Investigation into the role of Pak2 in the heart following myocardial infarction

A thesis submitted to the University of Manchester for the degree of Doctor of Philosophy in the Faculty of Biology, Medicine and Health

Lucy P L Collins

2020

Division of Cardiovascular Sciences, School of Medical Sciences

Contents

Word count: 46,267

List of figures

Abbreviations

%EF	% Ejection fraction
%FS	% Fractional shortening
αSMA	Alpha smooth muscle actin
AAV	Adeno-associated virus
ACE	Angiotensin converting enzyme
AID	Auto-inhibitory domain
AIF	Apoptosis inducing factor
ANP	Atrial natriuretic protein
Apaf1	Apoptotic protease activating factor 1
ASK1	Apoptosis signal-regulating kinase 1
ATF	Activating transcription factor
ATP	Adenosine triphosphate
AW	Anterior wall
AWs/d	Anterior wall thickness during systole/diastole
BNP	B-type natriuretic protein
CABG	Coronary artery bypass graft
CAD	Coronary artery disease
CARD	Caspase recruitment domain
cCasp	Cleaved caspase
CH	Cardiac hypertrophy
Chop	C/EBP homologous protein
CsCl	Caesium chloride
DAMPs	Danger associated molecular patterns
ddH_2O	Double distilled water
DHE	Dihydroethidium
DISC	Death-inducing signalling complex
DMEM	Dulbecco's modified Eagle's medium
DMSO	Dimethyl sulfoxide
DRP1	Dynamin related protein
ECG	Electrocardiography
ECM	Extracellular matrix
ER	Endoplasmic reticulum
ERAD	ER-associated degradation

ETC	Electron transport chain
FADD	Fas-associated death domain
FBS	Foetal bovine serum
H&E	Haematoxylin & Eosin
H/R	Hypoxia/reoxygenation
H_2O_2	Hydrogen peroxide
HF	Heart failure
HFrEF	Heart failure with reduced ejection fraction
HIF1	Hypoxia inducible factor 1
HW/TL	Heart weight/tibia length
I/R	Ischaemia/reperfusion
IAP	Inhibitor of apoptosis proteins
ICAD	Inhibitor of caspase-activated DNase
IRE1	Inositol-requiring kinase 1
IVS	Intraventricular septum
IVSs/d	End-systolic/diastolic intraventricular septum thickness
LAD	Left anterior descending coronary artery
LV	Left ventricle
LVPWs/d	Left ventricular posterior wall thickness at end-systole/diastole.
LW/BW	Lung weight/body weight
MI	Myocardial infarction
miR	MicroRNA
MLKL	Mixed lineage kinase domain-like protein
MMP	Matrix metalloproteinase
MOMP	Mitochondrial outer membrane permeabilization
mPTP	Mitochondrial permeability transition pore
MTT	Methylthiazolyldiphenyl-tetrazolium bromide
Pak	p21-activated kinase
Pak-2p34	34 kDa fragment of Pak2
$Pak2^{cko}$	Pak2 cardiomyocyte-specific knockout mice
$Pak2^{f/f}$	Pak2-floxed mice
PARP	Poly-ADP ribose polymerase
PBD	p21-binding domain
PCI	Percutaneous coronary intervention
PCR	Polymerase chain reaction

pEIF2α	Phosphorylated eukaryotic translation initiation factor-2 subunit alpha
PERK	Protein kinase-like endoplasmic reticulum kinase
PGAM	Phosphoglycerate mutase
pIRE1	Phosphorylated inositol-requiring kinase 1
PIX	Pak-interacting exchange factor
PRR	Pattern recognition receptors
qPCR	Quantitative PCR
RIDD	Regulated IRE1-dependent decay of mRNA
RIPs	Receptor-interacting protein kinases
RISC	RNA-induced silencing complex
ROS	Reactive oxygen specifies
s/dD	Left ventricular diameter end-systole/diastole
siRNA	Small interfering RNA
STEMI	ST-segment elevation MI
TAC	Transverse aortic constriction
tBid	Truncated Bid
tCasp	Total caspase
tEIF2α	Total eukaryotic translation initiation factor-2 subunit alpha
TGFβ	Transforming growth factor beta
TIMP	Tissue inhibitor of metalloproteinase
TM	Tunicamycin
TNFR	Tumour necrosis factor receptor
TNFα	Tumour necrosis factor α
TRADD	TNF-receptor type 1-associated death domain
TRAF2	Tumour necrosis factor receptor-associated factor 2
TRAIL	TNF-related apoptosis inducing ligand
TUNEL	Terminal deoxynucleotidyl transferase dUTP nick-end labelling
UPR	Unfolded protein response
XBP1	X-box binding protein 1
αMHC	Alpha myosin heavy chain
ΔΨ	Mitochondrial membrane potential

Abstract

Myocardial infarction (MI) and cardiac hypertrophy are two principal causes of heart failure, which affects millions of people worldwide and for which prognosis remains poor. Previous research has identified p21-activated kinase 2 (Pak2) as a cardioprotective molecule during cardiac hypertrophy by regulating the ER stress response. This project aimed to determine whether Pak2 has a protective role in the heart following MI. Pak2 cardiomyocyte-specific knockout mice ($Pak2^{cko}$) were used to investigate Pak2's role *in vivo*, and MI was induced through permanent ligation of the left anterior descending coronary artery. Western blot analysis demonstrated that Pak2 is activated in the acute MI response. Cardiac function was not affected by Pak2 knockout after two weeks. However, $Pak2^{cko}$ mice exhibited increased cell death and cardiac fibrosis two days following MI. Molecular analysis found an increase in protein levels of C/EBP homologous protein (Chop), demonstrating an impaired ER stress response in these mice. To investigate the role of Pak2 *in vitro,* H9c2 cardiomyoblasts were exposed to MI-mimicking stressors. Pak2 was found to be activated after 2 hours of hypoxia (100 % N_2) combined with nutrient starvation, and 1 hour after induction of oxidative stress by hydrogen peroxide (100 µM). Under these conditions, adenovirus-mediated Pak2 knockdown demonstrated that Pak2 deficiency leads to an impaired ER stress response. These findings suggest that Pak2 is a cardioprotective factor in response to MI-related stresses through modulation of the cardiomyocyte ER stress response.

Declaration

No portion of the work referred to in the thesis has been submitted in support of an application for another degree or qualification of this or any other university or other institute of learning.

Copyright statement

I. The author of this thesis (including any appendices and/or schedules to this thesis) owns certain copyright or related rights in it (the "Copyright") and she has given The University of Manchester certain rights to use such Copyright, including for administrative purposes.

II. Copies of this thesis, either in full or in extracts and whether in hard or electronic copy, may be made only in accordance with the Copyright, Designs and Patents Act 1988 (as amended) and regulations issued under it or, where appropriate, in accordance with licensing agreements which the University has from time to time. This page must form part of any such copies made. Presentation of Theses Policy You are required to submit your thesis electronically Page 11 of 25

III. The ownership of certain Copyright, patents, designs, trademarks and other intellectual property (the "Intellectual Property") and any reproductions of copyright works in the thesis, for example graphs and tables ("Reproductions"), which may be described in this thesis, may not be owned by the author and may be owned by third parties. Such Intellectual Property and Reproductions cannot and must not be made available for use without the prior written permission of the owner(s) of the relevant Intellectual Property and/or Reproductions.
Further information on the conditions under which disclosure, publication and commercialisation of this thesis, the Copyright and any Intellectual Property and/or Reproductions described in it may take place is available in the University IP Policy (see http://documents.manchester.ac.uk/DocuInfo.aspx?DocID=2442 0), in any relevant Thesis restriction declarations deposited in the University Library, The University Library's regulations (see http://www.library.manchester.ac.uk/about/regulations/) and in The University's policy on Presentation of Theses

Acknowledgements

I would like to thank the British Heart Foundation for accepting me on this programme and the University of Manchester for funding my research.

I would like to thank my supervisors Prof. Xin (Joy) Wang, Dr Wei (Vicky) Liu and Dr Elly Cartwright for all their support and guidance throughout my PhD. They gave me invaluable advice and I would not have been able to complete my PhD without them.

I would like to add further thanks to Elly for being an excellent programme director and for all her help and advice during the MRes year of this programme, dealing with mine and my cohort's many questions and queries.

The Wang/Liu labs have been a great group to work with over these years and I would like to thank them all – Pablo, Binh, Andrea, Cole, Yatong, Nimmi, Tayyiba and Rida. Special thanks to Pablo for dealing with all my questions and being a great desk buddy to chat to!

I would like to thank my BHF programme cohort – Shona, Steph, Lauren and Luke. It may have been a tough few years and it hasn't ended as we expected but we've had a great time. I wish them all the best in the future and hope that we keep in touch. Special thanks to Steph and Shona who, together with Eliza, got me through lockdown with our 'coffee mornings'.

Finally, I must thank my family for all of their backing and encouragement during not only my PhD but the many years before that. They have helped me more than they know. Mum and Amy, I look forward to celebrating this! In particular, I would like to thank Rob who has been my rock through this and has kept me going even when I wasn't sure I could.

Chapter 1 : Introduction

1.1 Heart failure

Heart failure (HF) is characterised as the inability of the heart to sufficiently pump enough blood around the body to meet the metabolic needs of all cells (Institute of Medicine (US) Committee on Social Security Cardiovascular Disability Criteria, 2010). It is a chronic condition that can be due either to the heart's inability to fill with enough blood, or due to the heart's failure to eject the blood with enough force. There are multiple forms of HF (Inamdar and Inamdar, 2016); for this project, the focus will be on the form known as heart failure with reduced ejection fraction (HFrEF). HFrEF, also described as systolic failure, is classified as the loss of left ventricular contraction capability, resulting in reduced ability of the heart to pump out enough blood into circulation. Symptoms of HFrEF include shortness of breath, oedema and fatigue (Chen *et al.*, 2019).

In 2014 it was estimated that around 26 million people were living with HF worldwide (Ponikowski *et al.*, 2014). Treatments include lifestyle changes, use of medication, such as angiotensin-converting enzyme (ACE) inhibitors, and surgical interventions if the cause is structural or caused by an issue with cardiac conduction. A study carried out in the UK between 2002 and 2014 found that the estimated total number of patients diagnosed with HF had increased by 12 %, with this attributed to the changing demographic, particularly the increasingly aging population (Conrad *et al.*, 2018). Further to this, a study published in 2017 found that, in the UK between 1998 and 2012, the survival rates of those diagnosed with HF has not improved, with 29.8 % survival at 10 years (Taylor *et al.*, 2017). These findings demonstrate the importance for not only improved treatment for HF, but also improved understanding about how it is caused and, therefore, how it may be prevented.

The leading causes of HF are diseases which cause cardiac injury, with hypertension-related diseases and myocardial infarction (MI) being two main causes. Hypertension places excessive strain on the heart muscle leading to pathological cardiac hypertrophy (CH). MI normally occurs due to a blockage in a coronary artery. This leads to cardiomyocyte death and reduces contractility in areas of the heart. Over time, remodelling to compensate fails, culminating in the development of HF. CH and MI will

be discussed in more detail below. Other cardiomyopathies can also lead to HF, though they will not be the focus of this project.

An important reason for the development of HF is the poor replicative ability of cardiomyocytes, given that they are terminally differentiated and hence post-mitotic, an event that occurs shortly after birth (Zebrowski *et al.*, 2015). Limited replication can occur but this decreases over time, and is only 0.3 % by the age of 75 (Bergmann *et al.*, 2009). Hence, any cardiac pathology that causes cardiac injury and cardiomyocyte death will likely lead to the development of HF due to the inability to replace lost cardiomyocytes; hearts with end-stage HF were found to have a cardiomyocyte apoptotic rate two hundred times higher than healthy hearts (Olivetti *et al.*, 1997).

1.2 Cardiac hypertrophy

Cardiac hypertrophy (CH) is an adaptive response of the heart to increased demand. It is characterised by the enlargement of the heart due to an increase in muscle mass. As previously stated, adult cardiomyocytes are terminally differentiated and have poor replicative ability. As such, during CH there is an increase in average cardiomyocyte size rather than an increase in cardiomyocyte number. There are two forms of CH, physiological and pathological, which are caused by differing overloading stimuli, which in turn stimulate separate molecular signalling pathways (McMullen and Jennings, 2007).

1.2.1 Physiological cardiac hypertrophy

Physiological CH is thought of as a beneficial adaptive response which does not detrimentally impact cardiac function. It results from the increased demand placed on the heart during events such as exercise or pregnancy, which cause a compensatory response. During physiological CH there is an increase in cardiomyocyte size, but they maintain normal cardiomyocyte structure and function (McMullen and Jennings, 2007). As such, physiological CH is often reversible; a study on Olympic athletes found that deconditioning for a mean of 13 weeks substantially reduced septal wall thickness (Maron *et al.*, 1993).

1.2.2 Pathological cardiac hypertrophy

Unlike physiological CH, pathological CH is often caused by underlying health issues, with the two main causes being hypertension and heart valve stenosis. It can also result from cardiac injury, for instance following MI (Kehat and Molkentin, 2010). The loss of contractility in the infarct area due to cardiomyocyte death causes compensation elsewhere in the heart. As such, excessive strain in these parts results in pathological CH that, over time, develops into HF.

The strain placed on cardiomyocytes during pathological CH results in increased cardiomyocyte necrosis and apoptosis (Teiger *et al.*, 1996). Fibrotic material replaces areas of cell death. This, unlike cardiomyocytes, cannot contract or propagate electrical stimuli, and hence reduces cardiac contractile capability. Combined reduction in contraction capability and diminished ventricular capacity reduces cardiac output (Capasso *et al.*, 1990). Furthermore, pathological CH causes abnormal gene expression in cardiomyocytes, with foetal genes, such as atrial and ventricular natriuretic peptides (ANP and BNP respectively), becoming upregulated (Cox and Marsh, 2014). Although this reactivation of genes not normally expressed in the adult heart is initially an adaptive response to stress, their expression alters cardiomyocyte contractility and calcium handling, and as such are key to the pathogenesis of pathological CH (Dirkx *et al.*, 2013).

Combined, these changes to cardiomyocyte function and cardiac structure detrimentally affect cardiac function. Over time the chronic strain placed on the heart results in HF.

1.3 Myocardial infarction

Myocardial infarction (MI) occurs when blood flow to an area of the myocardium becomes impeded due to a blockage in a coronary artery, preventing oxygen and nutrient supply to downstream cardiomyocytes. The main cause of MI is coronary artery disease (CAD). CAD is the narrowing of coronary arteries, normally due to atherosclerosis where accumulation of cholesterol and fatty deposits leads to the formation of plaques in vessel walls (Moreno, 2001). These plaques reduce lumen size and blood flow through the artery. MI occurs when a plaque becomes unstable and a thrombus forms in a coronary artery, obstructing blood flow to downstream cardiomyocytes (Figure 1.1A).

In the UK in 2019, over 100,000 people were admitted to hospital due to an MI, equivalent to one every 5 minutes (British Heart Foundation, 2020), and of the 17.9 million people that died from cardiovascular disease worldwide in 2016, 85 % were due to MI or stroke, demonstrating the ongoing need to focus research to tackle this disease (World Health Organisation, 2020). Current therapies improve initial mortality; however, due to the damaging effects that MI has on the heart, as will be discussed further in later sections, and the remodelling that occurs to compensate for this, improved survival correlates with increased incidence and risk of HF in survivors (Velagaleti *et al.*, 2008). This demonstrates the requirement for novel therapies to reduce initial damage, and prevent adverse cardiac remodelling following MI.

Loss of blood flow to downstream cardiomyocytes causes large levels of cells death. This delineates the heart into three regions – the infarct, border and remote regions (Figure 1.1B) (French and Kramer, 2007). The infarct region is comprised of tissue that has been directly affected by the loss of blood flow and is the site of most cell death. This is surrounded by a border zone of cardiomyocytes which are at risk and can easily be triggered to die. Areas of the heart that are further from the infarct region are termed as being in the remote region of the heart. These cells are not directly affected by an MI, but remodelling following MI, such as hypertrophy and increased interstitial fibrosis to compensate for the infarct area, affects cell function in this area. The key determinants of the progression to HF are the size of the infarct and the ability of the heart to repair and adapt to it.

1.3.1 Phases of MI

The biological response following MI can be separated into three main phases: (1) The inflammatory phase, (2) the proliferative phase and (3) the maturation phase (Figure 1.1C). Each of these phases have distinct functions and involve different cell types. The aim of all three phases it to aid in cardiac repair. These phases are described below.

The Inflammatory phase of MI

The initial response following MI involves a large number of cardiomyocytes undergoing cell death, predominantly sudden necrotic death. The release of cellular components that is typified by necrotic cell death, combined with damage to other myocardial tissue, leads to the release of danger-associated molecular patterns (DAMPs) (Weil and Neelamegham, 2019). These promote the infiltration of many immune cells into the myocardium, including neutrophils and monocytes, such as macrophages with an M1 pro-inflammatory phenotype. This initial inflammation is crucial for the removal of debris and aids in the formation of the infarct scar; however, persistent inflammation can cause immune-mediated tissue damage (Ong *et al.*, 2018).

The Proliferative phase of MI

The second phase of the response to MI is termed the proliferative phase and involves the formation of the scar in the infarct area. Formation of the scar is crucial to prevent cardiac rupture, which would result in sudden cardiac death. For the scar to be formed, fibroblast recruitment, proliferation, and differentiation into myofibroblasts is required. This allows the deposition of extracellular matrix (ECM) components, such as collagen fibres. Angiogenesis allows for vascularisation of this new tissue (Cochain *et al.*, 2013). In this stage the majority of inflammation is also concluded, and macrophages polarise towards a reparative (M2) phenotype, where they release anti-inflammatory and pro-fibrotic cytokines (Weil and Neelamegham, 2019).

The Maturation phase of MI

The final maturation phase of MI can occur weeks to months after the initial infarction. During this phase, myofibroblasts either de-differentiate back to fibroblasts or undergo apoptosis, and the scar matures through cross-linking of the ECM creating the final non-contractile scar (Frangogiannis, 2017; Nagaraju *et al.*, 2019). This phase is typified by changes in the remote region of the heart, with the loss of contractile capability of the scar area placing increased strain on the cardiomyocytes in this region. As such, there is increased inflammation and deposition of interstitial fibrosis in the remote region. Furthermore, cardiomyocytes become hypertrophic to compensate and, as in CH, this adaptive response ultimately can result in dilatation of the left ventricle and eventual progression to HF (French and Kramer, 2007).

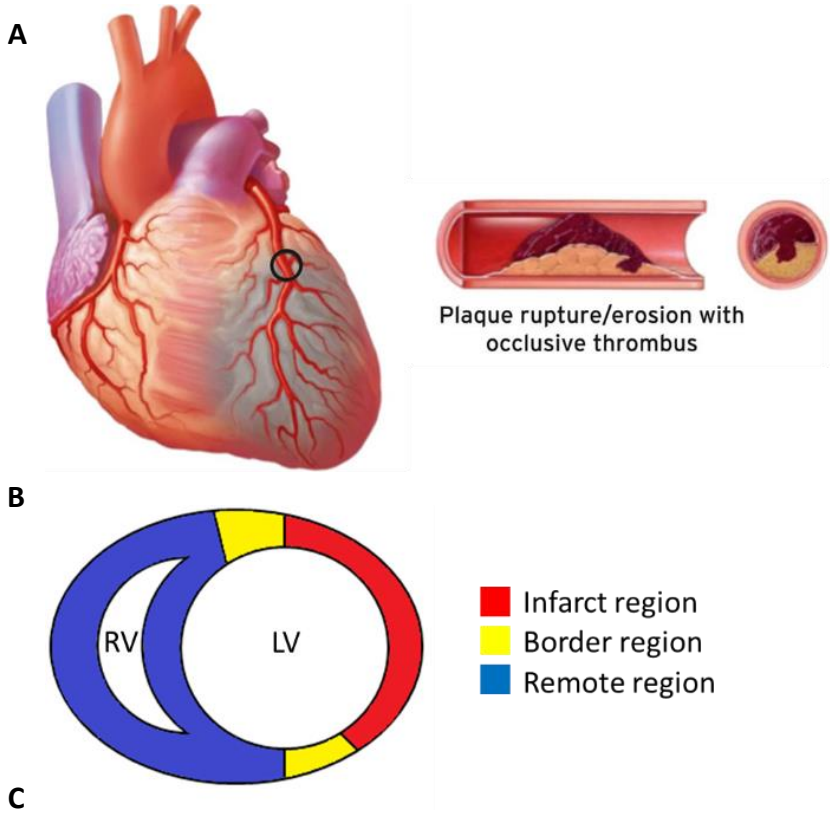

Figure 1.1 Cause of myocardial infarction and cellular and structural changes that occur in the heart following this. (A) Myocardial infarction (MI) occurs when an atherosclerotic plaque located in a coronary artery becomes destabilised and ruptures. This leads to the formation of a thrombus that impedes blood flow through the coronary artery, thus preventing blood flow to downstream cardiomyocytes. **(B)** Following MI, the heart tissue can be divided into three regions. The infarct region (red) is the site of immediate cell death following MI. In this region there is mass cell death which is replaced by fibrotic tissue to maintain heart structure. The border region (yellow) surrounds the infarct region. Cardiomyocytes in this region can be easily triggered to die, and so are known as 'at risk'. The remote region (blue) is not affected immediately by MI but a large amount of remodelling occurs here in the chronic stage to compensate for loss of contractility in the infarct region. **(C)** The cellular and structural changes that occur in the heart following MI follow three main phases, the inflammatory phase, the proliferative phase, and the maturation phase. Remodelling occurs over multiple months. ECM, extracellular matrix; LV, left ventricle; RV, right ventricle. Heart image in A is adapted from Thygesen *et al* (2018). Figure 1.1C is adapted from Ferrini *et al* (2019) and Weil & Neelamegham (2019)

1.4 Cell death is triggered by MI

As mentioned above, loss of oxygen and nutrient supply causes massive cell death following MI. It is estimated that 1 billion cardiomyocytes must die, on average, following MI for HF to occur (Murry *et al.*, 2006). Initial studies determined that two main forms of cell death take place after MI: apoptosis and necrosis. Whilst apoptosis is defined as an organised and regulated form of cell death that is non-inflammatory, necrosis and its programmed form, necroptosis, lead to a large inflammatory response due to the unregulated release of cellular contents.

1.4.1 Necrotic cell death

Necrosis-mediated cell death is considered to be a major form of cell death that occurs immediately following MI (Reimer *et al.*, 1977) since the loss of oxygen supply causes sudden cellular changes and prevents ATP-dependent apoptosis from occurring. Initially all necrotic death was thought to be unregulated; however, research over the past decade has identified a form of regulated necrosis, known as necroptosis (Dhuriya and Sharma, 2018). Both occur following MI. Necrotic cell death causes mass release of cellular components and, as such, causes substantial infiltration of immune cells and inflammatory response.

Necrosis

Coagulative necrosis is activated by external changes to the cellular environment, such as hypoxia. In short, loss of oxygen during MI prevents aerobic respiration, depleting ATP production and initiating anaerobic respiration. This leads to ion channel dysfunction, which causes accumulation of Ca^{2+} in the cytosol. To resolve this, some Ca^{2+} is taken up by the mitochondria which, together with loss of oxygen, impairs the electron transport chain, impeding ATP production and increasing levels if reactive oxygen species (ROS) (Chiong *et al.*, 2011). Oxidative burst results, which promotes the opening of the mitochondrial permeability transition pore (mPTP) leading to mitochondrial swelling as water moves down the osmotic gradient. Furthermore, increased cytosolic Ca^{2+} concentration leads to the influx of H_2O into the cell, causing cellular swelling and ultimately loss of membrane integrity and plasma membrane rupture, releasing cellular contents into the extracellular space (Kalogeris *et al.*, 2012). A recent study found that

in patients with ST-segment elevation MI (STEMI) optimal reperfusion therapy is required to occur within two hours of the MI, and if it is left longer there is significantly greater level of necrosis, which leads to increased infarct size and less salvageable tissue (Greulich *et al.*, 2019).

Necroptosis

Necroptosis is regulated by serine-threonine receptor-interacting protein kinases (RIPs) and targeting these using statins has shown to reduce infarct size (Smith *et al.*, 2007; Garvin *et al.*, 2018) (Figure 1.2). In short, necroptosis is initiated by binding of ligands to death receptors. Ligands include TNFα, which is upregulated following MI in humans (Halawa et al, 1999). RIP1 is recruited to the death receptor cytosolic domain and recruits RIP3 which autophosphorylates, leading to the formation of the necrosome. This allows for phosphorylation, and activation, of the mixed lineage kinase domain-like protein (MLKL). Active MLKL oligomerises and translocates to the plasma membrane, along with the necrosome, where it induces pore formation and cell rupture, leading to cell death (H. Wang *et al.*, 2014). RIP3-mediated activation of CAMKIIδ also leads to rupture and occurs independently of MLKL. The necrosome can also translocate to the mitochondria through association with PGAM5, a mitochondrial phosphatase that causes mitochondrial fragmentation alongside the GTPase Drp1. Loss of PGAM5 blocks necroptosis (Z. Wang *et al.*, 2012).

Unlike in apoptosis, during necroptosis DNA damage occurs in an unordered fashion, causing overactivation of the nuclear DNA repair enzyme PARP. Paradoxically this results in release of apoptosis inducing factor (AIF) from the mitochondria, causing further DNA damage (Culmsee *et al.*, 2005; Koh *et al.*, 2005; Moubarak *et al.*, 2007). Furthermore, PARP overactivation depletes levels of its substrate NAD^+. Synthesis to replace this causes ATP exhaustion, affecting ion channel function and leading to increased cytosolic concentrations of Na^{2+} and Cl^-. This drives water influx which results in cell swelling and rupture. PARP knockout in mice protects against necroptosis but not apoptosis (Ha and Snyder, 1999). As in necrosis, rupture of the plasma membrane leads to release of cellular contents and DAMPs, promoting an inflammatory response (Kaczmarek *et al.*, 2013; Pasparakis and Vandenabeele, 2015).

In vivo research has demonstrated necroptosis' role in MI-related cell death. RIP3 becomes upregulated following MI in mice, and $RIP3^{-/-}$ mice have improved ejection fraction and reduced CH 30 days following MI (Luedde *et al.*, 2014), demonstrating its importance in cardiac remodelling following injury. Similarly, molecular inhibition of RIP1 during I/R injury in mice improved cardiac function and reduced infarct size (Lim *et al.*, 2007; Smith *et al.*, 2007; Oerlemans *et al.*, 2012). Necroptotic markers, such as RIP1, are elevated in hearts of HF patients (Szobi *et al.*, 2017), supporting its role in remodelling and HF progression following MI.

Surprisingly, apoptosis and necroptosis signalling pathways act antagonistically. Both RIP1 and the pro-apoptotic caspase 8 bind death receptors, and active caspase 8 can cleave and inactivate RIP1, promoting apoptosis over necroptosis (Bohgaki *et al.*, 2011; O'Donnell *et al.*, 2011; Fritsch *et al.*, 2019; Newton *et al.*, 2019). This is required during embryogenesis, with global knockout of caspase 8 embryonically lethal due to excessive necroptosis (Kaiser *et al.*, 2011). The mechanism through which caspase 8-mediated inhibition of necroptosis is prevented *in vivo* is unclear. Regardless, it appears RIP1-RIP3 complexing at the death receptor is the molecular switch to promote necroptosis over apoptosis (Zhang *et al.*, 2009).

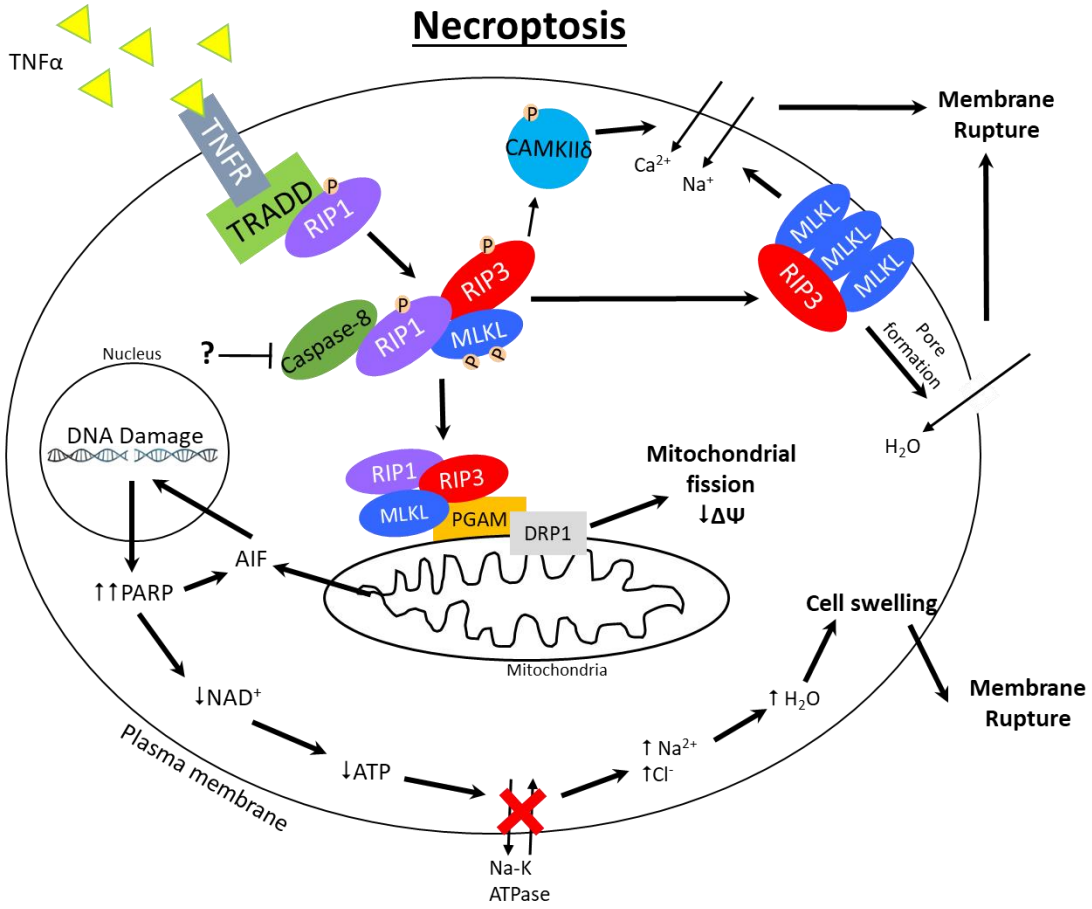

Figure 1.2 TNF-receptor mediated necroptosis cell death pathway. Extracellular ligand binding to death receptors causes recruitment of RIP1 to the death domain. Through an unknown mechanism, caspase 8-mediated inhibition of RIP1 is prevented. RIP1 recruits and activates RIP3, which recruits and phosphorylates MLKL, leading to the formation of the necrosome which translocates to the plasma membrane to promote pore formation. Pore formation is also caused through activation of CAMKIIδ by RIP3. The necrosome can also translocate to the mitochondria where it interacts with DRP1 to cause mitochondrial fission and loss of the mitochondrial membrane potential. DNA damage caused by extracellular stress leads to augmented PARP activation, leading to release of apoptosis inducing factor (AIF) from the mitochondria, augmenting DNA damage. Increased PARP also depletes NAD^+ reserves, and increased production reduces ATP levels. As a result, ion channel activity is reduced, leading to increased cytosolic levels of sodium and chloride ions, promoting water influx into the cell. This leads to cell swelling and, ultimately, rupture of the plasma membrane. MLKL, mixed lineage kinase domain-like protein; TNFα, tumour necrosis factor α; TNFR, tumour necrosis factor receptor; TRADD, TNF-receptor type 1-associated death domain; PARP, poly-ADP ribose polymerase; PGAM, phosphoglycerate mutase; DRP1, dynamin related protein; ΔΨ, mitochondrial membrane potential. Figure also used in the literature review for Lucy Collins' MRes dissertation.

1.4.2 Apoptotic cell death

Unlike necrosis, apoptotic cell death is highly regulated and non-inflammatory, and it requires the use of ATP. It is essential for regulation of the immune system (Opferman, 2008) and during development, with atypical apoptosis leading to abnormalities at birth (Mirkes, 2008; Su and Lenardo, 2008).

Increasing evidence demonstrates the importance of apoptosis in ventricular remodelling following MI, and it is also the key form of cell death during ischaemia/reperfusion (I/R) injury (Ikeda *et al.*, 1998; Eefting *et al.*, 2004), which is discussed later in the introduction. A study in rats showed that the apoptotic rate remained elevated in the remote regions of the heart up to four weeks following MI, and this was associated with increased ventricular dilation (Palojoki *et al.*, 2001). Furthermore, in a small cohort study, apoptotic rate strongly correlated with the progression to HF post-infarction, and this was associated with increased remodelling of the left ventricle (Abbate *et al.*, 2003).

Apoptotic cell death is highly regulated by caspases and Bcl-2 family proteins. There are two apoptotic pathways, the intrinsic and extrinsic pathways, both of which occur following MI. Crosstalk between the pathways can occur, and they converge on the same terminal pathway involving activation of effector caspases (Figure 1.3).

The intrinsic apoptotic pathway

The intrinsic pathway of apoptosis, also known as the mitochondrial pathway, is regulated by Bcl-2 family proteins. This family consists of both pro-apoptotic proteins, such as Bim, Bax, and Bid, as well as pro-survival proteins such as Bcl-2 and Bcl-xL. Overexpression of anti-apoptotic Bcl-2 in mice leads to reduced apoptosis following I/R (Chen *et al.*, 2001). External stress, such as hypoxia, loss of nutrient supply, and hypoxia/reoxygenation-induced release of ROS, leads to activation of a subset of pro-apoptotic Bcl-2 proteins known as BH3-only proteins. These activate pro-apoptotic Bcl-2 proteins such as Bax and Bak on the mitochondrial membrane, and promote the sequestration of pro-survival Bcl-2 proteins. This leads to irreversible mitochondrial outer membrane permeabilization (MOMP), which results in loss of the mitochondrial membrane potential (ΨM) and release of proteins and molecules into the cytosol that are normally sequestered within the mitochondria. For instance, following MOMP,

apoptosis inducing factor (AIF) is released into the cytosol and translocates to the nucleus where it causes DNA fragmentation (Daugas *et al.*, 2000). Cytochrome c is another important mitochondrial sequestered protein that is released following MOMP. Once in the cytosol, cytochrome c promotes the formation of the apoptosome through binding and promoting the oligomerization of apoptotic protease activating factor 1 (APAF1). The apoptosome contains a caspase recruitment domain (CARD) which allows for the recruitment of caspase 9 and its autoactivation. Active caspase 9 subsequently cleaves, thus activating, downstream effector caspases such as caspase 3 and 7. Caspase 9 also cleaves Bid, truncating it to form tBid, which promotes further mitochondrial changes and production of ROS. Smac, a protein released from the mitochondria during MOMP, inhibits inhibitors of apoptosis proteins (IAPs) which normally impede apoptosome formation and caspase 9 activation (Du *et al.*, 2000). Bax and Bak also promote mitochondrial fission and scission, leading to mitochondrial fragmentation (Suen *et al.*, 2008), further exacerbating release of mitochondrial-sequestered molecules. $Bax^{-/-}$ mice have smaller infarcts following MI (Hochhauser *et al.*, 2007).

The extrinsic apoptotic pathway

Unlike the intrinsic pathway, the extrinsic pathway of apoptosis is activated by ligand-receptor binding, leading to downstream signalling. Various receptors and their ligands can promote extrinsic apoptosis, such as FasL, TNFα and TRAIL (TNF-related apoptosis inducing ligand) binding their respective receptors (Wiley *et al.*, 1995; Krown *et al.*, 1996; Lee *et al.*, 2003). This binding leads to receptor-clustering and recruitment of adaptor death domains, such as the Fas-associated death domain (FADD). This complex is known as the death-inducing signalling complex (DISC). Plasma levels of FasL are elevated in patients following MI (Zhao *et al.*, 2009), and mice lacking functional Fas were shown to have 60 % fewer apoptotic cardiomyocytes following I/R (Nakamura *et al.*, 2000).

Formation of the DISC allows for the recruitment of pro-caspase 8 and 10 which become cleaved and activated. Active caspase 8 and 10 translocate from the plasma membrane to the cytosol where caspase 8 cleaves Bid, causing its truncation to tBid, resulting in its activation. This action allows for crosstalk between the intrinsic and extrinsic apoptotic pathways as tBid promotes Bax- and Bak-mediated MOMP (Li *et al.*, 1998). Both caspase

8 and 10 are capable of cleaving pro-caspase 3 and 7, leading to the activation of these executioner caspases.

Execution of apoptosis

The key executioner caspases of apoptosis, both the intrinsic and extrinsic pathways, are caspase 3 and 7. Both are upregulated in cardiac tissue from mice after I/R (Holly *et al.*, 1999). Inhibition of caspase 7 by overexpression of its regulator miR-23a was shown to improve ventricular function and reduce infarct size in rats following MI, though this was through reducing apoptosis of mesenchymal stem cells rather than cardiomyocytes (Mao *et al.*, 2014).

Executioner caspases cause the cellular changes associated with apoptosis, such as chromatin condensation, shrinkage of the cell, and DNA fragmentation. For instance, caspase 3 impedes the DNA repair machinery by cleaving PARP, thus preventing repair of DNA damage caused by ROS and AIF. Caspase 7 has been shown to compensate for loss of caspase 3 and can cleave PARP in its absence (Walsh *et al.*, 2008). Caspase 3 can also promote DNA fragmentation by cleaving the inhibitor of caspase-activated DNase (ICAD), thus causing its dissociation from the caspase-activated DNase (CAD), removing its inhibitory effect and allowing for CAD to cleave chromosomal DNA, resulting in chromatin condensation. Chromatin condensation is a key identifier of cells undergoing apoptosis.

Executioner caspases also cause the morphological changes associated with apoptosis. Caspase-mediated cleavage of ROCK-I, removing its inhibitory domain, renders it constitutively active (Walsh *et al.*, 2008). ROCK-I then causes blebbing of the cell (Coleman *et al.*, 2001; Sebbagh *et al.*, 2001). Following cell blebbing, cells are packed into apoptotic bodies, which are removed through phagocytosis by phagocytic cells such as macrophages. This prevents the inflammatory response caused by release of cellular components that is associated with necrotic cell death (Taylor *et al.*, 2008).

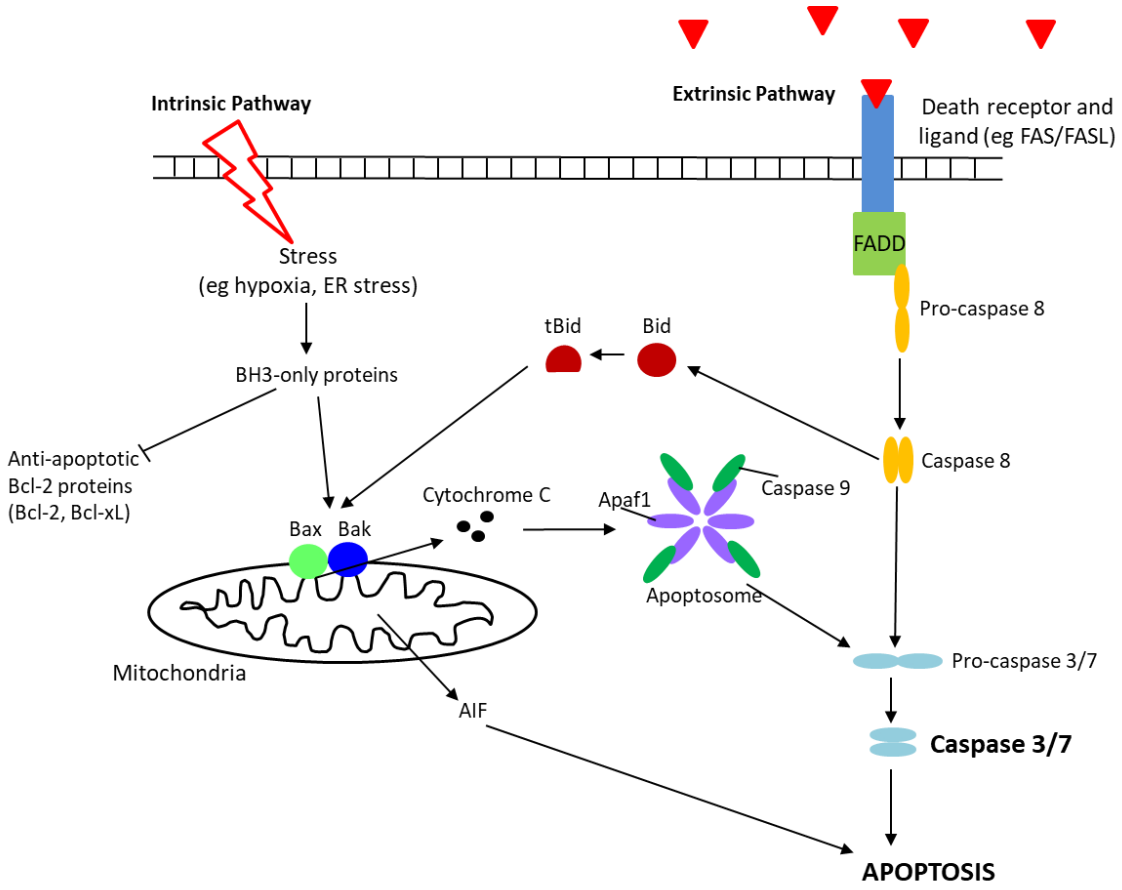

Figure 1.3 The apoptotic pathways. Apoptosis is triggered through two pathways, the intrinsic and extrinsic pathways. In the intrinsic pathways, extracellular stress, such as hypoxia, causes activation of BH3-ony proteins. These inhibit pro-survival Bcl-2 proteins and activate pro-apoptotic Bcl-2 proteins such as Bax and Bak. Bax and Bak stimulate mitochondrial outer membrane permeabilization, causing the release of mitochondria-sequestered proteins such as cytochrome C and apoptosis inducing factor (AIF). Cytochrome C triggers the formation of the apoptosome which cleaves the executioner pro-caspases 3 and 7, rendering them active. Release of SMAC from the mitochondria prevents inhibition of caspase 9 by the inhibitor of apoptosis protein (IAP). The extrinsic apoptotic pathway is activated by extracellular binding of ligands to their death receptors. This causes the formation of a death domain, to which pro-caspase 8 localises and becomes active. Active caspase 8 cleaves Bid, promoting MOMP, and also cleaves downstream executioner caspase pro-caspase 3 and 7. Once active these can cause the cellular and morphological changes associated with apoptosis such as DNA damage and blebbing. Apaf1, apoptotic protease activating factor 1; tBid, truncated Bid; FADD, Fas-associated death domain; ER, endoplasmic reticulum. Adapted from Hong et al (2008) and Ichim and Tait (2016). Diagram used in the literature review for Lucy Collins' MRes dissertation.

1.5 Inflammatory response following MI

Shortly following MI there is a large inflammatory response. As mentioned in section 1.4, MI causes massive cell death, of which much is necrotic and leads to the uncontrolled release of cellular debris into the intercellular space. This debris acts as danger-associated molecular patterns (DAMPs) which bind pattern recognition receptors (PRRs) on cells involved in the innate immune system, causing their activation (Prabhu and Frangogiannis, 2016). Furthermore, stressed cardiomyocytes have been shown to secrete DAMPs and cytokines to induce an immune response; for instance, they have been shown to release IL6, which has both pro- and anti-inflammatory properties following MI (Yamauchi-Takihara *et al.*, 1995). Following MI, there is also an increase in TNFα release, which has both pro-apoptotic and pro-hypertrophic effects (Irwin *et al.*, 1999). As well as release of pro-inflammatory mediators, hypoxia that occurs during MI damages vessel wall integrity, leading to increased vascular permeability, thus aiding infiltration of immune cells (Eltzschig and Eckle, 2011). Immune cell recruitment further amplifies the immune response as they too can release DAMPs and pro-inflammatory cytokines. Together, these factors initiate an inflammatory response that is required to remove necrotic debris and is also important for scar formation. Immune cells such as neutrophils release proteolytic enzymes and release ROS to degrade extracellular matrix components, aiding in the removal of cellular debris (Ma *et al.*, 2013). Removal of cell debris is required to prevent an exacerbated inflammatory response.

Following the initial MI inflammatory response, inflammation is predominantly resolved by a finely regulated but complex process during the reparative phase (Ong *et al.*, 2018). During this, macrophages polarise towards the M2 phenotype which is pro-reparative (Mouton *et al.*, 2018) and enables the release of anti-inflammatory cytokines such as IL-10 (Peet *et al.*, 2020). During this stage, the release of TGFβ by inflammatory cells can aid the activation of fibroblasts to promote deposition of fibrotic material to create the infarct scar (Ortega-Gómez *et al.*, 2013).

However, prolonged inflammation can cause immune-mediated damage to cardiac tissue and, if uncontrolled, can lead to structural remodelling that affects cardiac function and aids the progression to HF (Ono *et al.*, 1998; Dobaczewski *et al.*, 2010). For

instance, NFκB-mediated signalling is important for the post-MI inflammatory response, but over-exacerbation of this signalling has shown to be detrimental, leading to increased infarct size and reduced survival (Kawano *et al.*, 2006; Jin *et al.*, 2016). Blocking downstream signalling of NFκB has shown to improve survival in mice following MI and improve prognosis in human patients (Dai *et al.*, 2019). Furthermore, targeting inflammatory cytokines, such as blocking IL-1 signalling, reduces apoptosis and infarct size (Abbate *et al.*, 2008), and limits detrimental cardiac remodelling following MI (Bujak *et al.*, 2008), whilst promoting an anti-inflammatory response through exogenous IL-10 encourages cardiac repair and reduces left ventricular dilatation (Jung *et al.*, 2017).

1.6 Cardiac fibrosis

The cardiac ECM is crucial for supporting cardiac-resident cells and structures, and for aiding normal cardiac function (Rienks *et al.*, 2014). It consists of collagen type I, III, IV and VI, which are produced as pro-collagens and cleaved by peptidases to produce collagen fibres, along with other structural proteins. The ECM is dynamic, with a balance between release and deposition of ECM components, predominantly by fibroblasts, and turnover by matrix metalloproteinase (MMPs) which are regulated by tissue inhibitors of metalloproteinases (TIMPs).

Excessive cardiac fibrosis is a maladaptive process that is characterised as the disproportionate deposition of ECM components, predominantly collagen types I and III (Cleutjens *et al.*, 1995), in the cardiac muscle where it is not usually found. Initially, cardiac fibrosis develops to promote wound healing, but it often has detrimental outcomes. Increased cardiac fibrosis alters cardiac structure and function as it increases the stiffness of the myocardium and hinders normal contractile function due to its inability to conduct electrical stimuli, which can lead to arrythmias (Morita *et al.*, 2014).

Cardiac fibrosis is a hallmark of both CH and MI. Initially following an MI the inflammatory cells recruited to the infarct area release MMPs to release necrotic myocytes (Nielsen *et al.*, 2019). However, the massive cell death that occurs in the infarct region leaves a void that must be filled to maintain the heart's form. Due to this, a large amount of ECM components are deposited by myofibroblasts to repair this area. This is termed replacement fibrosis (Hinderer and Schenke-Layland, 2019). Insufficient replacement fibrosis can result in cardiac rupture (Shimazaki *et al.*, 2008). However,

continued strain on the heart due to the infarct results in increased interstitial fibrosis in non-infarcted regions; this is known as reactive fibrosis and, as with fibrosis during CH, aids in the progression to HF.

Deposition of fibrotic material is governed by fibroblasts. The pool of cardiac fibroblasts in the stressed heart is heterogeneous in its origin, as is well summarised by Ma et al (2018). It is comprised of resident fibroblasts as well as those that have migrated to the heart from other areas of the body such as the bone marrow and epicardium, as well as endothelial-derived fibroblasts which have undergone endothelial-mesenchymal transformation. Lineage tracing suggests that around 30 % cardiac fibroblasts in the hypertrophic heart derive from endothelial cells (Zeisberg *et al.*, 2007).

Differentiation of fibroblasts into myofibroblasts is important for the deposition of ECM and development of cardiac fibrosis, and only occurs when the heart is stressed or failing. Changes in the heart, such as mechanical tension, cause fibroblasts to transfer to a proto-myofibroblast state, whilst TGFβ and other cytokines promote the final differentiation to mature activated myofibroblasts (Boris Hinz *et al.*, 2001; Elson *et al.*, 2019). Myofibroblasts share phenotypic similarities with both fibroblasts and smooth muscle cells, in that they are fibroblasts which express contractile proteins, such as alpha smooth muscle actin (αSMA), and develop stress fibres. Myofibroblasts are superior at wound healing due to their increased motility, contractile capability, and ability to secrete high levels of ECM components. Furthermore, they secrete cytokines and recruit immune cells to the injury site, aiding the reparative response (Porter and Turner, 2009; Baum and Duffy, 2011). However, chronic myofibroblast activation and signalling has been shown to promote cardiac dysfunction (Meng *et al.*, 2018). In the maturation phase of MI, once a mature scar has formed, myofibroblasts either undergo de-differentiation back to fibroblasts, though the mechanism of this is not fully understood, or undergo apoptosis and are cleared by inflammatory cells.

TGFβ is a key regulator of cardiac fibrosis. Its level are significantly increased in the heart after MI (Wünsch *et al.*, 1991; Deten *et al.*, 2001). TGFβ, a growth factor, is produced by many cell types, including inflammatory cells and cardiomyocytes (Wu *et al.*, 2018). It is secreted by cells in a latent form bound to TGFβ-binding protein (LTBP) and latency-associated peptide (LAP). The full pathway for TGFβ activation is not clear, but it is known that several factors, such as ROS (Barcellos-Hoff and Dix, 1996), proteases and

MMPs (Yu and Stamenkovic, 2000), changes in pH (Lyons *et al.*, 1988) and binding of glycoproteins (Schultz-Cherry and Murphy-Ullrich, 1993) can lead to activation of TGFβ from its latent complex, allowing it to bind its receptors and initiate downstream signalling cascades. Upon binding to its receptor, TGFβ can initiate canonical SMAD2/3-dependent signalling pathways and non-canonical signalling pathways which are SMAD-independent. Both can regulate the TGFβ-mediated fibrotic response (Finnson *et al.*, 2020) and both have been implicated in the development of cardiac fibrosis, which is reviewed nicely by Hanna & Frangogiannis (2019). For instance, TGFβ is crucial for the differentiation of fibroblasts to myofibroblasts (Desmouliere *et al.*, 1993) and promotes the secretion of collagens I and III (Eghbali *et al.*, 1991) and TIMPS (Johnston and Gillis, 2017) from myofibroblasts, demonstrating how TGFβ promotes ECM deposition and suppresses MMP-mediated ECM degradation.

Targeting TGFβ for therapeutic purposes has been explored (Györfi *et al.*, 2018). However due to its involvement in many other cellular processes and elsewhere in the body, for instance its importance in the immune system (Sanjabi *et al.*, 2017), it is unlikely that directly targeting TGFβ will be feasible without producing harmful side effects. Furthermore, a study in mice found that inhibition of TGFβ through infusion of anti-TGFβ antibodies led to increased mortality and ventricular remodelling after MI, demonstrating the crucial balance between the pro-survival and detrimental effects of fibrosis in the infarcted heart (Frantz *et al.*, 2008).

1.7 Ischaemia/Reperfusion (I/R) injury

Current treatments of MI often involve restoring blood flow to infarcted areas and surrounding tissue. These treatments include percutaneous coronary intervention (PCI), where a stent is implanted by a catheter to reopen the occluded artery, the use of thrombolytic agents to dissolve the blockage, and coronary artery bypass graft (CABG) surgery, where blood vessels are transplanted from elsewhere in the body to restore blood flow to a region of the heart by bypassing the affected coronary artery. However, whilst these treatments improve initial mortality rates, they can also lead to further myocardial damage. This is because restoration of oxygen can cause ischaemia/reperfusion (I/R) injury, which either accelerates the cell death process, or initiates it in previously-healthy cells (Kloner, 1993). Reperfusion has shown to significantly elevate the percentage of cardiomyocytes undergoing apoptosis following MI (Z. Q. Zhao *et al.*, 2000) and post-conditioning in dogs significantly reduced infarct size irrespective of ischemic time (Zhao *et al.*, 2003).

As demonstrated in Figure 1.4, it is believed that reperfusion limits the progressive cell death that would be caused were ischaemia not resolved; however, reperfusion causes a sudden increase in cell death and resultant infarct size, above what it would be if I/R injury could be prevented (Yellon and Hausenloy, 2007). Thus, strategies targeting this phenomenon to reduce the cell death caused are of great interest. However, clinical studies targeting I/R injury have yet to prove successful in human patients (Hausenloy *et al.*, 2017).

Changes to calcium handling affect cellular responses during reperfusion. During ischaemia, the loss of oxygen prevents aerobic respiration and initiates anaerobic respiration. As such, cellular ATP levels are reduced along with a reduction in intracellular pH due to lactate accumulation. Whether a cell enters the cell death cycle is determined by the level and duration of oxygen depletion. In cells that survive this, often those found in the border region of the infarcted heart, restoration of oxygen during reperfusion causes a re-initiation of aerobic respiration and restoration of pH levels. However, alteration in cellular ion channels to restore the pH, reviewed elsewhere (Kalogeris *et al.*, 2012; Hausenloy and Yellon, 2013), result in a sudden and substantial increase in cytosolic calcium levels. To resolve this, Ca^{2+} is removed from the

cytosol into the mitochondria via the mitochondrial Ca^{2+} uniporter, but this in turn leads to excessively elevated mitochondrial Ca^{2+} levels. This triggers the opening of the mitochondrial permeability transition pore (mPTP), leading to reduced mitochondrial membrane potential that results in cell death, as mentioned in section 1.4.1 on necrosis. Targeting calcium handling using pharmacological agents has proven to reduce reperfusion-related cellular damage in pigs (Carry *et al.*, 1989) but has not yet shown positive results in human patients (Zeymer *et al.*, 2001).

Along with calcium, changes to cellular oxygen levels during reperfusion cause cellular damage. This is due to oxidative stress, which is termed as the imbalance between production of ROS and their clearance by antioxidants (Pizzino *et al.*, 2017). During ischaemia, substantial levels of ROS are produced because of the uncoupling of the electron transport chain (ETC) due to the loss of oxygen. However, the restoration of oxygen supply during reperfusion, allowing aerobic respiration to restart and hence reactivating the ETC, augments the release of ROS due to electron leak from the ETC. Furthermore, along with increased cytosolic Ca^{2+}, ROS promotes the opening of the mPTP during reperfusion, increasing the inner mitochondrial membrane permeability. This prevents the ETC from functioning normally, leading to further ROS production. ROS damage DNA, lipids, and proteins, which in turn leads to activation of cell death pathways. Elevated ROS can also contribute to the development of arrhythmias following reperfusion, as they decrease the activity of SERCA2 and reduce myofibrillar calcium sensitivity (Kaplan *et al.*, 2003; Zhou *et al.*, 2018). Studies targeting ROS in I/R have had mixed results, potentially due to the difficulty in introducing antioxidants into cells (Boissel *et al.*, 2000), though treatment of a free radical scavenger prior to reperfusion was found to reduce infarct size compared to those given a placebo in a small study on 100 patients (Tsujita *et al.*, 2006), suggesting potential therapeutic benefits.

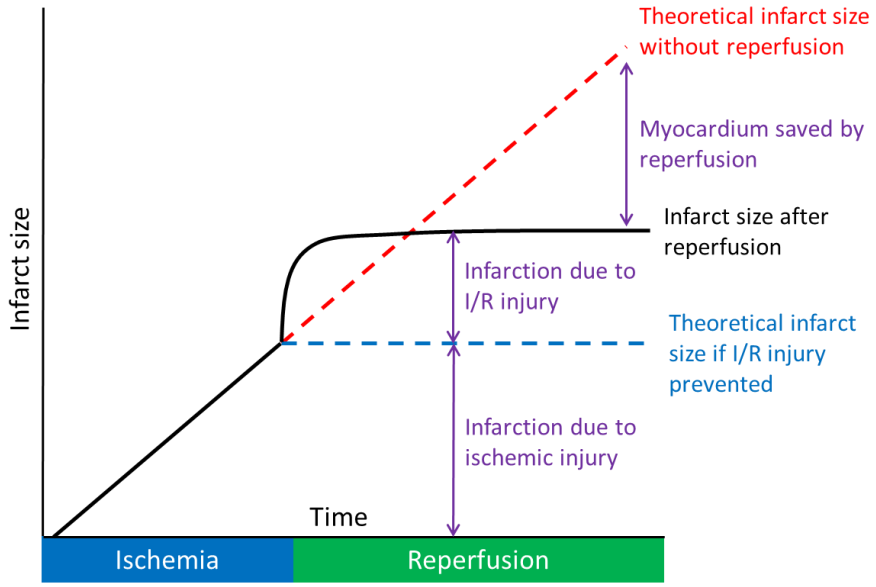

Figure 1.4 Schematic demonstrating the contribution of ischaemia/reperfusion (I/R) injury to infarct size. The black line demonstrates the infarct size following MI and I/R. The dashed red line indicates the theoretical infarct size if reperfusion had not occurred. The dashed blue line indicates the theoretical infarct size if I/R injury could be prevented. I/R, ischemia/reperfusion. Diagram adapted from Hausenloy & Yellon (2013)

1.8 Endoplasmic Reticulum (ER) stress

1.8.1 ER function and the adaptive unfolded protein response (UPR)

The endoplasmic reticulum (ER) is a major site of protein folding and maturation in the cell, particularly of ER-resident proteins, lysosomal proteins and secretory proteins. Changes in cellular stimuli, both pathological and physiological, alter ER homeostasis and function. For instance, cell exposure to nutrient starvation (Zhang *et al.*, 2010), ischaemia (Nakka *et al.*, 2010), viral-infection (He, 2006) and other cellular stresses can disrupt protein folding. Furthermore, increased protein transcription caused by some diseases, such as during CH, increases protein load (Guan *et al.*, 2011).

Where ER homeostasis is disrupted significantly, this leads to an accumulation of misfolded or unfolded proteins. These can damage the cell through interfering with normal ER function, and some aggregates of misfolded protein can be toxic (McLendon and Robbins, 2015). To adapt to protein fluctuations, a conserved cellular response known as the unfolded protein response (UPR) is initiated (Zhang *et al.*, 2016) (Figure 1.5). The UPR aims to restore normal protein homeostasis, and does so through halting protein translation, degrading misfolded proteins, and increasing production of ER chaperones to aid protein folding. There are three main branches of the UPR, which are coordinated by three separate ER-resident transmembrane proteins: IRE-1, ATF6, and PERK. Under basal conditions the ER chaperone Bip/GRP78 binds and forms stable complexes with these proteins, acting as a negative regulator (Bertolotti *et al.*, 2000; Lee, 2005). However, during ER stress, Bip dissociates from these in order to bind unfolded proteins, removing its inhibitory effect and leading to downstream UPR signalling. Through this, Bip acts as a key sensor of ER stress.

Double-stranded RNA-activated protein kinase-like endoplasmic reticulum kinase (PERK) is a member of the eukaryotic translation initiation factor family. It is a type I transmembrane protein that has a luminal stress-sensing domain and a cytoplasmic protein kinase domain. Upon ER stress, PERK becomes activated via oligomerisation and trans-autophosphorylation (Rozpedek *et al.*, 2016). Activated PERK phosphorylates the Ser51 residue of the alpha subunit of eukaryotic translation initiation factor-2 (eIF2α). eIF2α is a translation initiation factor composed of three subunits (α, β, γ) that requires cycling of GTP/GDP in order to function, with eIF2-GTP catalysing translational initiation,

leading to GTP hydrolysis to GDP, recycling of eIF2 and exchange of GDP with GTP. Phosphorylation of eIF2α by PERK leads to translation attenuation through stabilising the GDP-bound EIF2β complex, preventing GDP/GTP exchange and thus preventing translation initiation (Harding *et al.*, 1999). This attenuation of translation reduces the load of newly synthesised proteins, thus reducing the strain placed on the ER. Interestingly, eIF2α phosphorylation does cause increased translation of some stress-related genes, of which activating transcription factor 4 (ATF4) is one. ATF4 is a transcription factor that regulates transcription of genes involved in autophagy, apoptosis and the redox response, as well as ER chaperones Bip/GRP78 and GRP94 (B'Chir *et al.*, 2013). These glycoprotein chaperones have four roles in maintaining ER function: they aid in the folding of proteins, interact with protein-folding machinery in the ER, are a store of Ca^{2+}, and target misfolded proteins for degradation. GRP78/Bip and GRP94 share similar roles, though GRP94 has more selectivity in the proteins it binds, with specific affinity for those involved in the immune response, cell adhesion, and growth signalling (Zhu and Lee, 2015).

Inositol-requiring kinase 1 (IRE1), like PERK, is a type I ER resident transmembrane protein with a cytosolic kinase domain. Upon ER stress and Bip dissociation, IRE1 becomes activated through oligomerisation and trans-autophosphorylation. Once active, IRE1 splices X-box binding protein 1 (XBP1) mRNA through its nuclease activity, generating a spliced form of XBP1 (XBP1s). XBP1s is a transcription factor that translocates to the nucleus and promotes the upregulation of transcription for target genes, including ER chaperones, lipid synthesis-related genes, and those involved in ER-associated degradation (ERAD) (S. Wang *et al.*, 2018). ERAD is a process whereby proteins that have been irreparably misfolded are cleared from the ER and degraded in the cytosol by the proteasome (Meusser *et al.*, 2005). On top of these mostly pro-survival effects of IRE1 through XBP1 splicing, IRE1 has also been identified as affecting the ER homeostatic response by promoting a process known as regulated IRE1-dependent decay of mRNA (RIDD). RIDD is a mechanism through which ER-associated mRNAs can be degraded during prolonged ER stress. It can cause a pro-apoptotic response, as will be discussed in section 1.8.2. Interestingly, Moore and Hollien (2015) determined that RIDD is hindered by depletion of PERK, suggesting interaction between these two pathways.

Under basal conditions, activating transcription factor 6 (ATF6) is a transmembrane protein located in the ER membrane. However, upon dissociation of Bip during ER stress, it translocates to the Golgi apparatus where it is cleaved by site-1 and site-2 proteases (S1P/S2P) to form a 50 kDa fragment that acts as a transcription factor (ATF6f or cleaved ATF6) and translocates to the nucleus. Here, ATF6f promotes expression genes with an ER stress response element (ERSE) in their promoter, including ER chaperones, XBP1, and those related to ERAD (Belmont *et al.*, 2010).

1.8.2 Chronic ER stress and cell death

Activation of the UPR aims to restore normal ER function by reducing protein load through RIDD, ERAD and inhibiting protein translation, and by increasing protein folding by promoting expression of ER chaperones. However, prolonged or chronic activation of the UPR is an indication that the ER stress cannot be resolved. To prevent this from leading to cellular dysfunction, which may in some way impact surrounding cells, chronic ER stress can lead to UPR-mediated cell death. ER stress-mediated apoptosis is heavily influenced by IRE1, caspase-12 and the transcription factor CAAT enhancer-binding protein (C/EBP) homologous protein (Chop).

Chop is an important regulator of ER stress-initiated apoptosis, with MEF cells from $Chop^{-/-}$ mice exhibiting less apoptosis following ER stress induction than those from controls (Zinszner *et al.*, 1998). Its expression is upregulated by all three branches of the ER stress response. Chop can act as both a transcriptional repressor and activator. Chop suppresses anti-apoptotic Bcl-2 expression (McCullough *et al.*, 2001), thus affecting the ratio of it to pro-apoptotic Bcl-2 proteins, and can directly induce transcription of pro-apoptotic Bim (Puthalakath *et al.*, 2007). It augments oxidant injury in cells by causing depletion of cellular glutathione and enhancing ROS production, potentially through its influence on Bcl-2 expression (McCullough *et al.*, 2001). Chop can also induce cell death independent of Bcl-2 related proteins. For instance, it triggers calcium-dependent apoptosis through activating ER oxidase 1α (ERO1α) (Li *et al.*, 2009). Using wild type and $Chop^{-/-}$ mice, Li et al (2009) showed that activation of ERO1α by Chop leads to enhanced activity of the inositol 1,4,5-triphophate (IP3) receptor (IP3R), which in turn augments IP3-induced calcium release and calcium-mediated apoptosis. In addition, Chop can antagonise pro-survival effects of the UPR. Chop directly activates GADD34 (Marciniak

et al., 2004), a protein which directs protein phosphatase 1 (PP1) to dephosphorylate pEIF2α at Ser51, thus preventing pEIF2α-induced translational repression, leading to exacerbated protein overload. Inhibition of PP1 can protect against tunicamycin and I/R-induced apoptosis by restoring pEIF2α activity (C. L. Liu *et al.*, 2014).

In rodent models, caspase 12 is an ER-localised caspase that is important for ER stress-induced cell death. Caspase 12, like other caspases, resides in a procaspase form until cleavage to generate its active form. It is localised at the ER membrane and can be cleaved through two mechanisms (Liu *et al.*, 2016). Firstly, raised cytoplasmic Ca^{2+} levels cause calpain activation, which cleave procaspase-12. Secondly, procaspase-12 can colocalise with tumour necrosis factor receptor-associated factor 2 (TRAF2) under basal conditions; upon ER stress, procaspase-12 dissociates from TRAF2, and this leads to caspase 12 activation. Active caspase 12 cleaves and activates caspase 9, which is part of the apoptosome, thus promoting apoptosis (Morishima *et al.*, 2002). Of interest, full-length caspase 12 is enzymatically inactive in humans and plays no role in ER stress-induced cell death. Caspase 4 has been identified as a potential alternative to caspase 12 in human and is involved in ER stress-induced cell death (Hitomi *et al.*, 2004).

As well as promoting cell survival through cleavage of XBP1, IRE1 can also promote cell death during prolonged ER stress through alternative pathways. As mentioned in section 1.8.1, IRE1 promotes RIDD, where mRNA is degraded to reduce load on the ER. However, under sustained ER stress it is thought that RIDD may lead to the degradation of mRNAs that are important for cell survival, thus promoting apoptosis (Hollien and Weissman, 2006; Hollien *et al.*, 2009; Scull and Tabas, 2011). This phenomenon precedes and tracks progression to apoptosis during ER stress, and prevention of RIDD was found to inhibit apoptosis (Ghosh *et al.*, 2014). As well as acting as an endoribonuclease, IRE1 also interacts with TRAF2 via its cytosolic kinase domain. TRAF2 in turn activates apoptosis signal-regulating kinase 1 (ASK1) (Nishitoh *et al.*, 1998), a MAPKKK which activates JNK and p38, both of which can phosphorylate and activate the pro-apoptotic Bcl-2 protein Bax (Kim *et al.*, 2006). p38 can also enhance Chop activity (Wang and Ron, 1996), while Jnk activation promotes the release of cytochrome c from the mitochondria (Tournier *et al.*, 2000) and can inhibit the pro-survival protein Bcl-2 (Davis, 2000). IRE1 activation is also coupled with the inflammatory stress response through its interaction with TRAF2, which recruits IκB kinase (IKK), a regulator of the inhibitor of κB kinase (IκB). IKK

phosphorylation of IκB leads to its degradation, and release and activation of sequestered NFκB. Thus, IRE1 activation and recruitment of TRAF2 promotes NFκB activation and translocation to the nucleus, where it promotes an inflammatory stress response (Tam *et al.*, 2012). Evidently, IRE1 balances both pro-survival and pro-apoptotic signalling. The view that this branch of the ER stress response is the last to be activated (Szegezdi, Logue, *et al.*, 2006) could suggest that it is the final attempt to resolve ER stress and, if it fails, apoptosis is initiated to remove the cell and prevent damage to surrounding tissue.

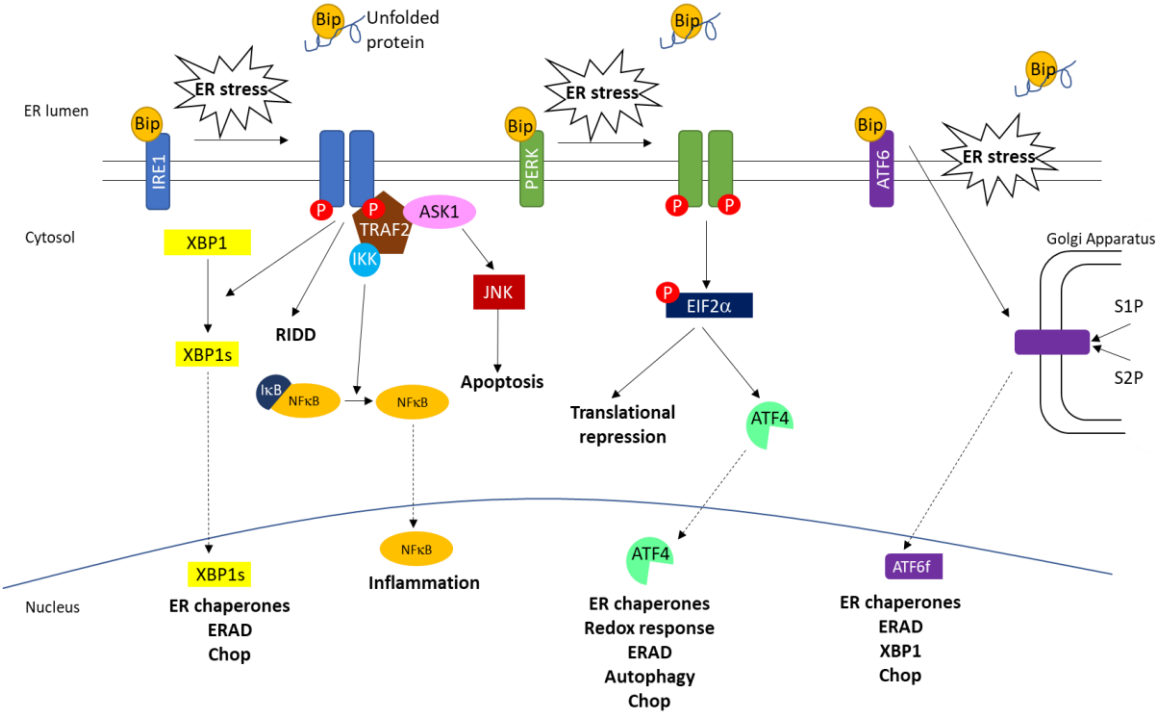

Figure 1.5 The unfolded proteins response (UPR). ER stress, such as an increase in unfolded or misfolded proteins, causes activation of three pathways (IRE1, PERK and ATF6) due to removal of Bip. Once active, IRE1 oligomerises and trans-autophosphorylates. Active IRE1 promotes the splicing of XBP1 into XBP1s, which translocates to the nucleus to promote gene expression for ER chaperones, ER-associated degradation (ERAD) genes, as well as pro-apoptotic genes such as Chop. Phosphorylated IRE1 can also promote regulated IRE1-dependent decay of mRNA (RIDD), as well as inflammation through activation of NFκB, and apoptosis through activation of JNK. Upon removal of Bip during ER stress, PERK becomes phosphorylated and activated. Active PERK activates EIF2α, leading to translation repression, and activates ATF4, leading to its translocation to the nucleus and altered gene expression associated with reducing protein load, autophagy, the redox response, and apoptosis. Finally, removal of Bip from ATF6 during ER stress causes its translocation to the golgi apparatus where it is cleaved by site-1 and site-2 proteases (S1P/S2P) to form a 50 kDa fragment (ATF6f) with transcription factor capabilities. This translocates to the nucleus where it promotes gene expression of ER chaperones, XBP1, and genes related to ERAD.

1.8.3 ER stress in the heart

The UPR is involved in the development of the cardiovascular system. Hearts from neonatal mice have elevated levels of GRP78/Bip compared to adult hearts, and this may be important for embryonic development (Mao *et al.*, 2006). Furthermore, global knockout of XBP1 is embryonically lethal in mice, with death occurring between embryonic days 10.5-14.5 due to increased cardiomyocyte death (Masaki *et al.*, 1999). Although the specific reason for this is not clear, it demonstrates that the UPR is activated not solely during disease.

Despite this, excessive ER stress and overactivation of the UPR has been identified in many disease models, including cancer (Urra *et al.*, 2016), metabolic diseases such as diabetes (Cnop *et al.*, 2012), and neurodegenerative diseases such as Alzheimer's disease and Parkinson's disease (Gerakis and Hetz, 2018; Colla, 2019). It has also been shown to play a role in diseases that affect the cardiovascular system (S. Wang *et al.*, 2018). Hypertension leads to increased Chop expression in the heart (Kassan *et al.*, 2012), and elevated levels of Bip and XBP1s splicing have been observed in tissue from HF patients (Dally *et al.*, 2009; Sawada *et al.*, 2010). Mice lacking Chop are less susceptible to the development of CH and cardiac fibrosis following transverse aortic constriction (TAC), in conjunction with reduced cardiomyocyte apoptosis and improved cardiac function compared to controls following this procedure (Fu *et al.*, 2010).

Interestingly, the PERK branch of the UPR appears to protect against the development of HF. Cardiomyocyte-specific PERK knockout mice have increased cardiac dysfunction and cell death following TAC compared to wild-type controls, together with increased Chop expression (X. Liu *et al.*, 2014). This protective role appears to be through PERK's ability to regulate SERCA2a expression, which is significantly reduced when PERK is absent, and hence regulate calcium handling which is impaired during the progression to HF (X. H. Liu *et al.*, 2011). However, this role of PERK appears to be detrimental in some cardiac diseases, with it implicated in the development of ventricular arrythmias during diabetic cardiomyopathy (Z. Liu *et al.*, 2014).

The protective arm of the UPR is downregulated during the development of heart disease. Duan et al (2015) identified that, during the progression towards CH and HF,

there is micro-RNA mediated inhibition of XBP1 and this may explain why XBP1, which is elevated in the early adaptive phase of ER stress, becomes downregulated.

1.8.4 ER stress in ischaemic heart disease

The UPR is activated following MI, with levels of PDI, an ER chaperone expressed during ER stress, upregulated 3-fold in tissue surrounding the infarct region (Severino *et al.*, 2007). Elevated levels of XBP1 and GRP78/Bip are evident in neonatal rat cardiomyocytes following exposure to hypoxia, and viral-infection with dominant negative XBP1 increased apoptosis following I/R, demonstrating the role of the UPR in cardiomyocyte death during MI-related events (Thuerauf *et al.*, 2006). As in other disease models, it appears initial activation of the UPR attempts to restore ER homeostasis by elevating levels of ER chaperones, XBP1 splicing and EIF2α-mediated translational repression. However, prolonged ischaemia, or reperfusion following ischaemia, leads to ER stress-mediated cell death, with increased levels of Chop, caspase 12 and executioner caspase activation (Szegezdi et al., 2006; Thuerauf et al., 2006; S. Wang et al., 2018).

Targeting the UPR following MI improves cardiac function. Transgenic overexpression of an endogenous calpain inhibitor, calpastin, was shown to blunt the ER stress response after MI, and led to significantly reduced scar area, cardiomyocyte cell death and ventricular dilatation (Li *et al.*, 2018) which was attributed to a reduction in Chop expression. Furthermore, overexpression of XBP1s *in vivo* significantly reduced the infarct area after I/R injury, whilst knockout of XBP1s impaired cardiac function (Z. V. Wang *et al.*, 2014) demonstrating the protective effects of this branch of the UPR. Ischemic postconditioning, which reduces the damage caused during I/R injury through intermittent reperfusion following infarction, appears to work, in part, through attenuating ER stress, with reduced protein levels of caspase 12 found (Liu *et al.*, 2008). Similar findings have also been shown during ischemic postconditioning in kidneys, with reduced Bip, ATF4, PERK, and XBP1 levels in the post-conditioned group (Mahfoudh-Boussaid *et al.*, 2012). Evidently, exploration into how the ER stress response is modulated during these conditions could provide a novel therapeutic strategy for the treatment of MI and I/R-related cardiac dysfunction.

1.9 P21-activated Kinases (Paks)

The p21-activated kinase (Pak) family of serine/threonine kinases are involved in numerous cellular processes (Rane and Minden, 2014). The family is split into two subfamilies, group I and group II, based on their protein structure. The group I Pak subfamily consists of Pak1, 2 and 3, whilst Pak4, 5 and 6 form the group II Paks. This project will focus on group I Paks. Group I Paks have a high level of structural homology with at least 83 % homology in their kinase domain, and a minimum of 88 % homology in their p21-binding domain (PBD) (Rane and Minden, 2014) (Figure 1.6A).

Paks were initially discovered as critical effector proteins for the Rho family GTPases Cdc42 and Rac1, which bind the PBD (Manser *et al.*, 1994). However, research into Paks has identified other sites in their structure through which they can be activated, such as proline-rich regions which enable the binding of proteins containing an SH3 domain (Z. Zhao *et al.*, 2000). The Pak-interacting exchange factor (PIX) is a known upstream Pak activator which binds a non-classical SH3-binding site on the Pak structure, enabling Pak recruitment to focal complexes during cell migration (Manser *et al.*, 1998; Loo *et al.*, 2004).

Inactive group I Paks exist in an auto-inhibitory homodimer configuration, whereby the auto-inhibitory domain (AID) of one Pak molecule binds the kinase domain of another Pak molecule. Binding of an upstream activator, such as Cdc42, causes conformational change of the Pak molecule, disrupting the AID-inhibition of the kinase domain, resulting in unfolding of the homodimer. As a result, Pak molecules can auto phosphorylate and become fully activated kinases (Figure 1.6B).

Specific residues in each Pak isoform are important phosphorylation sites for their activation. Thr^{402}, a residue located in the activation loop of the kinase domain in Pak2, is an essential residue for full Pak2 activation (Wu and Wang, 2003). Similarly, Thr^{423} in the kinase domain activation loop is crucial for Pak1 activation (Zenke *et al.*, 1999; King *et al.*, 2000). Mutations at these sites prevent activation of the respective Pak protein.

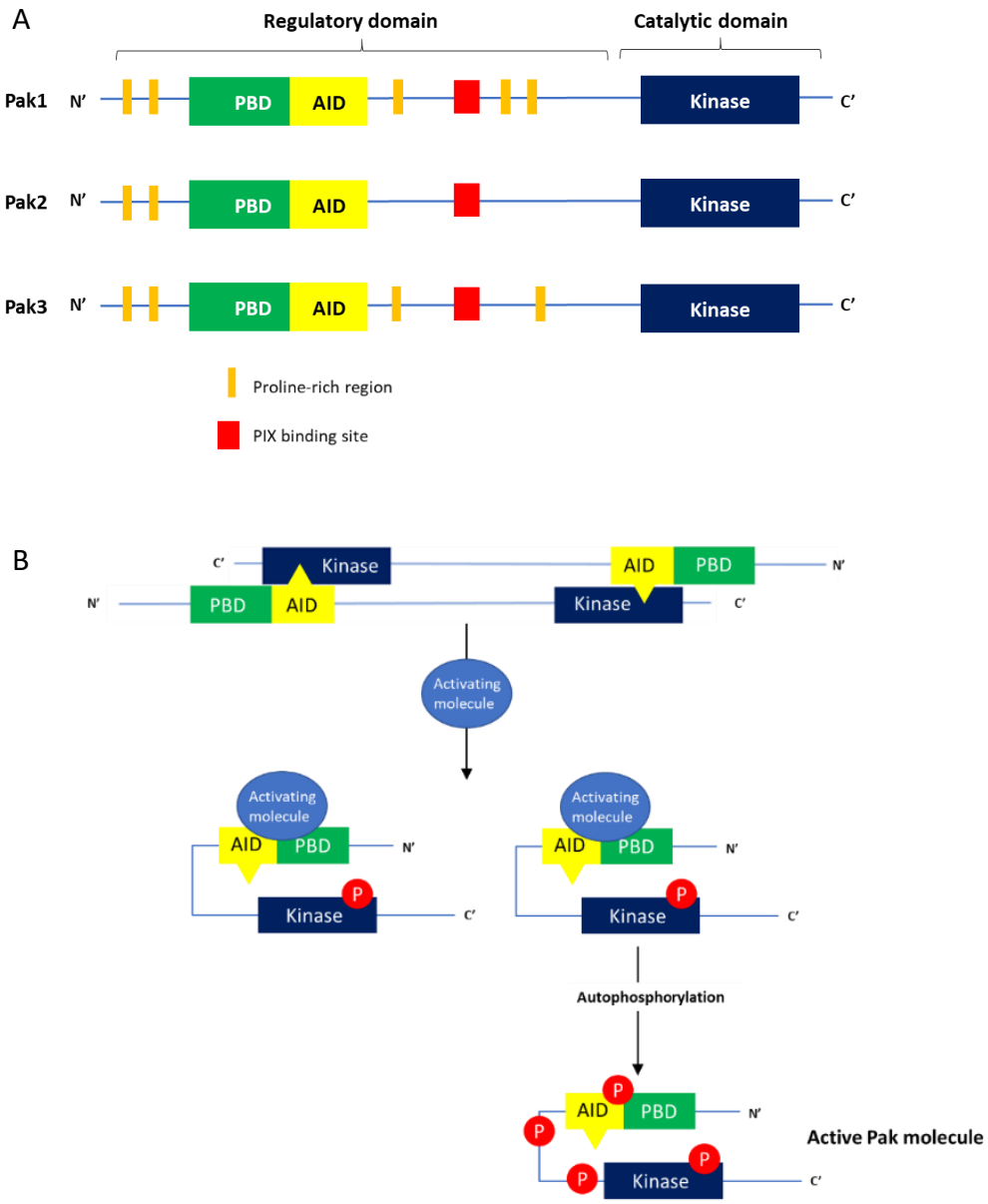

Figure 1.6 Structure and activation of group I p21-activated kinases (Paks). (A) Group I Paks have a high structural homology. The N-terminus contains regulatory domains, including the p21-binding domain (PBD) and the auto-inhibitory domain. At the C-terminus is the kinase domain through which active Paks carry out their catalytic function. All have proline-rich regions and a PIX binding site which aid in the binding of various upstream activators and downstream targets. **(B)** Inactive Paks are found in an auto-inhibitory homodimer conformation, with the autoinhibitory domain (AID) of one Pak protein bound to the kinase domain of another. Upon binding of an upstream activator, the AID-kinase domain interaction becomes disrupted, leading to conformational change of the Pak protein, allowing for autophosphorylation, rendering the Pak protein active. Figure adapted from Arias-Romero & Chernoff (2012).

1.10 Pak1 and Pak3 in heart disease

Pak1 is expressed in various organs including the brain and spleen (Fuchsova *et al.*, 2016). It is also expressed in the vasculature and heart where it can act not only through its kinase activity, but also through acting as a molecular scaffold (Ke *et al.*, 2013). In the heart, Pak1 has been shown to negatively regulate pathological CH, with cardiomyocyte-specific knockout of Pak1 ($Pak1^{cko}$) augmenting CH development in mice both following TAC and angiotensin II infusion (W. Liu *et al.*, 2011). This is due to Pak1's influence on JNK signalling. Global knockout of Pak1 in mice also protected against cardiac hypertrophy following isoproterenol administration, though this was through altering β-adrenergic signalling (Taglieri *et al.*, 2011). Interestingly, Pak1 promotes exercise-induced physiological CH through modulating calcineurin signalling (Davis *et al.*, 2015), further demonstrating the differing regulation of these two forms of CH.

Pak1 is also important for cardiac electrical conduction and, hence, cardiac contraction (Sheehan *et al.*, 2009). Ke et al (2007) found that Pak1 is abundantly expressed in pacemaker cells from the guinea pig sinoatrial node, and its overexpression suppressed the effect of isoproterenol on altering heart rate. Furthermore, Pak1 regulates calcium handling in cardiomyocytes through modulating SERCA2 activity (Y. Wang *et al.*, 2014). As a result of these effects, $Pak1^{cko}$ mice are more prone to arrythmias following stress (DeSantiago *et al.*, 2018).

Pak1 is protective following I/R through improving cardiac contractility (Monasky *et al.*, 2012). Pak1 is a known activator of PP2A (Westphal *et al.*, 1999), which once activated can dephosphorylate cardiac proteins such as cardiac troponin-I and myosin-binding protein C, resulting in increased myofilament Ca^{2+} sensitivity. Following ex vivo I/R, hearts from mice lacking Pak1 had reduced recovery of left ventricular developed pressure compared to wild type controls, indicating that these mice have impaired cardiac function (Monasky *et al.*, 2012). This was attributed to reduced phosphorylation of myosin light chain 2 following I/R when Pak1 was absent, which would lead to reduced ventricular power. Furthermore, Pak1's ability to phosphorylate and activate Akt, and vice versa, may suggest further protective roles of Pak1 during MI and I/R (Mao *et al.*, 2008; Y. Wang *et al.*, 2018). Akt overexpression in the mouse heart protects against cardiomyocyte apoptosis during I/R injury (Fujio *et al.*, 2000) and reduces infarct size

(Matsui *et al.*, 2001). Additionally, S1P, a known activator of Pak1, is important for ischaemic conditioning, and Akt activation is required for this, suggesting a protective S1P-Pak1-Akt pathway during ischaemia (Hofmann *et al.*, 2009).

The majority of research into Pak3 has regarded its role in the nervous system where it is highly expressed (Burbelo *et al.*, 1999; Rousseau *et al.*, 2003; Boda *et al.*, 2004; Duarte *et al.*, 2020). There is limited evidence on its role in the heart; one study has suggested that it may act as a pro-hypertrophic molecule since a Pak3 knockout model had improved survival and cardiac function following TAC (Xie and Xu, 2017). However, further research is required to corroborate this.

1.11 Pak2

Pak2, unlike other group I Paks, is expressed ubiquitously throughout the body. It is involved in numerous cellular processes such as cytoskeletal organisation (Zeng *et al.*, 2000), stem cell differentiation (Zeng *et al.*, 2015), and cancer metastasis (Coniglio *et al.*, 2008). Pak2 is essential in the development of the cardiovascular system as it is crucial for lumen formation and endothelial adhesion during development (Radu *et al.*, 2015). As such, mice with a global knockout of Pak2 die at embryonic day 8.5 with numerous complications including cardiovascular defects associated with increased vascular permeability (Hofmann, 2004). Studies in zebrafish have further shown that, in the brain, knockout of Pak2 increases vascular permeability resulting in cerebral haemorrhage (Buchner *et al.*, 2007), and this role of Pak2 is downstream of βPIX activation (Liu *et al.*, 2007). As a result, in order to study the effect of Pak2 in adult mice, tissue or cell-specific knockout models are used. Research into Pak2 has increased due to its high level of homology with Pak1 and its ubiquitous expression pattern, suggesting that it too may play protective roles during cardiovascular disease.

1.11.1 Pak2 in the cardiac hypertrophy and ER stress

Previous research has identified that, during cytostasis *in vitro*, Pak2 can localise to the ER and that this is required for it to regulate cell division (Huang *et al.*, 2003). Jung & Traugh (2005) theorise that binding of Cdc42 to Pak2 localises the complex to the ER where it enables Pak2 autophosphorylation.

Our previous study has demonstrated that Pak2 acts as a cardioprotective molecule in the heart during pressure-overload induced CH (Binder *et al.*, 2019). For the first year of this project, I assisted with completing experiments for the publication of this paper (see Appendix 1). In this study Pak2 was shown to protect against the development of pathological CH, with Pak2 activated in the hearts of mice one week following TAC, a model used to mimic pressure overload-induced CH. Pak2 cardiomyocyte-specific knockout ($Pak2^{cko}$) mice developed CH to a greater extent, and had significantly worse cardiac function following TAC compared to $Pak2^{f/f}$ control mice. Furthermore, $Pak2^{cko}$ mice had greater levels of cell death in the heart following TAC, demonstrating that Pak2 plays a cardioprotective role in the development of pathological CH.

The proposed model for this cardioprotective role is that, upon initiation of ER stress, Pak2 becomes activated. Activated Pak2 translocates to near the outer membrane of the ER where it phosphorylates PP2Ac, which would normally inhibit IRE1 phosphorylation via its phosphatase activity. Relief of IRE1 inhibition allows for its dimerization and autophosphorylation, leading to splicing of XBP1 and downstream expression of genes associated with ER chaperones and ERAD. As such, loss of Pak2 in the heart prevents this protective response, leading to increased expression of pro-apoptotic genes such as Chop, resulting in increased cardiomyocyte death which aids the progression to HF. This theory was supported by data showing that administration of an IRE1 activator, quercetin, via oral gavage for two weeks after TAC significantly improved cardiac function in $Pak2^{cko}$ mice. Furthermore, overexpression of spliced XBP1 via an adeno-associated virus 9 (AAV9) virus also improved cardiac function in $Pak2^{cko}$ mice after TAC, and significantly reduced the number of cardiomyocytes undergoing cell death. This data supports the theory that Pak2 acts through the IRE1-XBP1 branch of the UPR during ER stress, promoting an adaptive and pro-survival response.

As mentioned in Section 1.10, ER stress has been shown to occur during MI-related events. This demonstrates the potential for Pak2 to have a similarly protective role during MI, though due to the different stimuli that occur in these two diseases, further investigation is required to explore this possibility.

1.11.2 Pak2 in MI-related events

Pak2's role in MI has not previously been explored; however, it has been shown to have a role in many MI-related events, which will be discussed in this section.

Pak2 in ischaemia

Whilst Pak2's role in cardiac ischaemia and I/R has not been investigated *in vivo*, its role in ischaemia and I/R injury elsewhere in the body has been explored. Pak2 has shown to be upregulated following spinal I/R injury, and this upregulation was suggested to occur in order to promote a post-ischemic inflammatory response (Qi *et al.*, 2016). Furthermore, Elsherif et al (2014) showed that in a model of hindlimb ischaemia, Pak2 compensated for loss of Pak1 in $Pak1^{-/-}$ mice and allowed for maintained wound healing and neovascularisation. This demonstrates that Pak2 becomes activated following ischaemia and provides a protective and therapeutic response through aiding angiogenesis.

Pak2 in cardiac regeneration

The zebrafish model has been used to investigate Pak2's role in the heart, though in this model there are two Pak2 genes (pak2a and pak2b). In 2016, Peng et al (2016) demonstrated that Pak2 is important for cardiac regeneration following injury. They showed that Pak2 is activated in cardiomyocytes 7 days after injury to the ventricles, and this activation increases as cardiac regeneration ensues in the zebrafish heart. Furthermore, small molecule-mediated inhibition of Pak2 reduced cardiomyocyte proliferation, prevented cardiomyocyte dedifferentiation, and impeded heart regeneration. Pak2's role in proliferation has also been shown in cancer models. A recent study published in 2019 showed that in pancreatic cancer, Pak2 promoted cancer cell proliferation and migration, though no clear mechanism for how this occurs was demonstrated (Yao *et al.*, 2019). Since adult mammalian cardiomyocytes have a poor replicative capability, this suggests that, could the mechanism of Pak2's ability to

promote proliferation be further understood, it could be targeted for therapeutic purposes following MI where a large number of cardiomyocytes have died.

Pak2 and cardiac fibrosis

Pak2's role in fibrosis development and fibrosis-related signalling pathways also has contradictory findings. Yan et al (2012) found that in canine kidney epithelial cells Pak2 inhibits TGFβ signalling through associating with, and phosphorylating, Smad2/3, thus preventing downstream signal transduction. Pak2's impact on TGFβ signalling itself has not been explored in the context of fibrosis, though it has been shown to act downstream of TGFβ to promote fibrosis. In fibroblasts, but not epithelial cells, Pak2 was shown to be activated through Smad-independent TGFβ signalling involving c-Abl and PI3K, and this leads to increased proliferation and some of the morphological changes associated with myofibroblast differentiation (Wilkes *et al.*, 2003, 2005; Wilkes and Leof, 2006). This demonstrates the cell-type specificity of Pak2's role in TGFβ signalling, and as such its role in cardiac fibrosis must be investigated to determine whether it has an impact, and if so in what way.

Pak2 in angiogenesis

As mentioned at the beginning of Section 1.10, Pak2 is key for maintaining vascular integrity, and is important for lumen development during embryogenesis. Due to this, it is believed that Pak2 is important for angiogenesis, a process that is key for restoring blood flow to the damaged or infarcted heart, and this function may be due to Pak2 activation by Cdc42 (Koh *et al.*, 2008; Barry *et al.*, 2015). This is due to the ability of Pak2 to regulate endothelial cell proliferation, attachment, migration, and sprouting, demonstrated in both human and mouse *in vitro* models, through regulating the MAPK family member ERK5 (Radu *et al.*, 2015). Exosomes containing Rac1 and Pak2 have also been shown to induce angiogenesis (Gopal *et al.*, 2016).

Pak2 in cell death

Pak2's role in modulating cell death is complex and appears to vary depending on the stimuli and the tissue. Unlike other members of the Pak family, Pak2 can be activated both through the standard method of activation and by cleavage, and this cleavage appears to promote a pro-apoptotic response (Bokoch, 1998). Pak2 cleavage by caspase

3 occurs at residue Asp^{212} and generates two fragments, a 28 kDa fragment from the N-terminal of Pak2, and a 34 KDa C-terminal fragment, termed Pak2p34, which contains the kinase domain. This residue is also found in Pak1 but appears to be shielded, potentially by continuous proline residues around the site, preventing Pak1 cleavage (Rudel and Bokoch, 1997). Due to the loss of the AID, located in the N-terminal fragment, Pak2p34 is constitutively active, and further post-translational modification potentiates its pro-apoptotic effects (Vilas *et al.*, 2006). This cleavage appears to promote apoptosis through activation of JNK (Lee *et al.*, 1997; Rudel *et al.*, 1998), and inhibition of Pak2 cleavage limits apoptosis in isolated cells (Luo and Rubinsztein, 2009; Marlin *et al.*, 2011). Despite these findings, there has been no evidence demonstrating Pak2 cleavage in *in vivo* models or in the heart.

In contrast, canonical activation of full-length Pak2 promotes a protective pro-survival response. For instance, Pak2 overexpression suppresses apoptosis in fibroblasts, and this overexpression of constitutively active Pak2 was shown to lead to increased phosphorylation of the Bcl-2 protein Bad, preventing its pro-apoptotic abilities (Jakobi *et al.*, 2001). In a conditional Pak2 knockout model, loss of Pak2 in haematopoietic stem cells (HSC) induced leukopenia and mild anaemia (Zeng *et al.*, 2015). This study identified that loss of Pak2 decreased survival and proliferation of HSC progenitors, and skewed lineage differentiation. Pak2 can also prevent apoptosis stimulated by de-adhesion of epithelial cells, known as anoikis, by localising the adherens junctions and binding βPIX (Frank *et al.*, 2012). However, this pro-survival ability is thought to promote the ability of cancer cells to metastasise.

Furthermore, Pak2 can directly phosphorylate pro-apoptotic molecules to reduce apoptosis. For instance, Pak2 can directly phosphorylate caspase 7, an executioner caspase, and this can prevent apoptosis through two mechanisms (Eron *et al.*, 2017). Phosphorylation at Ser30 prevents caspase 9-mediated cleavage of caspase 7, preventing caspase 7 activation. Meanwhile, Pak2 phosphorylation of caspase 7 at Ser239 prevents caspase 7 binding its substrate, blocking its executioner abilities to cause apoptosis. In this study, it is suggested that the quantity of Pak2, and whether its activation supersedes caspase 7 cleavage, determines whether apoptosis proceeds. Targeting this activity of Pak2 could reduce chemotherapy-resistant tumour persistence (Marlin *et al.*, 2009; Li *et al.*, 2011).

Endogenous knockdown of Pak2 by microRNAs has shown to prevent apoptosis. MiR-4779 was found to prevent colon cancer cell growth by inducing apoptosis and cell cycle arrest through targeting Pak2 (Koo and Kwon, 2018), and suppression of Pak2 mRNA by miR-26a was shown to promote apoptosis in porcine Sertoli cells to regulate spermatogenesis (Ran *et al.*, 2018). This demonstrates that Pak2's pro-survival role is highly regulated, both in disease and in normal organ function.

1.12 Hypothesis

This project hypothesised that Pak2 is protective following myocardial infarction through ameliorating maladaptive ER stress.

1.13 Aims

The aims of this project were to:

1. Investigate changes of Pak2 expression and activation following myocardial infarction *in vivo* and related phenomena *in vitro.*
2. Determine whether cardiomyocyte-specific Pak2 knockout mice respond differently to floxed controls following myocardial infarction.
3. Assess the mechanism through which Pak2 acts during ischaemia-related events.

Chapter 2 : Materials and Methods

2.1 Mouse Models

All experiments involving animals were performed according to the project licence (P3A97F3D1) and the Animals (Scientific Procedures) Act 1986. Mice were exposed to a normal 12-hour light/dark cycle with free access to a standard chow diet and water. All animals used in this study were male.

2.1.1 Pak2^{cko} mouse model

Cardiac Pak2's role in cellular signalling pathways was investigated *in vivo* using Pak2 cardiomyocyte-specific knockout mice (Pak2^{cko}). To generate this line the Cre-LoxP system was used (Figure 2.1). Pak2 flox mice (Pak2$^{f/f}$), containing LoxP sites flanking exon 2 of the Pak2 gene (Radu *et al.*, 2015), were bred with mice previously generated to express Cre under the alpha myosin heavy chain (αMHC) promoter (Agah *et al.*, 1997), which is expressed solely in cardiomyocytes. As a result, litters contain both flox-positive Cre-positive Pak2^{cko} mice, and flox-positive Cre-negative Pak2$^{f/f}$ littermates.

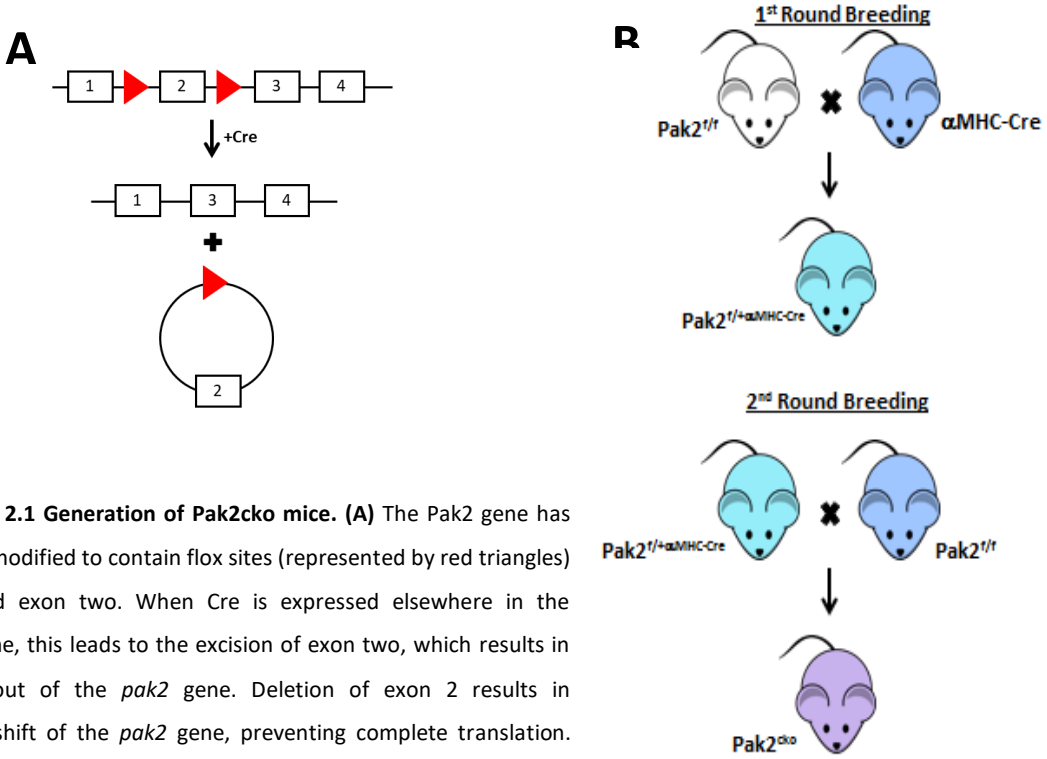

Figure 2.1 Generation of Pak2cko mice. (A) The Pak2 gene has been modified to contain flox sites (represented by red triangles) around exon two. When Cre is expressed elsewhere in the genome, this leads to the excision of exon two, which results in knockout of the *pak2* gene. Deletion of exon 2 results in frameshift of the *pak2* gene, preventing complete translation. **(B)** Breeding regime for the generation of $Pak2^{cko}$ mice. During the first round of breeding, $Pak2^{f/f}$ mice containing flox sites around exon two of the *pak2* gene are bred with mice containing the *Cre* gene under control of the αMHC promoter, which is only expressed in cardiomyocytes. This results in mice heterozygous for flox sites which also contain Cre under αMHC promoter control. In the second round of breeding, these mice are bred once more with $Pak2^{f/f}$ mice, resulting in mice homozygous for the flox sites, also expressing Cre, resulting in Pak2 cardiomyocyte-specific knockout mice ($Pak2^{cko}$).

2.2 Genotyping

Genotyping was performed to identify Pak2^{cko} mice from their Pak2$^{f/f}$ littermates.

2.2.1 DNA extraction

Ear tissue biopsies were taken from mice once weaned. 500 µL lysis buffer (Qiagen) and 5 µL proteinase K (Ambion) were added to each tissue sample, which were subsequently vortexed and left to lyse at 55°C overnight. The lysates were vortexed, 500 µL phenol/chloroform (25:24) added to dissolve the solvation shell, releasing nuclear material, and the samples centrifuged at 15,700 xg for 7 minutes. The upper aqueous layer, which contains the extracted DNA, was transferred to a fresh Eppendorf and 500 µL ice-cold isopropanol added. Samples were vortexed then centrifuged at 15,700 xg for 30 minutes at 4°C to precipitate the DNA. The supernatant was discarded and the DNA pellet washed with 500 µL 70 % ethanol, then centrifuged for 5 minutes at 15,700 xg at 4°C. The supernatant was discarded, and samples heated at 37°C for 10 minutes with the lid open to dry the pellet. 50 µL RNase-free H_2O was added, and the tube heated at 55°C for 60 minutes, to dissolve the DNA pellet. DNA concentration was determined using a Nanodrop 2000 (ThermoScientific) and diluted to around 100 ng/µL.

2.2.2 Polymerase Chain Reaction (PCR) and Gel Analysis

Per PCR reaction, 1 µL DNA sample was mixed with PCR master mix (Qiagen, HotStarTaq R Master Mix Kit), double distilled water (ddH_2O), and the respective primers (Tables 2.1 & 2.2). PCR was carried out using an Eppendorf mastercycler DNA Engine Thermal Cycler PCR machine, using the PCR reaction programme specific for the primers used (Table 2.3). The PCR product was run on an agarose gel (1.5 % w/v for Pak2, 1 % w/v for Cre) made using agarose (Melford Biolaboratories) dissolved in 1xTAE (Tris Acetate EDTA) buffer (40 mM Tris, 0.1 % v/v acetate acid, 1 mM EDTA, pH 8.5). 10 µL Safeview™ Nucleic Acid stain was added to the solution prior to it being set to allow for DNA band identification. Samples were run alongside a 100 bp ladder (NEB). Samples were mixed with 4 µL DNA loading buffer (0.25 w/v Bromophenol blue, 0.25 % w/v xylene cyanole, 25 mM EDTA, and 50 % v/v glycerol, Sigma-Aldrich) prior to being loaded into the gel and run for 1 hour at 100 volts using a BIO-RAD Power Pac 300, and subsequently imaged using a ChemiDoc™ MP System (170-8280).

Table 2.1. Primer Sequences for genotyping

Primer Name	Primer Sequence
Cre Forward	5'–GACGGAAATCCATCGCTCGAC–3'
Cre Reverse	5'–GACATGTTCAGGGATCGCCAG–3'
Pak2 Forward	5'–ATCTTCCCAGGCTCCTGACT–3'
Pak2 Reverse	5'–TGAAGCTGCATCAATCTATTCTG–3'

Table 2.2 PCR reaction mixture for genotyping

Reagent	Pak2 flox genotyping	Cre genotyping
	Volume	Volume
Master Mix	5 µL	5 µL
ddH_2O	3 µL	3 µL
Forward Primer	0.5 µL	0.5 µL
Reverse Primer	0.5 µL	0.5 µL
DNA sample	1 µL	1 µL

Table 2.3 PCR Reaction programmes for genotyping

		Cre		Pak2 flox	
		Temperature (°C)	Time	Temperature (°C)	Time
Initial Activation		95	15 seconds	95	15 seconds
30 cycles	Denaturation	95	1 minute	95	30 seconds
	Annealing	55	1 minute	57	30 seconds
	Extension	72	1 minute	72	30 seconds
Final Extension		72	5 minutes	72	7 minutes

2.3 Induction of Myocardial Infarction

Surgery to induce myocardial infarction (MI) was kindly performed by Dr Min Zi on 11–13-week-old mice. The chests of mice were shaved prior to surgery. Mice were anaesthetised using 3 % isoflurane in oxygen at flow rate of 1L/minute. Analgesia, 0.1mg/kg buprenorphine, was injected subcutaneously prior to surgery along with 0.1 mL saline (0.9 % w/v NaCl) to account for any blood loss. Mice were intubated and surgery was performed on a heat mat to minimise heat loss. MI was induced through permanent ligation, using an 8-0 Prolene® suture (Ethicon), of the lateral anterior descending (LAD) coronary artery. Following this, the chest and skin were closed using a 6-0 Prolene® suture (Ethicon). Mice were allowed to recover from anaesthesia in a warmed oxygen chamber and kept in a heated incubator for the remainder of the surgery day.

For initial experiments, ligation occurred just above the arterial bifurcation; this will henceforth be known as the 'severe' MI model. Due to the high mortality rate, further experiments used more mild MI models to investigate changes long term; the 'moderate' ligation model ligated 2 mm closer to the apex of the heart compared to the 'severe' model, whilst for the 'mild' model MI was induced by ligating the LAD 3 mm closer to the apex of the heart compared to the severe model. Sham controls underwent the same procedures during surgery but without ligation of the vessel. Any deaths following the procedure were recorded (Table 2.4). These were categorised based on the cause of death. Some mice were put down due to symptoms related to acute heart failure, including hunched posture, lack of movement, shivering and piloerection. Where mice were found dead the heart was examined, and it was noted if there was sign of cardiac rupture.

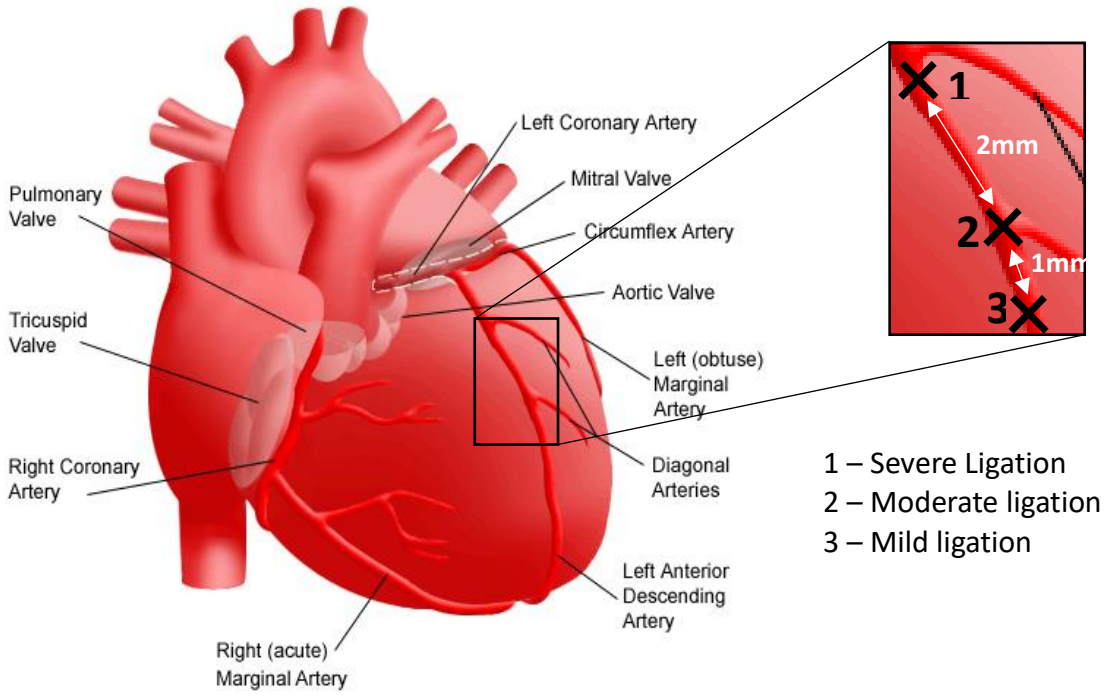

Figure 2.2 Ligation sites of the left anterior descending coronary artery (LAD) for MI surgeries during this project. Three severities of MI were used during this project. Severe ligation is the standard ligation point for other mouse strains but led to a high level of mortality after three days and so could not be used to investigate anything other than the acute MI response. This ligation point is just below the branch of the first diagonal artery. The moderate ligation point was located 2mm below the severe ligation point; this model also led to high mortality levels in the MHC-Pak2 strain. As such a mild model, where the LAD was ligated 1mm closer to the apex of the heart than the moderate ligation point, and 3mm closer the apex than the severe model, was also used during this project. Image obtained and modified from El Camino Health (2020)

Surgery	Genotype	Total animals	Total deaths	Cause of death		
				Put down – likely acute heart failure	Found dead – cardiac rupture	Found dead – no obvious cause
1-week severe MI	$Pak2^{f/f}$	4	3	2	1	-
	$Pak2^{cko}$	4	3	-	3	-
2-week moderate MI	$Pak2^{f/f}$	9	3	1	2	-
	$Pak2^{cko}$	5	3	3	-	-
2-week mild MI	$Pak2^{f/f}$	6	2	-	1	-
	$Pak2^{cko}$	6	1	1	-	1

Table 2.4 Deaths following MI in each model used in this study. Following all surgeries, any deaths were noted and the heart was assessed to determine cause of death. Deaths were categorised into three causes of death. (1) Mice were put down. This was likely due to the development of acute heart failure, with symptoms including hunched posture, low body temperature and laboured breathing. These symptoms exceeded the severity threshold allowed by the project licence meaning animals must be put down. (2) Mouse found dead due to obvious cardiac rupture. Rupture of the myocardium was visible. (3) Mouse found dead with no obvious cause of death. Where mice were found dead without evidence of a cardiac rupture or previous visible symptoms cause of death was unknown. Potential reasons for this could be sudden cardiac death caused by arrythmia.

2.4 Echocardiography, ECG and tissue collection

Echocardiography was performed at various time points following surgery to assess the difference in cardiac structure and function between the mouse groups. Chest hair was removed using hair removal cream to prevent it causing interference. Mice were anaesthetised using 2 % isoflurane induction, and isoflurane was maintained between 1-1.5 % during the procedure. Henley's medical ultrasound gel was used, and echocardiography was performed using a Visualsonics Vevo 770 micro-ultrasound system. One image was taken from a parasternal short axis view, from which one measurement was taken from parallel to the papillary muscles, and one image from the parasternal long-axis echocardiogram view, from which measurements were taken across three points from the base, middle and apex of the heart (Figure 2.3). Values were averaged over each view. From the images taken, left ventricular diameter end-diastole (dD) and systole (sD) could be measured, as well as the diameter of the end-diastolic intraventricular septum (dIVS) and end-systolic intraventricular septum (sIVS), and end-diastolic left ventricular post-wall thickness (dLVPW). From these measurements, fractional shortening, ejection fraction, and left ventricular mass could be measured using the equations below.

$$\text{Fractional shortening} = 100 \times \left(\frac{\text{dD} - \text{sD}}{\text{dD}}\right)$$

$$\text{Ejection Fraction} = 100 \times \left(\frac{1.05 \times (\text{dD}^3 - \text{sD}^3)}{1.05 \times \text{dD}^3}\right)$$

$$\text{Left Ventricular Mass} = 1.05 \times ((\text{dD} + \text{dIVS} + \text{dLVPW})^3 - \text{dD}^3)$$

Where 1.05 g/mL is the myocardial density. Fractional shortening is the percentage of the diastolic diameter that is lost during systole, whilst ejection fraction is the percentage of blood that is pumped out of both ventricles each contraction.

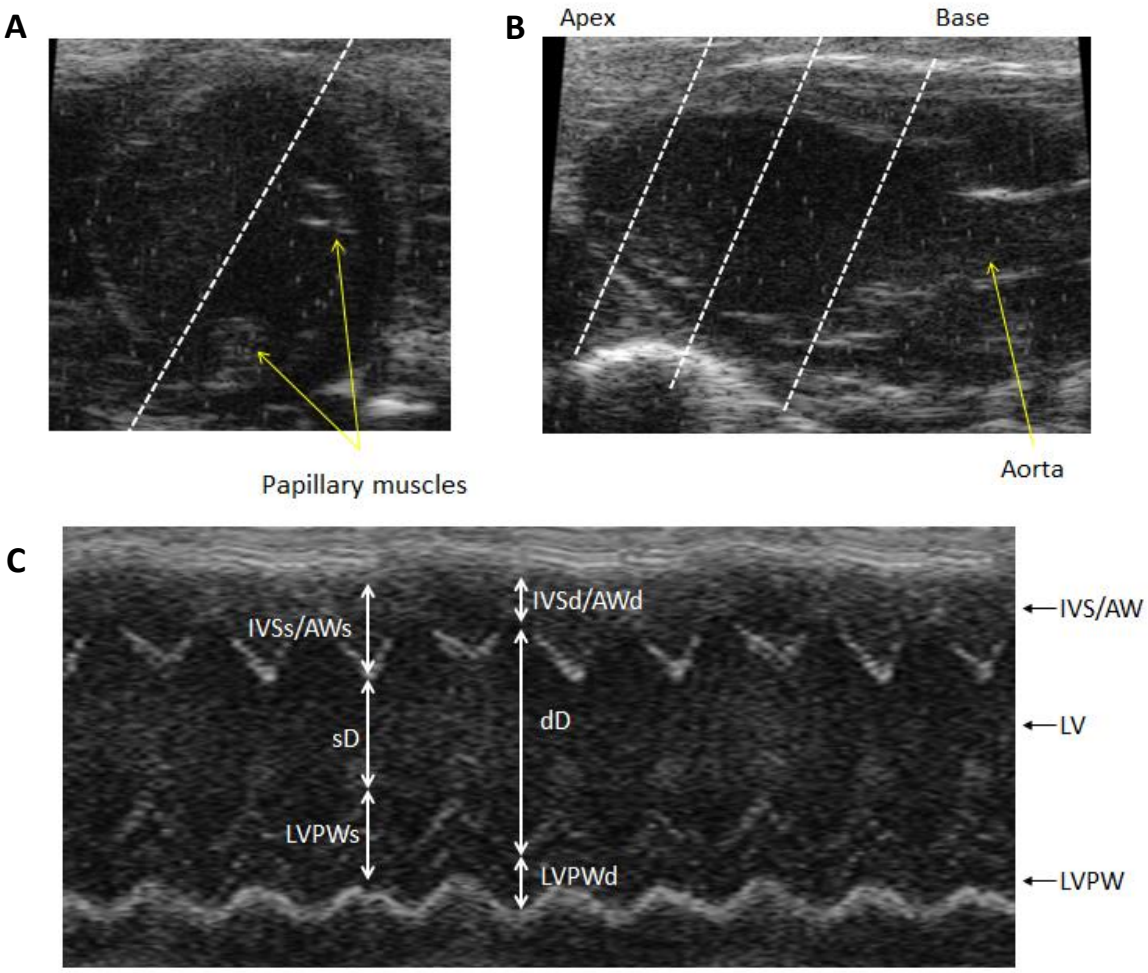

Figure 2.3 Diagrammatic explanation of echocardiographic analysis. (A) The heart was identified using the parasternal short axis view on a Visualsonics Vevo 770 micro-ultrasound system. In this view the papillary muscles could be identified. Measurements were taken from parallel to the papillary muscles. **(B)** Since MI affects areas of the heart differently, with the infarct only occurring below the ligation point, it was important to measure cardiac function throughout the heart. Therefore, three measurements were taken through the heart from the apex to the base using the parasternal long-axis echocardiogram view. Measurements were then averaged to give overall measurements for cardiac structure and function. **(C)** Echocardiographic parameters were measured using the M-mode. LV = left ventricle. LVPW = left ventricle posterior wall. IVS = intraventricular septum, this could be imaged in the short-axis view. AW = anterior wall, this could be visualised in the long-axis view. IVSs/d = thickness of the intraventricular septum at end-systole or -diastole. AWs/d = Anterior wall thickness during systole or diastole. s/dD = ventricular diameter end-systole or -diastole. LVPWs/d = thickness of the left ventricular posterior wall at end-systole or -diastole.

Conscious electrocardiography (ECG) was carried out to assess changes in cardiac rhythm and electrical conduction. ECG was performed on an ECGenie ECG machine (Mouse Specific Inc) using the Image Lab v8 software (BIO-RAD) and analysed using LabChart 8 (ADInstruments) (Figure 2.4). No blood collection was permitted in the same room during this to prevent against stressing the mice. From ECG traces several parameters were analysed (Figure 2.4 and Table 2.5). During conscious ECG the P wave is not always visible and as such parameters using this were not analysed.

Mice were culled via cervical dislocation as is described in the project licence (P3A97F3D1). The heart was excised and rinsed in phosphate-buffered saline (PBS) to remove blood trapped in the heart chambers. For tissue to be used for histological assessment, the heart was cut at the same cross-sectional point – 4 mm from the apex of the heart for hearts subjected to the severe/moderate MI procedure, and 3 mm from the apex of the heart for hearts given the mild MI procedure. All points were apical to the ligation site.

For hearts that required embedding in paraffin, hearts were fixed in 4 % paraformaldehyde (in PBS) and left on a shaker at 4°C for 5 hours. Hearts were washed in PBS for 30 minutes on a shaker and transferred to 50 % ethanol where they were kept at 4°C to be stored. Heart samples were dehydrated sequentially in increasing concentrations of ethanol (70 %, 90 %, 100 %) for two hours each. Samples were cleared in xylene overnight and subsequently embedded in paraffin. 5 µM sections were cut using a Leica RM2255 microtome.

Hearts for cryotomy were washed in PBS to remove excess blood, and subsequently placed in a mould filled with optimal cutting temperature compound (OCT). The moulds were then flash frozen by submerging in isopentane (2-methylbutane) which had been pre-chilled in dry ice. OCT-embedded samples were stored at -80°C and sections were cut on a Leica CM1950 Cryostat at 10 µm thickness.

For hearts from which protein or RNA were to be extracted, hearts were excised, washed in DEPC-treated PBS to remove excess blood, and stored at -80°C. DEPC treatment ensures solutions are RNase-free and hence reduces the chance of contamination.

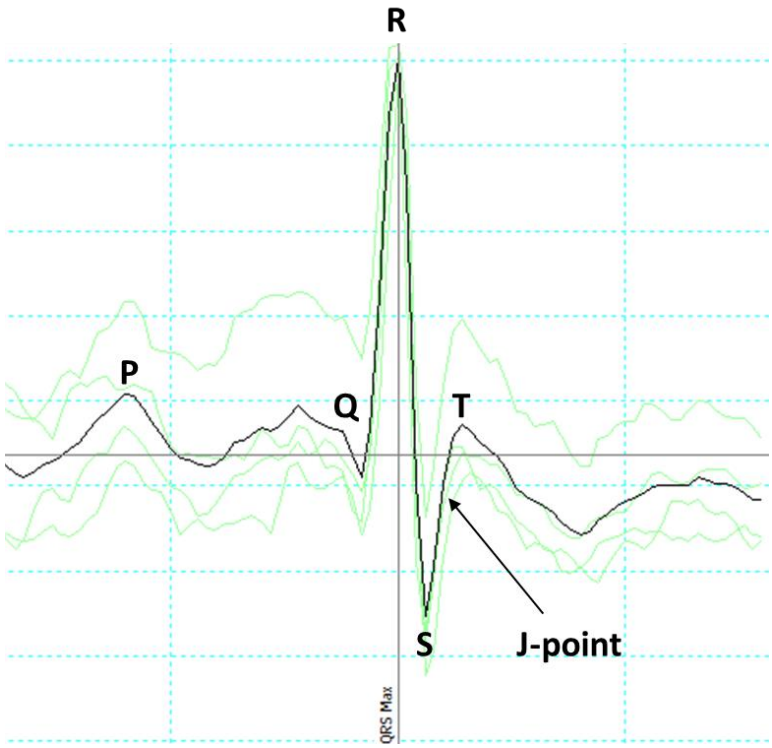

Figure 2.4 Representative electrocardiograph (ECG) trace. Using the LabChart software version 8, four beats were averaged into one trace, and a total of 10 traces were analysed. From each trace the P-wave, QRS complex, and T-wave could be identified. However, for some mice, particularly those given the MI procedure, it was not always possible for the P-wave to be identified. The P-wave is generated by the depolarisation of the atria. The QRS complex represents ventricular depolarisation and hence contraction. The end of the QRS complex is delineated as the J-point, where there is an inflection in the upstroke of the S-wave. The T-wave which follows the QRS complex represents ventricular repolarisation.

Table 2.5 Parameters measured from ECG traces

Parameter	Definition
Heart Rate (bpm)	The number of ventricular contractions, measured in beats per minute (bpm).
RR interval (ms)	The amount of time that has elapsed between two successive R-waves.
QRS interval (ms)	The duration in milliseconds of the QRS complex on an ECG trace
QT interval (ms)	The amount of time taken to move from the beginning of the Q wave to the end of the T wave.
QTc (ms)	The QTc is the corrected QT interval. The QT interval is corrected to the standard heart rate, allowing for a comparison of values at different heart rates.

2.5 Histological Staining

2.5.1 Masson's Trichrome Staining

Masson's trichrome staining stains fibrotic tissue blue and is used to analyse interstitial fibrosis. Sections were deparaffinized for one hour in xylene. They were subsequently re-hydrated in decreasing concentrations of IMS (100 %, 75 %, 50 %) and water for 5 minutes each. Slides were further fixed in Bouin's solution for two hours at room temperature. This substance acts as a mordant, improving dye penetration and staining. Following pre-treatment, slides were washed in water to remove any remaining fixative and then slides were placed in Harris' haematoxylin for 5 minutes. After washing in running water, slides were places in 1 % HCl in 70 % IMS for 10 seconds to allow differentiation. Differentiation removes excess background staining; alcohol makes the differentiation more controllable. Sections were washed in warm running water and then stained in Red solution (90 mL 1 %(w/v) Biebrich Scarlet, 10 mL 1 %(w/v) Acid Fuchsin, 1 mL Glacial Acetic acid) for four minutes. Slides were rinsed in water and then treated for 15 minutes in 2.5 %(w/v) phosphomolybdic acid before being stained with aniline blue (Sigma) for 3 minutes. Slides were rinsed briefly to avoid removal of too much aniline blue stain, before being treated in 1 % acetic acid for 1 minute. Slides were subsequently dehydrated in 100 % IMS three times for 5 minutes each and cleared in xylene for 20 minutes. Coverslips were mounted using Eukitt quick-hardening mounting medium (Sigma-Aldrich).

Masson's trichrome staining was imaged on a 3D Histech Pannoramic 250 flash slide scanner at x20 magnification. Analysis was carried out on the Fiji software using the colour deconvolution and thresholding method (Chen *et al.*, 2017). The investigator was blinded to the genotype and procedure during analysis. Percentage of the heart stained blue, not including the infarct area, was calculated as the percentage of interstitial fibrosis. For MI samples, the infarct size was calculated as total fibrosis in the heart minus the interstitial fibrosis.

2.5.2 Haematoxylin & Eosin Staining

Haematoxylin & eosin (H&E) staining stains the nucleus blue and the cytoplasm pink. From this stain, the average cardiomyocyte cross-sectional area can be measured, determining whether the surgery has resulted in alterations in average cell size which would indicate hypertrophy. Sections were deparaffinized for one hour in xylene then re-hydrated in decreasing concentrations of IMS (100 %, 75 %, 50 %) and water for 5 minutes each. Sections were stained in Harris' Haematoxylin for 5 minutes then rinsed twice in water. Sections were differentiated by placing in 1 % HCl in 70 % IMS for 10 seconds before being washed in warm running water for 5 minutes. Sections were placed briefly in cold water and then counterstained in Eosin for 1 minute. After washing twice in water to remove excess stain, the sections were dehydrated in 100 % IMS three times for 5 minutes each. Sections were cleared in xylene for 20 minutes. Coverslips were mounted using Eukitt quick-hardening mounting medium.

H&E staining was imaged on an Olympus single slide scanner microscope at x60 magnification using an oil-immersion lens. 10 images were taken per heart sample. The investigator was blinded to the genotype and procedure during analysis. Analysis was carried out using the ImageJ software with cross-sectional area manually calculated, measuring 10 cells per image to give an average cross-sectional area of 100 cells per sample.

2.5.3 TUNEL staining

Terminal deoxynucleotidyl transferase dUTP nick-end labelling (TUNEL) staining was performed to detect apoptotic cells in heart samples following MI. This stain labels the 3' hydroxyl termini of DNA double strand breaks which result from DNA fragmentation during apoptosis. The *in situ* Cell Death Detection Kit (Roche) was used to perform this staining. Paraffin-embedded tissue sections were de-waxed in xylene for one hour then rehydrated sequentially in 100 %, 75 % and 50 % IMS for 5 minutes each followed by 5 minutes in ddH_2O. One tissue section was circled using a PAP pen to create a hydrophobic barrier, so that solutions remained contained over the tissue of interest. 3 % H_2O_2 was placed on the tissue for 15 minutes to block endogenous peroxidase activity. This was then washed twice in ddH_2O and once in PBS for 10 minutes each. The tissue was permeabilised through two methods. Firstly, proteinase K (700 nM, Ambion) was added to the tissue and incubated at 37°C for 15 minutes. A second permeabilization step consisted of incubating the tissue in 0.1 % Triton X (Sigma) and 0.1 % Sodium citrate (in PBS) for 8 minutes at room temperature. Subsequently, the TUNEL enzyme was mixed 1:100 with the provided labelling agent and added to the tissue. The tissue was incubated with the enzyme in a humid chamber at 37°C for 1 hour. The tissue was blocked in 1 % bovine serum albumin (BSA, Sigma) for 1 hour at room temperature before being incubated in anti-mouse α-actinin primary antibody (1:100, A7811, Sigma) overnight at 4°C. The tissue was washed briefly in PBS before the secondary antibody was added and incubated at room temperature for 90 minutes. The secondary antibody used was Donkey anti-mouse (1:500, Alexa Fluor 594). The tissue was washed 3 times for 15 minutes each in PBS. Vectashield (Vector Laboratories), which contains DAPI staining, was added to the tissue and a coverslip was added.

Slides were imaged on a Zeiss fluorescent snapshot microscope at x20 magnification. 10 images were taken per heart sample, and the infarct area was avoided so that level of cell death in remote regions could be analysed. The investigator was blinded to the genotype during analysis. Analysis was carried out on ImageJ with the number of TUNEL-positive nuclei normalised to total number of DAPI-stained nuclei.

2.6 Cell Culture of H9c2 and Hek293T cells

H9c2 rat cardiomyoblasts and Human Embryonic Kidney 293T (Hek293T) cells were used during this project. All cells were incubated at 37°C, 5 % CO_2. Cells were maintained in Dulbecco's modified Eagle's medium (DMEM, Gibco) containing either 2 % or 10 % foetal bovine serum (FBS) along with penicillin (100 U/mL) and streptomycin (1 mg/mL) to avoid contamination. To split cells, media was removed and enough trypsin (TrypLe Express, Gibco) to cover the base of the flask was added. Incubation at 37°C for 2 minutes ensured cells dissociated from the culture surface. Cells were resuspended in media, the same volume as was added of trypsin, to prevent further damage to cells from trypsin, and the mixture was centrifuged for 5 minutes at 250 xg. The supernatant was removed, and the cells were resuspended in the required volume of pre-warmed media and redistributed in plates or flasks where necessary. When not required, cells were stored in liquid nitrogen suspended in DMEM media containing 10 % dimethyl sulfoxide (DMSO) and 20 % FBS.

2.7 Pak2 knockdown by Ad-shPak2

Pak2 knockdown was instigated via administration of adenovirus into which plasmids containing short-hairpin RNA (shRNA) had been packed. A control virus (Ad-shControl) was used alongside an adenovirus for Pak2 knockdown (Ad-shPak2). Sequences of the shRNA plasmids can be found in Table 2.6. These viruses were constructed prior to this project, though were re-purified and titrated using the same method described for Ad-Pak2 in section 2.12.

Table 2.6 shRNA sequences

Plasmid	Plasmid sequence
Sh-Control	GGAATCTCATTCGATGCATAC
Sh-Pak2	GGAGTTAAAGAATCCCAACAT

2.8 Pak2 knockdown by siRNA

Pak2 knockdown was also achieved through siRNA transfection (siPak2 ID: s218097). A scrambled sequence was used as a negative control siRNA (siScr, AGGUAGUGUAAUCGCCUUG [Sigma]). Lipofectamine LTX and Plus reagents (ThermoFischer) were used for transfection.

H9c2 cells were transfected in 6 well plates. Per well, 250 µl Opti-MEM (Gibco), 2 µl siRNA and 5 µl Plus reagent were incubated together at room temperature for 15 minutes. Subsequently 250 µl Opti-MEM and 10 µl LTX reagent were added and the mixture was incubated at room temperature for 30 minutes. The mixture was added to each well to be transfected and cells incubated at 37°C for 6 hours. Standard culture medium was added to the cells and cells were incubated at 37°C for 48 hours to achieve a knockdown.

2.9 Induction of oxidative stress

Oxidative stress, which occurs during MI due to changes in the ROS defence mechanisms, and during I/R injury, was induced by incubating cells in hydrogen peroxide (H_2O_2, Sigma). H9c2 cells were plated in six well plates at a confluence of 60-80 %. 100 µM H_2O_2 was added to fresh 10 % FBS DMEM media which was subsequently added to the cells. Control cells received fresh 10 % FBS DMEM media with H_2O added instead of H_2O_2.

2.10 Hypoxia induction and nutrient starvation

Hypoxia was induced in cells to determine the effect of oxygen deprivation on Pak2 expression and activation. Cells were seeded into 6-well plates at 60-80 % confluency and exposed to hypoxic conditions in a Billups-Rothenberg modular incubator, with 100 % N_2 introduced at a flow rate of 20 L/min for 5 minutes before the incubator was sealed. Time-points were carried out simultaneously, and cells which were not exposed to hypoxia were used as controls.

To recreate the loss of nutrient supply that occurs alongside hypoxia during MI, normal media was removed from H9c2 cells and cells washed with PBS to remove any remaining media. Fresh media containing no glucose and no FBS was added to cells, and cells were then exposed to hypoxic conditions for the relevant time. Control cells were kept at normoxic conditions in normal DMEM media containing 4.5 g/L glucose and 10 % FBS.

2.11 MTT cell viability assay

In order to evaluate the effect of Pak2 knockdown on cell survival following stress, cell viability was assessed using methylthiazolyldiphenyl-tetrazolium bromide (MTT, Sigma Aldrich). MTT is a colorimetric assay for assessing metabolic activity. Cells were plated equally in wells of a 96 well plate (TC-treated). Following gene knockdown and exposure to the treatment of choice, the media was discarded and 100 µL MTT solution (5 mg/mL in PBS) added to each well alongside 100 µL serum-free DMEM media (Gibco). Cells were incubated for 3 hours at 37°C before the solution was removed and the wells left to dry overnight at room temperature in the dark. 150 µL DMSO was to each well as an MTT solvent and the plate shaken for 15 minutes at room temperature whilst covered in foil to prevent light affecting the colorimetric results. Absorbance was measured on a Synergy HT microplate reader (Promega) at 570 nM wavelength with background subtracted at 630 nM. Cell viability was expressed as a percentage of untreated controls.

2.12 Ad-Pak2 virus generation, amplification and purification

2.12.1 Pak2 Adenovirus Generation

Primers (Table 2.7) were designed to bind the target gene, in this case constitutively active (T402E) Pak2 with a Flag insert at the N-terminal, and to contain a restriction site for a restriction enzyme found also in the entry vector (pENTR11, Invitrogen, Figure 2.5) but not found elsewhere in the target gene. In this case KpnI restriction enzyme was chosen for the sense primer and XhoI for the antisense primer. The pENTR11 vector already contains a Kozak sequence so this was not required in the primer. The T402E mutation of Pak2 mutates the amino acid threonine at location 402, an essential residue for Pak2 activation located in the catalytic loop of the Pak2 structure, to glutamic acid, an acidic substitution which leaves Pak2 kinase-active independent of the N-terminal regulatory region.

Table 2.7 Primer sequences for generation of Pak2 adenovirus

Use	Primer	Sequence
Pak2 T402E plasmid amplificaton	**Flag-Pak2T402E (forward with KpnI RE site)**	5'CGGGGTACCGAATGGACTACAAAGACCATGAC-3'
	Flag-Pak2T402E (reverse with XhoI RE site)	5'- CCGCTCGAGTTAACGGTTACTCTTC -3'
pENTR sequencing	**pENTR (forward)**	5'AGCAGGCTTCGAAGGAGATAG-3'
	pENTR (reverse)	5'-GTAACATCAGAGATTTTGAGACAC-3'
pDest sequencing	**T7 promoter/priming site**	5'-GACTTTGACCGTTTACGTGGAGAC-3'
	V5(C-term) reverse priming site	5'-ACCGAGGAGAGGGTTAGGGAT-3'

Bacterial transformation and maxiprep were performed to amplify the pENTR11 vector. 10 ng pENTR11 vector was added to 50 µL DH5α competent cells. Following incubation on ice for 30 minutes the cells were exposed to heat-shock at 42°C for 1 minute and then cooled on ice for 2 minutes. Subsequently, 200 µL LB broth (Sigma) was added and the cells shaken at 37°C for 1 hour. The solution was plated on LB agar plates containing kanamycin (100 µg/mL) and incubated at 37°C overnight. A single colony was picked, incubated in 200 mL LB broth containing kanamycin (100 µg/mL) and shaken at 37°C for 24 hours. The pENTR11 vector contains a gene conferring kanamycin resistance, meaning that use of this antibiotic allows for selection of colonies containing this vector. Following this, the vector was amplified using a Qiagen® Plasmid Maxi kit following the Manufacturer's instructions (a process termed Maxiprep).

A plasmid, sized 1656bp, which had been previously generated in the lab and contained the flag-Pak2 gene with a T402E mutation, was used. In order to ligate the primer to the plasmid, PCR was performed using a HiFidelity (Hotstar) PCR kit (Qiagen). 10 µL 5x buffer was mixed with 1 µL Hotstar polymerase and 1 µM of both the forward (sense) and reverse (antisense) primers (Table 2.7). 50 ng plasmid was added, and ddH_2O added up to 50 µL. PCR was carried out using the programme shown in Table 2.8.

Table 2.8 PCR reaction programme for Flag-Pak2(T402E) plasmid

		Temperature (°C)	Time
Initial Activation		95	5 minutes
30 cycles	Denaturation	94	15 seconds
	Annealing	65	1 minute
	Extension	72	1 minute
Final Extension		72	10 minutes

5 µL PCR product was run on a 1 % agarose gel to confirm the band was the correct length. 45 µL PCR product was purified using the Qiagen DNA purification kit. Both the pENTR11 vector and the purified flag-Pak2T402E plasmid were digested with the restriction enzymes HF-KpnI (NEB) and XhoI (NEB). 5 µL buffer was mixed with 1µg DNA, 1 µL of each restriction enzyme and ddH_2O added up to 50 µL. The digestion reaction was incubated for 1 hour at 37°C and then run on a 1 % gel for 45 minutes at 95 volts alongside 100 bp and 1 kb ladders (New England Biolabs). The bands for both the plasmid and vector were identified and removed, and DNA was extracted from the gel using the QIAquick gel extraction kit (Qiagen) following the manufacturer's instructions. Subsequently, the digested plasmid and vector were ligated using T4 DNA Ligase (NEB) in a 1:3 vector:insert ratio, with volumes calculated using the NEBioCalculator™ Ligation calculator (http://nebiocalculator.neb.com/#!/ligation). 1 µL T4 ligase was mixed with 2 µL T4 ligase buffer along with the calculated volumes of the vector and plasmid insert. ddH_2O was added to the reaction to make the final volume 20 µL. The reaction was incubated for 2 hours at room temperature.

Bacterial transformation was performed; the ligation mixture was added to 50 µL DH5α competent cells and incubated on ice for 30 minutes. Following one minute heat-shock at 42°C and 2 minutes incubation on ice, 200 µL LB broth was added and the mixture shaken at 37°C for one hour to allow bacterial replication. The transformation mixture was plated on LB agar plates containing kanamycin (100 µg/mL), and the plates incubated at 37°C overnight. Subsequently 6 individual colonies were picked and added to 5 mL LB broth and incubated overnight at 37°C on a shaker. DNA was extracted and purified using the QIAprep spin miniprep kit (Qiagen). The purified plasmid was sequenced by the University of Manchester DNA Sequencing Facility (University of Manchester). For sequencing, 150-300ng DNA was mixed with 5 µM of either the forward (sense) or reverse (antisense) primer (Table 2.7) and ddH_2O added up to 10 µL. Sequencing confirmed ligation of the Flag-Pak2T402E insert into the pENTR11 vector. The clone containing the correct sequence was amplified via bacterial transformation in 200 mL LB broth containing kanamycin (100 µg/mL) and subsequently underwent maxiprep, as described previously.

The pAd/CMV/V5-DEST™ gateway vector (Invitrogen, Figure 2.5) was chosen as the destination vector as it allows high-level, constitutive expression of the target gene.

Bacterial transformation and maxiprep allowed for vector amplification. This vector contains a ccdB gene, which is toxic to *E. coli* such as DH5α competent cells. Hence, ccdB-resistant *E. coli* (One Shot™ ccdB Survival™ 2T1^{R} competent cells) were used for bacterial transformation. 1 µL vector was added to 50 µL ccdB-resistant *E. coli*, which were then incubated on ice for 30 minutes, heat-shocked at 42°C for 1 minute and stored on ice for a further 2 minutes. The vector-containing bacteria were added to 250 µL S.O.C. medium (Invitrogen) and incubated at 37°C for 1 hour on a shaker before being added to 200 mL LB broth containing ampicillin (50 µg/mL) and cultured overnight at 37°C whilst shaking. The pAd/CMV/V5-DEST™ gateway vector contains a gene conferring ampicillin resistance, hence use of this antibiotic in plates or broth to culture bacteria allows selection for clones which contain this vector.

Recombination was carried out between the attL sites in pENTR11-Pak2T402E and the attR sites in pAd/CMV/V5-DEST to transfer the Pak2-T402E gene into the destination vector (Figure 2.5). 150 ng/µL entry vector was mixed with 300 ng/µL destination vector along with 2 µL LR-clonase (Invitrogen), to catalyse the reaction, and the mixture topped up to 10 µL with TE buffer. The reaction was incubated at 25°C overnight. The recombination mixture was subsequently plated on ampicillin-containing agar plates overnight, resulting in colonies of bacteria containing only the destination vector since the entry vector is not ampicillin-resistant. Following bacterial transformation, four colonies were picked and amplified using a QIAprep spin miniprep kit (Qiagen). To confirm that the flag-Pak2T402E gene had been inserted into the destination vector in the correct orientation and frame, the amplified plasmids were sequenced at the University of Manchester DNA Sequencing Facility (University of Manchester) using the relevant primers (Table 2.7). A plasmid containing the correct sequence was chosen and amplified via Maxiprep.

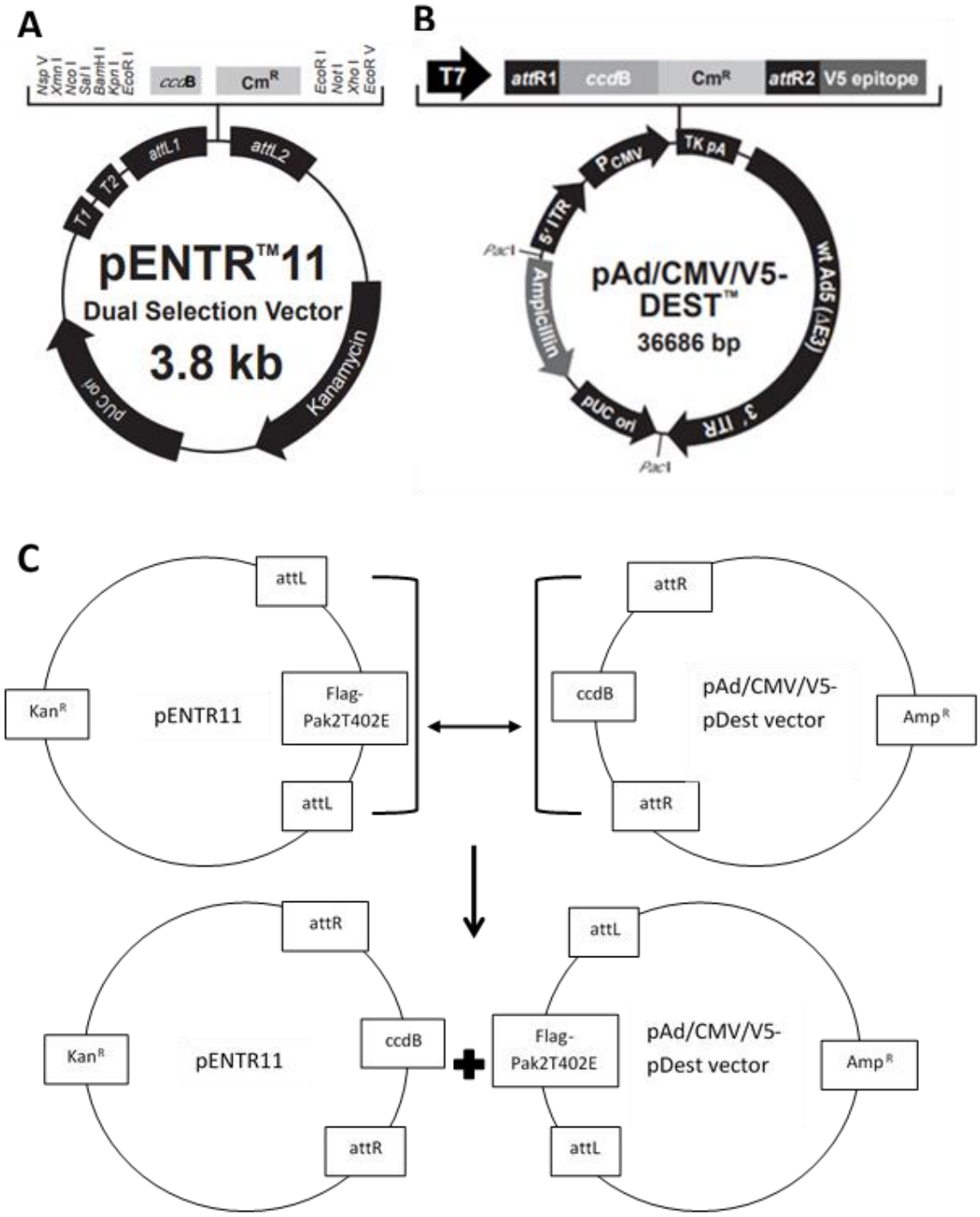

Figure 2.5 Vectors for the generation of Pak2-overexpressing adenovirus (A) Vector map for pENTR11 Dual selection vector (Invitrogen). **(B)** Vector map for pAd/CMV/V5-Dest vector (Invitrogen). **(C)** Diagram for transfer of Flag-Pak2T402E gene from pENTR11 vector to pAd/CMV/V5-Dest vector. Flag-Pak2T402E has previously been inserted into the pENTR11 vector through restriction enzyme digest with XhoI and KpnI and ligation using T4 ligase. Following bacterial recombination between the attL sites found in the pENTR11 vector and the attR sites found in the pAd/CMV/V5-pDest vector, the flag-Pak2T402E gene was transferred to the destination vector, which was verified through DNA sequencing. Kan^R = gene conferring kanamycin resistance; Amp^R = gene conferring Ampicillin resistance.

2.12.2 Pak2 adenovirus production

The plasmid DNA underwent digestion with the PacI restriction endonuclease to expose two inverted terminal repeats (ITRs) to aid virus uptake, replication and packaging in cells. 5µg plasmid DNA was mixed with 5 µL CutSmart buffer (NEB), 3 µL PacI (NEB), and ddH_2O up to 50 µL. The reaction was incubated at 37°C overnight. Subsequently, the PacI-restricted plasmid DNA was purified. 40 µL ice-cold isopropanol and 10 µL 3M sodium acetate was added to the DNA and the mixture stored on ice for 2 hours. The mixture was centrifuged for 10 minutes at 15,700 xg and the supernatant discarded. The DNA pellet was air dried, then resuspended in 20 µL RNA-free ddH_2O.

Hek293T cells were transfected with the purified plasmid. 625 µL Opti-MEM (Gibco) was mixed with 50 µL purified PacI-digested DNA. 625 µL Opti-MEM was also mixed with 12.5 µL lipofectamine 2000 (Invitrogen). Both reactions were incubated at room temperature for 5 minutes. They were subsequently mixed together and incubated at room temperature for 20 minutes. The mixture was added to a T25 flask (Corning) of Hek293T cells for 6 hours before being replaced with 2 % FBS DMEM media. The following day, the cells were split into a T75 flask. After 9 days, cells were collected once 80 % cytopathological effect (CPE) was apparent. Cells were collected in the media, spun at 250 xg for five minutes and resuspended in 500 µL PBS. Three rounds of freeze/thawing were carried out using a 37°C water bath and liquid nitrogen in order to break down the cell membrane and release virus particles trapped inside cells. Following centrifugation at 170 xg for 5 minutes, the resulting supernatant was stored at -80°C and used as a virus 'seed'.

2.12.3 Virus amplification

40 µL virus seed was added to a T75 flask (Corning) of 80 % confluent Hek293T cells. Cells were collected after 36 hours once 80 % CPE was apparent. Cells were detached using jet-force and collected in the media, centrifuged at 250 xg for 5 minutes and the cell pellet resuspended in 500 µL PBS. Following three rounds of freeze/thawing, described above, and centrifugation at 170 xg for 5 minutes, the supernatant was collected and used as a primary virus stock. The entire primary virus stock was added to 500 mL DMEM (2 %FBS, 1 % Glucose, 100 U/mL penicillin, 1 mg/mL streptomycin) which was distributed between 20 T162 flasks (Corning) of Hek293T at 80 % confluence. Cells

were collected around 36 hours later once 80 % CPE had been reached. Cells were harvested in the media, spun at 500 xg for 5 minutes and the supernatant discarded. All cell pellets were combined and washed in 20 mL sterile PBS and centrifuged for a further 5 minutes at 400 xg. The supernatant was discarded, and the cell pellets resuspended in 8 mL sterile PBS, before undergoing three cycles of freeze/thaw. Following centrifugation at 2600 xg for 15 minutes the supernatant was stored at -80°C until purification was carried out.

2.12.4 Virus purification

Adenovirus purification was carried out using a caesium chloride (CsCl) gradient. The recipes for all solutions used are described in Table 2.9.

The CsCl gradient was generated by floating 2.5 mL 1.33 g/mL CsCl solution on top of 1.5 mL 1.45 g/mL CsCl in a Beckman 14 mL centrifuge tube. The virus solution was layered on top of the gradient slowly and mineral oil (Sigma) placed on top. Centrifugation at 90,000 xg for 2 hours at 4°C was carried out in an Optima XE-90 swingout ultracentrifuge using a SW40 Ti swing-out rotor. Following centrifugation, three white bands were visible. The oil layer and the top two bands, which contain cellular debris and defective virus particles, respectively, were removed. The lowest band, containing active part-purified virus, was extracted and diluted with half a volume of TE buffer. It was subsequently layered on another CsCl gradient composed of 1.5 mL 1.33 g/mL CsCl floated on top of 1 mL 1.45 g/mL CsCl solution. The gradient was once more centrifuged at 90,000 xg for 2 hours at 4°C in an Optima XE-90 swingout ultracentrifuge using a SW40 Ti swing-out rotor. The virus band was removed as above and placed inside 15 cm dialysis tubing (pore size 24 Angstrom, Medicell) that had been previously soaked in sterilised water. The dialysis tubing, containing the virus, was soaked in 1 litre of buffer A for 1 hour, followed by buffer B for a further hour to replace CsCl. Following dialysis, the virus was removed from the tubing and stored at -80°C.

Table 2.9 Buffer recipes for virus purification

Buffer	Ingredients
TE Buffer (pH 7.8)	10 mM Tris hydrochloride 1 mM EDTA (Ethylenediaminetetraacetic acid)
1.45 g/mL CsCl solution	8.349 g CsCl (Sigma C4036) 11.4 mL TE buffer
1.33 g/mL CsCl solution	8.349 g CsCl (Sigma C4036) 16 mL TE buffer
Buffer A	10 mM Tris Base 1 mM $MgCl_2$ 135 mM NaCl
Buffer B	10 mM Tris Base 1 mM $MgCl_2$ 135 mM NaCl 10 % Glycerol

2.12.5 Virus Titration

Hek293T cells were seeded in a 96 well plate at a confluency of $1x10^4$ cells per well. This resulted in around 60 % confluence after 24 hours. The purified virus was serially diluted in 2 % FBS DMEM media 23 times from 10^{-2} dilution until $3.81x10^{-12}$ dilution (Table 2.10). The cell media was replaced with the serially diluted virus in triplicate, and the final three wells were used as negative controls with virus-free media. After 24 hours the virus-containing media was removed and replaced with 200 µL fresh 2 % FBS DMEM media. Seven days after the virus was initially added, the endpoint well was detected as the last well found to show CPE. From this, the plaque forming units per millilitre (Pfu/mL) could be calculated using Table 2.10.

Table 2.10 Information for the calculation of plaque forming units per millilitre (Pfu/mL) following virus titration

Well (triplicates)	1	2	3	4	5	6	7	8
Dilution	10^{-2}	10^{-3}	10^{-4}	10^{-5}	10^{-6}	10^{-7}	$2.5x10^{-7}$	$1.25x10^{-7}$
Pfu/mL	$1x10^3$	$1x10^4$	$1x10^5$	$1x10^6$	$1x10^7$	$2x10^7$	$4x10^7$	$8x10^7$
Well (triplicates)	9	10	11	12	13	14	15	16
Dilution	$6.25x10^{-8}$	$3.12x10^{-8}$	$1.56x10^{-8}$	$7.81x10^{-9}$	$3.91x10^{-9}$	$1.95x10^{-9}$	$9.77x10^{-10}$	$4.88x10^{-10}$
Pfu/mL	$1.6x10^8$	$3.2x10^8$	$6.4x10^8$	$1.28x10^9$	$2.56x10^9$	$5.12x10^9$	$1.02x10^{10}$	$2.05x10^{10}$
Well (triplicates)	17	18	19	20	21	22	23	24
Dilution	$2.44 x10^{-10}$	$1.22 x10^{-10}$	$6.1 x10^{-11}$	$3.05 x10^{-11}$	$1.53 x10^{-11}$	$7.63 x10^{-12}$	$3.81 x10^{-12}$	Negative control
Pfu/mL	$4.1x10^{10}$	$8.19x10^{10}$	$1.64x10^{11}$	$3.28x10^{11}$	$6.55x10^{11}$	$1.31x10^{12}$	$2.62x10^{12}$	n/a

To calculate the volume of virus required to cause the desired multiplicity of infection (MOI) in a well of a six well plate ($1x10^6$ cells), the equation below was used.

$$Quantity\ of\ virus\ to\ be\ added = \frac{MOI\ x\ number\ of\ cells\ to\ be\ infected}{Pfu/ml}$$

2.13 Immunofluorescence

2.13.1 CD68 staining of MI tissue samples

To evaluate changes in infiltration of inflammatory cells following MI, immunofluorescent staining for CD68, a macrophage-specific marker, was carried out on paraffin-embedded tissue samples from mice subjected to MI for two days.

Slides were de-waxed in xylene for 1 hour at room temperature before samples were re-hydrated in decreasing concentration of IMS in water (100 %, 75 %, 50 %) and finally ddH_2O for 10 minutes each. Antigen retrieval was carried out by immersing slides in pre-heated sodium citrate buffer (Table 2.11) for 30 minutes at 95°C. Sections were rinsed in ddH_2O for 5 minutes on a shaker to ensure all parts of the section were washed. A hydrophobic ring was placed around each section using a PAP pen and blocking buffer (Table 2.11) added to each section for 1 hour at room temperature in a humidified chamber to ensure sections did not dry out. Primary antibodies, CD68 and troponin (Table 2.12), were added in antibody buffer (Table 2.11) and slides were incubated overnight at 4°C in a humidified chamber. Following this, sections were washed in wash buffer three times at room for 10 minutes each. The relevant secondary antibodies (Table 2.12), diluted in antibody buffer, were then added and slides incubated at room temperature for 1 hour in a humidified chamber. Sections were washed three times for ten minutes in wash buffer whilst on a shaker before being quickly dipped in ddH_2O to remove any residue from the washes. Slides were left to air dry at room temperature in the dark to prevent bleaching. Slides were mounted with Vectashield® (Vector Laboratories) mounting medium containing DAPI and a coverslip was added.

Slides were imaged on a Zeiss fluorescence snapshot microscope at x20 magnification. Analysis was carried out on ImageJ software to determine CD68+ cells per mm^2.

Table 2.11 Buffer solutions for CD68 immunofluorescence

Buffer	Components
Sodium citrate buffer (1 L)	10 mM Tri-sodium citrate 0.5 % Tween 20 H_2O pH 6.0
Wash buffer (100 mL)	0.1 % Triton-X 1x PBS
Blocking buffer (50 mL)	10 % donkey serum 0.1 % Triton-X PBS
Antibody buffer (50 mL)	5 % donkey serum 0.1 % Triton-X PBS

Table 2.12 Immunoglobulins for immunostaining

Primary Antibody	Concentration	Source	Secondary antibody	Concentration	Source
Anti-CD68	1:100	Ab31630, Abcam	**Donkey anti-mouse (Alexa Fluor® 488)**	1:200	715-545-151, Stratech
Anti-troponin	1:100	Sc-8121, Santa Cruz	**Donkey anti-goat (Alexa Fluor® 594)**	1:200	705-585-174, Stratech

2.13.2 DHE staining of MI tissue samples

Dihydroethidium (DHE) staining was performed to assess whether there were changes in levels of reactive oxygen species (ROS) two days after MI. DHE is a fluorescent probe; in its unoxidized state it resides in the cytosol and exhibits blue fluorescence. However, when ROS is present this probe exhibits red fluorescence and intercalates with the cell's DNA. As a result, the cell's nucleus appears red. Due to this, relative fluorescence can be determined, allowing for the assessment of the level of oxidative stress in cells.

10 µm thick cryosections of two-day MI hearts were washed in PBS for 10 minutes. To ensure that the stain was confined to the heart section on the slide, a hydrophobic line was drawn around each heart section using a Pap pen. 50 µl DHE solution (2.5 µM; D23107 Invitrogen) was applied to each heart section, and a coverslip was added and sealed with nail polish to prevent it from moving. Slides were incubated at 37°C in a dark humid chamber for 30 minutes and imaged immediately at x20 on a Zeiss fluorescence snapshot microscope at excitation 518 nM. Average fluorescence was calculated using ImageJ software.

2.14 Quantitative PCR

Quantitative PCR (qPCR) was performed to assess changes in DNA transcription. Throughout this process RNase Zap (Sigma) was used to prevent any contamination.

2.14.1 RNA extraction from tissue

To extract RNA from tissue samples, snap-frozen heart tissue was cut into small pieces in DEPC-treated PBS and placed into a glass homogenizer tube along with 1 mL Trizol (Ambion Life Technologies). The tissue was homogenized using manual force until no tissue was visible. The solution was transferred to a clean Eppendorf tube. 300µl chloroform was added and the tube was shaken vigorously for one minute, then incubated at room temperature for 3 minutes. Samples were then centrifuged at 15,700 xg for 10 minutes at 4°C. The clear upper aqueous layer was removed from the tube and placed into a new clean Eppendorf tube. 600µl isopropanol was added and the solution incubated at room temperature for 30 minutes. After centrifugation at 13,400 xg at 4°C for 20 minutes the supernatant was removed and the pellet was washed with 1 mL 70 % ethanol, and centrifuged once more for 10 minutes at 13,400 xg at 4°C. The supernatant was removed and pellets were left to dry at 37°C for 5 minutes. The pellet was subsequently resuspended and dissolved in 20 µl RNase-free H_2O containing 1 µl SUPERase IN (Invitrogen).

2.14.2 DNase treatment

DNase treatment was carried out using the DNA-free DNA removal kit (Invitrogen). 0.1 volume of 10xDNase I buffer was added to each sample alongside 1µl DNase and samples were incubated at 37°C for 45 minutes. 0.1 volume of DNase inactivation agent was then added to inactivate the DNase, and the solution was mixed by flicking. Samples were incubated at room temperature for 2 minutes and then centrifuged at 9,300 xg for 1 minute at 4°C. The supernatant was transferred to a new Eppendorf tube. Samples could be stored at -80°C.

2.14.3 Reverse-transcriptase PCR

Reverse transcription was carried out to convert RNA into cDNA for analysis. RNA concentration was determined in each sample using a Nanodrop 2000 Spectrophotometer (ThermoScientific). LUNAScript RT (5X) (NEB) was added to a fresh 0.5 mL Eppendorf tube along with up to 1µg RNA sample. Nuclease-free H_2O was added to bring the total volume to 20 µl. The reverse transcriptase PCR was run using the programme in Table 2.13. cDNA concentration was determined using a Nanodrop 2000 spectrophotometer. Samples could be stored at -20°C.

Table 2.13 Reverse transcription PCR programme

Stage	Temperature (°C)	Time
Annealing	22	2 minutes
cDNA synthesis	55	10 minutes
Heat Inactivation	95	1 minute

2.14.4 qPCR

cDNA was diluted to 25 ng/µl using nuclease-free water. To each well in a 96 well plate, 10 µl SYBR™ Select qPCR master mix (Thermofischer Scientific), 2 µl Primer (Table 2.14), and 7 µl Nuclease-free H_2O was added alongside 20-30 ng cDNA. Samples were loaded in duplicate. qPCR was carried out using the Step One software (Applied Biosystems) on a StepOnePlus Real-time PCR machine using the programme defined in Table 2.15. 18S was used as a housekeeper gene for all samples, to which they were normalised. Results were analysed using the comparative CT ($2^{-\Delta\Delta CT}$) method (Livak and Schmittgen, 2001).

Table 2.14 qPCR primers

Primer	Species	Catalogue
Col1A2	Mouse	Qiagen, QT01055572
Col3A1	Mouse	Qiagen, QT01055516
IL6	Mouse	Qiagen, QT00098875
IL1β	Mouse	Qiagen, QT01048355
SOD2	Mouse	Qiagen, QT00161707
NPPA	Mouse	Qiagen, QT00250922
NPPB	Mouse	Qiagen, QT00107541
Col6a1	Mouse	Qiagen, QT00102060
Hgsnat	Mouse	Qiagen, QT00254653
Scara3	Mouse	Qiagen, QT00174258
Pdgfrb	Mouse	Qiagen, QT00113148
Pmp22	Mouse	Qiagen, QT00097104
Bloc1s1	Mouse	Qiagen, QT01063069
18S	Mouse	Qiagen, QT02448075

Table 2.15 qPCR programme

Stage	Temperature (°C)	Time	Number of cycles
Holding	95	10 mins	n/a
Cycling	95	15 seconds	40
	60	1 minute	
Melt Curve	95	15 seconds	n/a
	60	1 minute	
	95	15 seconds	

2.15 Immunoblot

Immunoblots were performed to assess changes in protein levels.

2.15.1 Protein extraction & quantification

To extract protein from tissue, tissue was first washed in DEPC-treated PBS and subsequently manually homogenised in 200 µl 1xTLB (Table 2.16). This was performed on ice to prevent protein denaturation. The homogenate was collected and incubated on ice for 30 minutes to ensure complete tissue digestion and cell lysis. Samples were centrifuged at 15,000 xg for 30 minutes at 4°C. The supernatant was collected and could either be stored at -80°C or used immediately.

To extract protein from cells, culture media was removed and wells washed with DEPC-PBS. 40 µL 1xTLB was added to each well and a cell scraper used to detach the cells. The collected solution was incubated on ice for 30 minutes to ensure all cells were lysed. Subsequently, samples were centrifuged at 15,000 xg for 30 minutes at 4°C and the supernatant, which contains the protein, was collected. This could either be stored at -80°C or used immediately.

Once extracted, relative protein quantification was determined. 2 µL protein sample was diluted in 98 µL ddH_2O, and 1 mL BIO-RAD protein assay dye (diluted 1:5 ddH_2O) added. A blank containing no protein sample was used to normalise against. The optical density (OD) was measured using a Jenway 6300 spectrophotometer set at 595 nM wavelength. Samples were diluted in 1xTLB until the protein concentration lay within 0.2-0.8 ABS. The equation below was used to determine the sample volumes required to ensure equal protein concentrations were loaded.

$$\frac{Lowest\ OD\ value\ x\ 10}{OD\ of\ sample\ to\ be\ loaded} = volume\ of\ sample\ to\ be\ loaded\ (\mu l)$$

Table 2.16 Recipes for solutions used during immunoblotting

Buffer	Components
5xTLB (Triton Lysis Buffer)	20 mM Tris Base
	137 mM NaCl
	2 mM EDTA pH 7.4
Adjusted to pH 7.4	1 % Triton X-100
	25 mM β-glycerophosphate
1xTLB (1 mL)	20 % 5xTLB
	10 % glycerol
	1 mM Na_3VO_4 (100 mM)
	1 mM phenylmethylsulfonyl fluoride (PMSF)
	1.54 µM Aprotinin
	21.6 µM Leupeptin
	578 µL ddH2O
10x Running Buffer	144 g Glycine
	30 g Tris Base
	ddH_2O up to 1L
1x Running Buffer	10 % 10x Running buffer
	1 % Sodium Dodecyl Sulfate (SDS)
	89 % ddH_2O
1xTransfer Buffer	10 % 10xRunning buffer
	20 % Methanol
	70 % ddH2O
10xTBS	87.68 g NaCl
	60.55 g Tris Base
Adjusted to pH 7.4	1 L ddH_2O
TBST	10 % 10xTBS
	1 % of 10 % Tween20
	89 % ddH_2O
6x Laemmli buffer	208 mM SDS
	180 mM Tris Base
Adjusted to pH6.8	15 % β-mercaptoethanol
	50 % Glycerol
	0.75 mM bromophenol blue

2.15.2 Polyacrylamide gel electrophoresis

Protein samples were separated using SDS-PAGE (Sodium Dodecyl Sulphate Polyacrylamide Gel Electrophoresis). 5 µL Laemmli buffer (Table 2.16) was added to the samples to be loaded. Samples were heated at 95°C for 5 minutes to denature the protein. Gel electrophoresis was carried out on a 10 % gel (Table 2.17) in 1xRunning buffer (Table 2.16) at 400 V, 20 mA/gel, 50 W for between 60-90 minutes alongside a PageRuler™ pre-stained protein ladder.

Table 2.17 Recipes for resolving and stocking gels for electrophoresis

Gel Component	10 % Resolving gel (5 mL)	Stacking Gel (2.5 mL)
30 % Protogel	1.67 mL	0.375 mL
1.5M pH8.8 Tris-HCl	1.25 mL	n/a
0.5M pH6.8 Tris-HCl	n/a	0.625 mL
ddH_2O	2.06 mL	1.5 mL
10 % ammonium persulfate	20.83 µL	25 µL
Tetramethylethylenediamine (TEMED)	1.95 µL	2.5 µL

2.15.3 Protein Transfer

Resolved proteins were transferred onto a polvinylidenedifluoride (PVDF) membrane (Immunobilon^{R}-P) via semi-dry transfer or wet transfer, for proteins under or over 120 kDa respectively. Semi-dry transfer was carried out on a TE77 ECL Semi-Dry Transfer Unit. Two pieces of thick Whatman™ paper were soaked in transfer buffer (Table 2.16) and placed into the unit. The PVDF membrane was first activated in methanol for 1 minute before being placed on the Whatman™ paper. The gel section containing the resolved proteins of interest was placed on top of the PVDF membrane, followed by another 2 pieces of Whatman™ paper soaked in transfer buffer. Bubbles were removed as these would interfere with protein transfer. Transfer was run at 15 V, 300 mA, 50 W for 2 hours 30 minutes. Wet transfer was used to transfer proteins over 120 kDa. Three pieces of thin Whatman™ paper were placed either side of the activated PVDF membrane and gel section, as with semi-dry transfer. Wet transfer was run at 50 V, 300 mA, 50 W for 3 hours in a wet transfer machine (BIO-RAD).

2.15.4 Blocking and detection

To limit non-specific background, the PVDF membrane was blocked in 3 % (w/v) non-fat milk (Sigma Aldrich) in TBS-T buffer (Table 2.16) for 1 hour at room-temperature. Subsequently, the membrane was immersed in the relevant primary antibody (Table 2.18) and incubated at 4°C overnight on a shaker. The membrane was then washed three times in TBS-T buffer for 10 minutes and the relevant secondary antibody (Table 2.18) added for 1 hour. After being washed four times in TBS-T for 10 minutes each, ECL detection reagent (GE Healthcare) was added to the membrane for 3 minutes and the membrane imaged on a ChemiDoc™ MP System. β-actin, GAPDH, or ERK1/2 were used as a loading controls where appropriate. Analysis was performed using ImageJ software.

Table 2.18 Antibodies used during immunoblotting

	Target protein	Dilution	Catalogue code and Source
Primary Antibodies	Anti-Pak2	1:1000	2608S, Cell Signalling Technology
	Anti-Pak1	1:1000	2602S, Cell Signalling Technology
	Anti-Flag	1:1000	F7425, Sigma-Aldrich
	Anti-pPak2	1:1000	2607S, Cell Signalling Technology
	Anti-β-actin	1:5000	Ab20272, Abcam
	Anti-GAPDH	1:1000	Ab9482, Abcam
	Anti-α-tubulin	1:1000	T6199, Sigma
	Anti-ERK1/2	1:1000	9102S, Cell Signalling Technology
	Anti-Bax	1:1000	Sc-493, Santa Cruz
	Anti-Bcl-2	1:1000	Sc-492, Santa Cruz
	Anti-cleaved caspase 3	1:1000	9661S, Cell Signalling Technology
	Anti-caspase 3	1:1000	9662S, Cell Signalling Technology
	Anti-cleaved caspase 7	1:1000	9491S Cell Signalling Technology
	Anti-caspase 7	1:1000	9492S, Cell Signalling Technology
	Anti-caspase 12	1:1000	Ab62484, abcam
	Anti-Bip/GRP78	1:1000	Ab21685, abcam
	Anti-GRP94	1:1000	2104S, Cell Signalling Technology
	Anti-Chop	1:1000	2895S, Cell Signalling Technology
	Anti-ATF6	1:1000	Ab37149, Abcam
	Anti-IRE1	1:1000	Ab37073, Abcam
	Anti-phospho-IRE1	1:1000	Ab48187, Abcam
	Anti-phospho-EIF2α	1:1000	9721S, Cell Signalling Technology
	Anti-EIF2α	1:1000	9722S, Cell Signalling Technology
	Anti-XBP1s	1:1000	Ab37152, Abcam
	Anti-ATF4	1:1000	11815S, Cell Signalling Technology
	Anti-TGFβ1	1:1000	Ab92486, Abcam
	Anti-αSMA	1:1000	Ab5694, Abcam
	Anti-SMAD7	1:1000	Ab216428, Abcam
	Anti-HIF1α	1:1000	Sc-13515, Santa Cruz
HRP-conjugated Secondary Antibodies	Anti-Rabbit IgG	1:1000	7074S, Cell Signalling Technology
	Anti-Mouse IgG	1:1000	7076S, Cell Signalling Technology

2.16 Statistical analysis

Statistical analysis was performed to determine whether Pak2 impacts the response to MI and MI-related stimuli. Data were analysed using GraphPad Prism 8 software. Data are expressed as mean ±standard error of the mean. A value of $p<0.05$ was considered statistically significant.

A Shapiro-Wilk normality test was carried out where allowed by the analysis software. Normally distributed data were analysed by parametric tests, whereas non-parametric tests were used for data that were not deemed to be normally distributed. Data were then analysed using an unpaired two-tailed Student's t-test or one-way ANOVA, or their non-parametric equivalents (the Mann-Whitney test or Kruskall-Wallis test, respectively), or a two-way ANOVA where appropriate. Post-hoc tests were performed where multiple comparisons were necessary. Following ANOVA analysis, Tukey's multiple comparison test was performed to determine differences between all data sets, whilst Dunnett's multiple comparison test was performed to identify differences between a treatment group and the control group. Dunn's multiple comparison test was employed following non-parametric analysis. Kaplan-Meier curves of survival were analysed using a Log-rank (Mantel-Cox) test. The statistical tests used for each data set are described in the respective figure legend.

Chapter 3 : Results 1: Investigating the function of cardiac Pak2 post-myocardial infarction

As mentioned in the introduction, recent research has identified Pak2 as a cardioprotective molecule during the development of cardiac hypertrophy and in the progression to heart failure through its ability to modulate the ER stress response (Binder *et al.*, 2019).

Cardiac hypertrophy (CH) and myocardial infarction (MI) share many similarities in how these diseases affect the heart. For instance, both cause increased cell death, increased extracellular matrix deposition, and cardiomyocyte hypertrophy. However, these two diseases are caused by very different stimuli, with CH often caused by hypertension-related diseases or valve disease, whilst MI is caused by a blockage, often a thrombus, in a coronary artery, leading to impeded blood flow to downstream cardiac tissue. Therefore, it is necessary to investigate whether loss of Pak2 in cardiomyocytes affects cardiac structure and function following MI. This will address aims 1 and 2 of this project.

The mouse model used to investigate these aims was a cardiomyocyte-specific knockout model, made using the Cre recombinase-*LoxP* system. In this system *LoxP* sites are located around exon 2 of the *pak2* gene. When Cre is expressed, it binds the *LoxP* sites, causing the excision of the DNA between the two *LoxP* sites. In the model used during this project Cre was driven by the alpha myosin heavy chain (αMHC) promoter as it is both cardiomyocyte-specific and highly efficient (Agah *et al.*, 1997). αMHC is the main isoform of MHC expressed in adult murine ventricles, with βMHC the main form expressed during foetal development. αMHC expression is very low in the foetal heart, but increases around birth, becoming the main isoform around neonatal day 8 (Pandya *et al.*, 2011).

3.1 ERK1/2 is a suitable western blot loading control for two-day MI protein samples

Considering that, following MI, many cellular responses are significantly altered, thus affecting protein levels of many different proteins, it was important to identify a suitable loading control that is not affected by MI so that protein changes in MI tissue could be assessed. It was found that the standard loading control GAPDH was suitable to be used for protein samples from one- and four-week MI tissue since there was no difference between sham and MI samples (data not shown). However, likely due to the effect of MI on the metabolic function on cardiac cells, GAPDH was found to not be suitable to assess protein changes in the acute (two day) phase following MI, with many MI samples showing a significant ($p<0.05$) reduction in GAPDH expression (Figure 3.1). Other standard loading controls were also assessed. Protein levels of structural loading controls, α-tubulin and β-actin, were found to be increased ($p<0.0001$) at two days following MI, likely due to the changes in cardiac structure that are brought on by an ischemic event, such as cell death and increased ECM deposition. ERK1/2 was identified as a suitable loading control for assessing protein levels in acute two day MI tissue from the remote region of the heart, given that its levels were not changed between sham and MI samples, and for this reason it was used for these experiments.

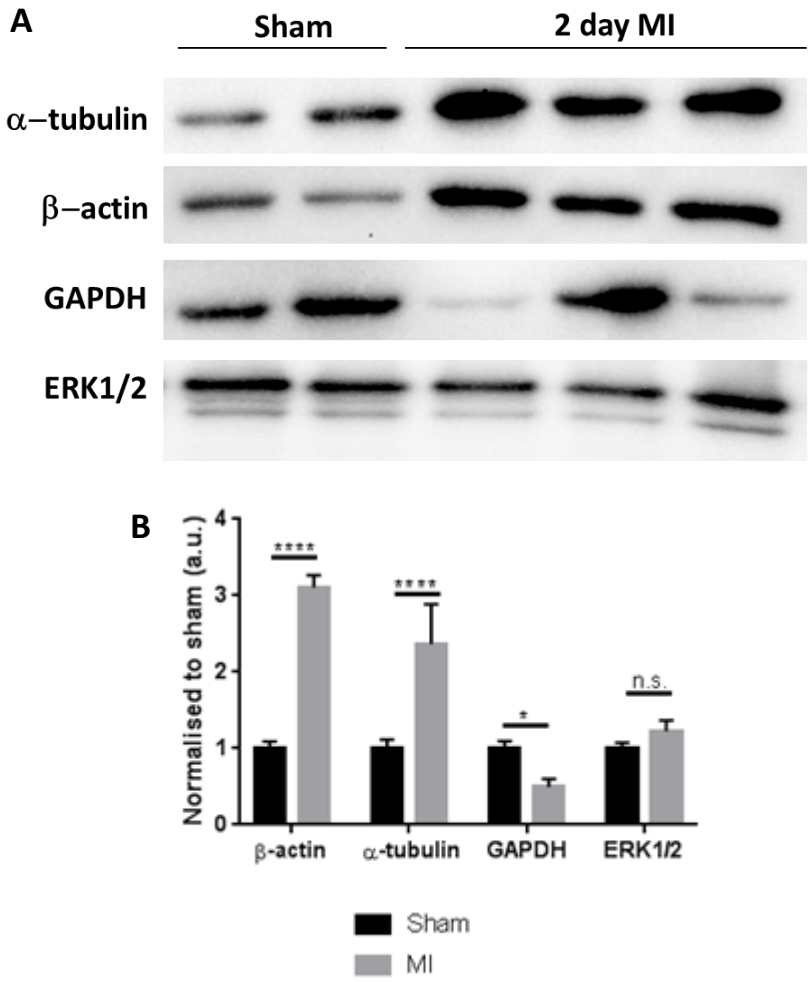

Figure 3.1 Identification of ERK1/2 as a suitable loading control for carrying out western blots using two day MI protein samples. **(A)** Representative western blots and **(B)** quantification of different standard loading controls, normalised to sham levels. Loading controls related to extracellular proteins, such as β-actin and α-tubulin were found to not be suitable loading controls for two day MI samples as they were significantly increased following MI, whilst GAPDH levels varied in MI samples, with the majority of samples showing a reduction in GAPDH protein levels following MI. ERK1/2 was found to have consistent protein levels in MI samples compared to sham controls. N=3-5. **** represents $p<0.0001$. * represents $p<0.05$. n.s. represents no significant difference. a.u. represents arbitrary units. Two-way ANOVA followed by Tukey's multiple comparison test.

3.2 Pak2 is activated *in vivo* following myocardial infarction

Pak2 regulation was assessed by immunoblotting for Pak2(Ser20). This is an autophosphorylation site which requires activation of Pak2 kinase. For the purposes of this thesis, it was taken as a measure of activity.

Pak2 phosphorylation was increased in cardiac tissue of mice subjected to MI two days following surgery (Figure 3.2A). Total levels of Pak2 were also raised. When normalised to these total Pak2 levels, levels of phosphorylated Pak2 remained elevated ($p<0.0001$). However, by one week and four weeks post-MI, protein levels of phosphorylated Pak2, normalised to total Pak2, had returned to basal levels (Figure 3.2B-D). This demonstrates that Pak2 is activated during the acute phase following MI and suggests that it acts during this phase. However, it is unknown whether the effects that it has during this time may affect long-term remodelling of the heart despite returning to basal levels.

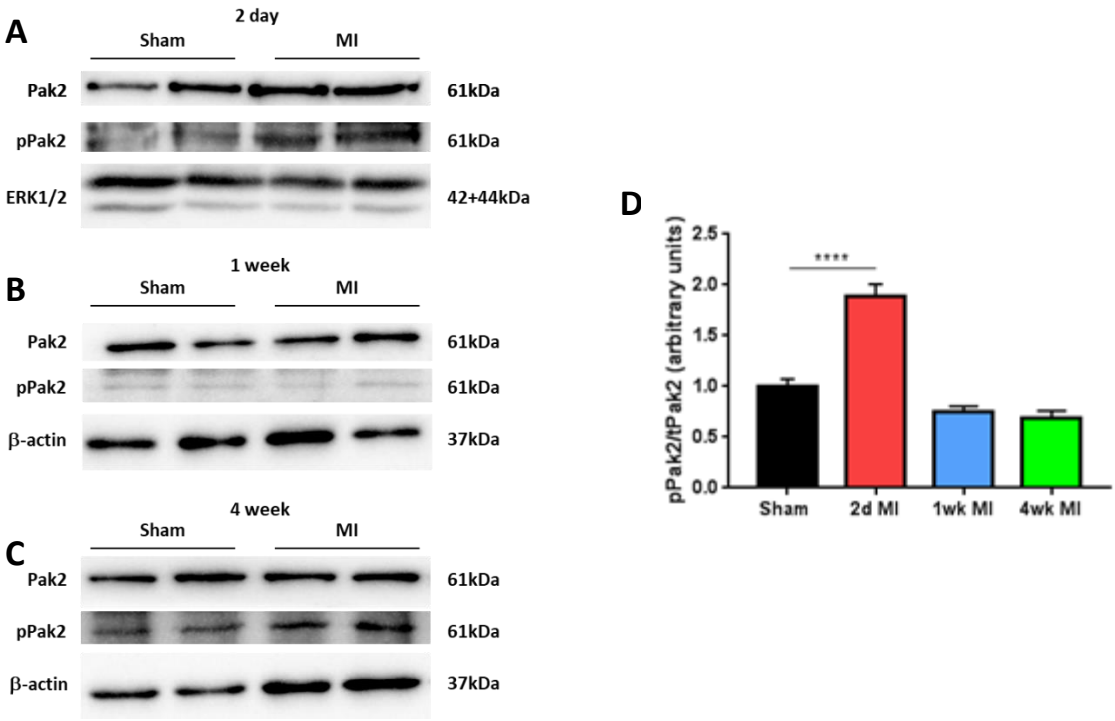

Figure 3.2 Pak2 is activated at two days following MI, but has returned to basal levels by one week and remains so at four weeks post-MI. Representative western blots of Pak2 and phosphorylated Pak2 from mouse hearts two days **(A)**, one week **(B)**, and four weeks **(C)** following MI, and quantification **(D)** of phosphorylated Pak2 proteins levels normalised to total Pak2 protein levels. ERK1/2 was used as a loading control for two-day samples. GAPDH was used as a loading control for 1-week and 4-week samples. N=3-5 with two technical repeats. **** represents a significant difference of $p<0.0001$. One-way ANOVA followed by a Dunnett's multiple comparison test.

3.3 Mouse Models

$Pak2^{cko}$ and $Pak2^{f/f}$ mice were identified through genotyping. Firstly, DNA samples were tested for the presence of loxP sites around the *pak2* gene (Figure 3.3A). The primers amplify a region of exon 2 of the *pak2* gene sized 307bp. The loxP sites add 93bp, making the fragment containing these sites 400bp. Hence, the *pak2* fragment in Pak2-floxed mice runs slower, allowing identification of mice containing these sites. Both $Pak2^{cko}$ and $Pak2^{f/f}$ mice contain loxP sites around exon 2, which is able to be identified by running alongside controls for wild type Pak2, Pak2 homozygous ($Pak2^{f/f}$) and heterozygous ($Pak2^{f/+}$) for loxP sites, and DNA from mice with flox sites around the mkk7 gene but not the Pak2 gene ($Mkk7^{f/f}$).

Following this, mice were genotyped for the presence of Cre, which lies under αMHC promoter control (Figure 3.3B). Mice which were flox-positive and Cre-positive were identified as $Pak2^{cko}$, whilst those without Cre were used as $Pak2^{f/f}$ controls. Pak2 knockout in the heart was confirmed by western blot, which showed a 75 % reduction in Pak2 protein levels in the heart (Figure 3.3C). Given that knockout of Pak2 only occurs in the cardiomyocytes, which have the MHC promoter, and cardiac tissue contains other cell types such as fibroblasts and endothelial cells, retention of some Pak2 expression in cardiac tissue was expected.

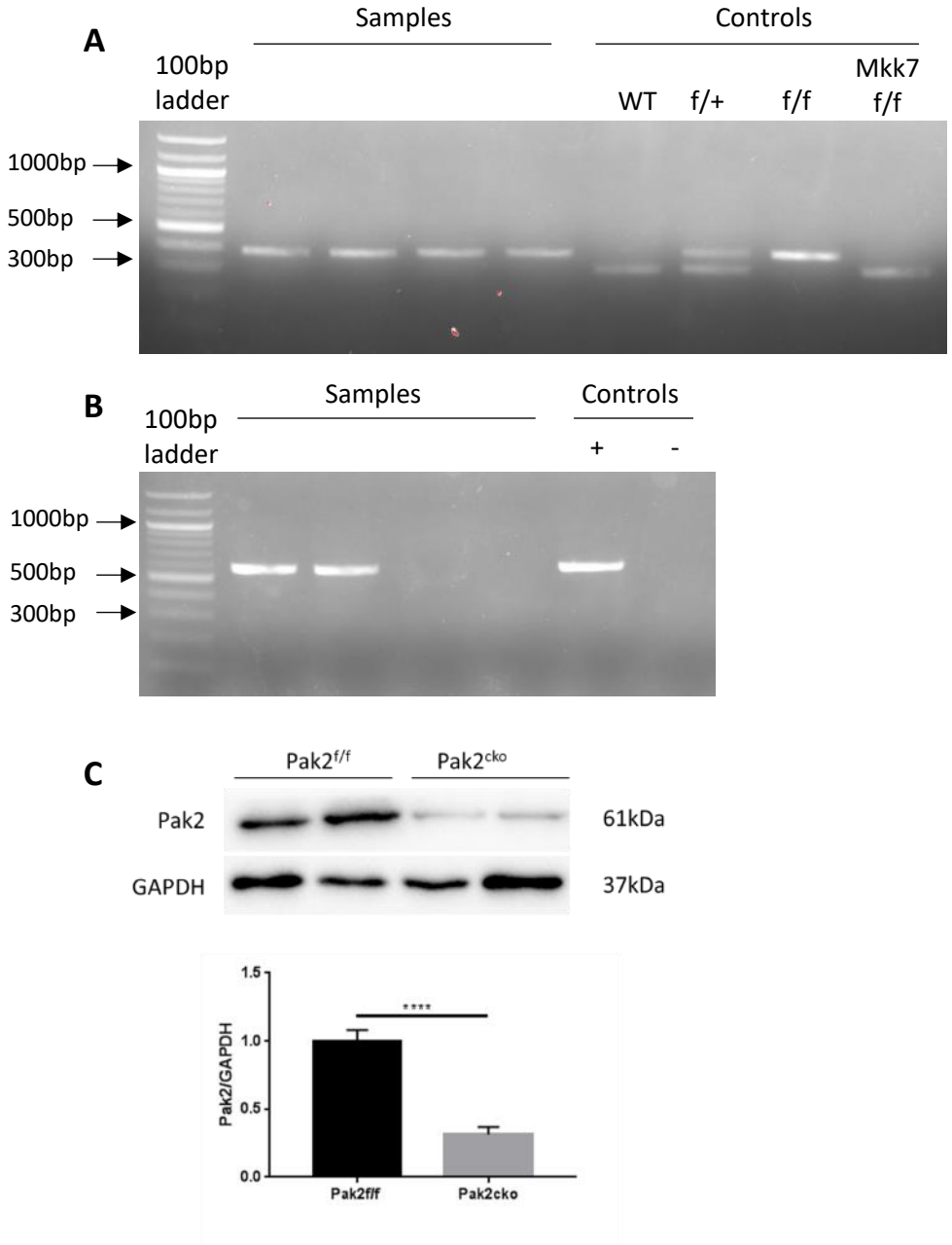

Figure 3.3 Identification of Pak2^{cko} and Pak2$^{f/f}$ mice. (A) All mice were homozygous for flox bands around exon 2 of the *pak2* gene. **(B)** Mice which presented a band when genotyped for the presence of Cre were hence Pak2 cardiomyocyte knockout mice (Pak2^{cko} mice). Those without a band were Pak2-floxed (Pak2$^{f/f}$) controls. **(C)** Representative western blot and quantification of Pak2 protein in heart from Pak2$^{f/f}$ and Pak2^{cko} mice. GAPDH was used as a western blot loading control. N=5. **** represents a significant difference of $p<0.0001$. Two-tailed unpaired t-test.

3.4 A 'mild' LAD ligation caused myocardial infarction but showed no discernible differences between $Pak2^{cko}$ mice and $Pak2^{f/f}$ control mice

3.4.1 'Mild' ligation of the LAD led to reduced cardiac function in both genotypes, but no differences between the genotypes were identified

The standard ligation point used in other strains, in this project termed the 'severe ligation', gave rise to a high mortality rate, greater than that which is allowed in the project licence, from three days following surgery (Appendix 2). For this reason, a 'mild ligation', whereby the left anterior descending coronary artery (LAD) was ligated 3 mm closer to the apex of the heart, was used initially to assess whether mice with a Pak2 deletion in cardiomyocytes are more susceptible to injury and the development of heart failure after MI. Surgery was performed on adult male mice; mice were aged 11-13 weeks at time of surgery with a body weight of 27.2 ±0.7 g and 27.9 ±0.6 g for $Pak2^{cko}$ mice and $Pak2^{f/f}$ mice, respectively (mean ±SEM).

Given the severity of the MI procedure, to have some deaths is not highly unexpected, and mortality following the mild MI procedure remained acceptable for the project licence, with two deaths out of six in the $Pak2^{f/f}$ MI group, and one out of six in the $Pak2^{cko}$ MI group (Figure 3.4A). Cardiac function was analysed, and tissue collected, two weeks after the surgery was performed. There was no evidence of pulmonary oedema in the MI groups (Figure 3.4B). Cardiac function was significantly impaired by the surgery (Figure 3.4C-E). Deterioration was evident one-week post-MI, though not to a significant level (Figure 3.4D). However, by two weeks post-surgery, reduced ejection fraction and fractional shortening was evident in both MI groups by a third and a half respectively, as well as evidence of ventricular dilatation with increased systolic left ventricular volume in mice subjected to MI. However, loss of Pak2 in cardiomyocytes did not appear to alter cardiac function following two-week MI, with no differences evident between the genotypes.

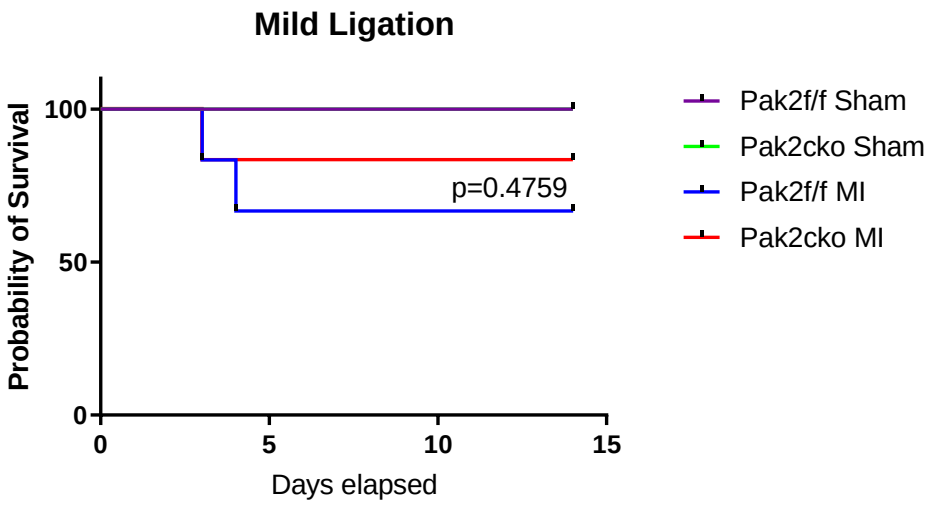
Mild Ligation
Probability of Survival
100
50
0
0
5
10
15
Days elapsed
p=0.4759
Pak2f/f Sham
Pak2cko Sham
Pak2f/f MI
Pak2cko MI

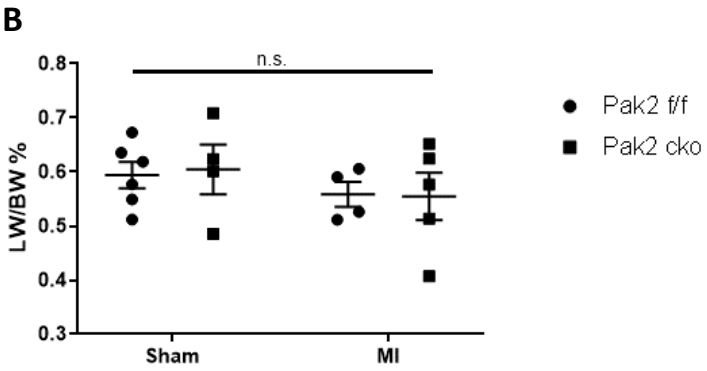
B
n.s.
LW/BW %
0.8
0.7
0.6
0.5
0.4
0.3
Sham
MI
Pak2 f/f
Pak2 cko

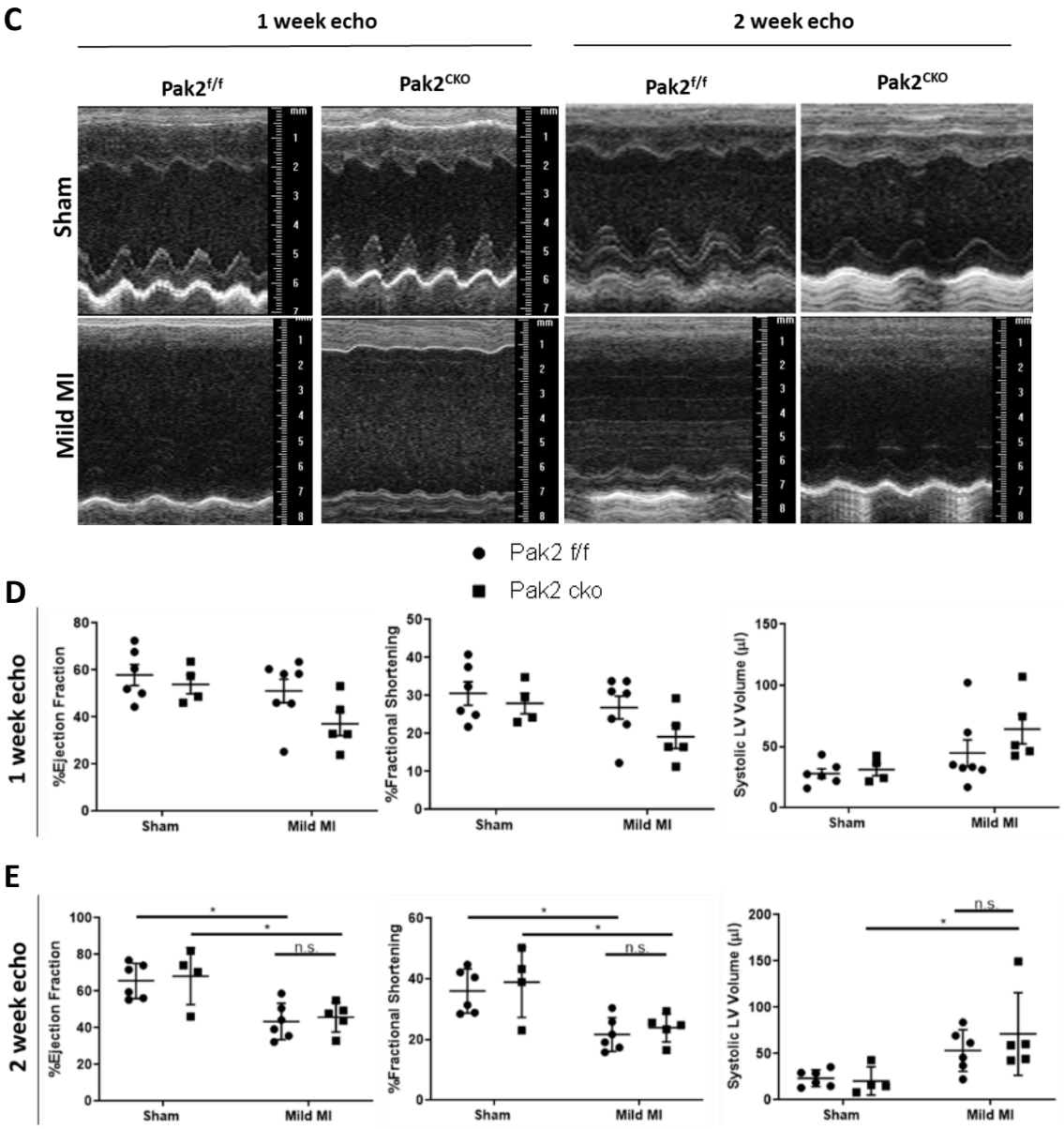

Figure 3.4 Mild MI ligation caused cardiac dysfunction. (A) Survival analysis demonstrated that 'mild' MI causes some deaths but remained within the mortality limits of the project licence. **(B)** The weight of the lungs (LW) normalised to body weight (BW) showed no change following MI in either genotype **(C-E)** Representative short-axis echocardiography images taken in M-mode and analysis of changes in ejection fraction, fractional shortening and systolic left ventricular (LV) volume one- and two-weeks following MI. Ejection fraction and fractional shortening were significantly reduced two weeks following MI, whilst there was an increase in systolic LV volume. n=4-6 for each group. * represents $p<0.05$. n.s. signifies no significant difference upon analysis of the results. Figure A was analysed using a Log-rank (Mantel-Cox) test; Figures B, D-E were analysed using a two-way ANOVA followed by Tukey's multiple comparison test.

3.4.2 'Mild' LAD ligation led to a defined infarct area but showed no clear genotype-specific differences in regard to infarct size and level of interstitial fibrosis

Loss of oxygen and nutrient supply caused by ligation of the LAD leads to cardiomyocyte death. As such, there is increased extracellular matrix deposition by cardiac fibroblasts, leading to increased fibrosis in the walls of the heart. This produces a distinct infarct area. At the two-week endpoint, hearts were excised and cut in half across the transverse axis 3 mm from the base of the heart. Masson's trichrome staining stains fibrotic material blue, allowing for analysis of the infarct area and interstitial fibrosis (Figure 3.5A). There was no difference ($p=0.3664$) in the size of the infarct between the $Pak2^{f/f}$ and $Pak2^{cko}$ mice (Figure 3.5B).

As well as causing fibrosis in the infarct area, the loss of cardiomyocytes in the infarct area of the heart causes mechanical stress elsewhere in the heart, leading to the development of fibrosis outside of the infarct zone in order to strengthen the remote regions of the heart. This was quantified as a percentage of the heart, not including the infarct, that stained positive for fibrosis (Figure 3.5C). There was increased interstitial fibrosis in many of the MI mice compared to the sham, but this was not significant ($p=0.3814$ and $p=0.6317$ for $Pak2^{f/f}$ and $Pak2^{cko}$ groups respectively). There was no difference ($p=0.9909$) between the two MI groups. The above data indicate that Pak2 deficiency does not affect infarct size and fibrotic remodelling in response to long-term MI.

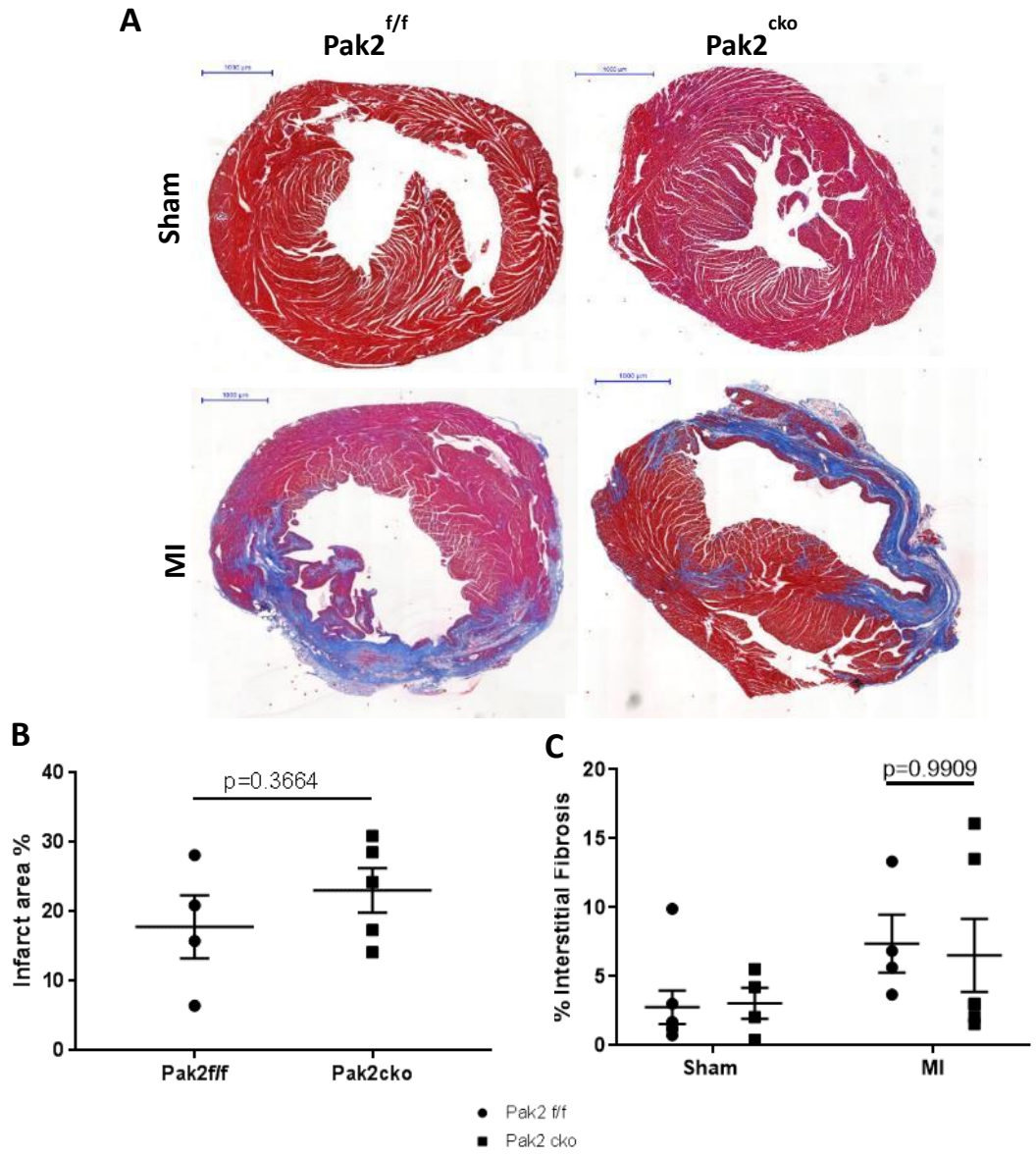

Figure 3.5 Cardiomyocyte-specific knockout of Pak2 does not affect the infarct size or level of interstitial fibrosis in mice two weeks following mild MI. Hearts were collected two weeks following initiation of MI by a 'mild' LAD ligation. They were stained using the masson's trichrome method **(A)** to allow determination of infarct size **(B)** and identification of interstitial fibrosis **(C)**. Analysis showed no significant difference between the groups regarding infarct size or percentage of the heart that was comprised of interstitial fibrosis. Scale bar in top left of each image represents 1000µm. N = 4-5 for each group. Figure B was analysed using a two-tailed unpaired t-test; figure C was analysed using a two-way ANOVA followed by Tukey's multiple comparison test.

3.4.3 Cardiac hypertrophy was evident two weeks after 'mild' LAD ligation, and may be augmented by loss of Pak2

As mentioned in the introduction, MI and CH are the two main causes of HF. However, MI can also lead to CH. The loss of contractility in the infarct area, due to the loss of cardiomyocytes and the replacement of these with non-contractile fibrotic material, leads to an increased burden on the remainder of the muscle to maintain the heart's ability to pump blood around the body. This increased stress leads to CH. Increases in cardiomyocyte cross-sectional area and other hallmarks of CH have been well-documented after MI (French and Kramer, 2007).

Since Pak2 protects against the development of pathological CH (Binder *et al.*, 2019), it was important to determine whether, two weeks following MI, hypertrophy was evident and whether loss of Pak2 altered this hypertrophic response. It was evident from echocardiographic analysis that CH had been initiated; the left ventricular (LV) mass was increased in both of the MI groups compared to their sham controls (p=0.0399 and p=0.0015 for $Pak2^{f/f}$ and $Pak2^{cko}$ groups respectively) (Figure 3.6A). $Pak2^{cko}$ mice given the MI procedure also had an increased LV mass compared to $Pak2^{f/f}$ mice given the same procedure (p=0.0499), suggesting an anti-hypertrophic role of Pak2.

Consistent with these findings, heart weight, normalised to tibia length, was significantly increased in both MI groups compared to sham (p=0.0265 and p=0.0015 for $Pak2^{f/f}$ and $Pak2^{cko}$ groups respectively) (Figure 3.6B). However, there was no significant difference (p=0.7371) between the two genotypes after MI. Haematoxylin and eosin (H&E) staining was performed on paraffin-embedded heart sections to assess changes in cardiomyocyte cross-sectional area. Analysis from this stain also showed no differences between the genotypes after MI in terms of cardiomyocyte cross-sectional area (p=0.3809) (Figure 3.6C-D).

These findings indicate that, two weeks after MI through mild ligation of the LAD, there is strong evidence that cardiac hypertrophy has been initiated in the MI groups. Echocardiographic results indicate that LV mass has been increased in $Pak2^{cko}$ mice after MI compared to $Pak2^{f/f}$ controls, suggesting that $Pak2^{cko}$ mice are developing cardiac hypertrophy at a greater level compared to $Pak2^{f/f}$ mice. However, since there was no

clear genotype-specific difference in total heart weight or average cross-sectional area, measured by analysing H&E staining, this finding is not conclusive.

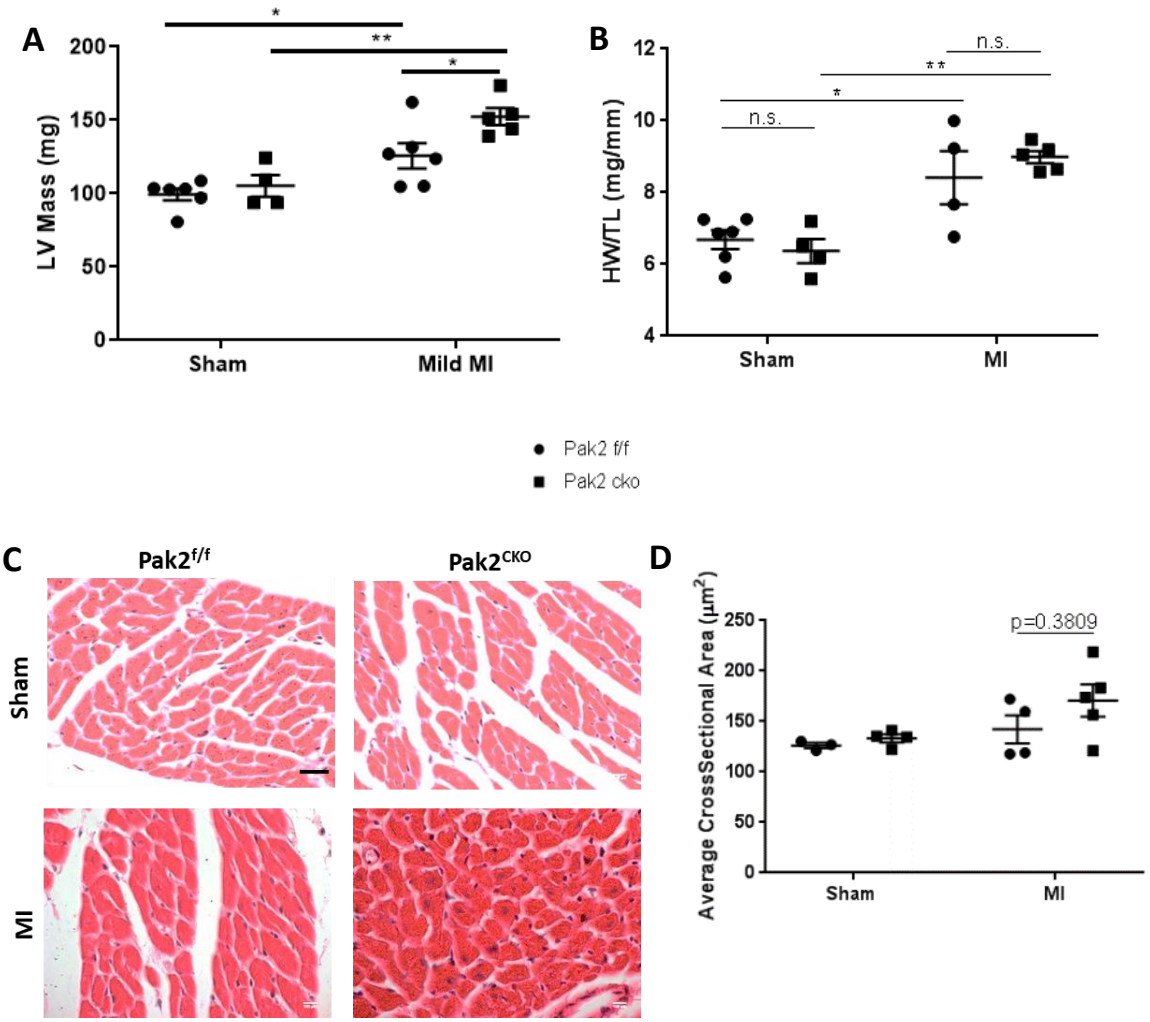

Figure 3.6 Cardiac hypertrophy had developed in hearts of mice subjected to MI two weeks after surgery. (A) Left ventricular (LV) mass, measured by echocardiography, was significantly increased in MI mice compared to sham controls. There was also an increased LV mass in Pak2^{cko} mice after MI compared to Pak2$^{f/f}$ mice. **(B)** Heart weight normalised to tibia length was significantly increased in MI mice. **(C-D)** Representative images of haematoxylin and eosin (H&E) staining and quantification showed no significant increase in average cross-sectional area in MI mice compared to sham controls. Scale bar in bottom right of Pak2$^{f/f}$ image represents 20µm. N= 4-8 for each group for echocardiographic analysis and animal parameters. N=3-5 for each group for H&E analysis. * represents p<0.05. ** represents p<0.01. Two-way ANOVA followed by Tukey's multiple comparison test.

3.4.4 A trend towards increased cardiomyocytes apoptosis was evident in Pak2^{cko} mice compared to Pak2$^{f/f}$ controls two weeks after 'mild' LAD ligation

MI leads to massive cell death not only in the infarct area, but also in the remote regions of the heart due to the mechanical stress placed on these regions due to the loss of contractility in the infarct zone. As such, cell death is a major contributor to cardiac dysfunction, and eventual heart failure, following MI. TUNEL staining is a fluorescent stain which allows the visualisation of cells in which their nuclei contain DNA breaks. DNA breaks occur during DNA fragmentation, a nuclear process that arises during cell death. As such, this stain allows for the visualisation of cells undergoing cell death, in particular apoptosis and necrosis.

TUNEL staining was performed to allow for the determination of how loss of Pak2 in the heart alters cell death in the remote and border regions of the heart. In the majority of the MI samples there was a clear increase in the number of TUNEL-positive nuclei compared to those in the sham group. As well as this, a trend ($p=0.1482$) showing increased cell death in the Pak2^{cko} MI group was evident compared to the Pak2$^{f/f}$ MI group (Figure 3.6).

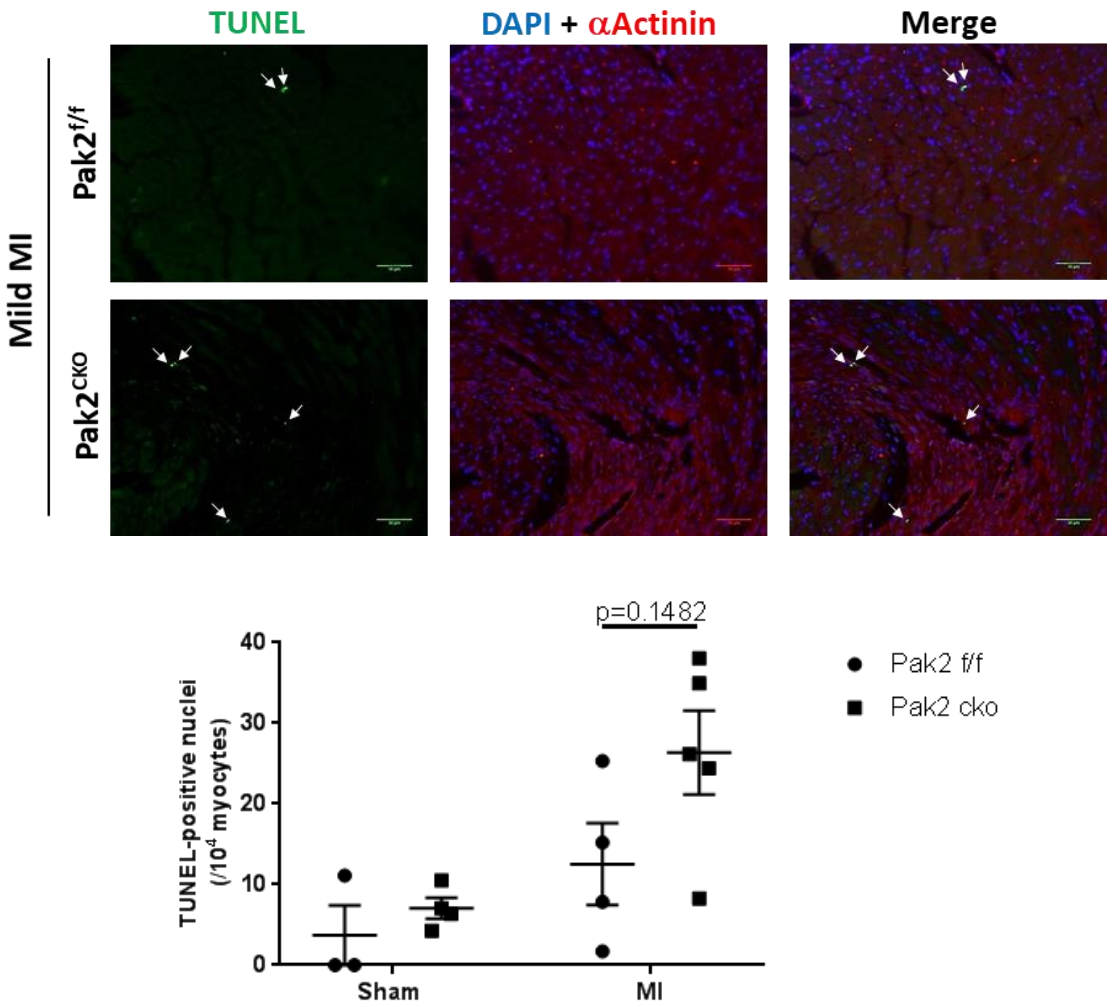

Figure 3.7 A trend towards increased cell death in Pak2cko mice following MI is evident. Representative images of TUNEL staining and quantification. Sections were triple stained with TUNEL (green), to identify cells undergoing cell death, DAPI (blue), to identify individual nuclei, and α-actinin (red), to mark for cardiomyocytes. Two weeks after mild LAD ligation there was a trend suggesting that $Pak2^{cko}$ mice had increased number of cells undergoing cell death in remote regions of the heart compared to $Pak2^{f/f}$ controls. White arrows indicate TUNEL-positive nuclei. N=3-5 for each group. Scale bar in bottom right of images represents 50μm. Two-way ANOVA followed by Tukey's multiple comparison test.

3.5 Pak2 knockout did not affect cardiac function and remodelling following 'moderate' MI

3.5.1 Mortality increased following increased ligation severity

Since there were no clear difference in cardiac function between genotypes after mild ligation, and as there was a large amount of variation in results in the MI groups, it was decided to increase the severity of the MI by raising the level of LAD ligation by 1 mm, thus enlarging the area of the heart that would be affected by the MI. This would potentially elucidate any difference that may have been masked in the mild model. This model was termed the 'moderate' MI model. Surgery was performed on adult male mice; mice were aged 11-13 weeks at time of surgery with a body weight of 26.1 ±0.8 g and 25.5 ±1.1 g for $Pak2^{cko}$ mice and $Pak2^{f/f}$ mice, respectively (mean ±SEM).

Increasing the severity increased the mortality more than expected (Figure 3.8). This was particularly evident in the $Pak2^{cko}$ MI group where there were 3 deaths out of 5, compared to the $Pak2^{f/f}$ MI group which had 3 deaths out of 9. As expected, there were no deaths in either of the sham groups. This high mortality surpassed the maximum mortality allowed on the project licence (~30 %), and thus no more surgeries were allowed to be performed. As a result, there is a low n number for the $Pak2^{cko}$ MI group meaning no conclusive results could be obtained, though trends could be viewed. Mice were analysed two weeks following surgery and tissue was collected for histological analysis.

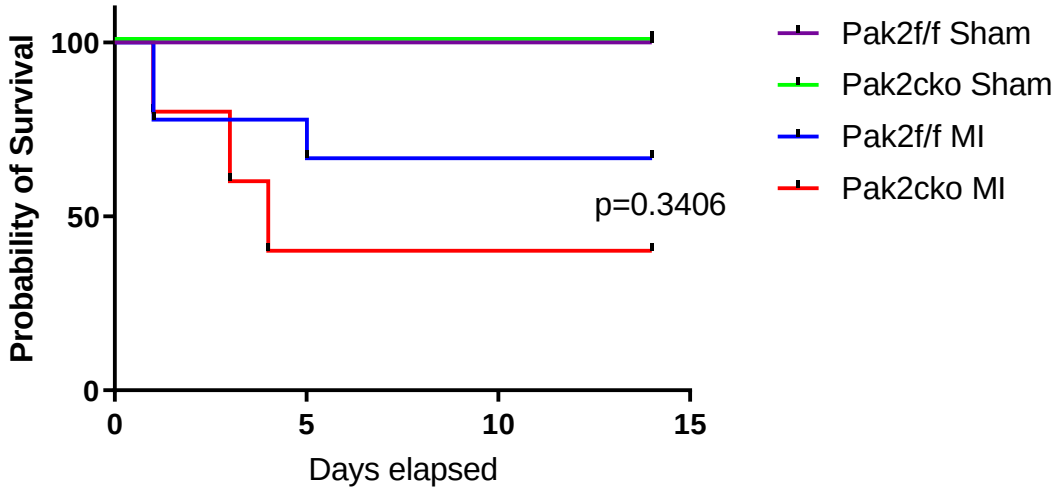

Figure 3.8 Mortality was greatly increased following moderate LAD ligation. Increased mortality was evident following moderate LAD ligation, particularly in the Pak2^{cko} MI group. N=5 for Pak2$^{f/f}$ sham group, of which there were 0 deaths. N=3 for Pak2^{cko} sham group, of which there were 0 deaths. N=9 for Pak2$^{f/f}$ MI group, of which there were 3 deaths (67% survival). N=5 for Pak2^{cko} MI group, of which there were 3 deaths (40% survival). All deaths occurred before day 7. Mortality surpassed the limit on the project licence so no more surgeries could be performed. Log-rank (Mantel-Cox) test.

3.5.2 'Moderate' MI produced high levels of variability in terms of cardiac function

Two weeks following induction of MI, a high level of variability was evident in both of the MI groups regarding cardiac function and this, combined with the low number of mice to analyse in the Pak2^{cko} group, meant that no real conclusions could be made from this data (Figure 3.9). It appears that this surgery, as with the 'mild' MI, leads to impaired cardiac function in both groups, with the majority of MI mice having reduced fractional shortening and ejection fraction (Figure 3.9A-B) and increased left ventricular volume during systole (Figure 3.9C) suggesting ventricular dilatation had occurred. There was no change in lung weight normalised to body weight, indicating that heart failure had not progressed to cause pulmonary oedema (Figure 3.9D).

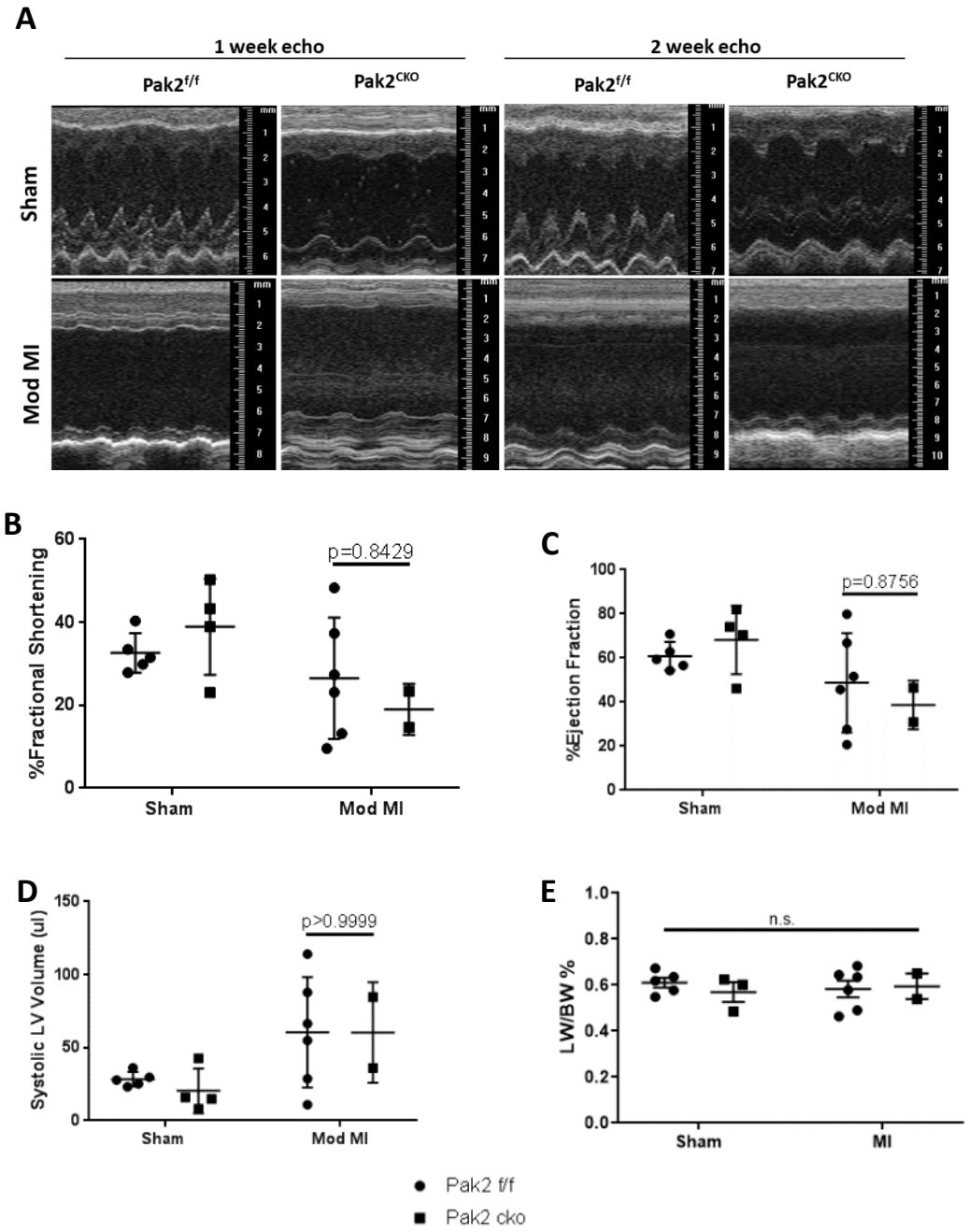

Figure 3.9 No conclusion could be made from echocardiographic data following 'moderate' LAD ligation due to the high level of variability. (A) Representative images of echocardiographs taken on a Visualsonics Vevo 770 micro-imaging system. **(B-D)** Calculated fractional shortening, ejection fraction and systolic left ventricular volume showed no effect of Pak2 knockout on cardiac function. High levels of variation following MI in both genotypes and the low n number of the Pak2^{cko} mice group meant no conclusions could be made. **(E) '**Moderate' MI caused no change in lung weight, represented as a percentage of body weight (LW/BW%) after two weeks. n.s. represents no significant difference. N=2-6 for each group. Two-way ANOVA followed by Tukey's multiple comparison test.

3.5.3 No discernible differences in level of fibrosis or infarct size were identified between the genotypes

At the endpoint of this experiment hearts were excised and cut across the transverse plane 4 mm from the apex of the heart, below the site of ligation. Hearts were then processed and embedded in paraffin for histological analysis. Masson's trichrome staining delineated the infarct area but showed no difference in infarct size or levels of interstitial fibrosis between the two genotypes (Figure 3.10). This is consistent with what was observed in mice subjected to mild ligation.

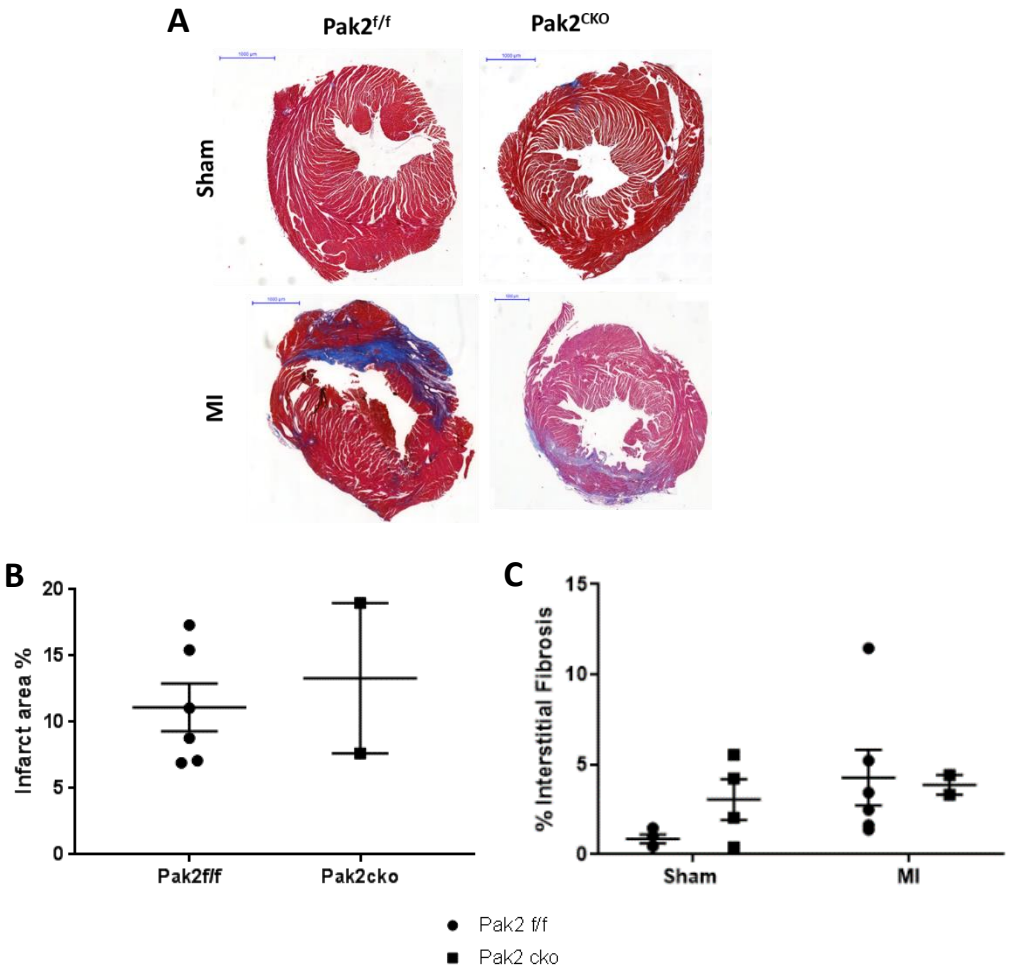

Figure 3.10 No differences were found between the genotypes regarding infarct size or level of interstitial fibrosis two weeks following 'moderate' LAD ligation. Hearts were collected two weeks following initiation of MI by 'moderate' ligation. **(A)** Representatives histological staining of masson's trichrome, which allowed analysis of infarct size **(B)** and level of interstitial fibrosis **(C)**. Scale bar in top left of each image represents 1000µm.N= 2-6 for each group. Figure B was analysed using a Mann-Whitney test; figure C was analysed using a two-way ANOVA followed by Tukey's multiple comparison test.

3.5.4 Pak2 disruption in the heart did not affect hypertrophic growth two weeks following 'moderate' MI ligation

Analysis of H&E staining revealed an increase in average cardiomyocyte cross-sectional area in the $Pak2^{f/f}$ MI group compared to shams ($P<0.01$) (Figure 3.11A-B). This finding demonstrates that two weeks after 'moderate' MI procedure CH has occurred in the remote regions of the heart, showing that an adaptive response is occurring to overcome the loss of contractility in infarct region. This finding was supported by an increase in left ventricular mass (Figure 3.11C, $p<0.01$) and an increase in heart weight normalised to tibia length (Figure 3.11D, $p<0.05$) in the $Pak2^{f/f}$ MI group compared to shams. However, the same was not found between the $Pak2^{cko}$ MI and sham groups ($p=0.7094$). No significant difference was identified between the two MI groups.

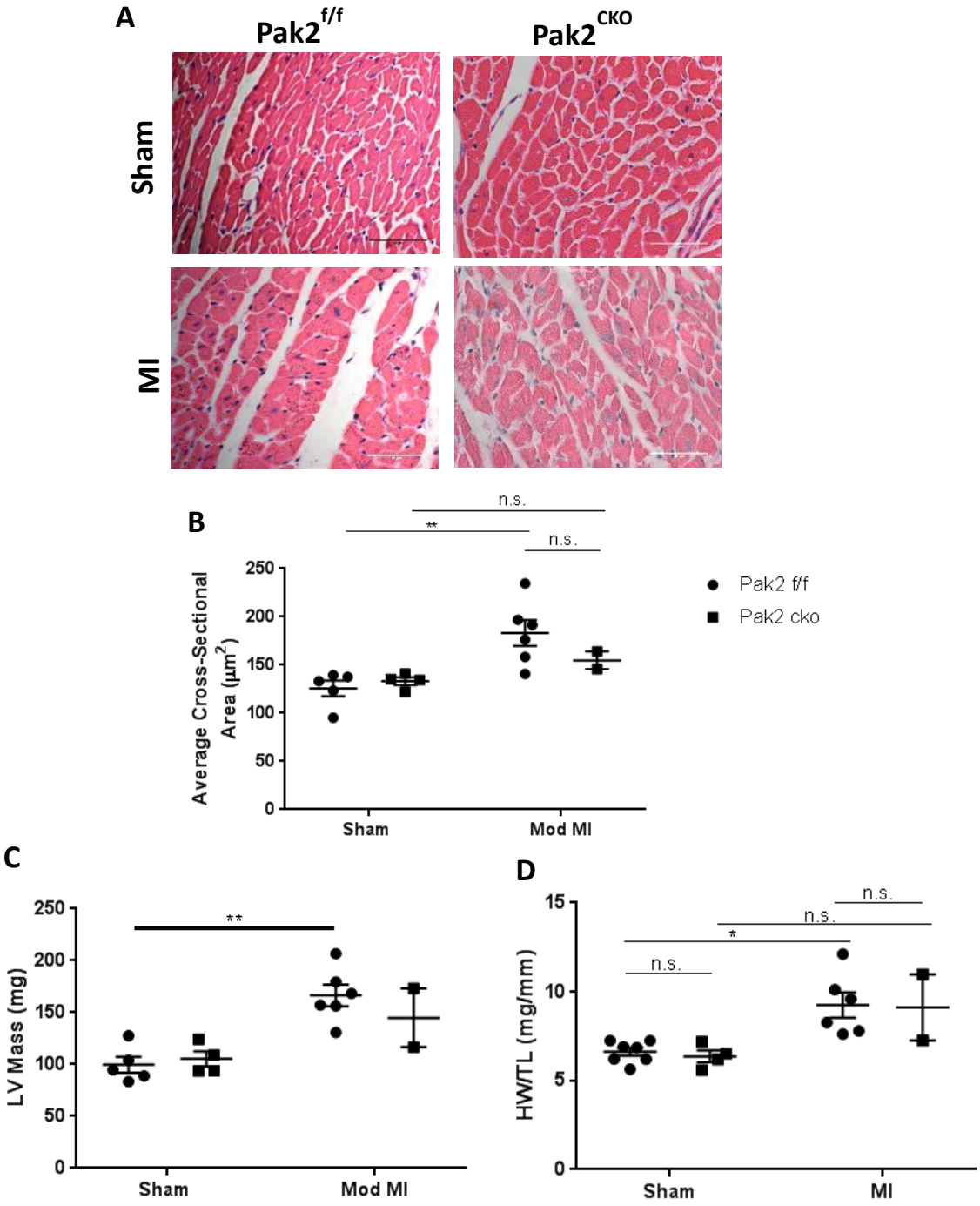

Figure 3.11 Cardiac hypertrophy was evident in MI groups two weeks after moderate LAD ligation. (A-B) Representative images of H&E staining and quantification showed a significant increase in in average cardiomyocyte cross-sectional area after moderate MI compared to shams. This was supported by an increase in left ventricular (LV) mass **(C)** calculated from echocardiographs, and in measurement of heart weight upon collection, normalised to tibia length **(D).** Scale bar in bottom right of H&E images represents 50µm. N=2-6 for each group. * represents $p<0.05$. ** represents $p<0.01$. n.s. represents no significant difference. Two-way ANOVA followed by Tukey's multiple comparison test.

3.5.5 There were comparable levels of cell death in Pak2$^{f/f}$ and Pak2^{cko} mice after two weeks MI

TUNEL staining of heart samples demonstrated that MI led to increased cardiomyocyte death in remote regions of the hearts of most mice subjected to the moderate model of MI (Figure 3.12). However, there were two Pak2$^{f/f}$ mice that had a very low number of TUNEL-positive cells in remote regions, demonstrating the variability of the moderate MI model.

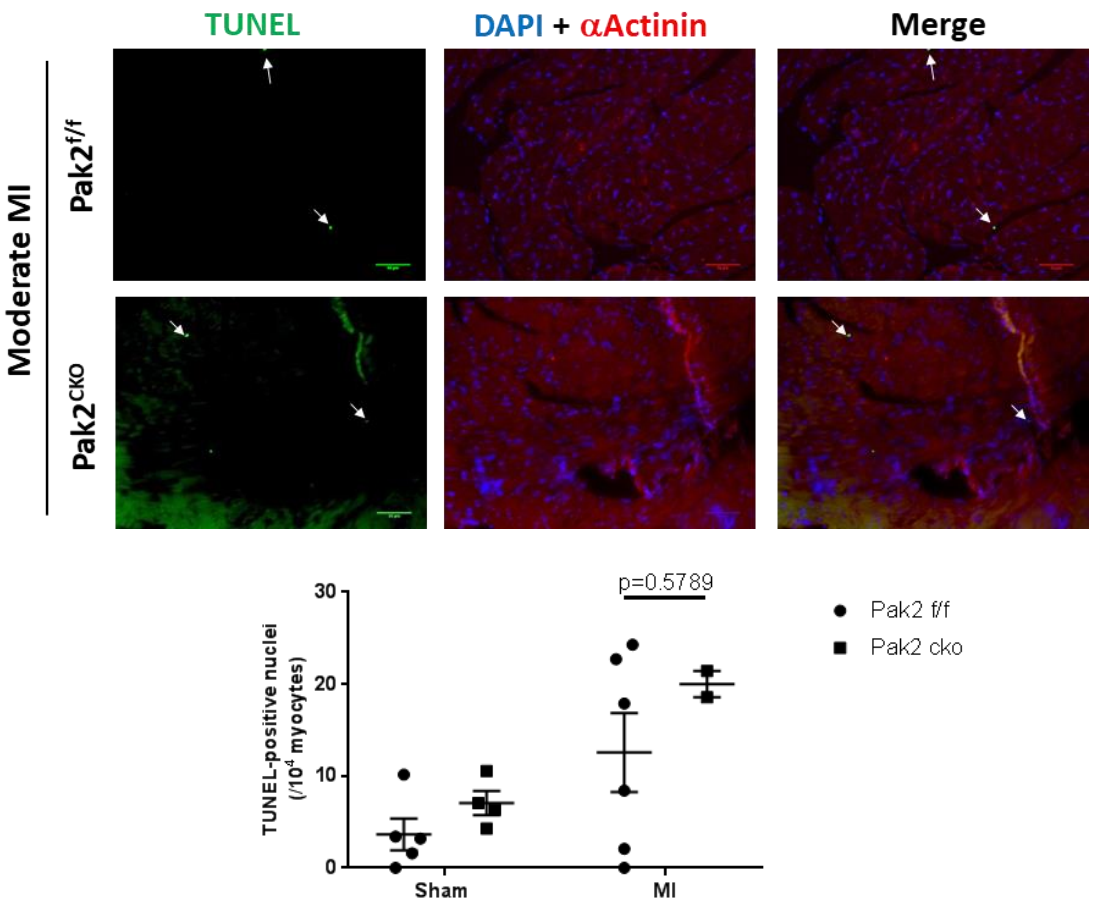

Figure 3.12 The majority of MI mice have increased cell death in remote regions of the heart two weeks after surgery. Representative TUNEL images and quantification of number of TUNEL-positive nuclei normalised to 10,000 myocytes. Sections were triple stained with TUNEL (green), to identify cells undergoing cell death, DAPI (blue), to identify individual nuclei, and α-actinin (red), to mark for cardiomyocytes. White arrows indicate TUNEL-positive nuclei. N=2-6 for each group. Scale bar in bottom right of images represents 50μm. Two-way ANOVA followed by Tukey's multiple comparison test.

3.6 Pak2^{cko} mice exhibited altered cellular responses two days after 'severe' MI was induced

3.6.1 Cardiac function is significantly deteriorated in both genotypes two days following 'severe' LAD ligation

Considering that the majority of deaths following acute MI occurred 3 or more days following surgery, it was decided to investigate whether loss of Pak2 alters cellular responses to MI after two days, before the majority of mortality occurred in this model. The severe model of MI was chosen as this is a standard LAD ligation point for other mouse models and so will likely lead to greater consistency. Surgery was performed on adult male mice; mice were aged 11-13 weeks at time of surgery with a body weight of 27.6 ±0.4 g and 27.6 ±0.4 g for Pak2^{cko} mice and Pak2$^{f/f}$ mice, respectively (mean ±SEM).

Two days following surgery using this 'severe' model of LAD ligation, cardiac function was already significantly impaired, as is evident from echocardiographic measurements (Figure 3.13A-D). Fractional shortening was significantly reduced ($p<0.001$ in each group) by around half, and similar findings ($p<0.001$) were found regarding ejection fraction showing that the ability of the heart to pump blood out to the body had been substantially diminished. The volume of the left ventricle during systole was significantly increased ($p<0.0001$) in both MI groups, demonstrating that ventricular dilatation had occurred. However, this was not yet sufficient to cause substantial HF as no pulmonary oedema was evident (Figure 3.13E). However, at this time point, there were no clear differences in any of the parameters to suggest that loss of Pak2 affects cardiac function after MI.

These findings show that this model is sufficient to cause reduced cardiac function two days after MI, and thus changes to cardiac structure and molecular signalling can be analysed to assess whether loss of Pak2 alters how the heart is affected following MI-induced stress.

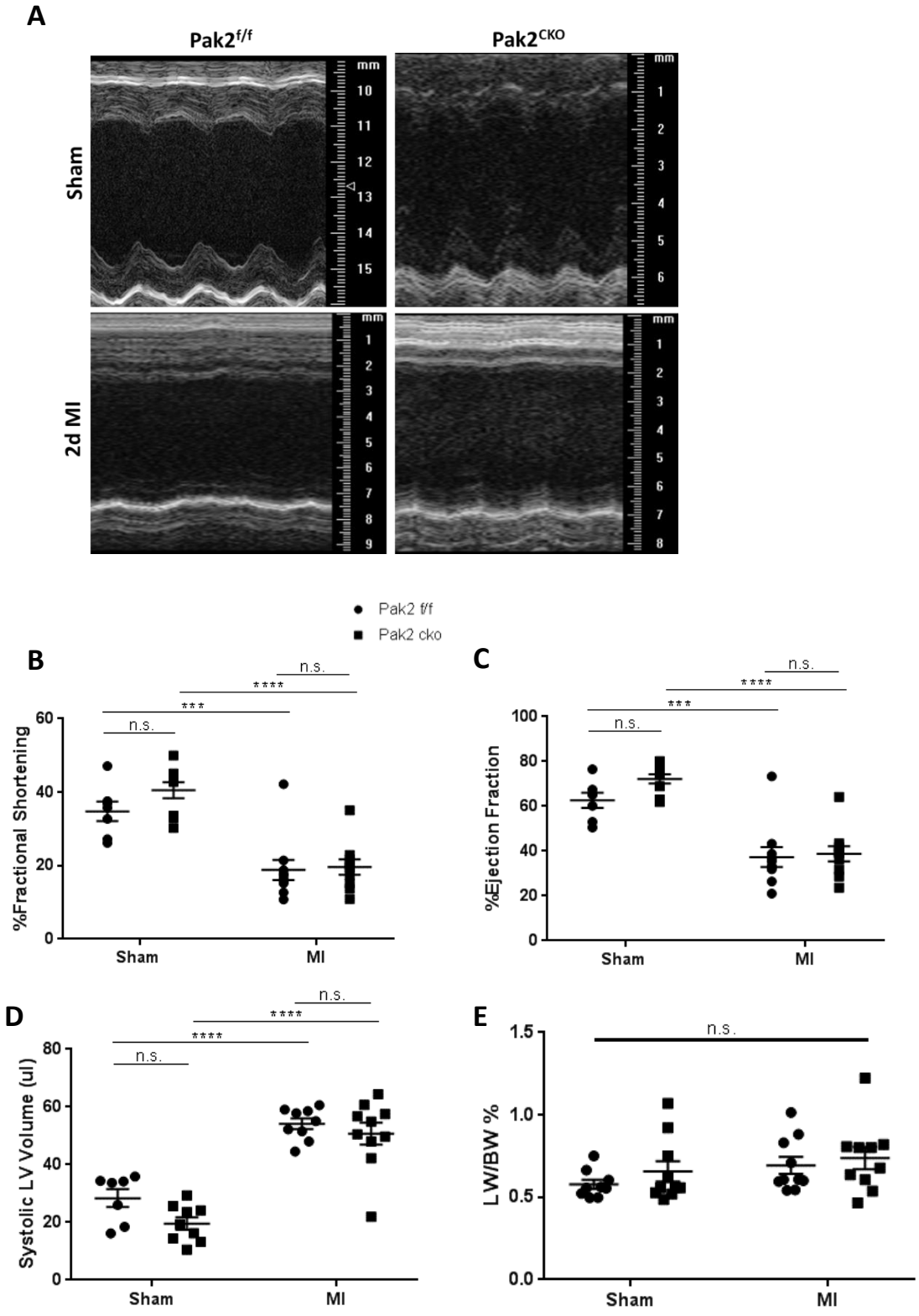

Figure 3.13 Cardiac function was severely affected two days after severe LAD ligation (A) Representative echocardiograms of sham and MI mice two days after surgery. Analysis showed a significant reduction in fractional shortening **(B)** and ejection fraction **(C)** in both MI groups after two days compared to sham controls. There was also a clear increase in left ventricular volume at the end of systole **(D)**. **(E)** Severe LAD ligation did not affect lung weight, normalised to body weight (LW/BW%). *** represents p<0.001. *** represents p<0.0001. n.s. represents no significance. N=9-10 for each group. Two-way ANOVA followed by Tukey's multiple comparison test.

3.6.2 No arrythmias were evident in either genotype after surgery

Changes in the cardiac conduction system have been observed in both animals and humans after MI (Bhar-Amato *et al.*, 2017). ECG analysis was carried out to identify whether arrhythmias have developed following MI, and whether this could explain the deaths following surgery in the moderate and severe MI models after three days. There was a low number of mice in each group (n=3-5 in each group) but from the results obtained there were no differences in any of the ECG parameters measured (Table 3.1), either between the sham and the MI groups, or between the genotypes.

Parameter	$Pak2^{f/f}$ sham	$Pak2^{cko}$ sham	$Pak2^{f/f}$ MI	$Pak2^{cko}$ MI	Significant?
Heart Rate (BPM)	640.0 ±1.2	680.2 ±28.7	689.2 ±23.2	720.9 ±41.3	n.s.
RR interval (ms)	93.5 ±0.4	89.0 ±3.8	88.2 ±3.2	79.9 ±3.8	n.s.
QRS interval (ms)	10.3 ±0.9	11.4 ±0.7	10.1 ±0.5	9.6 ±0.8	n.s.
QT interval (ms)	19.8 ±1.1	20.3 ±1.4	18.9 ±1.8	16.6 ±0.6	n.s.
QTc (ms)	64.9 ±3.6	68.3 ±5.6	64.0 ±6.2	57.9 ±3.8	n.s.

Table 3.1 At the two-day endpoint cardiac electrical conduction did not appear to be affected by surgery or genotype. No significant difference (n.s.) was identified between the groups for any of the parameters. N=3-5 for each group. Two-way ANOVA followed by Tukey's multiple comparison test.

3.6.3 Hypertrophic markers are induced by acute MI

Two days after MI, hearts were excised and cut transversely 4 mm from the apex of the heart. Hearts were then processed and paraffin-embedded for histological analysis. H&E staining showed no significant change in average cardiomyocyte cross-sectional area after MI either between the sham and MI groups ($p=0.0645$ and $p=0.4057$ for $Pak2^{f/f}$ and $Pak2^{cko}$ groups respectively), or between the genotypes after MI ($p=0.1497$) (Figure 3.14A-B). Similarly, there was no difference in LV mass measured during echocardiography (Figure 3.14C). However, heart weight normalised to tibia length, measured following excision of the heart, showed a significant increase in heart weight in both genotypes after MI ($p<0.001$), though knockout of Pak2 had no impact on this ($p>0.9999$).

qPCR analysis supported the theory that hypertrophic signalling had already been initiated two days following induction of MI (Figure 3.14E-F). Two foetal genes associated with pathological CH are atrial natriuretic peptide (ANP, *NPPA*) and brain natriuretic peptide (BNP, *NPPB).* During the initiation of CH, the increased stretch of cardiomyocytes re-activates foetal gene expression (Dirkx *et al.*, 2013), with ANP and BNP two markers of this phenomena. RNA analysis showed that these two genes are upregulated two days after MI in both $Pak2^{f/f}$ and $Pak2^{cko}$ mice, with a significant increase in BNP expression 4-6-fold in MI mice. There is a slight increase in $Pak2^{cko}$ mice compared to $Pak2^{f/f}$ mice in terms of BNP expression after MI, though this is not significant ($p=0.5356$).

These findings suggest that hypertrophic signalling has been initiated two days following MI.

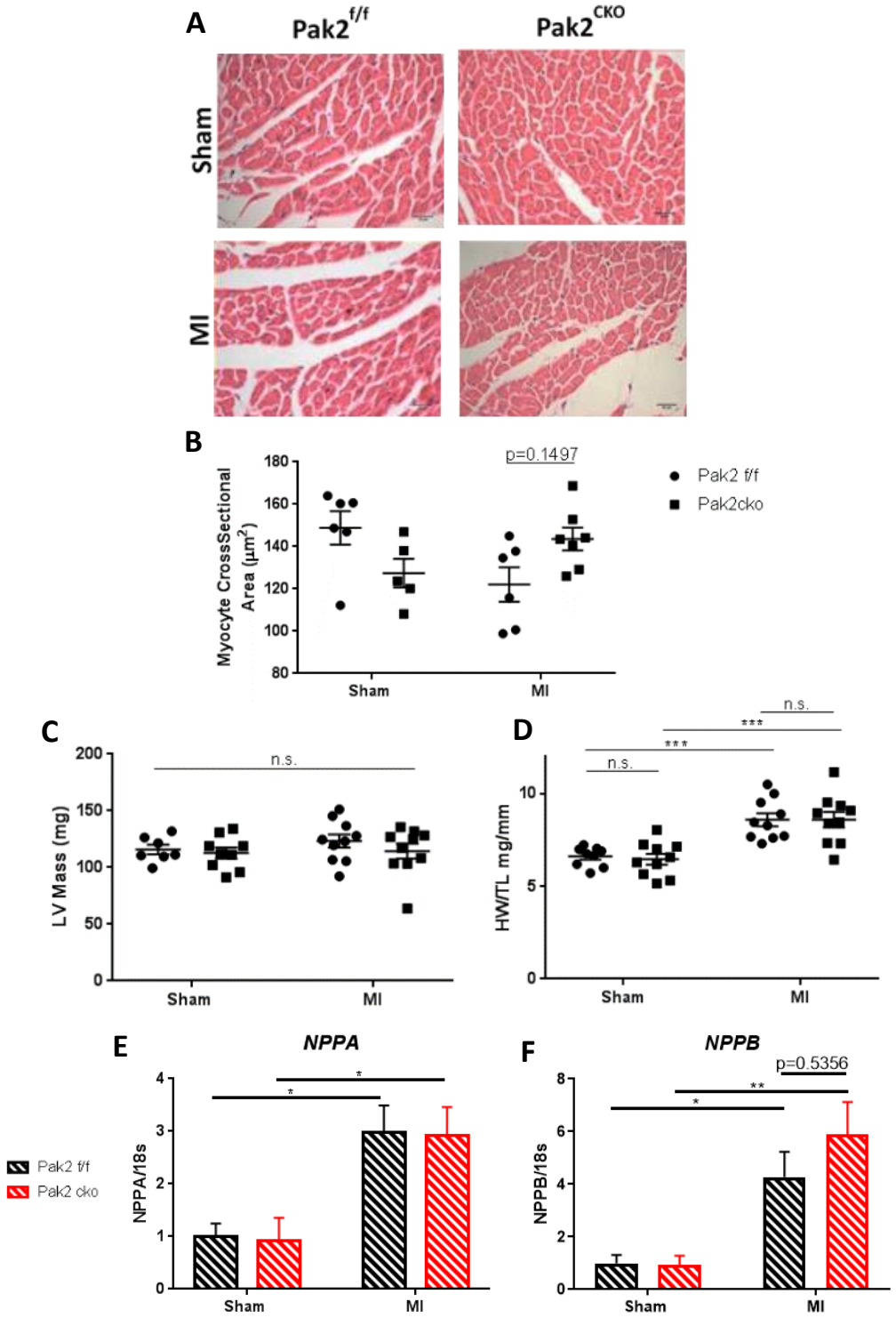

Figure 3.14 Cardiac hypertrophy has been initiated two days after severe MI surgery. (A-B) Representative images of H&E staining and quantification of average myocyte cross-sectional area showed no change in cardiomyocyte size two days after surgery, with no difference between the sham or MI mice, or between the genotypes. Scale bar in bottom right of H&E images represents 20µm. **(C)** There was no difference in left ventricular (LV) mass, measured via echocardiography. **(D)** There was increased total heart weight, normalised to tibia length (HW/TL) upon collection of tissue, with an increased weight in both MI groups. **(E-F)** qPCR analysis showed increased expression of ANP (*NPPA*) and BNP *(NPPB)*, two markers of cardiac hypertrophy, in the hearts of MI mice. All expression analysis was normalised to the housekeeper gene 18S. n=5-10 for A-D, n= 4-6 for figures E and F. * represents p<0.05. ** represents p<0.01. *** represents p<0.001. n.s. represents no significant difference. Two-way ANOVA followed by Tukey's multiple comparison test.

3.6.4 Pak2^{cko} mice exhibit increased levels of fibrosis following MI

Knockout of Pak2 in cardiomyocytes led to increased fibrosis in the heart of mice following MI. Masson's trichrome staining demonstrated a trend (p=0.0889) towards increased staining of fibrotic tissue in the heart (Figure 3.15A-B). At two days following MI it is not possible to delineate the infarct area since the proliferative phase following MI usually occurs 4-14 days following the initial infarction, and it is during this phase in which the majority of the extracellular matrix deposition occurs (Ferrini *et al.*, 2019; Weil and Neelamegham, 2019). Hence, total level of cardiac fibrosis, with no distinction between infarct-related and interstitial fibrosis, was determined.

The two main isoforms of collagen deposited in the heart after injury are collagen I (Col1A1) and collagen III (Col3A1). qPCR analysis demonstrated that transcription of these were increased in both genotypes after MI compared to control mice which had undergone a sham procedure (Figure 3.15C-D). However, at the transcriptional level there was no clear difference (p>0.9999 for both Collagen I and III) between the Pak2$^{f/f}$ and Pak2^{cko} groups after MI.

However, assessment of protein levels of fibrosis-related molecules via western blot supported the findings from the Masson's trichrome staining (Figure 3.16A-D). Protein levels of alpha-smooth muscle actin (αSMA) were increased in both MI groups, but levels were around three times higher in Pak2^{cko} mice after MI compared to the Pak2$^{f/f}$ controls (Figure 3.16C). αSMA is a marker of myofibroblasts following their differentiation from fibroblasts. This differentiation increases the capability of myofibroblasts to deposit extracellular matrix and allows them to secrete cytokines, maintaining the inflammatory response (Baum and Duffy, 2011).

Furthermore, protein levels of TGFβ were significantly (p<0.05) increased in Pak2^{cko} mice compared to Pak2$^{f/f}$ mice after MI (Figure 3.16D). TGFβ is a signalling molecule that is a key pro-fibrotic regulator. It is released by many cell types in its latent form. Upon binding its receptor, the TGFβ receptor, it leads to pro-fibrotic gene expression, and it is an important regulator of myofibroblast differentiation.

As expected, protein levels of Smad7 were significantly reduced by around 50 % in both MI groups (Figure 3.16E). Smad7 is a negative regulator of fibrosis that is able to

suppress TGFβ signalling (Wang *et al.*, 2002; Chung *et al.*, 2013), and thus its downregulation in MI hearts is unsurprising.

An unexpected finding was the increase in total Pak2 levels after MI, even in cardiac tissue from $Pak2^{cko}$ mice after MI, which have total Pak2 levels similar to those of $Pak2^{f/f}$ sham mice (Figure 3.16A-B). Considering that these mice have Pak2 knockout specifically in cardiomyocytes this demonstrates that, either there must be an increase in Pak2 protein expression in other cell types in the heart, or there must be an influx of cells expressing Pak2 into the heart.

These findings suggest that loss of Pak2 in cardiomyocytes may either increase the fibrotic response, or accelerate the development of fibrosis, in the heart. However, the mechanism through which this occurs is unclear.

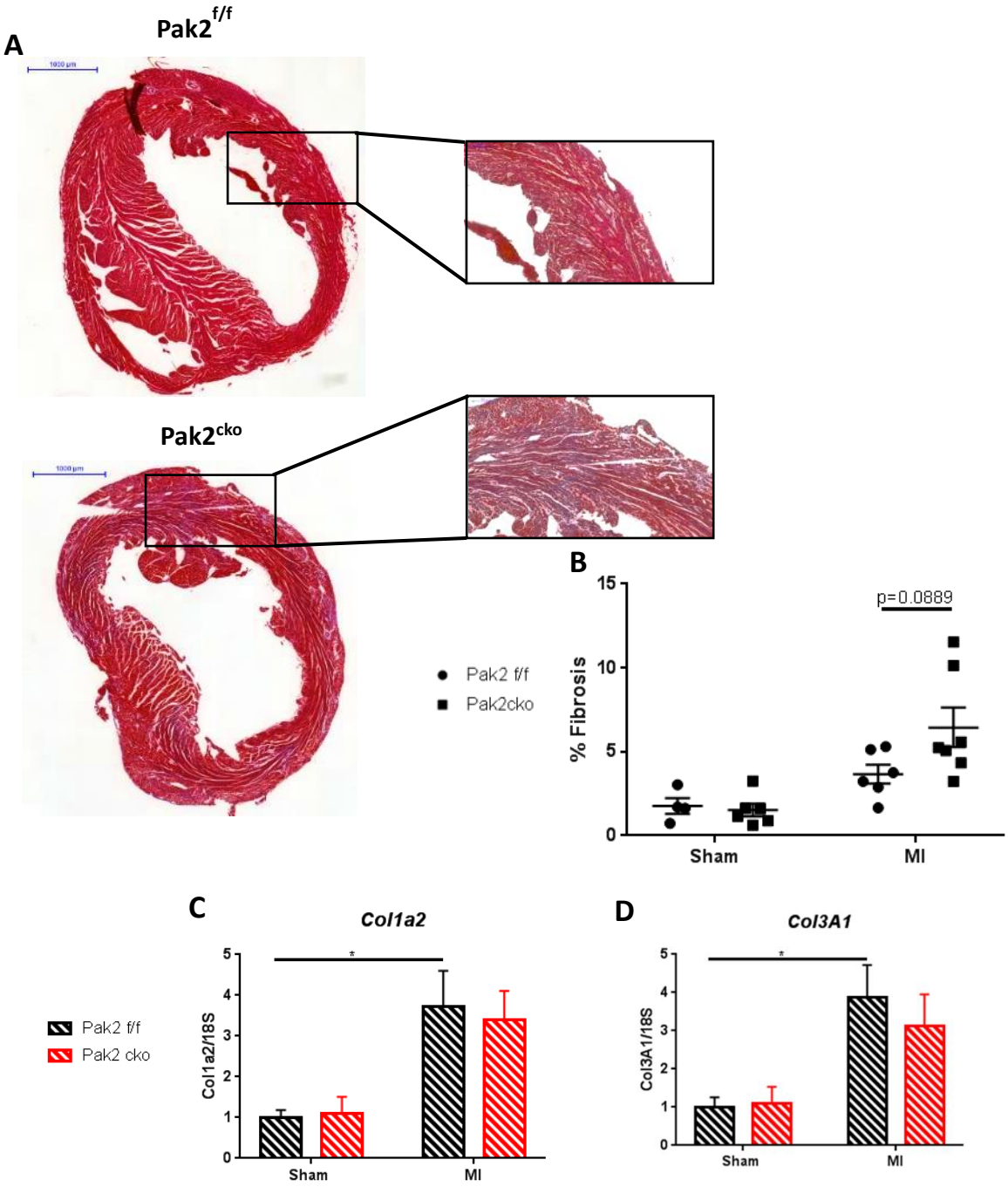

Figure 3.15 At two days following MI loss of cardiac Pak2 appeared to increase levels of fibrosis. (A-B) Representative images of masson's trichrome staining of hearts from Pak2$^{f/f}$ and Pak2^{cko} mice after two days MI and quantification of percentage of the heart stained positive for fibrosis. There was a strong trend suggesting increased fibrosis in the hearts of Pak2^{cko} mice after MI. Scale bar in top left of Masson's trichrome images represents 1000µm. **(C-D)** qPCR analysis showed a three- to four-fold increase in expression of collagen I (*Col1a2*) and collagen 3 (*Col3A1*) in the hearts of MI mice compared to sham controls. All expression analysis was normalised to the housekeeper gene 18S. n=4-7 for each group. * represents p<0.05. Two-way ANOVA followed by Tukey's multiple comparison test.

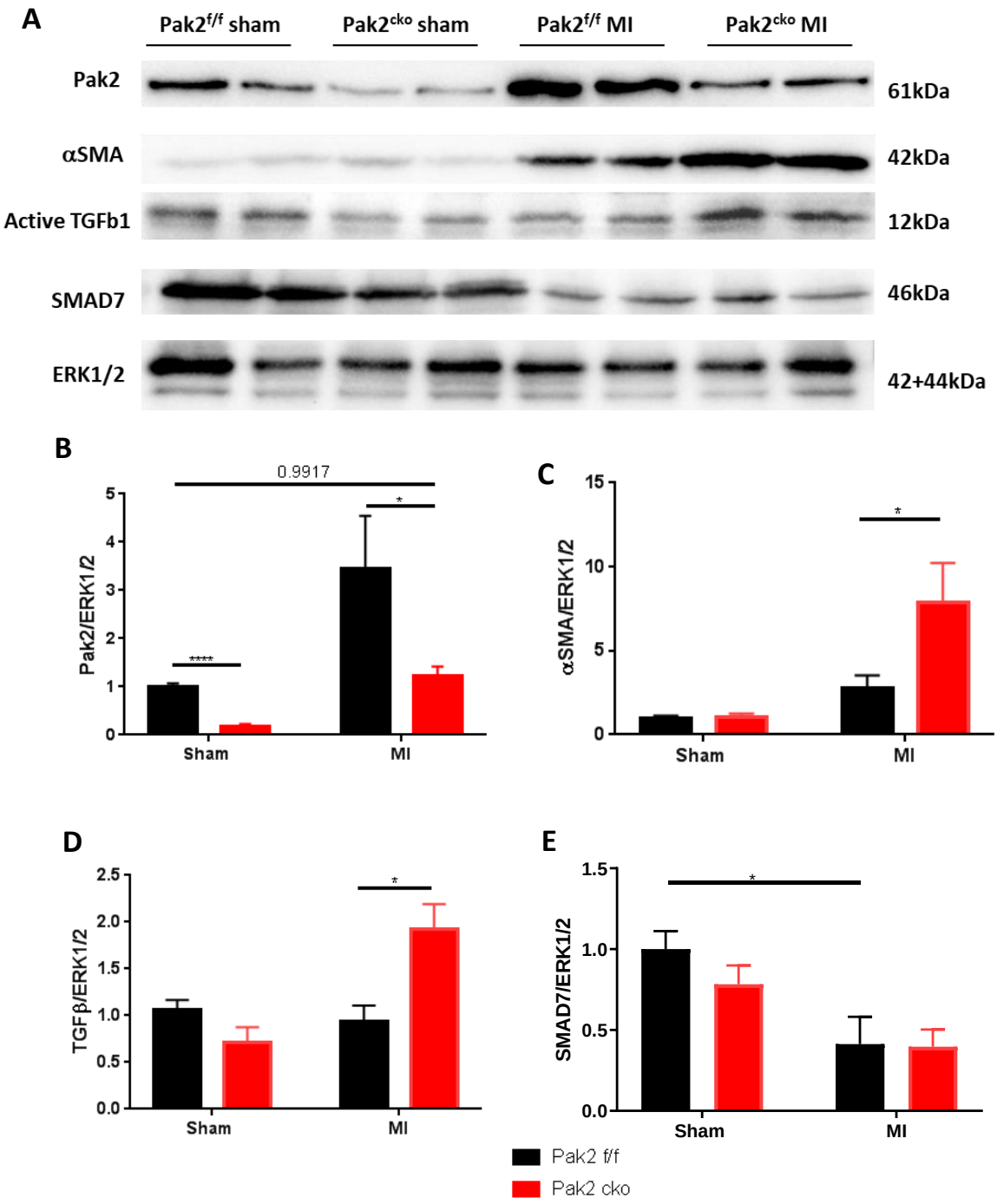

Figure 3.16 Pro-fibrotic markers are significantly increased in Pak2^{cko} mice after MI. (A) Representative western blot images of cardiac proteins involved in fibrosis. ERK1/2 was used as a loading control. **(B)** Increased protein levels of Pak2 were evident after MI, even in Pak2^{cko} mice. **(C)** Protein levels of αSMA, a marker of myofibroblasts, were significantly increased in Pak2^{cko} mice after MI compared to Pak2$^{f/f}$ mice. **(D)** TGFβ signalling was increased in Pak2^{cko} mice after MI. **(E)** Protein levels of SMAD7, an anti-fibrotic marker, were reduced in both MI groups compared to sham controls. N=4-6 for each group. * represents $p<0.05$. Two-way ANOVA followed by Tukey's multiple comparison test.

3.6.5 Pak2 loss did not alter the increased inflammatory response post-acute MI

Infiltration of inflammatory cells into the heart is a hallmark of MI. It was important to verify that this inflammation was caused by this model of MI, and to assess whether cardiomyocyte-specific loss of Pak2 alters this response.

CD68 is a protein that is highly expressed on monocytes, and it is often used as a marker for macrophages. Immunohistochemistry for CD68 revealed a significant increase in the number of CD68-positive cells in the hearts of mice subjected to MI compared to sham controls, with around double the number of these cells evident per mm^2 (Figure 3.17A-B). No genotype-specific difference was observed.

Levels of circulating cytokines in the heart were assessed through quantitative PCR since levels of these molecules are too low to detect changes by western blot. As expected, transcripts of *IL6* and *IL1*β, two pro-inflammatory cytokines, were significantly increased in MI hearts but were not impacted by the loss of Pak2 in cardiomyocytes (Figure 3.17C-D).

These findings verify that levels of inflammation and infiltration of inflammatory cells have increased following MI. There is no evidence to suggest that loss of Pak2 in cardiomyocytes affects the inflammatory response.

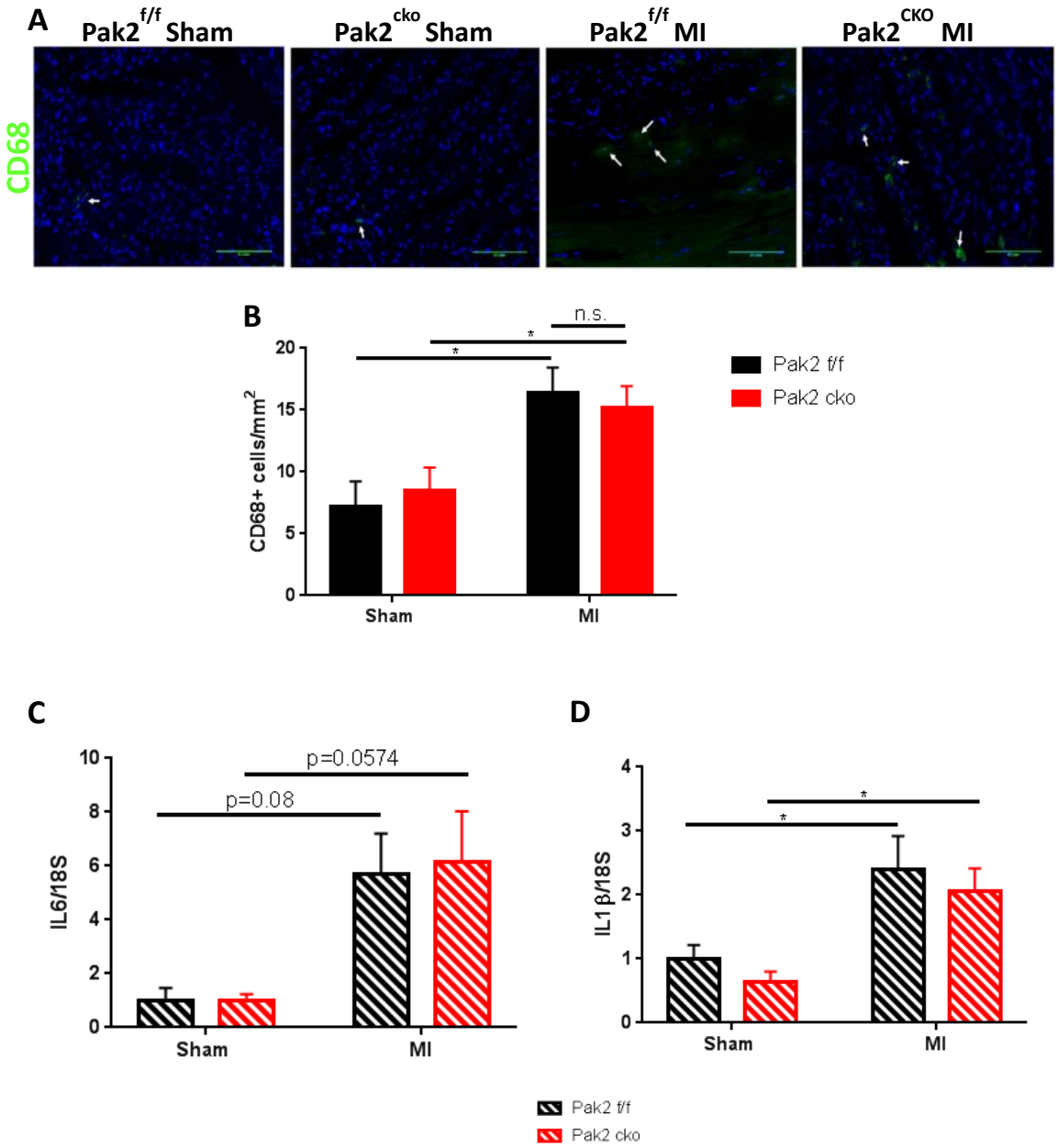

Figure 3.17 Myocardial infarction leads to increased inflammation in the heart. (A-B) Representative images of CD68 immunohistochemistry and quantification showed increased numbers of CD68-positive cells (green) in the hearts of MI mice, but no difference between genotypes. DAPI staining (blue) allowed identification of individual nuclei. White arrows indicate CD68-positive cells. Scale bar in bottom right of images represents 0.1mm. qPCR analysis of inflammatory markers *IL6* **(C)** and *IL1β* **(D)** showed increased cytokine expression in the heart after MI compared to sham controls. All expression analysis was normalised to the housekeeper gene 18S. n=4-6 for each group. n.s represents no significance. * represents $p<0.05$. Two-way ANOVA followed by Tukey's multiple comparison test.

3.6.6 Expression of downstream molecules of the ER stress response were altered in Pak2^{cko} mice

The ER stress response is comprised of three main pathways: the ATF6 pathway, the IRE1 pathway, and the PERK pathway. Previous research has identified that Pak2 is cardioprotective through its ability to modulate the ER stress response, in particular the IRE1 branch, with reduced IRE1 phosphorylation and splicing of its downstream target XBP1 found to occur in Pak2^{cko} mice during the development of CH and progression to HF (Binder *et al.*, 2019). It was important to elucidate whether the same occurs in Pak2^{cko} mice following MI, considering that, although they share many similarities in their outcome, they are triggered by very different stimuli.

Western blot analysis of cardiac tissue from mice two days following MI provided inconclusive results on what branch of the ER stress pathway Pak2 affects during MI (Figure 3.18). There was no clear difference between the Pak2$^{f/f}$ and Pak2^{cko} mice following MI regarding protein levels of cleaved ATF6, phosphorylated IRE1, nor the downstream effector of the PERK pathway, phosphorylated EIF2α (Figure 3.18B-D). However, Pak2^{cko} mice after MI had increased cardiac protein levels of Chop, a downstream pro-apoptotic effector of the ER stress response. This demonstrates that the UPR has been activated, and that one or more of these branches have been affected by loss of Pak2 in cardiomyocytes (Figure 3.18E). However, two days after MI the upstream effects of Pak2^{cko} on the ER stress response are no longer detectable.

As well as being involved in canonical ER stress pathways through which it can cleave XBP1, promoting an adaptive cellular response, IRE1 is also a regulator of regulated IRE1-dependant decay of mRNA (RIDD) which is often viewed as detrimental to cell survival. Six RIDD substrates which are commonly used as markers for this highly conserved process were assessed using qPCR – *col6a1*, *hgsnat, scara3, pdgfrb*, *pmp22*, and *bloc1s1* (Hollien *et al.*, 2009; Maurel *et al.*, 2014) (Figure 3.19). mRNA levels of four of these substrates were unaffected by MI. However, *hgsnat* and *pmp22* mRNA levels were elevated 2.5- and 3-fold, respectively, in Pak2$^{f/f}$ controls following MI compared to sham controls. Interestingly, this elevation in mRNA levels of these two RIDD substrates was not evident in Pak2^{cko} mice, suggesting that there is the possibility that their mRNAs are degraded, potentially via augmented RIDD due to Pak2 disruption.

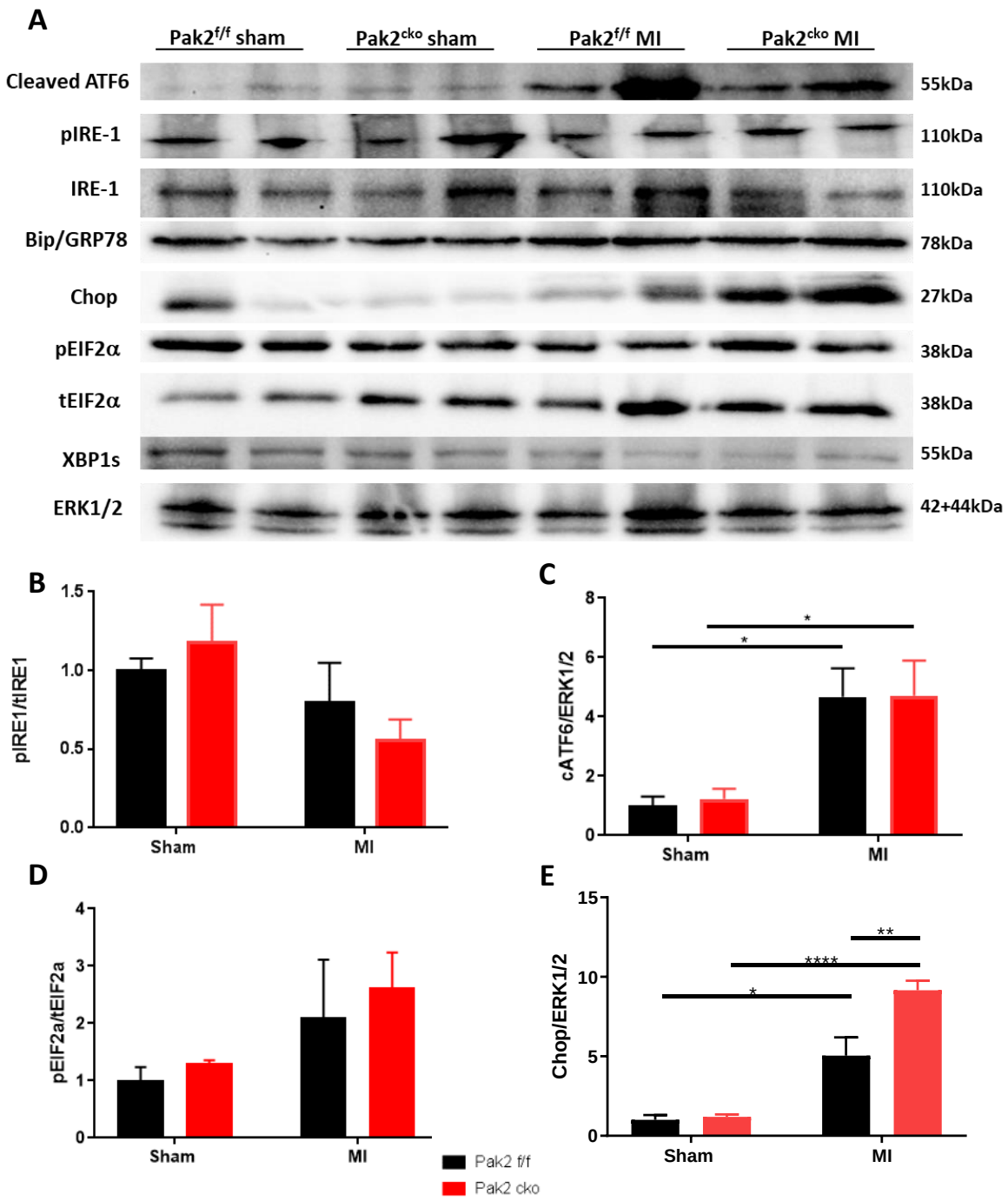

Figure 3.18 Downstream ER stress effectors are increased in hearts from Pak2^{cko} mice after MI but it is unclear through which pathway this has occurred. (A) Representative western blots of ER stress-related molecules. ERK1/2 was used as a loading control. There were no clear changes in phosphorylated IRE1 **(B)**, cleaved ATF6 **(C)** or pEIF2α **(D)**, a downstream molecule of the PERK pathway, between Pak2^{cko} mice and Pak2$^{f/f}$ mice after MI. However, Pak2^{cko} mice had significantly elevated protein levels of Chop **(E)**, a downstream effector of the ER stress pathways, after MI. N=4-6 per group. * represents $p<0.05$. ** represents $p<0.01$. Two-way ANOVA followed by Tukey's multiple comparison test.

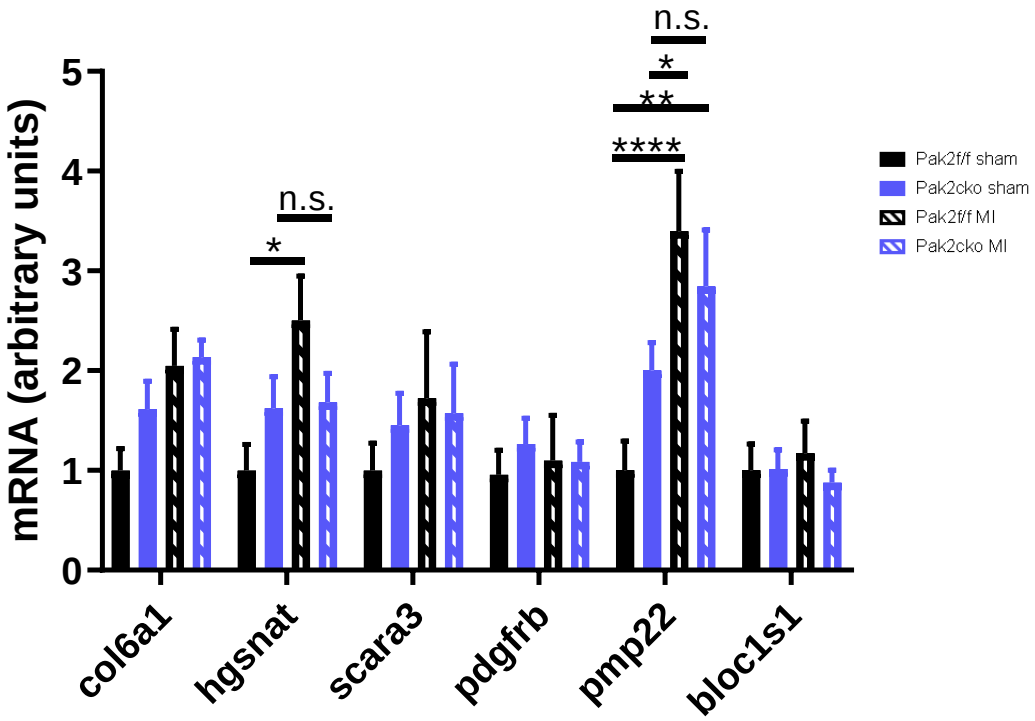

Figure 3.19 The RIDD process may be activated by loss of Pak2. qPCR analysis of six common RIDD substrates in two-day MI tissue samples showed that some, such as *hgsnat* and *pmp22*, are upregulated after MI, whilst others are unaffected. Of the two that were upregulated, loss of Pak2 lessened or prevented the elevation in mRNA levels following MI, suggesting the potential that loss of Pak2 may lead to activation of the RIDD process, resulting in mRNA cleavage and degradation. N=4-6. N.s. = no significant difference. * represents $p<0.05$. ** represents $p<0.01$. **** represents $p<0.0001$. Two-way ANOVA followed by Tukey's multiple comparison test.

3.6.7 Loss of Pak2 in the heart exacerbates cell death after MI

At two days following MI $Pak2^{cko}$ mice which had undergone the severe MI procedure had significantly greater levels of cardiomyocytes undergoing cell death compared to $Pak2^{f/f}$ mice which had experienced the same procedure. This was demonstrated using multiple techniques.

Two days after MI, TUNEL staining demonstrated that $Pak2^{cko}$ mice had significantly ($p<0.01$) more TUNEL-positive cardiomyocytes in the remote regions of the heart compared to $Pak2^{f/f}$ mice (Figure 3.20). This difference was not found between the sham groups.

Molecular analysis supported this finding and demonstrated that this was due to increased levels of apoptotic cardiomyocytes in the hearts of $Pak2^{cko}$ mice after MI. Western blot analysis of cell death markers revealed that, following MI, $Pak2^{cko}$ mice had significantly ($p=0.028$) greater protein levels of pro-apoptotic Bax protein normalised to pro-survival Bcl-2 protein (Figure 3.21A-B). Bax is a crucial regulator of apoptosis since it is important in the opening of the mitochondrial permeability pore leading to release of mitochondrial-sequestered pro-apoptotic factors such as cytochrome C and AIF, and it has also been shown to promote necrosis (Whelan *et al.*, 2012). Furthermore, there was also a trend ($p=0.0712$) showing increased protein levels of cleaved caspase 7 in the hearts of $Pak2^{cko}$ mice after MI compared to $Pak2^{f/f}$ mice (Figure 3.21C). Cleavage of caspase 7 is a final stage of apoptosis, with cleaved caspase 7 acting as an executioner caspase alongside cleaved caspase 3.

Hence, these findings indicate that $Pak2^{cko}$ mice have significantly greater levels of apoptosis in the heart after MI compared to $Pak2^{f/f}$ mice, demonstrating that loss of Pak2 augments the cell death response.

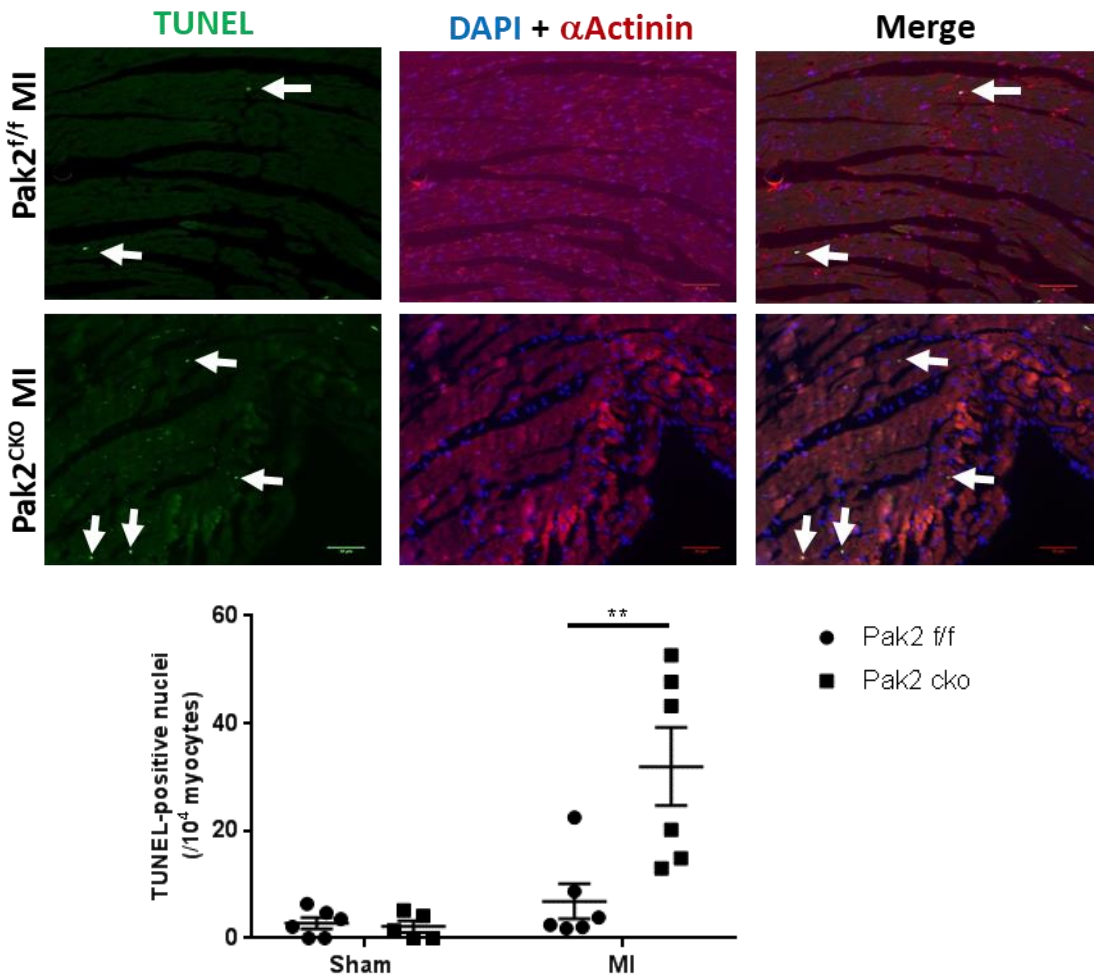

Figure 3.20 Pak2 protects against cell death following MI. Representative TUNEL staining and quantification. Sections were triple stained with TUNEL (green), to identify cells undergoing cell death, DAPI (blue), to identify individual nuclei, and α-actinin (red), to mark for cardiomyocytes. Pak2^{cko} mice after MI had significantly greater levels of TUNEL-positive cells, indicating cells undergoing cell death, in the remote regions of the heart, compared to Pak2$^{f/f}$ mice. White arrows indicate TUNEL-positive nuclei. Scale bar in bottom right of image represents 50µm. ** represents $p<0.01$. n=5-6 for each group. Two-way ANOVA followed by Tukey's multiple comparison test.

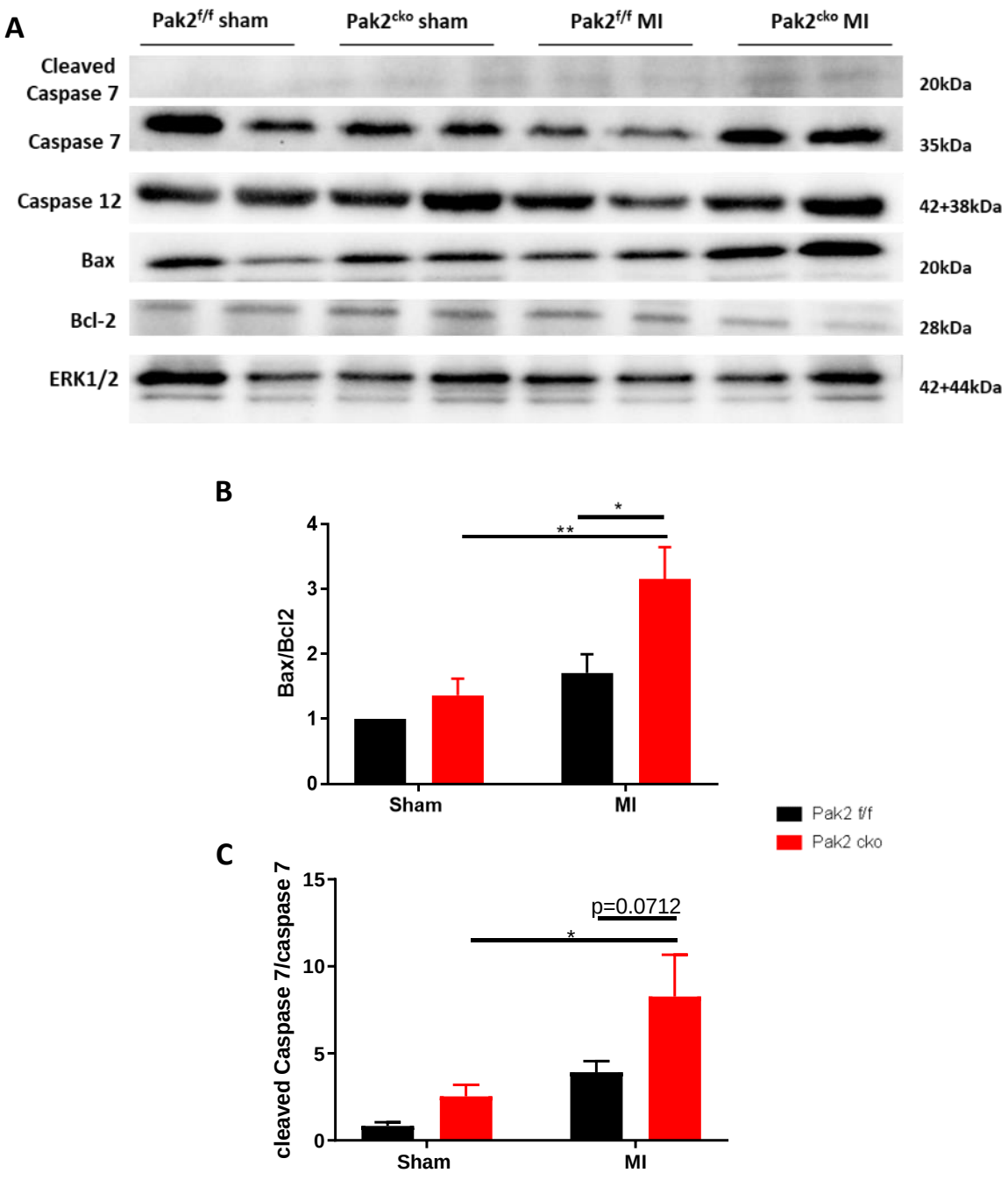

Figure 3.21 Knockout of Pak2 augments apoptosis following MI. (A) Representative western blot images of cell death-related proteins in cardiac tissue from sham and MI mice two days after surgery. ERK1/2 was used as a loading control. After MI, Pak2^{cko} mice had elevated protein levels of pro-apoptotic molecules Bax, normalised to pro-survival Bcl-2 **(B)**, and cleaved caspase 7, normalised to total levels of caspase 7 **(C)**. N=4-6 per group. * represents $p<0.05$. Two-way ANOVA followed by Tukey's multiple comparison test.

3.6.8 Oxidative stress is evident two days following MI induction

Oxidative stress occurs due to a disturbance in the balance between production of reactive oxygen species (ROS) and their detoxification by antioxidants. This imbalance in the redox state can have toxic effects on cellular responses and lead to cell death due to free radical-mediated damage of proteins, lipids, and DNA. High levels of oxidative stress are known to occur during I/R injury once blood flow has been restored following MI (González-Montero *et al.*, 2018). It was important to determine whether there was evidence for oxidative stress following permanent coronary occlusion where there is no effort to re-perfuse the hearts, since some reperfusion may still occur due to angiogenesis, leading to oxidative stress. Furthermore, changes in other cellular processes, including ER stress, can result in oxidative stress (Burgos-Morón *et al.*, 2019).

Two days following MI there was a significant 25 % increase in the intensity of staining for dihydroethidium (DHE), a fluorescent probe that can detect ROS generation, in the hearts of mice subjected to MI compared to their sham controls (Figure 3.22A-B). In the presence of ROS DHE is converted to ethidium, which in turn binds to nucleic acid, staining it as a fluorescent probe allowing for relative intensity to be measured.

Furthermore, qPCR analysis of SOD2 demonstrated a potential reduction in superoxide dismutase (*SOD2)* expression in both the $Pak2^{f/f}$ and $Pak2^{cko}$ mice after MI (Figure 3.22C). SOD2 is an enzyme that converts superoxide (O_2^-) into hydrogen peroxide (H_2O_2) which can then be further converted into water (H_2O). By doing this SOD2 can clear reactive oxygen species and therefore reduce the potential for DNA damage and cell death. Therefore, reduced expression of *SOD2* in MI mice shows a reduced capability to manage the redox state, and hence demonstrates oxidative stress is transpiring.

These findings demonstrate that cellular levels of ROS have increased, and the ability of cells to respond to ROS has decreased in the acute phase following MI.

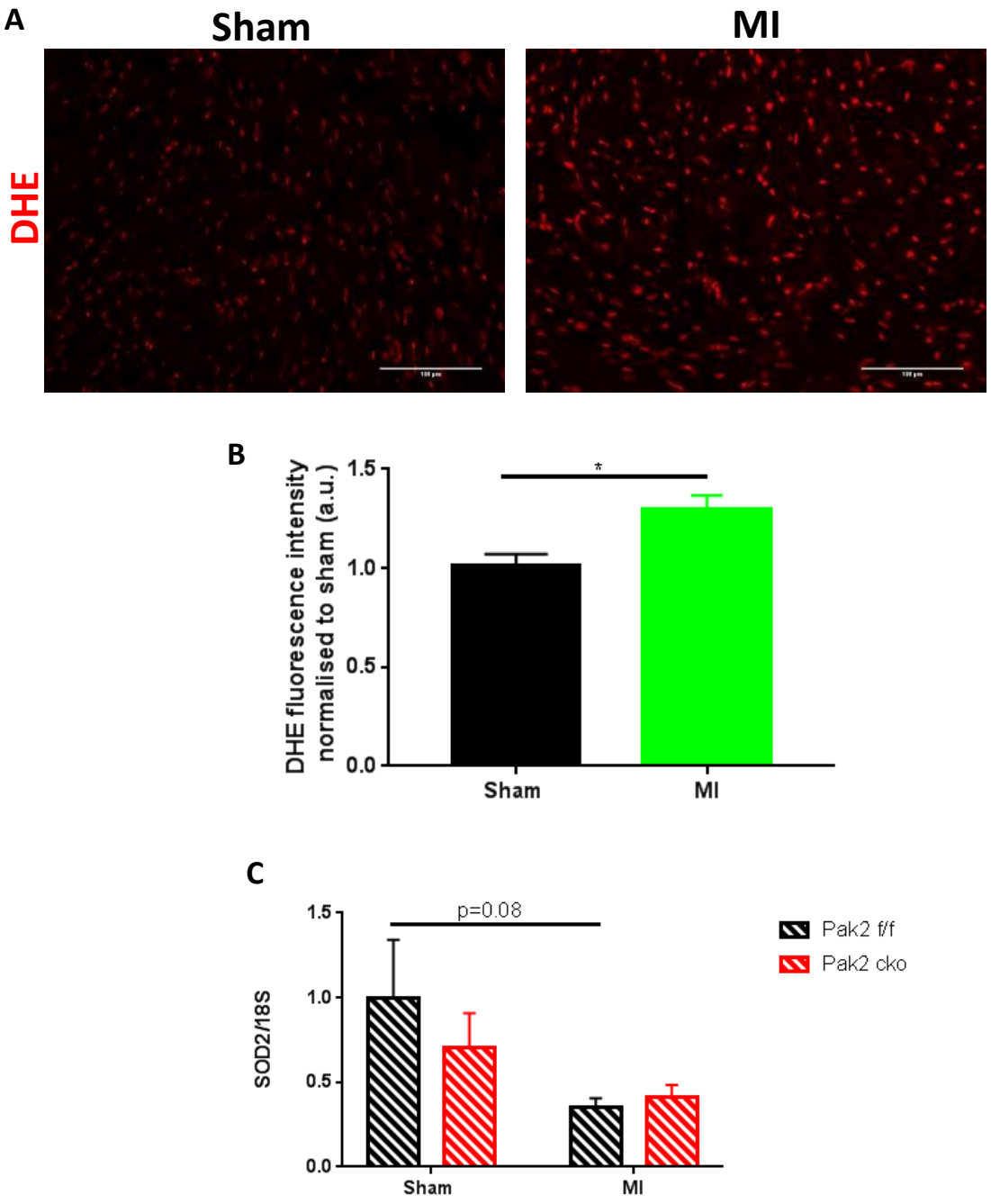

Figure 3.22 Oxidative stress is evident two days after initiation of MI. (A-B) Representative images of DHE immunofluorescent staining, and its quantification, demonstrated a significant 25% increase in fluorescent intensity in hearts two days after MI induction compared to sham controls. Scale bar in bottom right of DHE images represents 100µm. **(C)** A trend suggesting a reduction in *SOD2* expression, an enzyme responsible for ROS processing, was evident in hearts after two days MI. Expression analysis was normalised to the housekeeper gene 18S. N=5-6 for each group. * represents $p<0.05$. Figure B was analysed using an unpaired two-tailed t-test; figure C was analysed using a two-way ANOVA followed by Tukey's multiple comparison test.

3.7 Brief summary

The data presented in this chapter demonstrate that Pak2 is activated in the acute phase following myocardial infarction. Loss of Pak2 does not appear to affect cardiac function by two weeks following MI. However, knockout of Pak2 in cardiomyocytes leads to accelerated deposition of fibrotic material in the heart, an altered ER stress response, and elevated cardiomyocyte apoptosis following MI.

Chapter 4: Results 2: Pak2's role in cardiomyocyte survival following MI-related events *in vitro*

During MI cardiomyocytes are exposed to numerous stressors due to the loss of blood flow caused by coronary artery occlusion. For instance, occlusion prevents the supply of oxygen, thus impeding cellular metabolic activities, as well as the supply of nutrients such as glucose and amino acids. Additionally, as shown in Chapter 3, some reoxygenation occurs following MI, potentially due to angiogenesis, and this can lead to increased production of ROS and oxidative stress.

Evidence from Chapter 3 demonstrated that Pak2 becomes activated in the acute stages following MI and protects cardiomyocytes from MI-induced apoptosis. This chapter will use *in vitro* techniques to further identify the mechanism through which Pak2 is cardioprotective. Use of *in vitro* models will allow for the assessment of the impact of specific cellular stressors on Pak2 in cardiac cells. The ease of cellular manipulation *in vitro* enables greater investigation into the mechanism through which Pak2 may exert its cardioprotective effects which were not able to be elucidated in an *in vivo* model. This will address aim 3 of this project.

4.1 Knockdown of Pak2 was achieved using Ad-shPak2 and si-Pak2

A previously generated adenovirus containing short hairpin RNA (shRNA) complementary for Pak2 (Ad-shPak2) was successfully amplified and titrated alongside a negative control virus (Ad-shControl). Short hairpin RNA causes targeted gene silencing by RNA interference through a mechanism similar to that of micro-RNAs (miRNAs). Once integrated into the host genome, the shRNA is transcribed, processed by ribonucleases and incorporated into an RNA-induced silencing complex (RISC). The complementarity of the shRNA to its target guides the RISC to the mRNA of the gene of interest, where it is cleaved leading to gene silencing. The titre of the Ad-shControl was $2.62x10^{12}$ pfu/mL, and $6.55x10^{11}$ pfu/mL for Ad-shPak2. Both viruses were used at an MOI of 25. This led to a 60 % reduction ($p<0.001$) in Pak2 expression after 48 hours in H9c2 cardiomyoblasts treated with Ad-shPak2 compared to those exposed to the Ad-shControl virus (Figure 4.1A-B).

An alternative method for knockdown of Pak2 *in vitro* was transfection with Pak2 small interfering RNA (siRNA) for 48 hours. siRNA regulates gene expression through RNA interference. Like shRNAs, siRNAs function similarly to that of miRNAs; upon transfection into cells, an siRNA complexes with the RISC. RISC-siRNAs can bind to target mRNAs through sequence complementarity and promote their degradation through inducing mRNA cleavage. This prevents translation of the target gene, in this case Pak2. Transfection of siPak2 successfully produced a 75 % reduction ($p<0.01$) in Pak2 expression in H9c2 cells compared to cells transfected with a control siRNA encoding a scrambled mRNA sequence (Figure 4.1C-D).

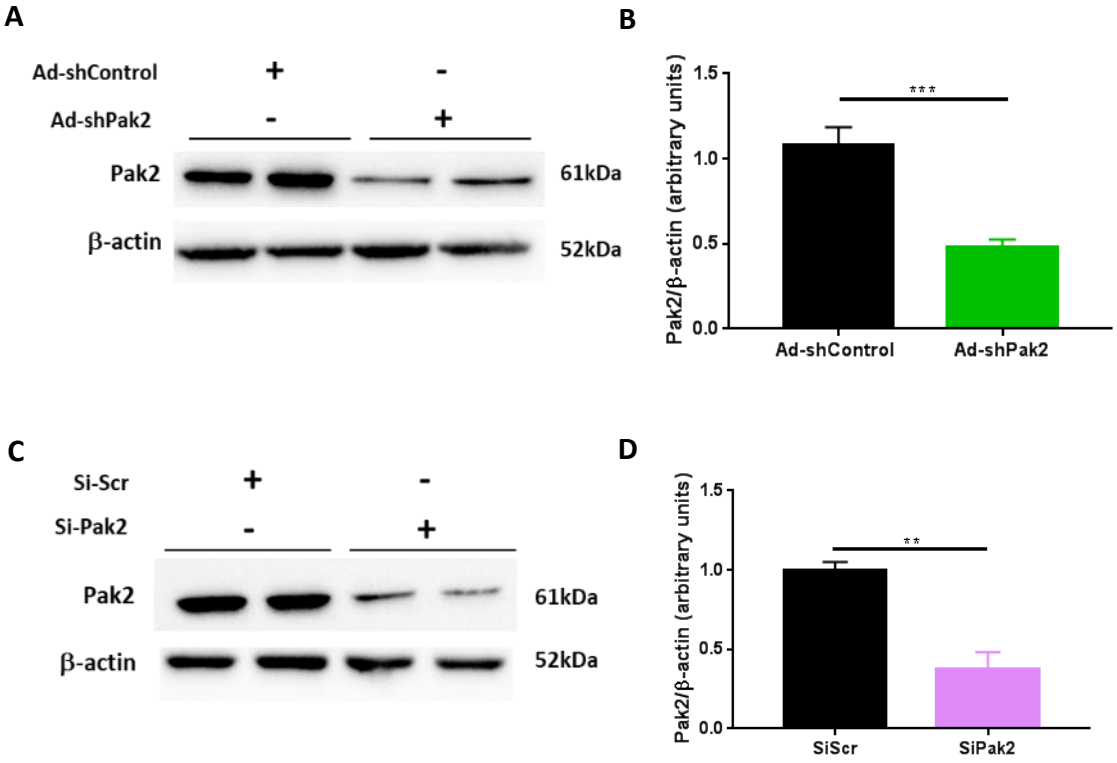

Figure 4.1 Verification of Pak2 knockdown by Ad-shPak2 and si-Pak2. (A-B) Representative western blots showing knockdown of total Pak2 protein by 60% in H9c2 cells following 48-hour treatment with Ad-shPak2 compared to Ad-shControl. **(C-D)** Representative western blots showing knockdown of total Pak2 protein by 75% in H9c2 cells following 48-hour transfection with si-Pak2 compared to control cells transfected with si-Scrambled (Si-Scr). β-actin was used as a loading control. n=4 for each group. ** represents $p<0.01$. *** represents $p<0.001$. Unpaired two-tailed t-test.

4.2 Hypoxia alone is not sufficient to cause significant Pak2 activation

4.2.1 Initiation of hypoxia signalling was verified by upregulation of hypoxia-related molecules

H9c2 cardiomyoblasts were exposed to 100 % nitrogen (N_2) in a Billups-Rothenberg modular hypoxia chamber at a flow rate of 10l/min to reproduce hypoxia and the activation of signalling cascades. To verify that hypoxia signalling had been initiated, protein levels of HIF1α, a hypoxia-related protein, were analysed by western blot.

The transcription factor HIF-1 (Hypoxia-inducible factor 1) is composed of two subunits, HIF1α and HIF1β. Whilst HIF1β is constitutively expressed, under normoxic conditions HIF1α is targeted for degradation. HIF1α is oxygen regulated; upon detection of hypoxic conditions, for instance in cardiomyocytes during MI, HIF1α is upregulated and stabilised (Wei *et al.*, 2010; X. Wang *et al.*, 2012). This allows interaction between the two subunits, enabling HIF-1 to mediate the effect of hypoxia on the cell. Hence, HIF1α is used to verify that hypoxia-related signalling has been initiated. HIF1α was significantly upregulated ($p<0.05$) two hours after incubation of H9c2 cardiomyoblasts in the Billups-Rothenberg modular hypoxia chamber (Figure 4.2), demonstrating that this is a suitable model of hypoxia.

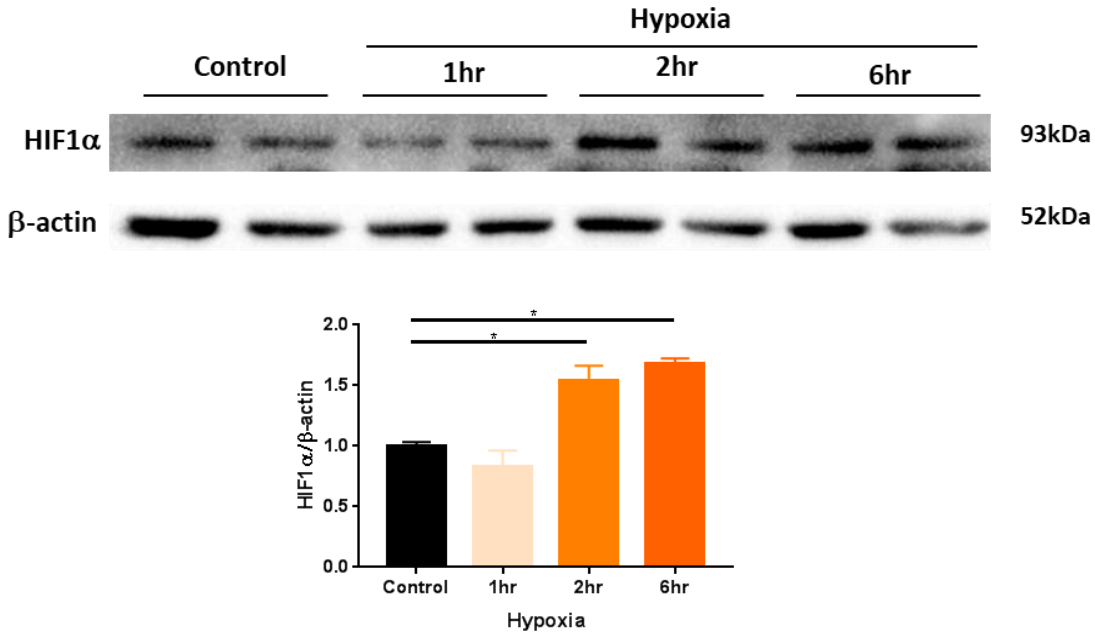

Figure 4.2 HIF1α, a marker of hypoxic signalling, is activated two hours after incubation of H9c2 cells in hypoxic conditions. Representative western blots and quantification. β-actin was used as a loading control. N=2 for each group. * represents $p<0.05$. Kruskal-Wallis test followed by Dunn's multiple comparisons test.

4.2.2 There is no obvious activation of Pak2 *in vitro* following hypoxia alone

During MI, the loss of blood flow downstream of the blockage or ligation point results in loss of oxygen supply to cardiomyocytes. As such, it was important to ascertain whether Pak2 becomes activated in hypoxic conditions and, if so, whether this could explain the level of Pak2 activation evident in mouse hearts two days following MI.

Cultured H9c2 cells were exposed to hypoxic conditions for 1 hour, 2 hours and 6 hours in standard DMEM media containing 4.5 % glucose and 10 % FBS. Control H9c2 cells were incubated at normoxic conditions. Protein levels of Pak2 and its activated form, phosphorylated Pak2, were assessed via western blot (Figure 4.3). There was no clear Pak2 activation caused by hypoxia. Levels of phosphorylated Pak2, normalised to total Pak2 seemed to increase, but not significantly, after two hours incubation in hypoxic conditions. However, there was a high level of variability, with large error bars representing a standard error of the mean of 0.6698.

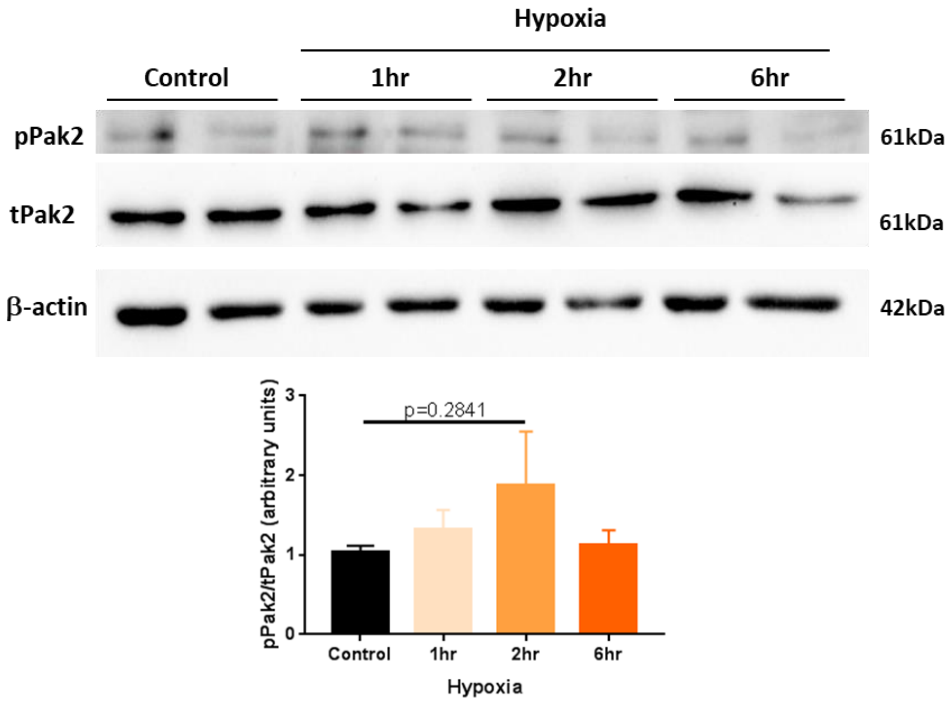

Figure 4.3 There is no clear Pak2 activation after incubation of H9c2 cells in hypoxic conditions. Representative western blots of phosphorylated Pak2 (pPak2) and total Pak2 (tPak2). pPak2 levels were normalised against tPak2. There was no significant change in Pak2 activation in H9c2 cardiomyoblasts after exposure to hypoxic conditions for 1 hour, 2 hours of 6 hours. β-actin was used as a loading control. N=6. Kruskall-Wallis test followed by Dunn's multiple comparison test.

4.2.3 Hypoxia leads to activation of some, but not all, ER stress response pathways

Despite Pak2 not clearly being activated by hypoxia alone, it was important to assess how pathways of interest are altered by this stress as it may indicate why Pak2 may not play a role during this form of cellular stress. ER stress and cell death related pathways were screened via western blot to assess how they respond to hypoxia (Figure 4.4).

By two hours after exposure of H9c2 cells to hypoxic conditions (100 % N_2), there was evidence for activation of the ATF6 and PERK pathways of the ER stress response. Upon activation, ATF6 translocates from the ER membrane to the Golgi apparatus where it undergoes selective proteolysis by site-1 and site-2 protease. This cleavage produces an ATF6 fragment, here termed cleaved ATF6, which translocates to the nucleus to influence gene expression (Hillary and Fitzgerald, 2018). Two hours after induction of hypoxia, there was a trend ($p=0.0518$) showing increased cleavage of ATF6 by around 50 % (Figure 4.4B). A second branch of the UPR involves the protein PERK. Dissociation of the chaperone Bip during ER stress allows for PERK oligomerisation and trans-autophosphorylation, rendering it active. This enables it to phosphorylate its downstream target EIF2α (Teske *et al.*, 2011). Following exposure of H9c2 cardiomyoblasts to hypoxic conditions, western blot analysis revealed protein levels of phosphorylated EIF2α (pEIF2α) were significantly ($p<0.01$) raised four-fold after two hours hypoxia, and were raised to an even greater extent, to almost six-fold basal levels ($p<0.001$), after exposure to hypoxic conditions for six hours (Figure 4.4C). The final branch of the ER stress response involves the protein IRE1, which Pak2 has previously been shown to act through under stress conditions. Like PERK, upon ER stress-mediated dissociation of Bip from IRE1, it oligomerises and trans-autophosphorylates, becoming active. In H9c2 cells exposed to hypoxic conditions there did not appear to be any change in the level of IRE1 phosphorylation at any of the timepoints tested (Figure 4.4D).

To assess whether hypoxia leads to cell death, protein levels of cleaved caspase 7 were assessed and normalised to total caspase 7 protein levels. Caspase 7 is an effector caspase in the apoptotic response. It works alongside caspase 3 to bring about the cellular and morphological changes that occur during apoptosis. As an executioner caspase, caspase 7 activation via its cleavage represents the irreversible cell decision to

undergo apoptosis, and as such can be used to assess cells that are undergoing apoptosis. Levels of cleaved caspase 7 appeared to be unchanged in H9c2 cardiomyoblasts exposed to hypoxia for one- and two-hours hypoxia. However, after exposure to hypoxic conditions for six hours, levels of cleaved caspase 7 were significantly increased ($p<0.05$) by around 300 % (Figure 4.4E).

These findings demonstrate that the UPR and cell death pathways are activated during hypoxia despite no activation of Pak2 though interestingly the IRE1 branch, through which Pak2 has previously been shown to act, did not appear to be activated in the time points tested.

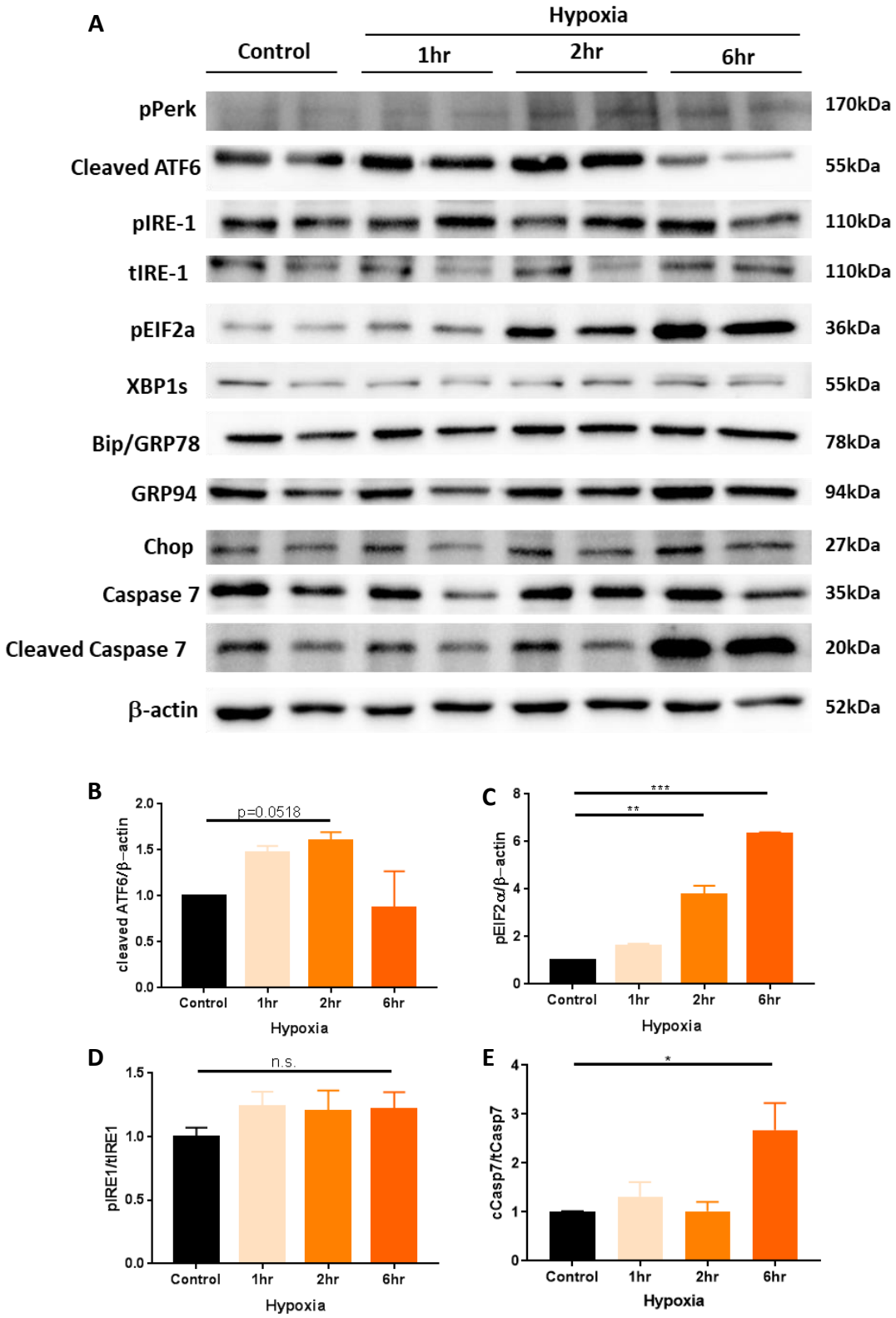

Figure 4.4 Assessment of changes to ER stress and cell death pathways in cells exposed to hypoxic (100% N_2) conditions. Representative western blots **(A)** and quantification **(B-E)** of ER stress-related and cell death-related proteins. β-actin was used as a loading control. pIRE1 = phosphorylated IRE1; tIRE1 = total IRE1; pEIF2α = phosphorylated EIF2α; pPerk = phosphorylated PERK; cCasp7 = cleaved caspase 7; tCasp7 = total caspase 7. N=4-6. * represents p<0.05. ** represents p<0.01. *** represents p<0.001. One-way ANOVA followed by Tukey's multiple comparisons test.

4.3 Pak2 modulation alters the ER and cell death response following combined hypoxia and nutrient starvation in vitro

4.3.1 Pak2 is activated *in vitro* following combined hypoxia and nutrient starvation

During MI, loss of blood flow downstream of the blockage not only prevents oxygen supply to downstream cardiomyocytes, but also supply of nutrients and glucose. To mimic these conditions *in vitro*, H9c2 cardiomyoblasts were incubated in media containing 0g/l glucose and no foetal bovine serum (FBS). Cells were then incubated in a hypoxia chamber that had been filled with 100 % N_2.

Protein levels of Pak2 and phosphorylated Pak2 were assessed via western blot in cells that had been nutrient-deprived and oxygen starved for 1 hour, 2 hours and 6 hours (Figure 4.5). Total Pak2 levels did not change over this time. Phosphorylated Pak2 was significantly increased two-fold in H9c2 cells after two hours of nutrient and oxygen starvation compared to control cells which had been incubated concurrently in normoxic conditions in media containing 4.5g/l glucose and 10 % FBS.

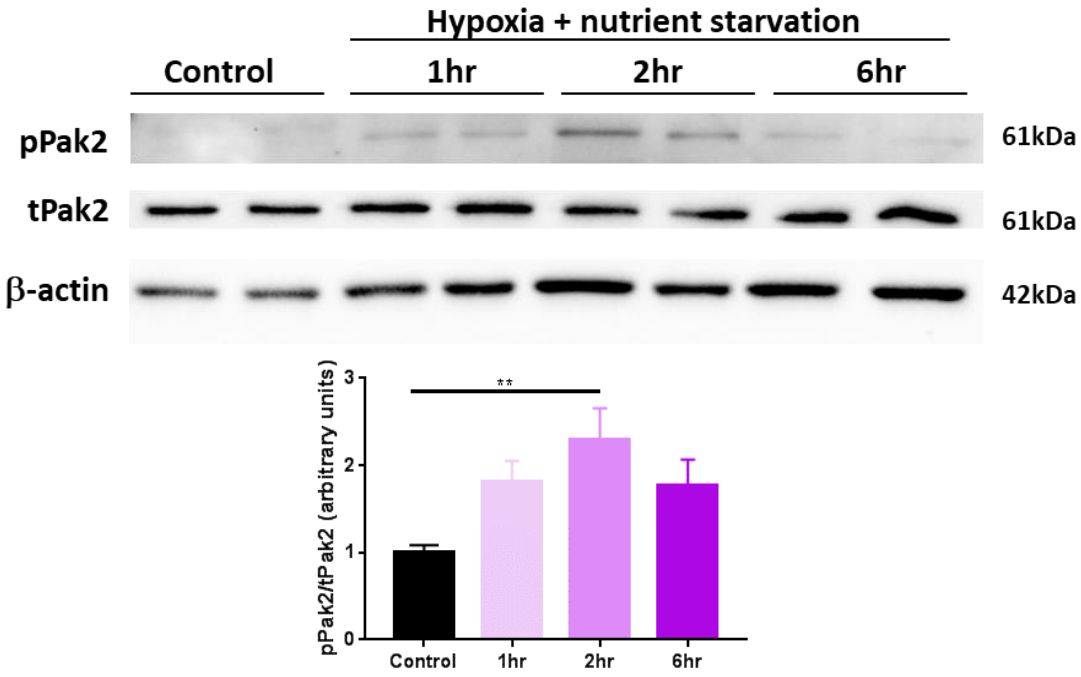

Figure 4.5 Pak2 was activated in H9c2 cells after two hours exposure to hypoxic conditions and nutrient starvation. Representative western blots of phosphorylated Pak2 (pPak2) and total Pak2 (tPak2), using β-actin as a loading control. pPak2 levels were normalised against tPak2. N=4. ** represents $p<0.01$. One-way ANOVA followed by Dunnett's multiple comparison test.

4.3.2 Combined, hypoxia and nutrient starvation activate the ER stress and cell death responses

ER stress and cell death related pathways were screened to assess how they are altered by combined hypoxia and nutrient starvation (Figure 4.6). Cells were incubated in serum-free media containing no glucose and exposed to hypoxic conditions in a Billups-Rothenberg modular incubator chamber for 1 hour, 2 hours or 6 hours. Control cells were incubated in normal media containing 4.5g/L glucose and 10 % foetal bovine serum and kept at normoxic conditions.

Combined hypoxia and nutrient starvation led to activation of all 3 branches of the ER stress response (Figure 4.6B-D), including the IRE1 branch which was not activated by hypoxia alone. This activation of the IRE1 branch was confirmed by assessing levels of spliced XBP1 which lies downstream of IRE1; this too was increased following hypoxia and nutrient starvation (Figure 4.6E). The downstream effector of PERK, phosphorylated EIF2α, was used as a proxy for activation of the PERK pathway. Protein levels of the pro-apoptotic effector molecule Chop was also found to be elevated during hypoxia and nutrient starvation (Figure 4.6F). Interestingly, this stress did not appear to alter protein levels of two ER chaperones, Bip and GRP94, within the 6 hour timeframe used in this experiment.

Cell death was induced by loss of oxygen and nutrient supply, with significant activation of the executioner caspase caspase 7 evident after 6 hours (Figure 4.6G). However, there were no significant change in the ratio of pro-apoptotic Bax protein to pro-survival Bcl-2 (Figure 4.6H), both of which are involved in the intrinsic apoptotic pathway.

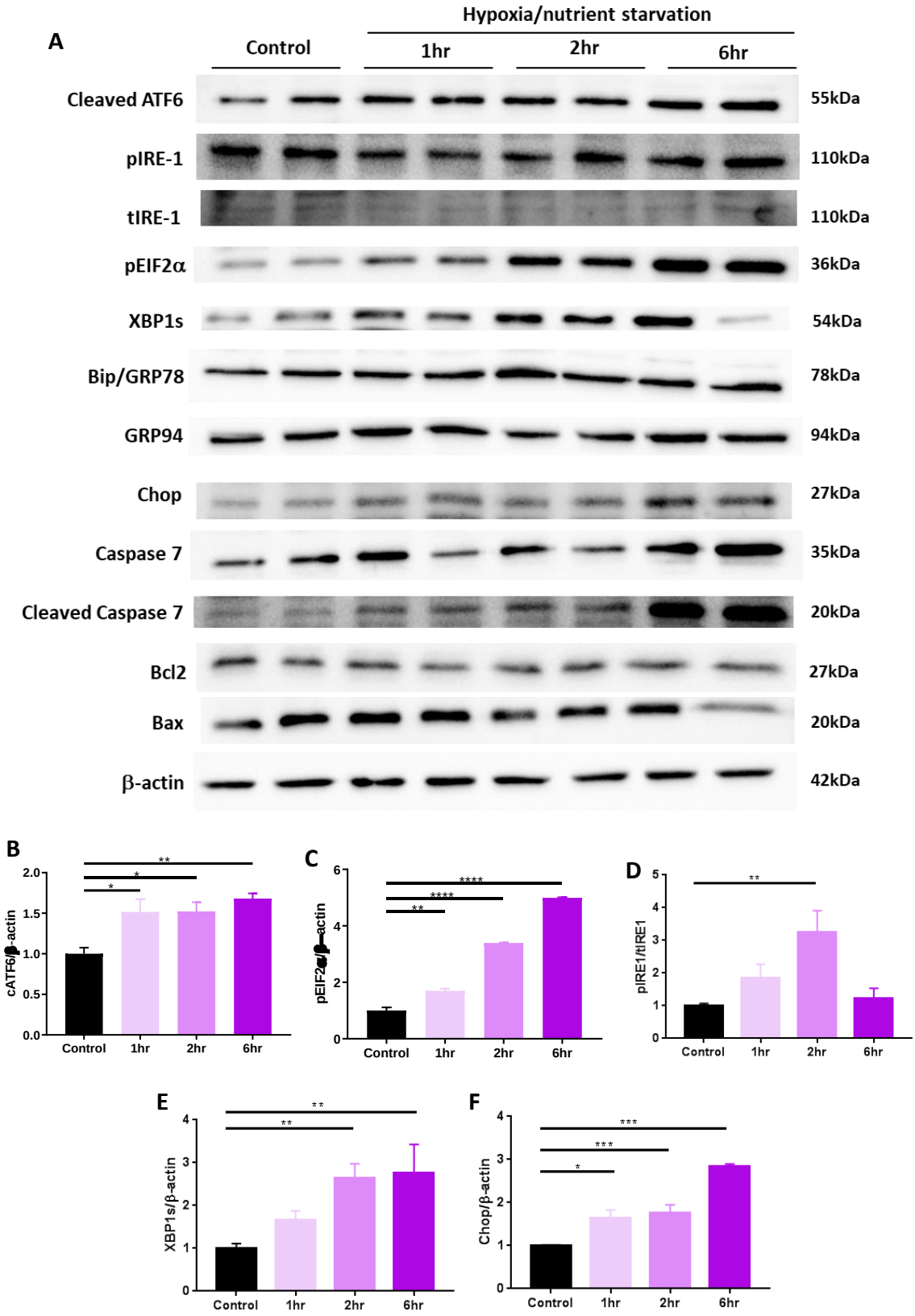
A
Hypoxia/nutrient starvation
Control
1hr
2hr
6hr
Cleaved ATF6
55kDa
pIRE-1
110kDa
tIRE-1
110kDa
pEIF2α
36kDa
XBP1s
54kDa
Bip/GRP78
78kDa
GRP94
94kDa
Chop
27kDa
Caspase 7
35kDa
Cleaved Caspase 7
20kDa
Bcl2
27kDa
Bax
20kDa
β-actin
42kDa
B
cATF6/β-actin
C
pEIF2α/β-actin
D
pIRE1/tIRE1
E
XBP1s/β-actin
F
Chop/β-actin
Control
1hr
2hr
6hr

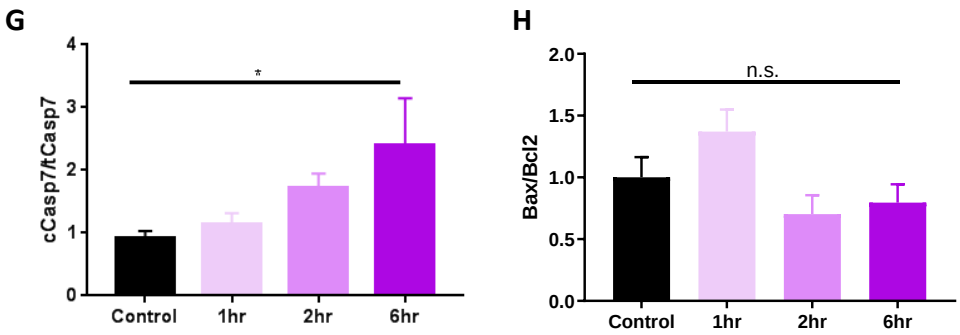

Figure 4.6 Assessment of changes to ER stress and cell death pathways in cells exposed to hypoxia (100% N_2) and nutrient starvation. Representative western blots **(A)** and quantification **(B-H)** of ER stress-related and cell death-related proteins. β-actin was used as a loading control. pIRE1 = phosphorylated IRE1; tIRE1 = total IRE1; pEIF2α = phosphorylated EIF2α; pPerk = phosphorylated PERK; cCasp7 = cleaved caspase 7; tCasp7 = total caspase 7. N=4-6. * represents p<0.05. ** represents p<0.01. *** represents p<0.001. **** represents p<0.0001. n.s. represents no significant difference. One-way ANOVA followed by Tukey's multiple comparisons test.

4.3.3 Knockdown of Pak2 leads to reduced activation of the IRE1-XBP1 pathway during the response to hypoxia/nutrient starvation

H9c2 cardiomyoblasts were used to investigate whether Pak2 plays a role in the UPR during combined hypoxia and nutrient starvation. Knockdown was induced using siRNA for 48 hours, either specific to cause Pak2 knockdown or a scrambled sequence for controls. This was followed by exposure to hypoxia and nutrient starvation for 2 hours (Figure 4.7). Control cells were plated in media containing 4.5mg/l glucose and 10 % FBS, and incubated at normoxic conditions.

After 2 hours of hypoxia and nutrient starvation, knockdown of Pak2 had no impact on activation of the ATF6 pathway or PERK pathway, indicated by the phosphorylation of EIF2α, of the UPR. However, a reduction in Pak2 levels led to impaired activation of IRE1 following this stress, with reduced levels of its phosphorylated form normalised to total IRE1 protein levels (Figure 4.7B). Furthermore, Pak2 knockdown led to reduced splicing of IRE1's downstream target XBP1 (Figure 4.7C). This pathway of the UPR is cardioprotective (S. Wang *et al.*, 2018), with transgenic overexpression of XBP1s shown to reduce infarct size and preserve cardiac function following ischaemia/reperfusion injury (Z. V. Wang *et al.*, 2014). Furthermore, Pak2 knockdown also led to greater protein levels of the pro-apoptotic molecule Chop (Figure 4.7D). Chop can promote cell death through numerous mechanisms including regulating Bcl-2 proteins and death receptors, as well as promoting DNA damage and interfering with the cell cycle (Hu *et al.*, 2019).

These findings suggest that Pak2 promotes a cardioprotective ER stress response during hypoxia and nutrient starvation through promoting the activation of the IRE1-XBP1 axis of the UPR, and a reduction in Pak2 leads to increased levels of pro-apoptotic effector proteins.

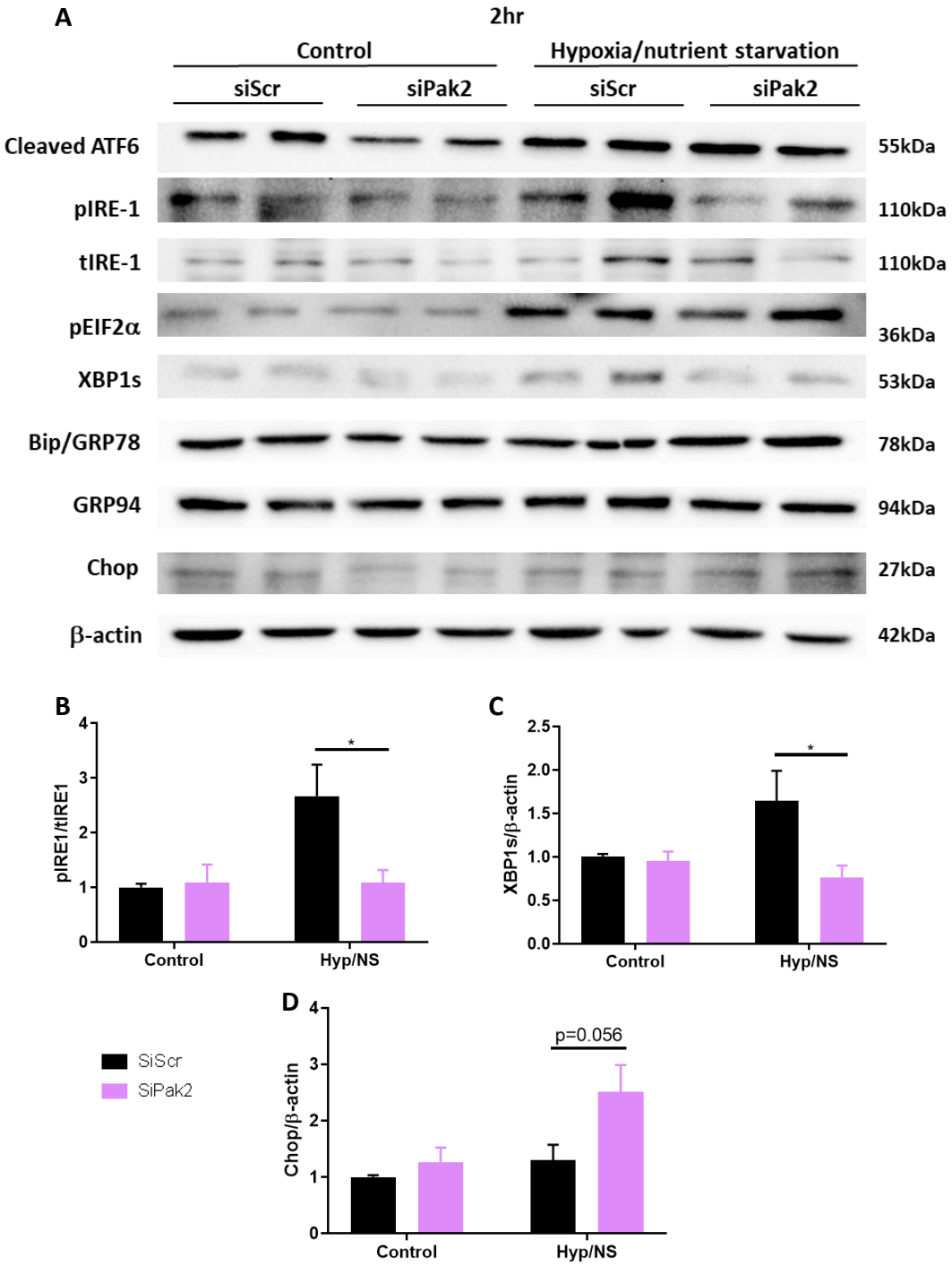

Figure 4.7 Knockdown of Pak2 in H9c2 cells impairs the activation of the IRE1 branch of the ER stress response during exposure to hypoxia and nutrient starvation. Representative western blots **(A)** and quantification **(B-D)** of ER stress-related proteins. β-actin was used as a loading control. N=4. Hyp/NS = hypoxia and nutrient starvation; pIRE1 = phosphorylated IRE1; tIRE1 = total IRE1. * represents $p<0.05$. Two-way ANOVA followed by Tukey's multiple comparisons test.

4.3.4 Knockdown of Pak2 accelerates the apoptotic response following hypoxia and nutrient starvation *in vitro*

Considering the changes to the ER stress response caused by reduced protein levels of Pak2 during hypoxia and nutrient starvation, it was important to ascertain whether these changes alter the survival of cardiac cells. Knockdown of Pak2 was induced via siRNA in H9c2 cardiomyoblasts and cells were subsequently exposed to hypoxia and nutrient starvation. A variety of apoptosis-related proteins were assessed for changes via western blot (Figure 4.8).

After incubation in hypoxic conditions in media lacking nutrients, reduced levels of Pak2 led to a two-fold elevation in the cleavage of the key pro-apoptotic molecule caspase 7 (Figure 4.8A-B) compared to cells exposed to this stress in which Pak2 levels have been unaltered. Pak2 knockdown did not appear to alter protein levels of the pro-apoptotic Bcl-2 protein Bax in this *in vitro* model.

However, the increase in cell death caused by loss of Pak2 is no longer seen by six hours of hypoxia/nutrient starvation (Figure 4.8C). Interestingly, at this time point, cells in which Pak2 knockdown has been induced have reduced levels of cleaved caspase 7 compared to controls (Figure 4.8D). Similar to the two-hour time point, no changes are seen in any other apoptosis-related protein that was assessed, including caspase 12 and Bax, though as previously stated changes or lack of changes in levels of these proteins do not conclusively indicate that apoptosis will or will not occur.

These findings suggest that loss of Pak2 accelerates the apoptotic response during hypoxia and nutrient starvation.

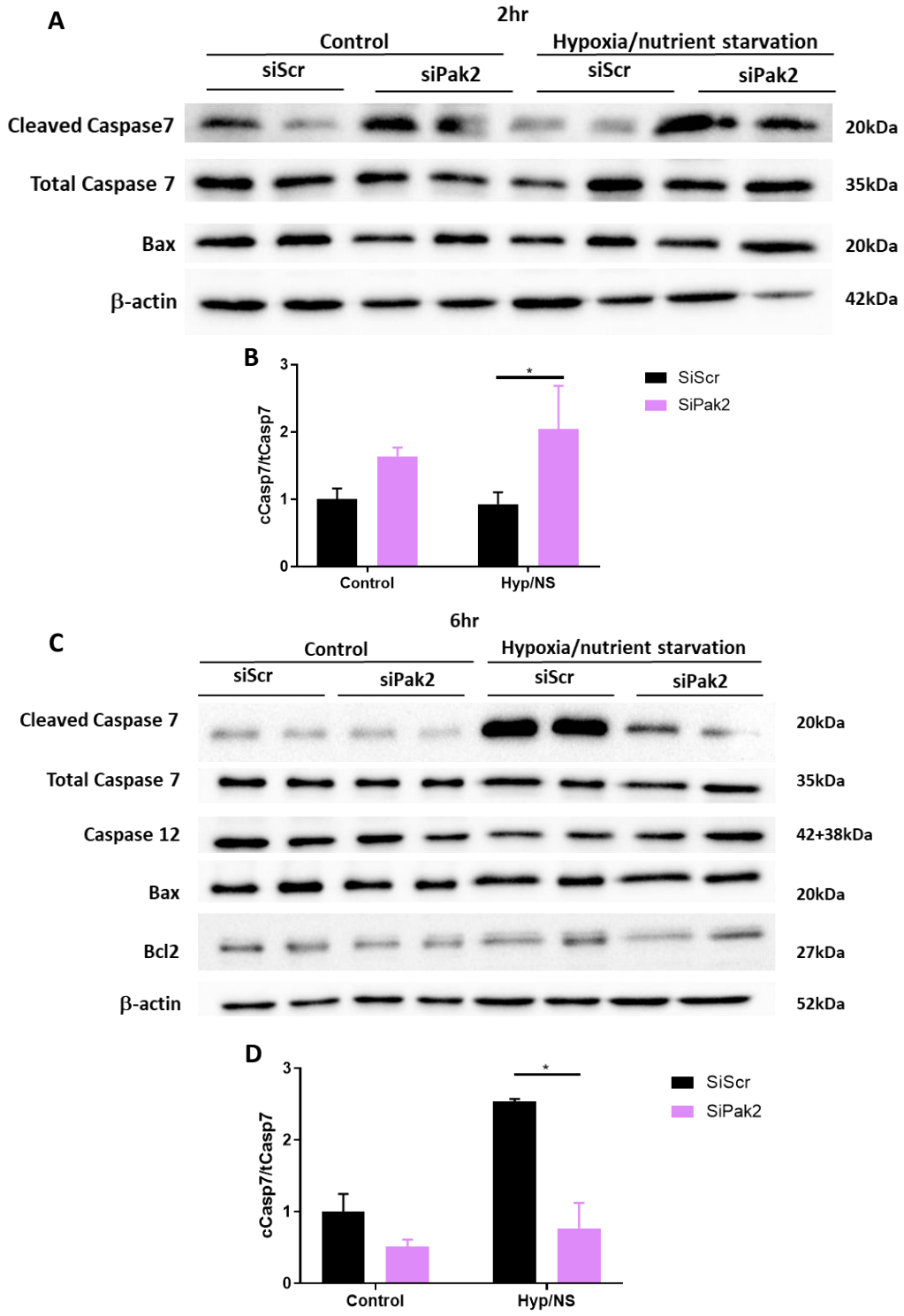

Figure 4.8 Loss of Pak2 accelerates apoptosis in H9c2 cells exposed to hypoxia and nutrient starvation. (A-B) Representative western blots and quantification of apoptosis-related proteins after two hours of hypoxia/nutrient starvation. Reduced Pak2 levels by siRNA (siPak2) led to elevated cleavage of caspase 7. **(C-D)** Representative western blots and quantification of apoptosis-related proteins after 6 hours of hypoxia/nutrient starvation. Cells with reduced levels of Pak2 (siPak2) have lower levels of caspase 7 cleavage compared to control cells (siScr) exposed to the same stress. β-actin was used as a loading control. N=2-4 per group. Hyp/NS = hypoxia and nutrient starvation; cCasp7 = cleaved caspase 7; tCasp7 = total caspase 7. Two-way ANOVA followed by Tukey's multiple comparisons test.

4.4 Pak2 is a critical mediator of the ER stress response and cell death response following oxidative stress

As demonstrated in Chapter 3, increased levels of ROS were found in MI samples two days following surgery. This suggests that, as well as the initial stress from loss of oxygen and nutrients, oxidative stress has also been caused and will affect cellular responses. Furthermore, oxidative stress is also an important cause of the massive cell death that occurs during I/R injury which is increasingly common in humans due to the increased use of stenting and bypass surgery.

For these reasons, it was important to determine whether the Pak2 activation found to occur two days following MI was due to the increased levels of ROS in cardiomyocytes at this time point. Furthermore, if this is the case, it could demonstrate the importance of investigating the role of Pak2 in I/R injury in future research.

4.4.1 Pak2 is activated *in vitro* following induction of oxidative stress

100µM H_2O_2 was added to cultured H9c2 cardiomyoblasts for 1 hour, 2 hours, or 6 hours alongside control cells which had the same volume of H_2O added. H_2O_2 induces oxidative stress as it is a reactive oxygen species. H_2O_2 is a normal oxygen metabolite during aerobic metabolism. However, in high doses, such as during I/R injury, it is converted to hydroxyl radicals (OH•) which cause cellular and DNA damage.

Expression and phosphorylation of Pak2 were assessed via western blot (Figure 4.9). Pak2 became activated by 1 hour after induction of oxidative stress by H_2O_2, with protein levels of phosphorylated Pak2 (pPak2) increased almost two-fold compared to control cells treated with water. This level of activation appears to diminish after this time, with pPak2 levels at 2 and 6 hours after induction no different to those found in control cells.

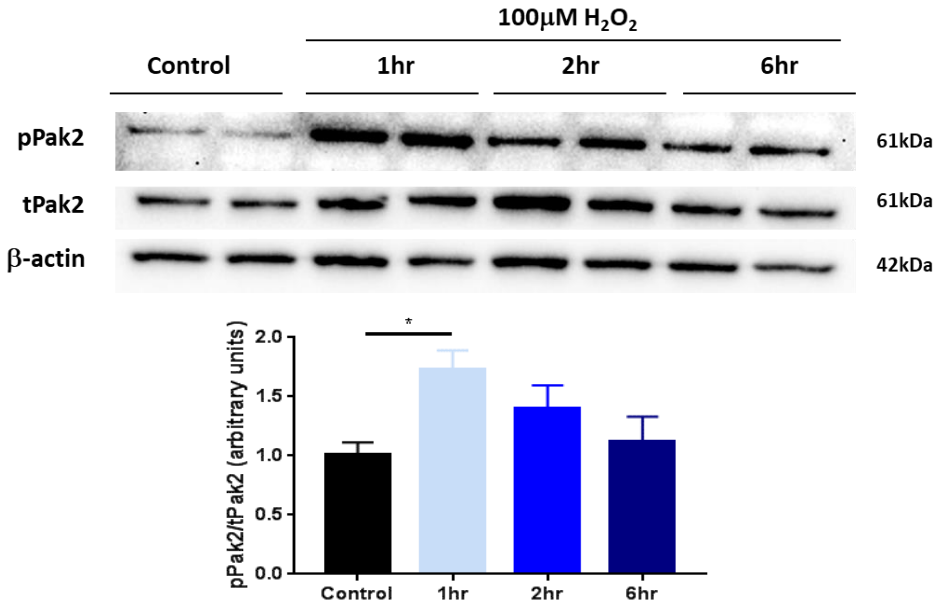

Figure 4.9 Pak2 is activated one hour after induction of oxidative stress. Representative western blots and quantification showed that levels of phosphorylated Pak2 (pPak2), normalised to total Pak2 (tPak2), are significantly increased in H9c2 cells after incubation in 100µM H_2O_2 for 1 hour. β-actin was used as a loading control. * represents $p<0.05$. n=6 per group. Kruskall-Wallis test followed by Dunn's multiple comparison test.

4.4.2 Oxidative stress activates the ER stress and cell death responses

In order to determine how oxidative stress affects cellular responses, alterations in levels of ER stress (Figure 4.10) and cell death (Figure 4.11) related proteins were screened at different time points following oxidative stress induction in H9c2 cardiomyoblasts, and compared to basal levels.

The three branches of the UPR were screened and showed that oxidative stress induced by addition of 100µM H_2O_2 caused no change in cleavage of ATF6. However, both the IRE1 and PERK pathways were activated, with increased phosphorylation of IRE1, and increased expression of both pEIF2α and ATF4 which lie downstream of PERK activation. Furthermore, there was evidence for increased expression of the ER chaperone Bip and the effector Chop.

Similarly, changes in apoptosis were investigated in protein extracts from H9c2 cells treated with 100µM H_2O_2. Cleavage of the effector caspases 3 and 7 was increased 3.5- and 2-fold respectively by 6 hours after oxidative stress induction, demonstrating that the apoptotic pathway has been activated. There was no clear change in protein expression of the Bcl-2 related pro-apoptotic protein Bax. However, whether its cellular location, which affects its cellular function, has changed cannot be assessed via western blot.

These findings demonstrate that both the ER stress and cell death pathways have been initiated after induction of oxidative stress, and thus the effect on these pathways of altered Pak2 expression *in vitro* can be investigated.

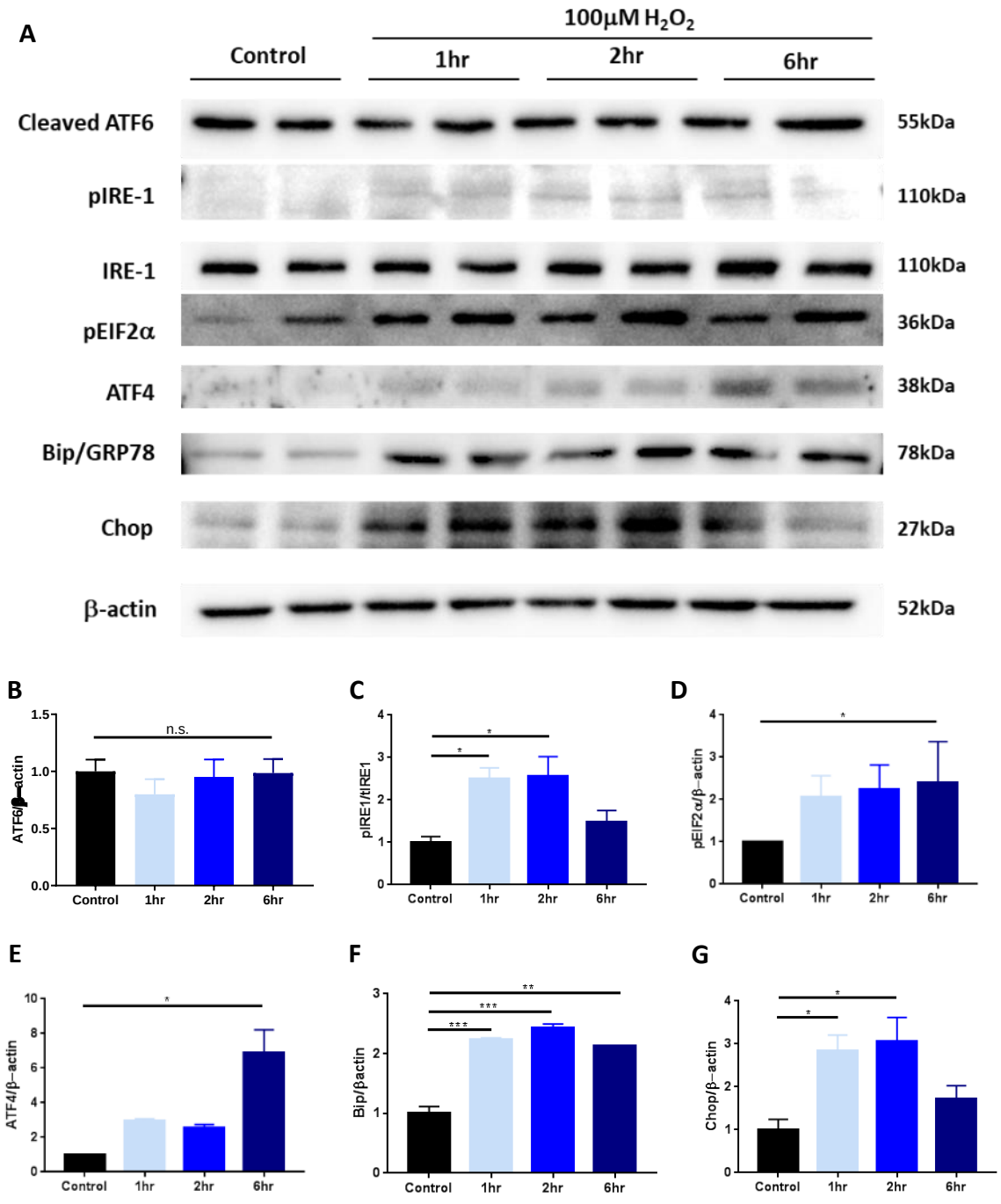

Figure 4.10 The unfolded protein response is activated in response to oxidative stress in H9c2 cells. Representative western blots **(A)** and quantification **(B-G)** of ER stress-related proteins. β-actin was used as a loading control. N=2-4. pIRE1 = phosphorylated IRE1; tIRE1 = total IRE1; pEIF2α = phosphorylated EIF2α. * represents p<0.05. ** represents p<0.01. *** represents p<0.001. n.s. represents no significant difference. Figures B, C, D, and G were analysed using a one-way ANOVA followed by Tukey's multiple comparison test; figures E and F were analysed using a Kurskall-Wallis test followed by Dunn's multiple comparison test.

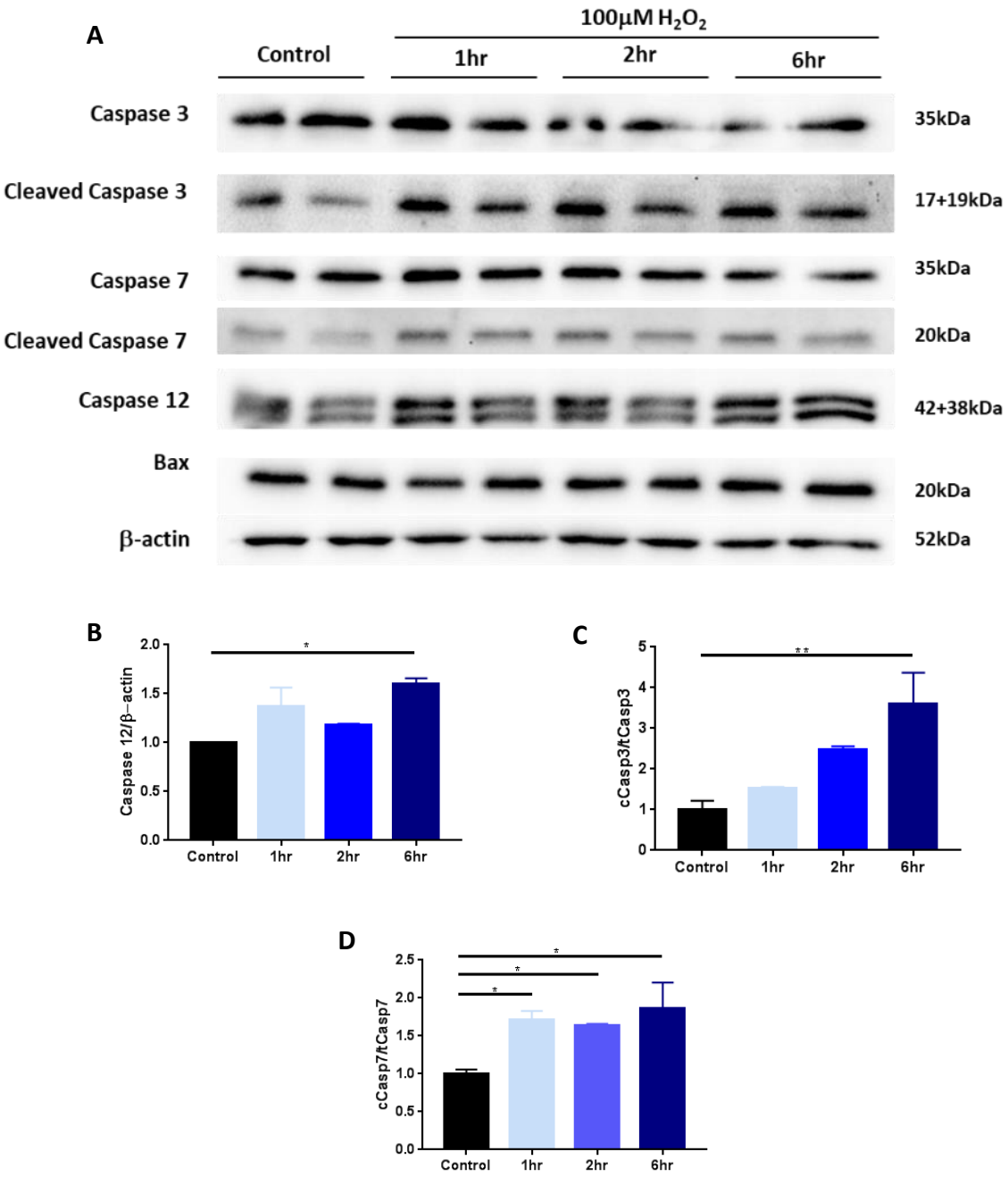

Figure 4.11 Induction of oxidative stress activates cell death pathways in H9c2 cardiomyoblasts. Representative western blots **(A)** and quantification **(B-D)** of cell death-related proteins. β-actin was used as a loading control. cCasp7 = cleaved caspase 7; tCasp7 = total caspase 7; cCasp3 = cleaved caspase 3; tCasp3 = total caspase 3. N=4. * represents $p<0.05$. ** represents $p<0.01$. Figures B and D were analysed using a one-way ANOVA followed by Tukey's multiple comparison test; figure C was analysed using a Kurskall-Wallis test followed by Dunn's multiple comparison test.

4.4.3 Knockdown of Pak2 alters the ER stress response in response to short term oxidative stress

Considering that Pak2 was activated one hour after induction of oxidative stress by 100µM H_2O_2 in H9c2 cells, we wanted to investigate whether knockdown of Pak2 using adenovirus expressing shPak2 would affect the ER stress response at this time point (Figure 4.12).

Knockdown of Pak2 in H9c2 cardiomyoblasts significantly altered the ER stress response during oxidative stress. There was a significant ($p<0.05$) reduction in levels of phosphorylated IRE1 by around 50 % in Pak2 knockdown cells, bringing levels down to those found in untreated cells (Figure 4.12B). Furthermore, downstream XBP1 splicing was similarly significantly reduced ($p<0.001$) (Figure 4.12C). There appeared to be no change in the level of ER chaperones Bip and GRP94. However, expression of the pro-apoptotic effector Chop was significantly raised almost 3-fold (Figure 4.12D) in H9c2 cardiomyoblasts exposed to oxidative stress where Pak2 had been knocked-down. The ATF6 and PERK branches appear unaffected by reduced Pak2. Considering this, it suggests that the increase in Chop is due to the reduced protective effect from the XBP1 axis of the IRE1 branch of the UPR.

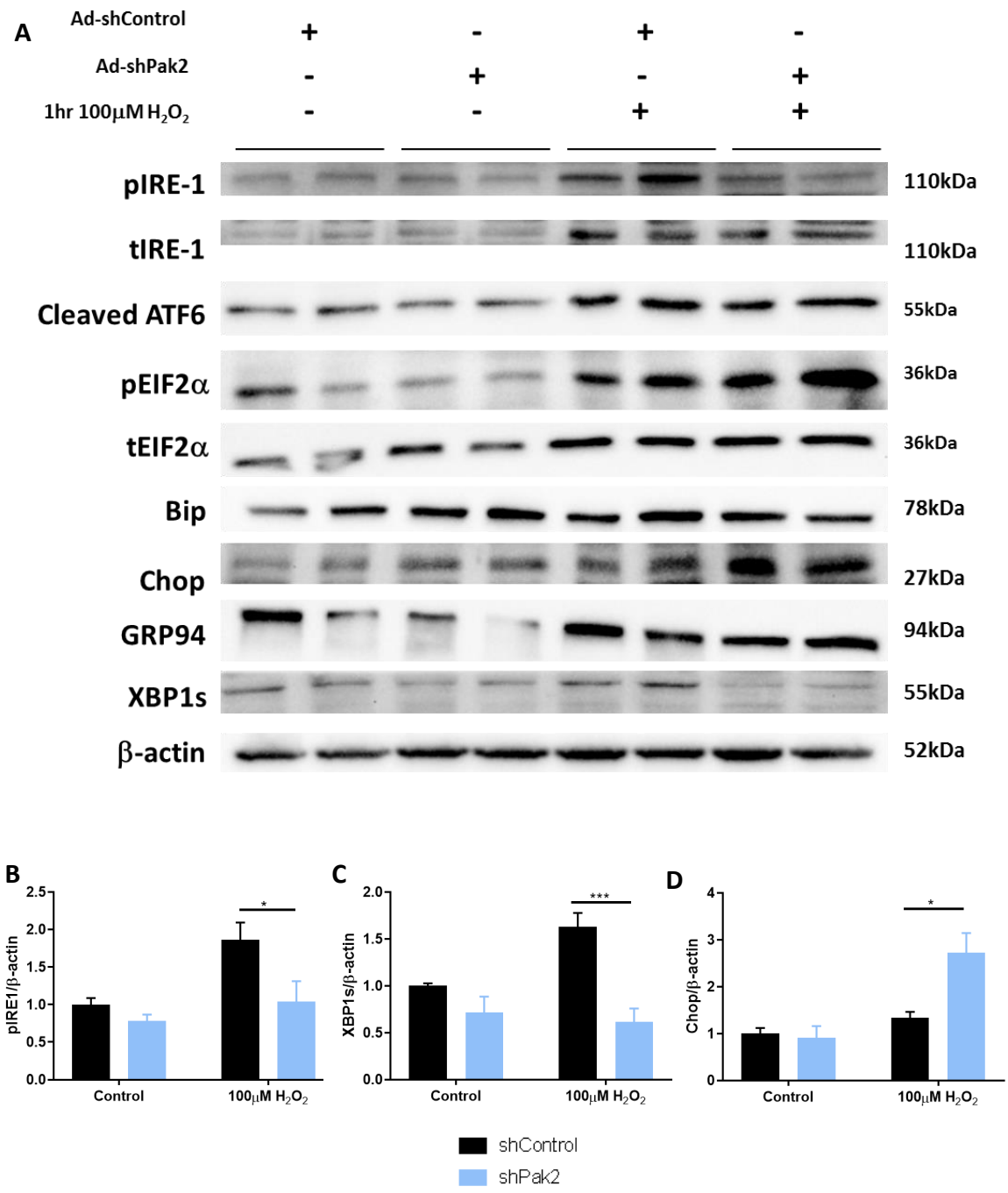

Figure 4.12 Knockdown of Pak2 in H9c2 cells impairs the IRE-1 branch of the ER stress response one hour after induction of oxidative stress. Representative western blots **(A)** and quantification **(B-D)** of ER stress-related proteins. β-actin was used as a loading control. N=4. * represents $p<0.05$. *** represents $p<0.001$. Two-way ANOVA followed by Tukey's multiple comparison test.

4.4.4 Knockdown of Pak2 exacerbates cell death during prolonged oxidative stress

To investigate whether loss of Pak2 alters the level of cell death caused by oxidative stress, knockdown of Pak2 was induced in H9c2 cardiomyoblasts using siRNA (siPak2) and then oxidative stress was triggered by incubating cells in media containing 100 µM H_2O_2. siRNA containing a scrambled sequence (siScr) was used as a control for siPak2. Cell extracts were collected after 6 hours as this allowed time for cell death to occur and potential differences to be seen. Changes were verified via western blot (Figure 4.13).

Knockdown of Pak2 led to significantly ($p<0.05$) increased cleavage of caspase 7 normalised to total caspase 7 levels (Figure 4.13B). Caspase 7 is a key executioner caspase in the apoptotic process. Once cleaved, alongside the other executioner caspase caspase 3, apoptosis is irreversible, and cleaved caspase 7 promotes cellular changes through cleaving structural and regulatory proteins (Crawford and Wells, 2011).

Knockdown of Pak2 did not affect protein levels of caspase 12 after 6 hours, and nor did it affect proteins involved in the intrinsic apoptotic pathway, specifically the ratio between pro-apoptotic Bax and pro-survival Bcl-2. However, as previously stated, whether their cellular location has been affected cannot be assessed by western blot.

To support the view that Pak2 is protective during oxidative stress, cell viability was assessed using the MTT assay. This colorimetric assay measures cell metabolic activity; cell death caused by oxidative stress leads to a reduction in metabolic activity which can be quantified relative to controls. H9c2 cells were plated evenly in 96-plate wells, knockdown of Pak2 was induced via siPak2, with siRNA used as a control, and cells were exposed to oxidative stress using 100 µM H_2O_2 (Figure 4.14). At 6- and 18-hours following induction of oxidative stress, loss of Pak2 significantly reduced cell viability compared to control cells at the same time point. By 24 hours this difference was no longer evident. This corroborates the findings that Pak2 protects cardiomyoblasts from the cell death process during oxidative stress.

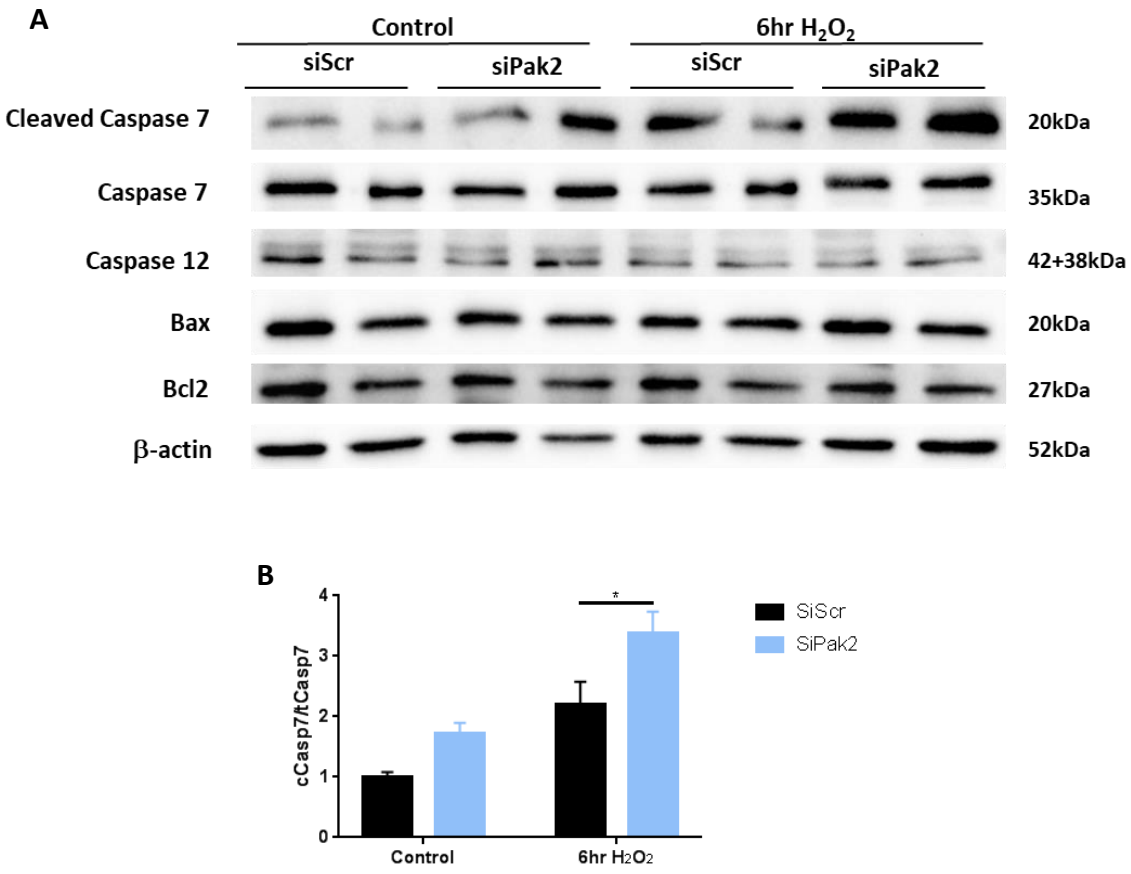

Figure 4.13 Pak2 protects against apoptosis during oxidative stress. Representative western blots **(A)** of apoptosis-related proteins and quantification of caspase 7 cleavage normalised to total caspase 7 protein levels **(B)** demonstrated that knockdown of Pak2 by siRNA (siPak2) leads to increased cleavage of caspase 7 six hours after induction of oxidative stress by 100μM H_2O_2. N=4. cCasp7 = cleaved caspase 7; tCasp7 = total caspase 7. * represents $p<0.05$. Two-way ANOVA followed by Tukey's multiple comparison test.

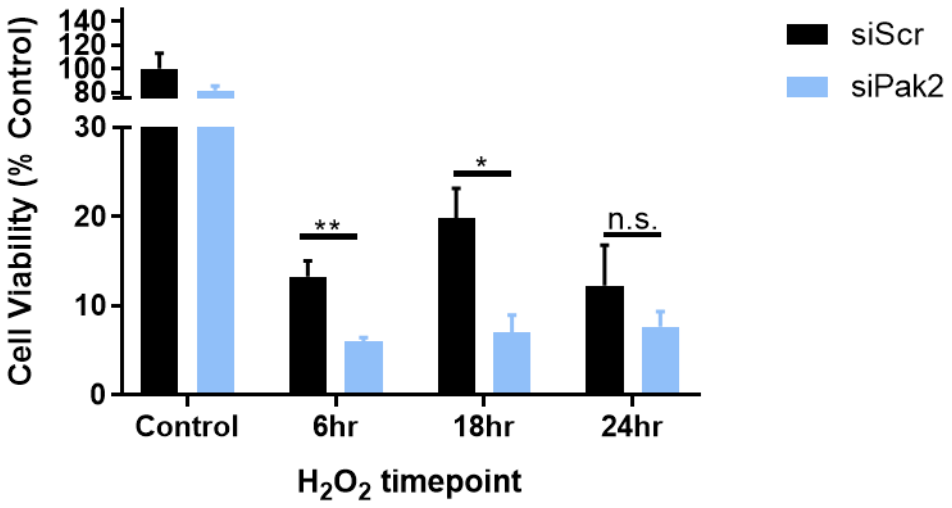

Figure 4.14 Knockdown of Pak2 reduced H9c2 cardiomyoblast viability during chronic oxidative stress. Quantification of cell viability determined using the MTT assay demonstrated reduced cell viability in cells in which Pak2 had been knocked down using siRNA (siPak2) compared to those with normal Pak2 levels (siScr) 6 hours and 18 hours after induction of oxidative stress by 100μM H_2O_2. N=5 with two technical repeats. * represents p<.05. ** represents p<0.01. n.s. represents no significant difference. Two-way ANOVA followed by Tukey's multiple comparison test.

4.5 Production of a Pak2-overexpressing adenovirus

In order to generate a Pak2-overexpressing adenovirus, a plasmid containing constitutively active human Pak2 (Pak2T402E) was used. In this plasmid, Thr^{402} of the Pak2 amino acid sequence has been mutated to glutamic acid (E); this mimics Pak2 autophosphorylation, making the mutant Pak2 constitutively and catalytically active (Renkema *et al.*, 2002). This plasmid was successfully ligated with primers to incorporate a KpnI restriction site 5' of the Pak2 gene fragment and a XhoI restriction site at the 3' end. This plasmid was amplified, and the size verified following PCR on a 1 % gel (Figure 4.15A). The band was identified as the correct size (around 1656bp). Sequencing was carried out to prove that the fragment had successfully been incorporated first into the pENTR11 entry vector (Figure 4.16) and then transferred into the pAd/CMV/V5-Dest vector (Figure 4.17). To allow optimal transfection of the vector into Hek293T cells, PacI digestion was carried out, and digestion was verified on a 1 % gel (Figure 4.15B).

Following transfection, amplification, purification and titration, the titre of the Pak2 overexpression adenovirus (AdPak2) was $4.1x10^{10}$ pfu/ml. Using this, the adenovirus was then infected in H9c2 cells at either 25 or 50MOI (Figure 4.15C-D). Flag protein was only detected in cells infected with AdPak2. Pak2 overexpression levels were verified by immunoblotting, which showed that 25MOI AdPak2 results in a four-fold increase in Pak2 protein after 24 hours incubation. 50MOI virus caused further increase in Pak2 protein levels, increasing levels six-fold compared to control cells. Pak1, like Pak2, is a member of the group I Pak family, but did not compensate for Pak2 loss, with no difference identified in Pak1 protein levels compared to control in cells incubated in 25MOI AdPak2 ($p=0.33$) or 50MOI AdPak2 ($p=0.19$). This virus can be used for future *in vitro* studies where the impact of Pak2 overexpression would be of interest, such as whether elevated Pak2 can reduce cell death or reverse cardiac pathologies that it has been implicated in, such as cardiac hypertrophy.

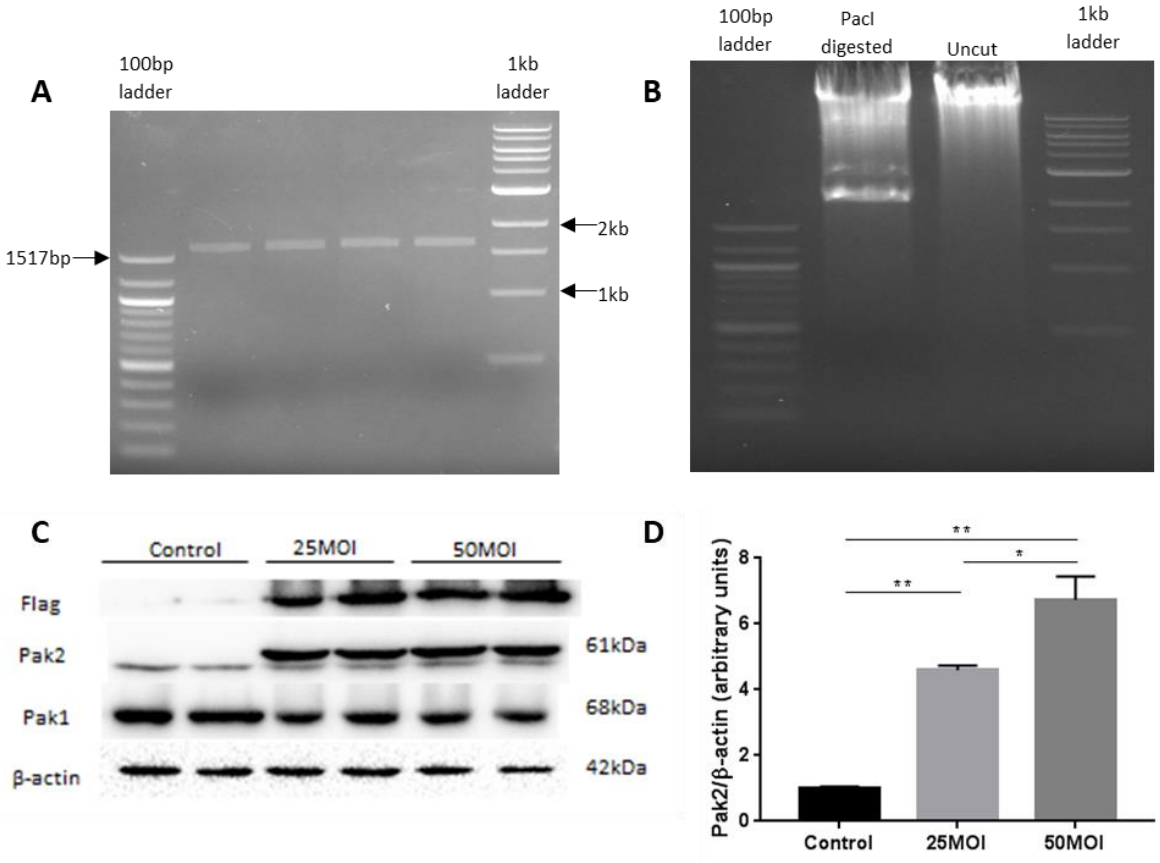

Figure 4.15 Generation and verification of AdPak2 virus. (A) Identification of Flag-Pak2T402E fragment. **(B)** Verification of PacI digestion of pDest-Pak2 plasmid prior to transfection. **(C-D)** Representative western blots and quantification of Pak2 protein levels following AdPak2 virus infection. Flag protein was only detected in cells infected with the adenovirus. Ectopic Pak2 levels were increased four-fold in H9c2 cells infected with 25MOI AdPak2, and over six-fold in those infected with 50MOI AdPak2. The upper strong band represents the ectopic Pak2 expression caused by the virus, the lower weaker band is the endogenous Pak2. N=2. *represents $p<0.05$, **represents $p<0.01$. Kruskall-Wallis test followed by Dunn's multiple comparisons test.

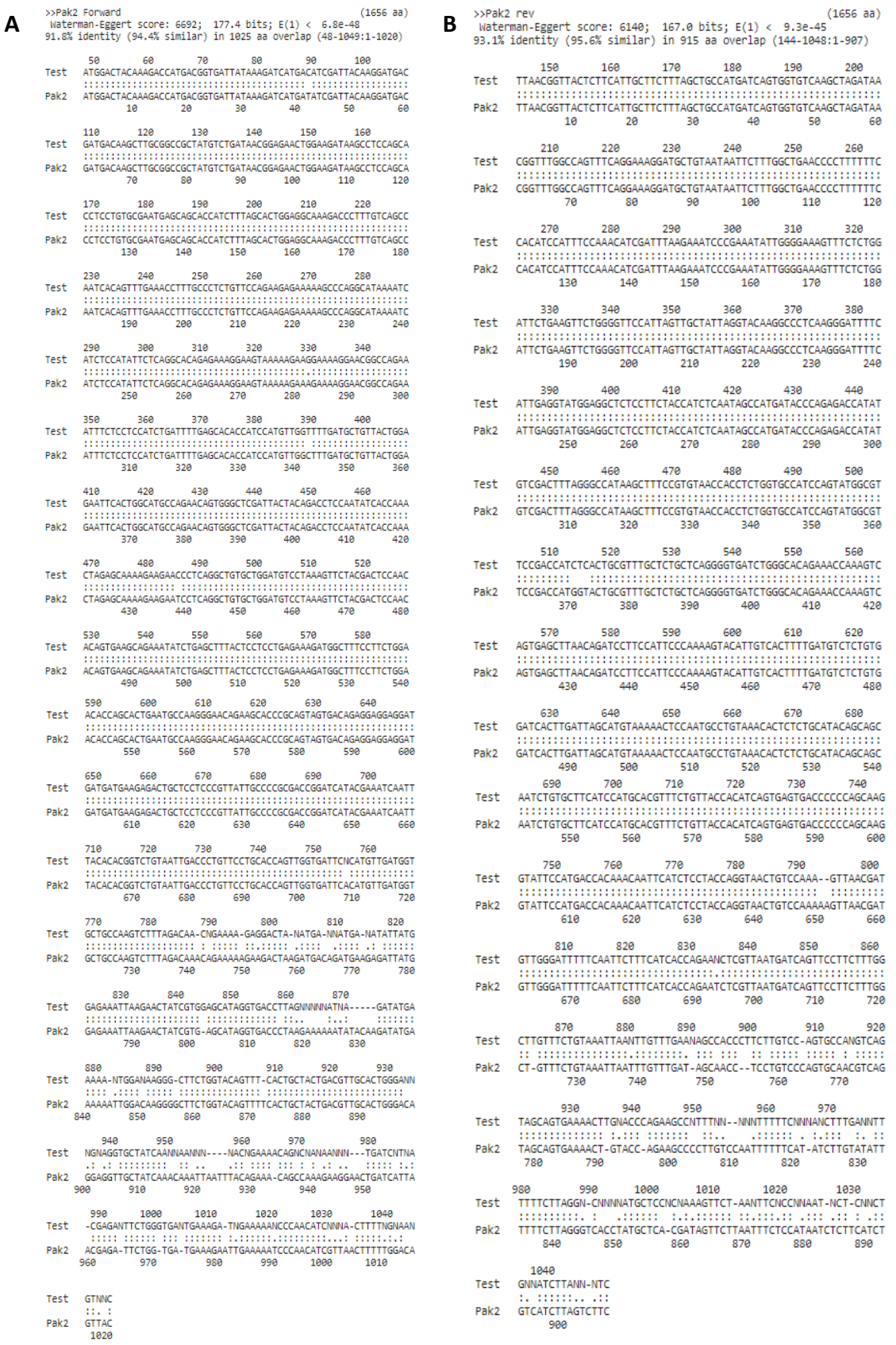

Figure 4.16 Sequencing of pENTR11-containing Pak2 plasmid. Forward **(A)** and reverse **(B)** sequencing to verify that the pENTR11 plasmid that had been generated contained the required Pak2 sequence. There was a high level of alignment (>94%) in each direction.

A

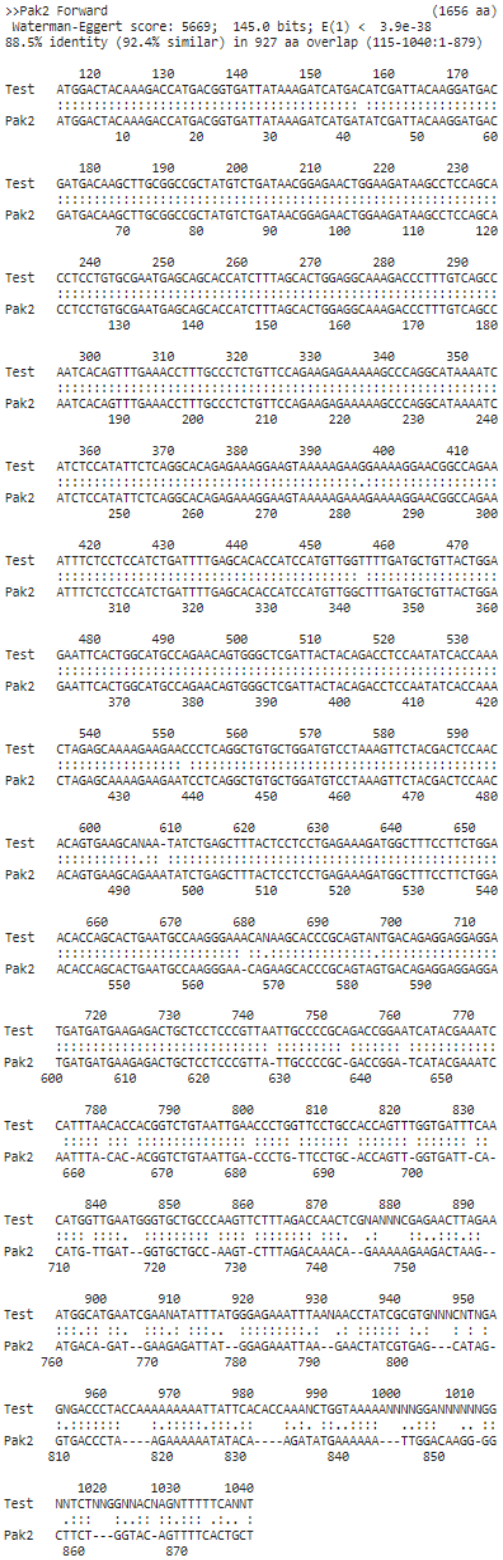

B

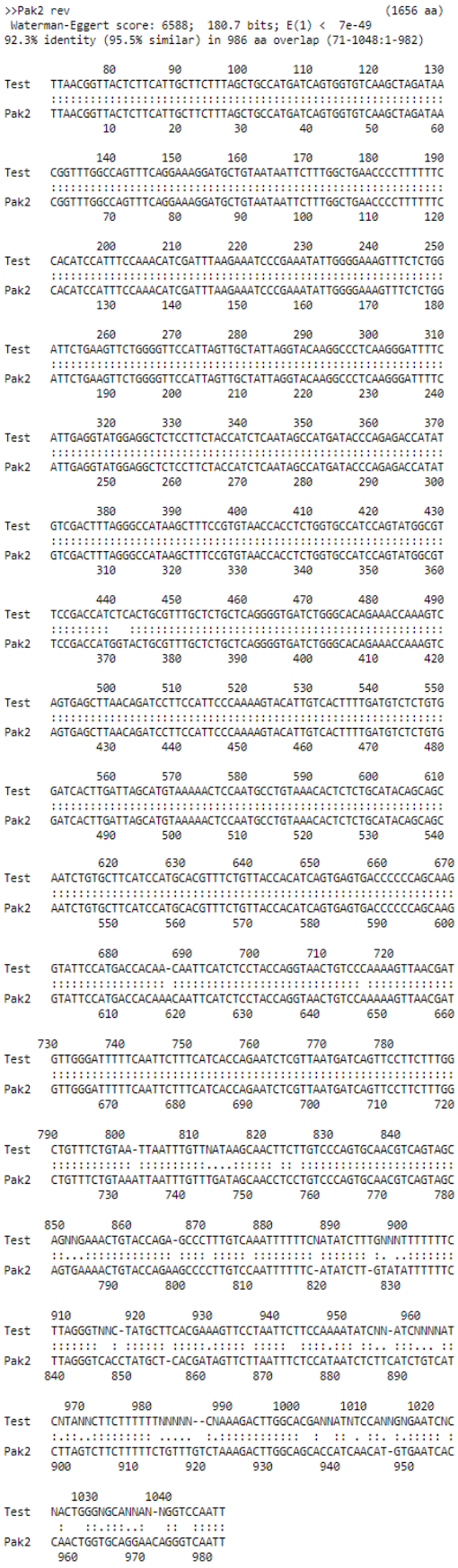

Figure 4.17 Sequencing of pAd/CMV/V5-Dest -containing Pak2 plasmid. Forward **(A)** and reverse **(B)** sequencing to verify that the pAd/CMV/V5-Dest plasmid that had been generated contained the required Pak2 sequence. There was a high level of alignment (>92%) in both directions.

4.6 Brief summary

The data presented in this chapter demonstrate that, during MI-related stress, Pak2 promotes activation of the cardioprotective IRE1-XBP1 axis of the unfolded protein response, and loss of Pak2 *in vitro* exacerbates apoptosis. Pak2 is not activated by hypoxia alone but is activated when this is combined with nutrient starvation. Furthermore, Pak2 is activated and protective during oxidative stress, demonstrating the potential that it may play a cardioprotective role during I/R injury as well as following myocardial infarction.

Chapter 5: Discussion

5.1 Summary of findings from this study

This project demonstrated that Pak2 is activated in the acute phase following myocardial infarction (MI), with increased total Pak2 expression, and increased Pak2 phosphorylation, two days following MI in mice. Using cardiomyocyte-specific Pak2 knockout mice ($Pak2^{cko}$), this study showed that Pak2 regulates the ER stress response during MI, with $Pak2^{cko}$ mice found to have upregulated protein levels of the pro-apoptotic ER stress effector molecule Chop in the heart. Furthermore, loss of Pak2 may increase mortality following MI, and leads to increased fibrosis and cardiomyocyte death in the acute MI phase. Using *in vitro* models, it was found that Pak2 is not activated by hypoxia, but when combined with nutrient starvation Pak2 activation is observed. Furthermore, Pak2 is activated following induction of oxidative stress, demonstrating that it could be a crucial molecule during I/R injury. Under both of these *in vitro* conditions, a reduction in Pak2 protein led to a dysregulated ER stress response, with impaired activation of IRE1 and its downstream target XBP1, and an increase in Chop. Furthermore, loss of Pak2 led to an increase in apoptotic markers, demonstrating its pro-survival role in the ischaemia-stressed heart.

5.2 Pak2 becomes activated following MI

Protein analysis of hearts obtained from $Pak2^{f/f}$ mice at different timepoints following MI identified that Pak2 becomes activated, indicated by its phosphorylation at residue Ser20, two days following MI. This residue is one of eight which become autophosphorylated during full Pak2 activation and it is commonly used in studies to assess Pak2 activation (Gatti *et al.*, 1999; Gao *et al.*, 2014). To confirm this activation, a kinase assay of Pak2's known downstream substrates could be carried out. This has previously been performed in the Wang lab, with a correlation between Pak2 phosphorylation and kinase activity observed. Activated Pak2 levels remained elevated when normalised to total Pak2. This suggests that Pak2 may have roles during the acute inflammatory phase following MI. During this phase the majority of cardiomyocyte death occurs alongside massive infiltration of inflammatory cells and release of pro-inflammatory cytokines (Weil and Neelamegham, 2019). As will be discussed later, loss of Pak2 was shown to exacerbate the apoptotic process leading to increased cell death, and thus activation in this phase may act to limit cardiomyocyte death. In remote regions of the heart, no difference in infiltration of macrophages, demonstrated by CD68 staining, or levels of the inflammatory cytokines IL1β and IL6, was evident between $Pak2^{f/f}$ and $Pak2^{cko}$ mice, though a more thorough analysis of inflammatory changes in the heart would be required to confirm that loss of Pak2 does not affect the inflammatory response. For instance, flow cytometry could be carried out on isolated immune cell populations from hearts following MI (Rusinkevich *et al.*, 2019). This would give greater detail on the changes in different immune cell populations, and how loss of Pak2 might affect them.

Interestingly, total Pak2 levels were also elevated two days following severe MI ligation, and this was found to occur in both $Pak2^{f/f}$ and $Pak2^{cko}$ mice after MI. The elevation of Pak2 levels in $Pak2^{cko}$ mice suggests that this is not due to changes of Pak2 in cardiomyocytes, but rather other cell types found within the heart. This could either be due to an increase in Pak2 expression in cardiac-resident cells, or through an influx of cells expressing Pak2. Alternatively, MI may affect Pak2 degradation. This finding would need to be investigated in greater detail, such as through isolating individual cardiac-resident cells, such as fibroblasts, and examining fluctuations in Pak2 in these cells during ischemic stress.

Pak2 phosphorylation was no longer elevated compared to sham one week or four weeks following MI. This suggests that Pak2 may not have a direct role in remodelling following MI, but does not exclude the possibility. There is the potential that Pak2 activation in the acute phase may impact on long-term remodelling. Interestingly, in a hypertrophic mouse model, Pak2 was found to be activated one week following induction of pressure overload-induced cardiac stress, and its phosphorylation was reduced to below basal levels after five weeks, suggesting exhaustion of Pak2 activation (Binder *et al.*, 2019). Since similar findings were not found following MI this further demonstrates the differences between these two models. During transverse aortic constriction (TAC) to induce pressure-overload induced pathological CH, the stress on the heart is constant over time, and chronic. However, following permanent ligation of the left anterior descending (LAD) coronary artery to cause an MI the effect is instant, and though the resulting effects are chronic, the initial stimulus is acute. As such, this suggests that Pak2 is activated as a result of the effects of loss of blood flow caused during MI, such as loss of oxygen and nutrients, or other external stress stimuli.

To assess the potential causes of Pak2 activation following MI, phosphorylation of Pak2 was assessed *in vitro* in H9c2 cardiomyoblasts following MI-related stresses. Interestingly, Pak2 was not found to be activated by hypoxia alone. This suggests that Pak2 may not be involved in the hypoxic response despite this stress having been shown to alter ER functions (Chipurupalli *et al.*, 2019). However, Pak2 was activated when hypoxia was combined with nutrient starvation. This activation occurred two hours after the stress was initiated. Nutrient starvation and hypoxia activate many common pathways, such as the mTOR and AMPK pathways (Humpton and Vousden, 2016); however, the speed at which these are activated differ between the models. Furthermore, nutrient starvation also disrupts lipid and carbohydrate metabolism pathways which are not directly impacted by hypoxia. In order to fully understand the reason behind Pak2's differential activation, the upstream activation mechanism of Pak2 under these stresses must be determined.

An interesting finding of this study was the identification that Pak2 becomes activated one hour after induction of oxidative stress by administration of 100μM H_2O_2. It was not tested whether Pak2 becomes activated earlier than 1 hour. This activation appears to protect against apoptosis during oxidative stress, with knockdown of Pak2 leading to

increased caspase 7 cleavage and reduced cell viability up to 18 hours after stress induction. This differs to recent findings by Huang et al (2020) who found that during oxidative stress Pak2 promotes apoptosis in Hek293T cells. They showed that this is due to activation of Pak2 by caspase 3 cleavage, and that this could be prevented by pre-activation of Pak2 by Cdc42 through its canonical activation pathway. However, there are many differences between this study and the one carried out in this project. Firstly, Hek293 cells are originally derived from human embryonic kidneys and are therefore significantly different to cardiac cells. Secondly, this study used longer time points, up to 12 hours, and a much greater concentration of H_2O_2 at 1 mM. Any of these differences might explain the disparity between the two findings.

Given that Pak2 was shown to be activated after oxidative stress, and considering that oxidative stress has also been shown to occur in CH (Lee *et al.*, 2014), it would be interesting to assess whether oxidative stress may play a role in Pak2's activation in this model. Intriguingly, oxidative stress is also caused by ER stress, such as in cells treated with tunicamycin (TM) (Kim *et al.*, 2018) demonstrating a potential positive feedback loop. Since Pak2 is known to become activated following two hours TM treatment (Binder *et al.*, 2019), it would be of interest to investigate whether this activation is caused by ER stress-induced oxidative stress or due to other changes caused by ER stress. To investigate this, antioxidants, such as vitamin C or N-acetyl cysteine (NAC) could be added before, during, or after TM-induced ER stress to assess whether this alters the activation of Pak2. If this were found to occur, it could suggest a common pathway through which Pak2 becomes activated.

5.3 Pak2 might reduce mortality following myocardial infarction

Following MI surgery there was high mortality in both genotypes. Upon refinement and usage of the moderate LAD ligation, this mortality appeared to be higher in $Pak2^{cko}$ mice compared to $Pak2^{f/f}$ controls (Figure 3.8). Hearts were assessed following death to attempt to determine cause (Table 2.4). There are three main causes of death following MI: cardiac rupture, arrythmia, and acute HF.

Cardiac rupture occurs when part of the heart muscle becomes torn, allowing blood to escape the heart chambers, thus leading to rapid death as the heart cannot pump blood around the body (Gao *et al.*, 2005). It often occurs suddenly with no prior symptoms. There are two classifications following MI; type I occurs within the first 24 hours post-MI and is due to a sudden tear, type II is caused by erosion of the infarct, usually more than 24 hours post-MI. Some ruptures were evident in both $Pak2^{cko}$ and $Pak2^{f/f}$ that were found dead following MI, but it was not a consistent finding and due to the development of adhesions and damage to the heart during extraction could not always be identified with certainty. Initial fibrosis, termed reparative fibrosis, aids in protecting against cardiac rupture (Talman and Ruskoaho, 2016). Thus, given that $Pak2^{cko}$ mice had increased cardiac fibrosis compared to $Pak2^{f/f}$ two days after MI, this suggests that these mice might be less prone to rupture.

Following MI, in both humans and animals, arrythmias can develop and this can lead to sudden cardiac death. Sudden cardiac death incidence is greatly increased in humans following MI and is most likely to occur within the first 30 days post-infarction (Zaman and Kovoor, 2014). Loss of oxygen during MI causes cardiac cells to become depolarised (Klabunde, 2017), leading to altered impulse formation if this occurs in cells involved in the cardiac conduction system, or altered impulse propagation if non-pacemaker cardiomyocytes are affected. Furthermore, cell death and replacement with fibrotic material can lead to altered impulse propagation and electrical block as fibrotic tissue is non-conductive. Altered impulse propagation could lead to re-entry and tachyarrhythmia. In this study no arrythmias were identified in either genotype, measured using conscious ECG two days after MI; however, this would not identify sudden or intermittent arrythmias. Continuous ECG recordings would be required to identify these.

Some mice had to be put down following MI due to progression to acute HF (HF). Symptoms for this were a hunched posture, low body temperature, laboured breathing, piloerection, and slowed or minimal movement of the animal. In acute HF, symptoms develop quickly, and it is more common after MI than not (Harjola *et al.*, 2020). As previously mentioned, loss of Pak2 in the heart has shown to accelerate the progression to HF following CH (Binder *et al.*, 2019); however, this HF is chronic rather than acute. Given the elevated levels of cell death in the hearts of $Pak2^{cko}$ mice after MI, it could be postulated that this sudden increase in cell death does not allow for the heart to compensate through hypertrophic responses, and thus progresses to HF immediately.

5.4 Pak2 has an anti-apoptotic role following MI

In the literature, there is a functional dichotomy surrounding Pak2's role in cell death and cell survival. This is due to its unique ability among the Pak family to be activated not only through the canonical upstream binding pathway, but also through cleavage by caspase 3 (Bokoch, 1998). Once cleaved, the 34 kDa Pak2 fragment (Pak-2p34) containing the kinase domain can translocate to the nucleus where it promotes apoptosis. However, this has not been shown to occur naturally *in vivo*. Jakobi et al (2003) identified that this fragment is regulated by ubiquitination and targeted for degradation by the proteasome. Therefore, if it were to occur *in vivo* it might be cleared quickly, and therefore not identifiable. To investigate this, proteasomal pathways would need to be disrupted to prevent its potential degradation. The majority of the studies investigating this phenomenon use cell lines, and the only study using an *in vivo* model to investigate this performed their experiments on isolated cells rather than examining effects *in vivo* (Marlin *et al.*, 2011). Therefore, it is possible that the generation and pro-death function of this fragment is an artefact of *in vitro* experiments. There is currently no evidence of Pak2 cleavage occurring in the heart (Binder *et al.*, 2019).

Unlike the Pak-2p34 fragment, full length Pak2 resides in the cytosol due to a nuclear export signal motif located in the regulatory domain of its structure (Jakobi *et al.*, 2003). Here, following the standard activation mechanism, full length Pak2 can promote cell survival (Jakobi *et al.*, 2001; Eron *et al.*, 2017). In this study, we identified that Pak2 can protect against apoptosis following MI, with loss of Pak2 in cardiomyocytes leading to

increased cardiomyocyte apoptosis, visualised by TUNEL staining, and increased protein levels of the cleaved active form of the executioner caspase 7 and the pro-apoptotic Bcl-2 protein Bax. This finding mirrors those found in a model of pathological CH (Binder *et al.*, 2019), thus supporting the view that Pak2 is cardioprotective in the heart during disease.

Findings from *in vitro* experiments during this project further support Pak2 as pro-survival molecule following MI-related stress. Pak2 knockdown led to elevated cleavage of caspase 7 following induction of oxidative stress for six hours. This was shown to reduce cell viability up to 18 hours after stress was initiated. The level of Pak2 activation after six hours was not investigated; therefore, it would be of interest to assess whether Pak2 levels become elevated again beyond this, thus leading to chronic effects on cell viability.

Furthermore, *in vitro* knockdown of Pak2 was shown to accelerate the cleavage of caspase 7 in H9c2 cells following hypoxia and nutrient starvation, with elevated levels of its cleavage identified after two hours. However, in control cells this increased cleavage of caspase 7 caused by hypoxia/nutrient starvation was not apparent until after six hours. By this time caspase 7 cleavage levels in Pak2 knockdown cells had returned to basal levels, suggesting a model whereby Pak2 delays the peak of apoptosis (Figure 5.1). To investigate whether knockdown of Pak2 leads to increased levels of apoptosis, or merely accelerates the process, further experiments would be required, such as the MTT assay to assess changes in cell viability over multiple timepoints.

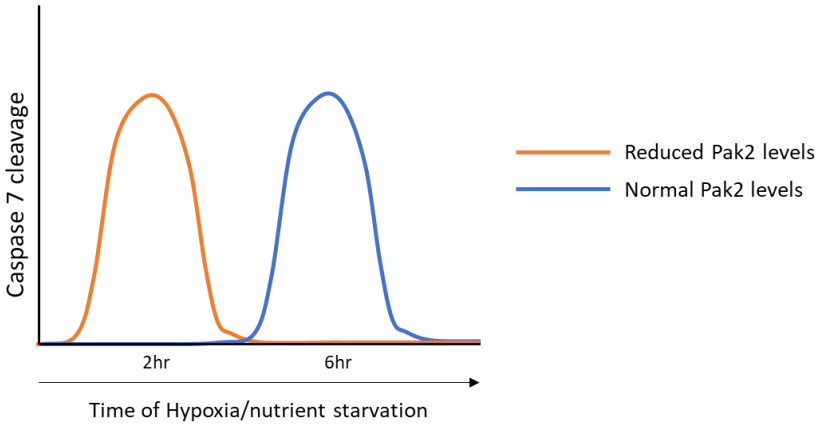

Figure 5.1 Potential of Pak2 to delay caspase 7 cleavage. From the data in this study, reduced levels of Pak2 caused by siRNA mediated Pak2 knockdown led to increased caspase 7 cleavage, a terminal point of apoptotic signalling, at two hours following initial exposure to combined hypoxia and nutrient starvation. However, this elevation was no apparent in control cells at this time point, and was not seen until six hours after stress initiation. However, by six hours cleaved caspase 7 protein levels had returned to basal levels in Pak2 knockdown cells, suggesting it accelerates the process and acts in a wave-like pattern. What remains unknown is whether the height of these peaks is the same and, as such, whether the overall level of apoptosis is similar, and that Pak2 merely delays it, or whether loss of Pak2 also leads to increased apoptosis as well as accelerating the process.

The exact mechanism through which Pak2 exerts its cardioprotective role is not fully elucidated in the MI model used in this study. However, it is possible, and potentially likely, that this is through its ability to promote resolution of ER stress, and as such when it is absent there are greater levels of unresolved ER stress. This would likely lead to an increase in unfolded or misfolded proteins which are proteotoxic (McLendon and Robbins, 2015). Unresolved ER stress was demonstrated in the heart of $Pak2^{cko}$ mice following MI by increased protein levels of pro-apoptotic Chop. Chop acts as a transcriptional regulator and can promote apoptosis through multiple mechanisms, which is reviewed thoroughly by Hu et al (2019). For instance, under ER stress, Chop can downregulate the expression of pro-survival Bcl-2 proteins Bcl-2 and Bcl-XL and can upregulate pro-apoptotic Bim. It can also promote apoptotic cellular changes, such as triggering DNA damage by activating GADD34 (Marciniak *et al.*, 2004). It is not clear that Pak2 directly reduces Chop expression, but that a dysregulated ER stress response caused by lack of Pak2 leads to its transcription.

Interestingly, Pak2 has also been shown to directly interact with and inhibit the activity of caspase 7. Li et al (2011) found that in human breast cancer cells, Pak2 expression is highly upregulated and this promotes chemotherapy-resistance; knockdown of Pak2

increased caspase 7 activation and activity, which led to increased apoptosis *in vitro*. They identified that Pak2 can co-localise and interact with caspase 7, and phosphorylate it at 3 sites – S30, T173 and S239. Eron et al (2017) identified that this phosphorylation represents two distinct mechanisms by which Pak2 can mediate caspase 7 inhibition. Phosphorylation of caspase 7 by Pak2 at residue S30 allosterically impedes the interaction between caspase 7 and caspase 9, thus impeding caspase 9-mediated cleavage of caspase 7 to activate it. Meanwhile, phosphorylation of caspase 7 by Pak2 at residue S239 prevents caspase 7 from binding to its substrates, regardless of its activation status, thus preventing its effector role in promoting apoptosis-related cellular changes. Considering that data from this current study found that Pak2 knockout in the heart following MI, and knockdown in cells following MI-related stress, led to increased caspase 7 cleavage and apoptosis, it would be of interest to identify whether Pak2-caspase 7 interaction occurs in the heart. To assess this *in vivo*, immunofluorescence staining followed by confocal microscopy could be performed to identify whether these two molecules co-localise during MI. *In vitro*, this could be achieved using the Pak2 overexpression adenovirus generated during this project in isolated adult cardiomyocytes followed by immunoprecipitation to determine any interaction between the two molecules.

5.5 Loss of cardiac Pak2 appears to augment the fibrotic response following MI

Another finding of this study was Pak2's impact on the deposition of fibrotic material in the acute phase following MI. At two days post-surgery, $Pak2^{cko}$ mice had elevated levels of Masson's trichrome staining in the heart compared to $Pak2^{f/f}$ controls, though this finding was not significant (p=0.0889). Masson's trichrome is a stain for collagen fibres. Alternative stains such as Picrosirius red, which also stains collagen fibres, could be utilised alongside it to confirm this finding (Cabibi *et al.*, 2015).

Reinforcing the hypothesis that loss of Pak2 increases fibrosis development, protein analysis identified that $Pak2^{cko}$ mice had elevated levels of TGFβ and α-smooth muscle actin (αSMA) in the heart two days following MI. TGFβ is a key pro-fibrotic cytokine that is released in a latent form by cells including cardiomyocytes and inflammatory cells. It is crucial for myofibroblast differentiation and increased contractility (Bernard *et al.*, 2015). αSMA is not normally expressed in cardiac fibroblasts, but is expressed in differentiated myofibroblasts. As such it is commonly used as a marker for myofibroblast activation (Tomasek *et al.*, 2002). αSMA is key for improving myofibroblast contractility and force generation, thus aiding their function in forming the mature scar (B. Hinz *et al.*, 2001).

αSMA is also expressed in vascular smooth muscle cells (Fatigati and Murphy, 1984; Skalli *et al.*, 1989), thus it could be speculated that there is an increase in angiogenesis and thus new vessels in $Pak2^{cko}$ mice. It would be of interest to investigate Pak2's role in angiogenesis post-MI due to its known role in vessel development during embryogenesis (Radu *et al.*, 2015), though since Pak2 was not knocked-out in endothelial cells in this study it is unlikely that it would act through the same mechanism in this context . When the increase in αSMA protein levels is combined with increased TGFβ, together with a trend towards increased staining of fibrosis in $Pak2^{cko}$ mice, this suggests that the elevation of αSMA is due to enhanced fibrotic signalling and greater numbers of myofibroblasts.

The proliferative phase following MI normally commences ~4-7 days following the initial insult (Carlson *et al.*, 2011; Weil and Neelamegham, 2019). $Pak2^{cko}$ mice had increased fibrosis two days following MI but there was no difference between the genotypes

regarding infarct size or level of interstitial fibrosis two weeks following mild MI. This suggests that loss of Pak2 may accelerate the fibrotic response rather than exacerbate it.

As mentioned above, the findings in this study suggest that Pak2 promotes an anti-fibrotic response. This differs to what has previously been reported in our lab, with $Pak2^{cko}$ mice after TAC having less fibrosis compared to $Pak2^{f/f}$ controls (Binder *et al.*, 2019). However, despite this, Pak2's impact on fibrotic development after TAC is ambiguous as transgenic mice overexpressing Pak2 also had elevated fibrosis, indicated by Masson's trichrome staining in the heart two weeks after TAC. Thus, further evidence is required to support its role in fibrosis during CH. The differences between the TAC and MI models and their impact on cellular changes in the heart mean that Pak2 may play varying roles depending on the stimuli. Other research has also found contradictory findings of Pak2's role in fibrosis, suggesting that there may be a greater level of regulation of its role in this. For instance, in MDCK epithelial cells, Pak2 inhibits fibrotic development by associating with, and blocking the activation of, Smad2/3 by TGFβ, thus preventing TGFβ signalling through these proteins (Yan *et al.*, 2012). Conversely, in fibroblasts, Pak2 can be activated by the non-canonical Smad-independent pathway of TGFβ-induced fibrosis through activation involving PI3K and Rac1 (Wilkes *et al.*, 2003, 2005; Wilkes and Leof, 2006). However, both these studies place Pak2 as downstream of TGFβ, different to the findings in our study which suggest it is upstream. Thus it would be of interest to investigate how Pak2 may alter TGFβ transcription, release, activation and signalling in greater detail in the context of heart disease, considering that fibrosis plays a crucial role in the remodelling of the myocardium during disease and the progression to HF (González *et al.*, 2018).

There is currently no explanation for how or why Pak2 may prevent early fibrotic development, though there could be a link between loss of Pak2 promoting cell death and also promoting fibrosis development. As shown in this study, Pak2 increases cell death following MI. A noteworthy point of interest is that a dysregulated ER stress response and an increase in Chop protein levels has been associated with an increase in fibrosis (Lenna and Trojanowska, 2012). For instance, Chop-deficient mice had greatly reduced hepatic fibrosis following bile duct ligation (Tamaki *et al.*, 2008). Furthermore, in the heart, a chemical chaperone drug, 4-PBA, has been shown to alleviate ER stress

and lead to reduced cardiac fibrosis (Park *et al.*, 2012). Hence, the dysregulation of the ER stress response caused by loss of cardiac Pak2 may be related to an increase in cardiac fibrosis found in this model.

Cell death-induced inflammation can promote cardiac fibrosis (Kania *et al.*, 2009). However, the type of cell death that Pak2 was shown to influence in this study was apoptosis, which is non-inflammatory as cell contents are removed through phagocytosis rather than the release of cellular contents into the extracellular space which occurs during necrotic cell death. It would be of interest to investigate whether Pak2 can also alter necrotic or necroptotic cell death as these cause inflammation. The inflammatory response and recruitment of inflammatory cells can promote fibrosis as inflammatory cells release TGFβ. If loss of Pak2 were found to promote these forms of cell death, it could explain why there is an increase of TGFβ in $Pak2^{cko}$ mice. However, in this study some parts of the inflammatory response following MI were assessed to investigate whether there were differences between the genotypes following MI, including macrophage infiltration and levels of the pro-inflammatory cytokines IL1β and IL6. No differences in these were identified between the genotypes. This suggests that Pak2 loss does not affect the inflammatory response following MI, though further investigation into changes in other cell types, such as neutrophils, would be required to make this finding conclusive. Conversely, some studies have reported that Pak2 may exacerbate the inflammatory response. For instance, both Pak1 and Pak2 are upstream regulators of NOX in neutrophils, and they are also important for cytoskeletal regulation and migration of inflammatory cells, both of which are reviewed thoroughly by Taglieri et al (2014). However, as mentioned, the cell-specificity of this knockout model makes it unlikely that this can explain the findings in this study. It is worth noting that Pak1, with which Pak2 shares many structural similarities and for which Pak2 can compensate for the loss of (Elsherif *et al.*, 2014), also regulates cardiac fibrosis during disease; Pak1 cardiomyocyte-specific knockout mice exhibit increased interstitial fibrosis compared to $Pak1^{f/f}$ controls 2- and 5-weeks following TAC (W. Liu *et al.*, 2011).

If the increase in TGFβ in the heart is not due to an increase in inflammatory cells, and considering that the model used in this *in vivo* study was cardiomyocyte-specific knockout mice, it is possible that loss of Pak2 may lead to an increase of TGFβ release from cardiomyocytes which could then have a paracrine effect to stimulate

myofibroblast differentiation. To investigate this, it would be important to assess how Pak2 knockout affects known transcriptional regulators of TGFβ such as p38, JNK, and ERK, as well as translational regulators such as PI3K and Akt (Xiao *et al.*, 2008). As mentioned previously in this section, Pak2 has been shown to be activated by PI3K in fibroblasts during TGFβ signalling (Wilkes and Leof, 2006; Hough *et al.*, 2012), though it has not been investigated whether Pak2 itself can influence PI3K. Regarding Akt, there is evidence that Pak2 can activate Akt in some contexts, such as during Rac1-mediated pro-survival pathway in keratinocytes (Wilkes *et al.*, 2005), but not others, with one study suggesting that Pak2 and Akt are two separate pathways downstream of PI3K in fibroblasts (Tang *et al.*, 2000). Furthermore, Pak1 can be activated by Akt (Tang *et al.*, 2000; Zhou *et al.*, 2003) and is a well-known activator of Akt in cardiomyocytes through which it can prevent against arrhythmias following I/R injury (Egom et al., 2010) and may also have other cardioprotective effects such as promoting cell survival, which is blocked by Akt inhibition (Egom et al., 2011; Mao et al., 2008).

Pak2's role in influencing fibrosis-related signalling, such as TGFβ release, in cardiomyocytes has not been previously investigated and, given the already recognised cell-specific differences in Pak2's roles, it would be of great importance to investigate this directly rather than make conclusions from studies in other cell types. An experiment that could be carried out to study this would be to isolate cells from $Pak2^{cko}$ and $Pak2^{f/f}$ mouse hearts. These can then be exposed to hypoxic stress *ex vivo* (Anttila *et al.*, 2017). From this, cardiomyocytes and fibroblasts could be isolated and cultured together, and a contractility assay, which indicates fibroblast activation (Pincha *et al.*, 2018), performed to investigate whether loss of Pak2 in cardiomyocytes is directly responsible for increased myofibroblast activation and the consequential increase in fibrosis following MI.

5.6 Pak2 might protect against cardiac hypertrophy following MI

Pathological CH occurs in remote regions of the infarcted heart to compensate for the loss of contractility in the infarct. It is triggered by both biochemical and mechanical stimuli, for instance through stretch receptors, norepinephrine (NE), endothelin-1, and angiotensin II (St. John Sutton and Sharpe, 2000). During pathological CH, cardiomyocytes increase in size rather than number since cardiomyocytes have a low replicative capability (Bergmann *et al.*, 2009), and these cells also exhibit abnormal gene expression with a reversal back to a foetal gene programme which can impair cardiac contractility (Cox and Marsh, 2014). Whilst initially compensatory, this remodelling can aid in the progression to HF following MI (Galli and Lombardi, 2016).

Evidence from the two-week mild MI model suggested that Pak2 may slow the development of CH following MI, though this result is not conclusive. $Pak2^{cko}$ mice at this timepoint had increased left ventricular mass compared to $Pak2^{f/f}$ controls, which was measured through echocardiography where the heart structure can be visualised. However, there was no increase in heart weight when normalised to tibia length, though the high level of variability in $Pak2^{f/f}$ MI group results may have impacted this. This measurement can produce higher variability as it is affected by human error during removal of the heart; for instance, if not all blood is removed from chambers this can affect results, or similarly if some heart tissue is removed unintentionally when removing connective tissue and the aorta. There was also no difference between the genotypes in this model in terms of cardiomyocyte size, which was measured from heart sections stained with haematoxylin and eosin. However, this technique also did not identify hypertrophy in two-day severe MI samples which had evidence of CH from other methods. Potentially, the difference in average cardiomyocyte size needs to be assessed throughout the heart rather than at one level. To do this serial sectioning of the heart could be carried out and staining done at multiple levels (Ojha *et al.*, 2008). This might improve the validity of this result. Similarly, no genotype differences were identified in the two-week moderate MI model, though due to the high mortality and high variability in the results from this model, these results cannot be used to make conclusions. Evidence from the two-day severe MI model shows that hypertrophic signalling is initiated promptly following MI, with an increase in the hypertrophic markers ANP and BNP at the mRNA level evident in both genotypes at this timepoint. These findings

demonstrate that potentially longer time points are required to fully determine whether Pak2 affects hypertrophic remodelling in the damaged heart following MI. For instance, evaluation at five weeks following MI may be beneficial to assess Pak2's impact on cardiac remodelling following MI as it can take many weeks, and this would also increase the understanding of Pak2's role in the progression from MI to HF.

It is necessary to investigate Pak2's role in CH and HF progression after MI since previous evidence has demonstrated that Pak2 is activated by hypertrophic stress and protects against the development of pathological CH, with loss of Pak2 in cardiomyocytes augmenting the hypertrophic response following TAC (Binder *et al.*, 2019). Transgenic overexpression of Pak2 also reduced CH under stress. This paper postulates that loss of Pak2 promotes hypertrophy through dysregulation of the UPR; ER stress can lead to increased concentrations of cytosolic Ca^{2+}, which can promote CH (Son *et al.*, 2014; Dewenter *et al.*, 2017). Interestingly, Vettel et al (2012) identified that Pak2 can act as a positive regulator of pathological CH, lying downstream of Rac1 during α_1-adrenergic-induced stress. However, this study was carried out solely in an *in vitro* model which lacks the normal cardiomyocyte environment of other cell types and mechanical forces, and using neonatal rat cardiomyocytes, which have an immature nature and do not represent normal signalling pathways that occur in the adult cardiomyocyte (Yang *et al.*, 2014). Thus, further experimentation, potentially using more relevant isolated adult ventricular myocytes, is required to determine the exact mechanism through which Pak2 exerts its anti-hypertrophic role *in vivo*.

Pak1 has also been demonstrated to act as a negative regulator of CH caused by both angiotensin II-infusion (R. Wang *et al.*, 2014) and TAC (W. Liu *et al.*, 2011), and is identified as an upstream activator of JNK signalling, which can antagonise CH through regulating and inhibiting NFAT (Liang *et al.*, 2003). Considering the structural similarities of Pak1 and Pak2 (Rane and Minden, 2014), and how Pak2 can compensate for the loss of Pak1 in a model of hindlimb ischaemia (Elsherif *et al.*, 2014), this further proports the notion of some form of obsolescence between these two isoforms. Though considering the ubiquitous expression pattern of Pak2 compared to the tissue-specific expression of Pak1, it suggests that Pak2's role may be wider reaching.

5.7 Loss of Pak2 in cardiomyocytes alters the ER stress response

ER stress and the UPR are critical mediators of cell survival during MI and I/R (Zhang *et al.*, 2017). Loss of oxygen and nutrients disrupts normal ER function, resulting in accumulation of misfolded or unfolded proteins, which leads to ER stress and activates the UPR. Furthermore, oxidative stress can lead to ER stress as redox homeostasis is required for normal protein folding and disulphide bond formation (Chong *et al.*, 2017). Conversely, activation of the UPR can also lead to increased oxidative stress, thus demonstrating a positive feedback loop (Chong *et al.*, 2017). All three pathways of the UPR – PERK, ATF6 and IRE1 – have been shown to activate following MI- and I/R-related stress (Liu & Dudley, 2016), and targeting therapies to relieve ER stress protects against cell death and reduces infarct size (Song *et al.*, 2011; Z. V. Wang *et al.*, 2014; Li *et al.*, 2015).

In the *in vivo* portion of this study, Pak2 was shown to promote a pro-survival ER stress response following MI, with loss of Pak2 in cardiomyocytes leading to increased expression of the pro-apoptotic ER stress effector molecule Chop. However, at two days post-MI it was not evident through which ER stress pathway Pak2 promotes this protective effect since expression of Chop is regulated by all three branches of the UPR (Hu *et al.*, 2019). To assess this, carrying out earlier timepoints would be required to determine how activation of the three branches differs in $Pak2^{cko}$ mice compared to $Pak2^{f/f}$ controls.

Since it was not clear from *in vivo* data what pathway Pak2 regulates during the response to MI, the impact of loss of Pak2 on the UPR during MI-related stress was investigated *in vitro*. During both oxidative stress and loss of oxygen and nutrients, Pak2 knockdown led to impaired activation of the IRE1 branch of the UPR, whilst the ATF6 and PERK pathways were unaffected. The IRE1 branch of the UPR is multifaceted, promoting cardioprotective effects through activation of XBP1, and apoptosis through ASK1-JNK signalling (S. Wang *et al.*, 2018). Western blot analysis demonstrated that knockdown of Pak2 reduced splicing of XBP1 and increased Chop. When combined with increased apoptotic markers in Pak2 knockdown cells, this suggests Pak2 promotes the cardioprotective IRE1-XBP1 axis. However, changes in the ASK1 and JNK pathways should also be assessed. The IRE1-XBP1 pathway has previously been shown to be

protective in the heart, with XBP1 overexpression reducing infarct size following I/R, and its knockdown exacerbating cardiac dysfunction (Z. V. Wang *et al.*, 2014). Furthermore, neonatal rat ventricular myocytes infected with an adenovirus encoding dominant-negative XBP1 are more likely to undergo apoptosis during hypoxia/reoxygenation than those infected with a control virus (Thuerauf *et al.*, 2006). A study carried out in isolated cardiomyocytes exposed to hypoxia/reoxygenation (H/R) also found that Pak2 is protective through modulating ER stress (Wang *et al.*, 2019). However, interestingly, this study identified that Pak2 is downregulated during H/R, and knockdown of Pak2 leads to increased protein levels of PERK and GRP78/Bip, neither of which occurred in the models used in this project. This could be due to the differences in the models and treatments used, as well as the use of melatonin in the study, though further investigation is necessary to determine the cause for the different findings.

The findings from this project resemble those found regarding Pak2's role in the heart during pressure-overload induced CH. In this model Pak2 was shown to localise near the ER membrane where it promoted the IRE1-XBP1 branch of the UPR by phosphorylating and inactivating PP2A, with $Pak2^{cko}$ mice exhibiting increased cell death and reduced cardiac function, exacerbating the progression to HF (Binder *et al.*, 2019). Activation of IRE1 using quercetin, and overexpression of XBP1s via AAV9 delivery, alleviated the ER dysfunction in the hearts of $Pak2^{cko}$ mice, confirming this mechanism. The commonality of Pak2's protective effects in the heart demonstrates that the Pak2 pathway could be targeted to treat multiple cardiac pathologies.

In 2006, Hollien & Weissman (2006) identified that IRE1 also regulates the degradation of certain mRNAs. This degradation is caused by IRE1-dependent splicing, and the determination of which mRNAs are targeted is governed by their localisation and sequence. This process is termed regulated IRE1-dependent decay of mRNA (RIDD) and is highly conserved (Maurel *et al.*, 2014). Initially RIDD can be protective through reducing ER load. However, prolonged RIDD that occurs during sustained ER stress promotes cell death as mRNAs encoding pro-survival proteins and miRNAs are targeted for degradation (Han *et al.*, 2009; Lerner *et al.*, 2012; Upton *et al.*, 2012). *In vivo* data from this project suggests that RIDD is augmented by loss of Pak2 in cardiomyocytes. mRNA levels of two common RIDD targets, *hgsnat* and *pmp22*, were elevated in $Pak2^{f/f}$ mice after MI, but the same was not found in $Pak2^{cko}$ mice. This suggests that either the

expression of these genes is reduced, or that their mRNA is being degraded, potentially through RIDD. This finding would need to be explored further in order to verify it, but it could suggest that loss of Pak2 promotes the targeting of IRE1 to promote pro-apoptotic pathways over pro-survival splicing of XBP1. How the different axis of IRE1 are activated is unclear, though Han et al (2009) identified that, *in vitro*, inhibition of IRE1's kinase activity promotes XBP1 splicing whilst avoiding RIDD and apoptosis. However, how this mechanism might be regulated *in vivo* is unknown. It would be of interest to investigate how Pak2 may promote the cardioprotective over pro-death axis to improve understanding of its mechanism.

5.8 *In vivo* model analysis and limitations

Despite the increasing use of reperfusion therapies to treat MI and limit the damage to the myocardium caused by ongoing ischaemia, there are some patients for which these therapies are either not feasible or significantly delayed (Li *et al.*, 2017; Chacko *et al.*, 2020). The permanent ligation model of MI used in this study allows for identification of changes in the myocardium that occur without the confoundment of reperfusion. As such, this model permitted screening of the effect of Pak2 on cellular and structural changes in the heart without the potential effect that reperfusion may have on its role. Nevertheless, the *in vivo* study carried out as part of this project had limitations that would have impacted results and will need to be taken into consideration when evaluating Pak2's role in the heart. Some conditions, such as using non-comorbid mice, were chosen to prevent potential variation and to limit confounding factors that may impact results and allow solely the impact of loss of Pak2 on results to be determined. Furthermore, it must be noted that I/R is a more relevant disease model to intimate the human condition in the western world where reperfusion therapies are more common. This could not be done as it is not permitted under the current Home Office project licence.

All mice used in this study were male. Epidemiological studies on MI have found that, whilst the majority of people who suffer an MI are male, it is still a major cause of mortality and morbidity in women (Moshki *et al.*, 2015). For instance, in the UK in 2018, there were 24,599 deaths due to MI, of which 15,143 were male, and 9,456 were female (British Heart Foundation, 2020). Research is often carried out on male mice as this

removes the potential effect on results that may occur as a result of hormonal fluctuations, which might increase variation. However, because of differences between males and females, it has been demonstrated that there are often gender-related variations in results. For instance, in terms of MI-related events, men are more likely to suffer from an MI due to occlusive coronary artery disease (CAD), and usually suffer from an MI around 10 years earlier than women (Regitz-Zagrosek and Kararigas, 2017). Meanwhile, women are more likely to suffer from ischemic heart disease due to non-obstructive CAD or microvascular dysfunction, where blood flow is not completely impeded but leads to myocardial ischaemia. Moreover, a study from 1999 in the United States of America found that younger women have increased mortality following MI compared to aged-matched male patients, though this difference is no longer seen after the age of 74 (Vaccarino *et al.*, 1999). Women also have a higher risk of developing HF following MI than men (Lam *et al.*, 2015). Evidently, further studies are required to investigate whether Pak2 has a gender-based effect, and to assess whether it is cardioprotective for the whole population.

The mice used in this study did not share many of the comorbidities that are found in many patients which suffer an MI. For instance, surgery was performed on mice aged, on average, 12 weeks old. The maximum mouse life expectancy is around three years, thus the mice used in this study were relatively young (Ben-Haim *et al.*, 2018). By comparison, over 80 % patients who suffered from an MI in the UK in 2018 were over 65 years old (British Heart Foundation, 2020). There are many age-related differences, such as immune development, bone density, and drug metabolism, that may impact on findings and reduce their translational capacity (Jackson *et al.*, 2017). Other comorbidities associated with MI are increased body weight, diabetes, hypertension and smoking (Teng *et al.*, 2020). It is unknown whether these may impact Pak2's role during MI. To overcome this, MI could be performed on comorbid mice; however, given the high mortality of this mouse strain already, this may further reduce survival, but would be beneficial to study if Home Office approval could be obtained. The use of young, healthy mice for studies into diseases that often affect the aged population is a common problem and has been recognised as a persistent constraint on research carried out worldwide (Jackson *et al.*, 2017). As such, it may require greater regulatory input for this to be rectified.

The high mortality rate of the Pak2 genetically modified mice during MI was unexpected, particularly the fact that it was not only high in $Pak2^{cko}$ mice but in $Pak2^{f/f}$ control mice as well. This suggests that this strain has potentially developed other mutations through inbreeding that is common when using laboratory-based genetically modified mice (Zeldovich, 2017; Dumont, 2019) and strain-dependent variability in research on MI is a recognised phenomenon (Gao *et al.*, 2005). As a result, during this project, a back-crossing scheme was performed (described in Figure 5.2) where $Pak2^{cko}$ mice were crossed with C57BL/6J mice, the genetic background from which the Pak2-MHC strain was originally generated (Radu *et al.*, 2015). Due to time constraints, it was not possible to assess whether this would improve the overall survival following MI, though if so this may increase the ease of carrying out research into Pak2's role during MI.

The high mortality that occurred following MI experiments reduced the power of the results. Although a mild model allowed for two-week analysis following MI, the reduced severity of this model may conceal some effects of the loss of cardiac Pak2. Furthermore, results could be skewed since only those that survive surgery and the initial high-risk time-points are assessed at the final endpoint. Therefore, those that would have made a significant difference at the chronic timepoint were not available to be analysed. The poor survival of animals, and the drive by the Home Office to reduce animal usage, also meant that not all experiments could be carried out. For instance, triphenyl tetrazolium chloride (TTC) staining is commonly used to assess total infarct size in each model (Ojha *et al.*, 2008). However, to assess this the whole heart must be fixed and stain and cannot be used for other experiments. To still allow for infarct size to be estimated, I used Masson's trichrome staining. By ensuring that all animal hearts were sectioned at the same point, this meant that an estimate of infarct size could be given, though it is recognised that this may not fully represent total infarct size. A further improvement on this would be to inject potassium chloride into the heart prior to its removal (Virag and Lust, 2011). This would ensure that hearts are fixed in position during diastole, and thus remove any variation that may occur due to contractile position.

Due to the small size of the mouse heart, small differences in ligation point can greatly affect results. Whilst surgery was performed by a competent surgeon who has performed permanent ligation of the LAD coronary artery before, there is still potential for technical differences. This was particularly evident in the moderate ligation model,

where the fractional shortening two weeks following MI varied in Pak2$^{f/f}$ mice from 9.59 % to 48.3 % (Figure 3.9). This could be due to incomplete ligation in some mice, or anatomical differences meaning that the severity differs. Measuring circulating plasma levels of cardiac troponin could be carried out to standardise the level of cardiac injury and remove any outliers (Frobert *et al.*, 2015). This was not done as blood collection to measure this must occur 24 hours following surgery and given the fragility and high mortality of this mouse strain following MI it was determined that the risk the increased stress that this would place on the mice was too great.

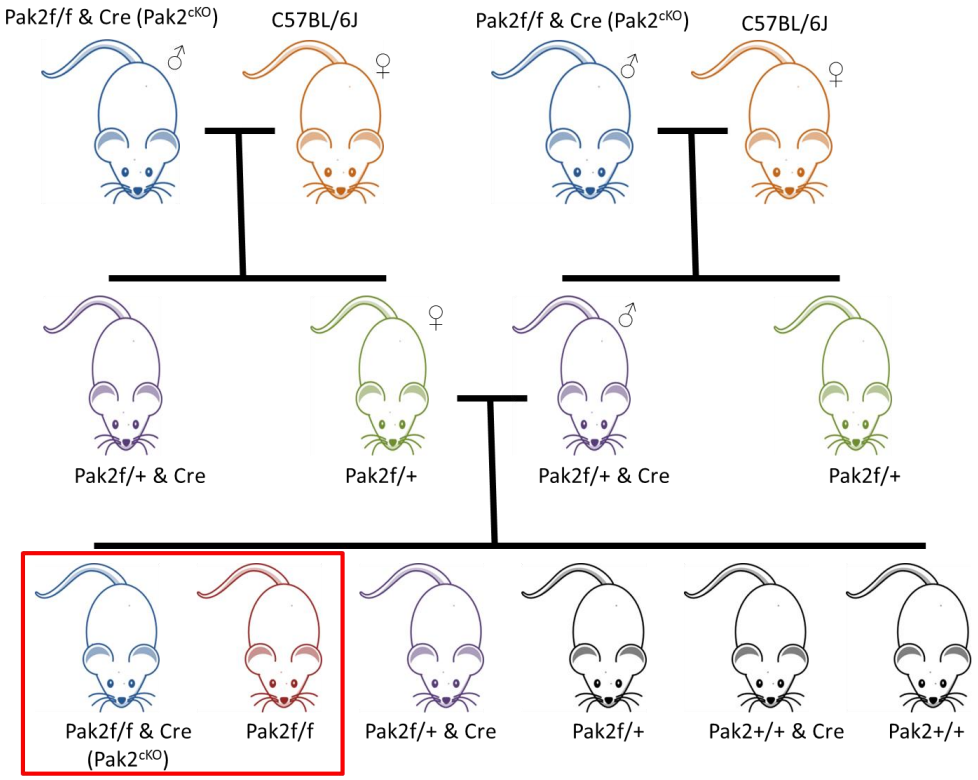

Figure 5.2 Breeding scheme for back-crossing of the Pak2-MHC strain. Current Pak2 cardiomyocyte-specific knockout mice (Pak2^{cko}), which are homozygous for flox-sites (f/f) around exon 2 of the Pak2 gene and contain the Cre element under control of the MHC promoter, were crossed with C57BL/6J mice, the strain from which the Pak2-MHC strain was originally generated. From this, two potential genotypes were produced: both were heterozygous for flox sites (f/+), half also contained the MHC-Cre genotype. From these offspring, a mouse containing Cre and a mouse without the Cre element were crossed. From this there were six potential genotypes of offspring: those without flox sites (Pak2+/+), those heterozygous for flox sites (Pak2f/+) and those homozygous for flox sites (Pak2f/f), each of which could also contain the Cre element. From these, the final strain could be continued using those delineated by the red box.

5.9 *In vitro* model analysis and limitations

The *in vitro* study of this project was carried out in H9c2 cardiomyoblasts. This cell line was originally derived from embryonic ventricular rat tissue, and as such resembles immature cardiomyocytes (Kimes and Brandt, 1976). They have been used in many studies on cardiovascular diseases, for instance to investigate cardiotoxic agents (L.-Q. Ma *et al.*, 2018; Lage *et al.*, 2019), and to investigate pathways involved in cardiovascular diseases (Merten *et al.*, 2007; Giacomo *et al.*, 2010; Zhang *et al.*, 2013). Where possible, experiments in this current study were carried out on cells with a passage number less than 20 as longer passages may affect results (Witek *et al.*, 2016). H9c2 cells have translational limitations as they are non-human, and they are also immature, shown by their propensity to proliferate. Furthermore, all cell lines have the potential for random genetic mutations to arise through their continuous replication, which may impact on results without the researcher's knowledge. However, many publications continue to use this cell line as a proxy for adult cardiomyocytes, and a study in 2015 found that H9c2 cells share more similarities with primary cardiomyocytes than other cell lines in terms of their response to hypoxia-reoxygenation, for which they have an increased sensitivity (Kuznetsov *et al.*, 2015).

Due to time constraints, results could not be confirmed in a more translational model; however, future work would include verification of these results in isolated adult rat ventricular cardiomyocytes. The effect of Pak2 *in vitro* could also be assessed in human cell models, such as human embryonic stem cell- or induced pluripotent stem cells-derived cardiomyocytes to further improve the translational capacity of these results, though these too have limitations, which are reviewed extensively elsewhere (Karakikes *et al.*, 2015; Jiang *et al.*, 2018; Gintant *et al.*, 2019). A limitation of all these models is that they are cardiomyocytes in isolation, and as such cannot mimic the multi-cellular environment of the adult heart which consists of many cell types.

To mimic the hypoxic environment caused by coronary artery occlusion *in vivo* and in human patients, cells were cultured in 100 % N_2 in a Billups-Rothenberg modular incubator chamber. Testing from our lab identified that, although sealed, oxygen does still leak into the chamber, and as such these conditions were termed hypoxic rather than anoxic. This mimics *in vivo* conditions where angiogenesis will restore some blood

flow back to affected tissue. Furthermore, even in the permanent ligation model other vessel branches can still supply some oxygen supply to cardiomyocytes, thus creating the border region of the infarct.

Hypoxia was combined with nutrient starvation. Loss of nutrients was mimicked *in vitro* through culturing cells in media lacking glucose or foetal bovine serum. This was to imitate the loss of nutrient supply to cardiomyocytes caused by permanent coronary artery ligation. Upon loss of oxygen, and hence increased anaerobic respiration, there is an increase demand for glucose as the substrate for ATP production (Wong *et al.*, 2016). Therefore, nutrient starvation would further impede the cells' response to hypoxia. Loss of nutrients can promote autophagy, as well as apoptosis and necrosis, as the cell attempts to survive by degrading unnecessary protein and organelles to generate fatty and amino acids to be used for ATP production (Russell *et al.*, 2014). Therefore, it would be of interest to also investigate whether Pak2 impacts the autophagic response, though this was not the focus of this current project.

The final *in vitro* MI-related condition in which Pak2's role was assessed was oxidative stress. Some oxidative stress was shown to occur in mice two days following MI without reperfusion, with increased Dihydroethidium (DHE) staining in heart tissue. DHE is a fluorescent probe that is oxidised in the presence of superoxide molecules, leading to increased fluorescence in the red spectrum that can be identified through fluorescent microscopy. There was also reduced gene expression of the antioxidant superoxide dismutase 2 (SOD2), which is consistent with previous findings that this gene is downregulated during oxidative stress (Zhang *et al.*, 2019). Loss of Pak2 did not affect SOD2 expression, suggesting that Pak2 may not play a role in promoting the removal of redox molecules, though further molecules would need to be investigated to determine this conclusively. The finding that oxidative stress occurs in the permanent ligation model of MI demonstrated the importance to investigate whether this may impact on Pak2's role in the heart. Cellular oxidative stress was initiated *in vitro* by culturing cells in 100 µM hydrogen peroxide (H_2O_2). 100 µM was used as this has been proven to cause oxidative stress and initiate cell death in H9c2 cells (Zhang *et al.*, 2013). H_2O_2 is produced following the conversion of $O_2^{\bullet-}$ by SODs. From this it is further detoxified by the cell (Kurian *et al.*, 2016). It causes cellular damage to macromolecules, including DNA,

proteins, and lipids, and can also alters calcium handling, thus leading to arrythmias (Zhang *et al.*, 2019).

5.10 Pak2 as a potential therapeutic target

Therapies to treat MI focus predominantly on restoration of blood flow, including drugs such as fibrinolytic agents, like tissue plasminogen activator (tPA), and surgeries including percutaneous coronary intervention (PCI) and coronary artery bypass grafts (CABG). However, whilst these restore blood flow, thus preventing the ongoing damage to the myocardium caused by ischaemia, they do not prevent the death of those already undergoing cell death, and conversely cause further cell death through I/R injury, where oxygen restoral causes oxidative burst. Consequently, there is a need to directly target the cell death caused by MI, and if possible, by reperfusion. This would hopefully aid in the prevention of HF development considering that around 1 billion cardiomyocytes are predicted to die for HF to develop (Murry *et al.*, 2006), and considering that HF following MI is an increasing issue (Velagaleti *et al.*, 2008).

The findings from this and previous studies suggest that targeting and promoting Pak2 activity in the heart could be beneficial and a potential therapeutic target. However, before this can be achieved, a full understanding of the effect of Pak2 in the diseased heart needs to be ascertained. For instance, the findings from this study, which show that Pak2 can influence both fibrosis and cell death, demonstrate its potential varied effects. Therefore, should it be possible to target Pak2, or either upstream or downstream molecules in its cardioprotective pathway, it would be important that this was specific to avoid any off-target effects, especially as Pak2 is ubiquitously expressed meaning therapy could affect other cell-types and tissues.

At what time point following MI or reperfusion Pak2 could be targeted to achieve the most benefit would need to be investigated. To understand this there needs to be a greater knowledge of how and when Pak2 becomes activated, its exact mechanism of protective effect, and whether it plays a greater role during ischaemia or reperfusion. Furthermore, any long-term effects of Pak2 overexpression in cardiomyocytes would need to be explored, though transgenic overexpression of Pak2 in mice does not appear to cause any adverse effects (Binder *et al.*, 2019).

However, Pak2 may not be an ideal candidate target therapeutically. Pak2 has been well-studied throughout the body for its role during cancer progression and metastasis. It is expressed in numerous cancer types, and it is an unfavourable prognostic marker for pancreatic, prostate and gastric cancer (Gao *et al.*, 2014). This is due to Pak2's role in promoting survival, which, whilst beneficial in the heart during disease, also implicates it in tumour progression where it promotes the survival of malignant cells. For instance, Pak2 can regulate cytoskeletal structure; upregulation of Pak2 in malignant tumours antagonises the phosphorylation of myosin light chain (MLC) through downregulation of RhoA (Coniglio *et al.*, 2008), potentially explaining the antagonistic nature of Rac1 and RhoA signalling (Sander *et al.*, 1999; Nimnual *et al.*, 2003). Reduced phosphorylation of MLC in turn reduces focal adhesion size, meaning cell movement is easier, plus knockdown of Pak2 prevents formation of new focal adhesions, demonstrating that Pak2 aids in focal adhesion formation that is required for metastasis (Coniglio *et al.*, 2008). This is supported by the finding of reduced migration of ovarian cancer cells when Pak2 is knocked down (Flate and Stalvey, 2014). In an *in vitro* model of pancreatic cancer, Pak2 was also shown to promote cancer cell proliferation through regulating MMP2 and 9, PCNA and Ki67 (Yao *et al.*, 2019), and down-regulation of Pak2 by miR-137 prevented Pak2-mediated proliferation of melanoma cells (Hao *et al.*, 2015). Although cardiac tumours are reasonably rare, they can occur and be both benign and malignant, both of which can impact cardiac function and lead to death (Cresti *et al.*, 2016). Therefore, it would be imperative that no treatment to promote Pak2 in the heart could inadvertently have pro-tumour effects.

The findings of Pak2's role in cancer has meant that it has been identified as a potential therapeutic target for preventing cancer progression, potentially via Pak2 inhibitors or inhibitors of its upstream activators (Edlinger *et al.*, 2017; Liu *et al.*, 2020). However, considering the findings from this and previous studies identifying Pak2 as protective in the heart during disease, any of these cancer therapies would need to be highly targeted and investigated for potential cardiotoxic effects.

5.11 Future work

Although there was evidence of oxidative stress in hearts two days following MI by permanent LAD ligation, with increased ROS levels demonstrated by DHE staining, and reduced expression of the anti-oxidant SOD2, oxidative stress is known to play a greater role in cell damage and death during I/R injury. This is because restoration of oxygen supply causes oxidative burst and dysregulation of the electron transport chain (González-Montero *et al.*, 2018). Due to the finding of Pak2's protective role *in vitro* during oxidative stress, it must be investigated whether Pak2^{cko} mice respond differently to controls following I/R injury. This model is not permitted by the Home Office under the current project licence; however, should it be permitted under future licences this will be investigated. The hypothesis that Pak2 will be protective during I/R injury is supported by findings from other labs that Pak2 becomes activated and protects against cardiomyocyte death following hypoxia/reoxygenation *in vitro*, though different upstream mechanisms for this have been described (Wang *et al.*, 2019; Xu *et al.*, 2020).

The experiments carried out in this study focused on Pak2's role in apoptosis. However, apoptosis is not the only form of cell death that occurs following MI. Necroptosis, a caspase-independent form of programmed cell death, has been shown to contribute to cardiomyocyte death following MI, in particular to promote detrimental remodelling (Luedde *et al.*, 2014). Studies have shown that ER stress during MI and I/R can promote necroptosis as well as apoptosis (Zhu *et al.*, 2018) and targeting this reduces infarct size after coronary artery ligation (Chang *et al.*, 2019). Considering the well-established role of Pak2 in regulating ER function and protecting against cytotoxic ER stress, it would be of interest to investigate whether Pak2 can protect against ER stress-induced necroptosis.

Although this study identified that Pak2 becomes activated following initiation of MI-related stress, it remains unclear the exact mechanism or upstream pathway that leads to its activation. Identifying this would improve overall understanding of signalling that occurs during MI, and potentially how this protective pathway could be utilised for therapeutic purposes. Pak2 has numerous binding sites on its structure through which its conformational change-induced activation could be stimulated. A complexity of this is the high number of upstream activators of Pak2 that have been identified (Z. Zhao *et*

al., 2000; Wilkes *et al.*, 2003; Huang *et al.*, 2020; Mei *et al.*, 2020). To first investigate this, common activators of Pak2, such as Cdc42, Rac1, and PIX, could be assessed through RNAi screening. Recent studies have demonstrated that Pak2's activation during hypoxia/reoxygenation *in vitro* may be due to binding of AMPK (Wang *et al.*, 2019), and AMPK has also shown to activate Pak2 in the brain of rats exposed to intermittent hypoxia (Mei *et al.*, 2020). AMPK is protective following MI and I/R, with its inhibition leading to impaired cardiac function and increased apoptosis in the heart (Russell *et al.*, 2004; Moussa and Li, 2012). Thus, it would be of great interest to assess whether modulation of AMPK during MI alters Pak2 phosphorylation *in vivo*, and whether this alters the protective effects of Pak2 demonstrated in this study.

There are currently no drugs developed to specifically target and activate Pak2; therefore, gene therapy could be a viable option as it can be directed to the heart specifically. Experiments in mice to overexpress Pak2 have used the adeno-associated virus-9 (AAV9) (Binder *et al.*, 2019). Recombinant AAVs (rAAVs) are preferred to other virus vectors for therapies due to their efficient and long-term transgene expression, meaning a single dosage may be sufficient (Svensson *et al.*, 1999). Furthermore, unlike other viral vectors, they have low immunogenicity, making them more suitable for therapies (Somanathan *et al.*, 2010; Verdera *et al.*, 2020). AAV9 is used to target cardiac tissue as it has superior gene transfer capability in this organ than other AAV serotypes (Bish *et al.*, 2008). In mice it has shown to have benefits from a single dose and can be targeted to specific regions of the heart using different promoters (Ni *et al.*, 2019; Yadav *et al.*, 2019). AAVs have already been piloted for gene therapies in humans and have demonstrated beneficial effects (Mendell *et al.*, 2017). However, despite the low immunogenicity of AAV vectors compared to others, immune responses following gene transfer have been reported and represent a hindrance to their use in the clinic (Ronzitti *et al.*, 2020). Furthermore, considering the homology between the capsid of naturally occurring AAVs and rAAVs, previous exposure could occur and lead to inherent immunity, thus reducing the effectiveness of gene delivery (Calcedo *et al.*, 2009; Boutin *et al.*, 2010). Additionally, detrimental effects of high doses of AAV9 have been reported in large animal models, including damage to the liver and sensory neurons independent of an immune response (Hinderer *et al.*, 2018), demonstrating that doses must be kept to a minimum.

5.12 Conclusion

To conclude, this study has demonstrated that Pak2 is activated during the acute phase of MI, and this is likely required for cardioprotection. Pak2 acts as a pro-survival molecule in cardiomyocytes during MI and MI-related stress through modulation of the ER stress response to promote the activation of the protective IRE-XBP1 branch. Pak2 may also act as an anti-fibrotic molecule in the heart following stress, and might also protect against the development of cardiac hypertrophy in remote regions, both of which could be beneficial in preventing the progression to HF following MI. However, further research is required to investigate and consolidate these results. These findings demonstrate the therapeutic potential of targeting Pak2 signalling to prevent the progression to heart failure.

Chapter 6: Appendix

6.1 Appendix 1

The first year of this PhD project included carrying out experiments to complete the submission and revisions for the paper:

"Pak2 as a novel therapeutic target for cardioprotective endoplasmic reticulum stress response" (*Circulation Research* 124(5): 696-711)

> Authors: Binder P, Wang S, Radu M, Zin M, **Collins L**, Khan S, Li Y, Sekeres K, Humphreys N, Swanton E, Reid A, Pu F, Oceandy D, Guan K, Hille S, Frey N, Muller O, Cartwright E, Chernoff J, Wang X, Liu W

Lucy Collins was responsible for breeding and maintenance of the Pak2 cardiomyocyte-specific knockout ($Pak2^{cko}$) mouse model during this time. She isolated all adult rat cardiomyocytes used throughout this paper and performed the immunohistochemistry co-localisation staining displayed in Figure 1 and Supplementary figure I. She also generated and amplified the primers used for production of the AAV9-XBP1s overexpression virus and assisted in the delivery and functional analysis of this virus in $Pak2^{cko}$ mice after transverse aortic constriction (TAC) (Figure 6M and Supplemental figure XVIF). Together with P.B. she administered the flavonol quercetin via oral gavage to produce pharmacological activation of IRE1 in $Pak2^{cko}$ mice and assessed the impact of this on cardiac function in mice following TAC (Figure 6K, Supplemental figure XVIC). She contributed to the writing of the methods.

6.2 Appendix 2

Initial MI experiments were carried out on mice using the standard model (termed the severe ligation model in this project) where the LAD was ligated at the same ligation point used in other mouse lines and mice were kept until the endpoint at day 7. However, within this time point, there was 75 % mortality in both genotype groups following MI, with 3 of the 4 MI mice dying. As such, no conclusions could be made from this model. The mortality exceeded what is permitted on the Home Office project licence and so no more experiments using this surgical model for this time point was permitted.

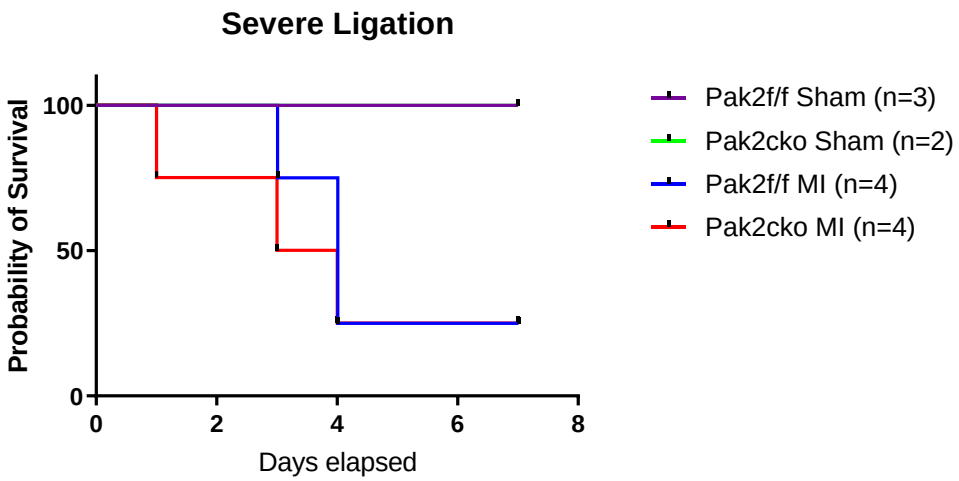

Supplementary Figure 2.1 Survival data following severe MI ligation. Both genotypes had 75% mortality within 7 days following severe MI ligation. There were no deaths in either sham group. N=4 for each MI group, n=3 for $Pak2^{f/f}$ sham group, n=2 for $Pak2^{cko}$ sham group.

Chapter 7: Bibliography

Abbate, A., Biondi-Zoccai, G. G. L., Bussani, R., Dobrina, A., Camilot, D., Feroce, F., Rossiello, R., Baldi, F., Silvestri, F., Biasucci, L. M., *et al.* (2003) 'Increased myocardial apoptosis in patients with unfavorable left ventricular remodeling and early symptomatic post-infarction heart failure', *Journal of the American College of Cardiology*, 41(5), pp. 753–760.

Abbate, A., Salloum, F. N., Vecile, E., Das, A., Hoke, N. N., Straino, S., Giuseppe, G. L., Biondi-Zoccai, Houser, J. E., Qureshi, I. Z., *et al.* (2008) 'Anakinra, a recombinant human interleukin-1 receptor antagonist, inhibits apoptosis in experimental acute myocardial infarction', *Circulation*, 117(20), pp. 2670–2683.

Agah, R., Frenkel, P. A., French, B. A., Michael, L. H., Overbeek, P. A. and Schneider, M. D. (1997) 'Gene recombination in postmitotic cells. Targeted expression of Cre recombinase provokes cardiac-restricted, site-specific rearrangement in adult ventricular muscle in vivo.', *The Journal of Clinical Investigation*, 100(1), pp. 169–79.

Anttila, K., Streng, T., Pispa, J., Vainio, M. and Nikinmaa, M. (2017) 'Hypoxia exposure and B-type natriuretic peptide release from Langendorff heart of rats', *Acta Physiologica*, 220(1), pp. 28–35.

B'Chir, W., Maurin, A. C., Carraro, V., Averous, J., Jousse, C., Muranishi, Y., Parry, L., Stepien, G., Fafournoux, P. and Bruhat, A. (2013) 'The eIF2α/ATF4 pathway is essential for stress-induced autophagy gene expression', *Nucleic Acids Research*, 41(16), pp. 7683–7699.

Barcellos-Hoff, M. H. and Dix, T. A. (1996) 'Redox-mediated activation of latent transforming growth factor-beta 1.', *Molecular Endocrinology*, 10(9), pp. 1077–1083.

Barry, D. M., Xu, K., Meadows, S. M., Zheng, Y., Norden, P. R., Davis, G. E. and Cleaver, O. (2015) 'Cdc42 is required for cytoskeletal support of endothelial cell adhesion during blood vessel formation in mice', *Development*, 142(17), pp. 3058–3070.

Baum, J. and Duffy, H. S. (2011) 'Fibroblasts and myofibroblasts: What are we talking about?', *Journal of Cardiovascular Pharmacology*, pp. 376–379.

Belmont, P. J., Chen, W. J., San Pedro, M. N., Thuerauf, D. J., Lowe, N. G., Gude, N., Hilton, B., Wolkowicz, R., Sussman, M. A. and Glembotski, C. C. (2010) 'Roles for endoplasmic

reticulum-associated degradation and the novel endoplasmic reticulum stress response gene derlin-3 in the ischemic heart', *Circulation Research*, 106(2), pp. 307–316.

Ben-Haim, M. S., Kanfi, Y., Mitchell, S. J., Maoz, N., Vaughan, K. L., Amariglio, N., Lerrer, B., De Cabo, R., Rechavi, G. and Cohen, H. Y. (2018) 'Breaking the ceiling of human maximal life span', *Journals of Gerontology - Series A Biological Sciences and Medical Sciences*, 73(11), pp. 1465–1471.

Bergmann, O., Bhardwaj, R. D., Bernard, S., Zdunek, S., Barnabé-Heider, F., Walsh, S., Zupicich, J., Alkass, K., Buchholz, B. A., Druid, H., *et al.* (2009) 'Evidence for cardiomyocyte renewal in humans.', *Science*, 324(5923), pp. 98–102.

Bernard, K., Logsdon, N. J., Ravi, S., Xie, N., Persons, B. P., Rangarajan, S., Zmijewski, J. W., Mitra, K., Liu, G., Darley-Usmar, V. M., *et al.* (2015) 'Metabolic reprogramming is required for myofibroblast contractility and differentiation', *Journal of Biological Chemistry*, 290(42), pp. 25427–25438.

Bertolotti, A., Zhang, Y., Hendershot, L. M., Harding, H. P. and Ron, D. (2000) 'Dynamic interaction of BiP and ER stress transducers in the unfolded-protein response.', *Nature Cell Biology*, 2(6), pp. 326–332.

Bhar-Amato, J., Davies, W. and Agarwal, S. (2017) 'Ventricular arrhythmia after acute myocardial infarction: "The perfect storm"', *Arrhythmia and Electrophysiology Review*, 6(3), pp. 134–139.

Binder, P., Wang, S., Radu, M., Zin, M., Collins, L., Khan, S., Li, Y., Sekeres, K., Humphreys, N., Swanton, E., *et al.* (2019) 'Pak2 as a novel therapeutic target for cardioprotective endoplasmic reticulum stress response', *Circulation Research*, 124(5), pp. 696–711.

Bish, L. T., Morine, K., Sleeper, M. M., Sanmiguel, J., Wu, D., Gao, G., Wilson, J. M. and Sweeney, H. L. (2008) 'Adeno-associated virus (AAV) serotype 9 provides global cardiac gene transfer superior to AAV1, AAV6, AAV7, and AAV8 in the mouse and rat', *Human Gene Therapy*, 19(12), pp. 1359–1368.

Boda, B., Alberi, S., Nikonenko, I., Node-Langlois, R., Jourdain, P., Moosmayer, M., Parisi-Jourdain, L. and Muller, D. (2004) 'The mental retardation protein PAK3 contributes to synapse formation and plasticity in hippocampus', *Journal of Neuroscience*, 24(48), pp.

10816–10825.

Bohgaki, T., Mozo, J., Salmena, L., Matysiak-Zablocki, E., Bohgaki, M., Sanchez, O., Strasser, A., Hakem, A. and Hakem, R. (2011) 'Caspase-8 inactivation in T cells increases necroptosis and suppresses autoimmunity in Bim-/- mice', *Journal of Cell Biology*, 195(2), pp. 277–291.

Boissel, J. P., Aldor, Erd, Gaul, Kuhn, Leisch, Lenzhofer, Mlczoch, Peschorn, Tiso, *et al.* (2000) 'Effect of 48-h intravenous trimetazidine on short- and long-term outcomes of patients with acute myocardial infarction, with and without thrombolytic therapy: A double-blind, placebo-controlled, randomized trial', *European Heart Journal*, 21(18), pp. 1537–1546.

Bokoch, G. M. (1998) 'Caspase-mediated activation of PAK2 during apoptosis: Proteolytic kinase activation as a general mechanism of apoptotic signal transduction?', *Cell Death and Differentiation*, 5(8), pp. 637–645.

Boutin, S., Monteilhet, V., Veron, P., Leborgne, C., Benveniste, O., Montus, M. F. and Masurier, C. (2010) 'Prevalence of serum IgG and neutralizing factors against adeno-associated virus (AAV) types 1, 2, 5, 6, 8, and 9 in the healthy population: Implications for gene therapy using AAV vectors', *Human Gene Therapy*, 21(6), pp. 704–712.

British Heart Foundation (2020) *UK factsheet - January 2021*.

Buchner, D. A., Su, F., Yamaoka, J. S., Kamei, M., Shavit, J. A., Barthel, L. K., McGee, B., Amigo, J. D., Kim, S., Hanosh, A. W., *et al.* (2007) 'pak2a mutations cause cerebral hemorrhage in redhead zebrafish', *Proceedings of the National Academy of Sciences*, 104(35), pp. 13996–14001.

Bujak, M., Dobaczewski, M., Chatila, K., Mendoza, L. H., Li, N., Reddy, A. and Frangogiannis, N. G. (2008) 'Interleukin-1 receptor type I signaling critically regulates infarct healing and cardiac remodeling', *American Journal of Pathology*, 173(1), pp. 57–67.

Burbelo, P. D., Kozak, C. A., Finegold, A. A., Hall, A. and Pirone, D. M. (1999) 'Cloning, central nervous system expression and chromosomal mapping of the mouse PAK-1 and PAK-3 genes', *Gene*, 232(2), pp. 209–215.

Burgos-Morón, Abad-Jiménez, Marañón, Iannantuoni, Escribano-López, López-Domènech, Salom, Jover, Mora, Roldan, *et al.* (2019) 'Relationship between oxidative stress, ER stress, and inflammation in type 2 diabetes: The battle continues', *Journal of Clinical Medicine*, 8(9), p. 1385.

Cabibi, D., Bronte, F., Porcasi, R., Ingrao, S., Giannone, A. G., Maida, M., Grazia Bavetta, M., Petta, S., Di Marco, V. and Calvaruso, V. (2015) 'Comparison of histochemical stainings in evaluation of liver fibrosis and correlation with transient elastography in chronic hepatitis', *Analytical Cellular Pathology*, 2015(431750).

Calcedo, R., Vandenberghe, L. H., Gao, G., Lin, J. and Wilson, J. M. (2009) 'Worldwide epidemiology of neutralizing antibodies to adeno-associated viruses', *The Journal of Infectious Diseases*, 199(3), pp. 381–390.

Capasso, J. M., Palackal, T., Olivetti, G. and Anversa, P. (1990) 'Left ventricular failure induced by long-term hypertension in rats', *Circulation Research*, 66(5), pp. 1400–1412.

Carlson, S., Trial, J., Soeller, C. and Entman, M. L. (2011) 'Cardiac mesenchymal stem cells contribute to scar formation after myocardial infarction', *Cardiovascular Research*, 91(1), pp. 99–107.

Carry, M. M., Peng, C. F., Mrak, R. E., Straub, K. D., Murphy, M. L. and Fody, E. P. (1989) 'Reperfusion injury in ischemic myocardium: Protective effects of ruthenium red and of nitroprusside', *American Journal of Cardiovascular Pathology*, 2(4), pp. 335–344.

Chacko, L., Howard, J. P., Rajkumar, C., Nowbar, A. N., Kane, C., Mahdi, D., Foley, M., Shun-Shin, M., Cole, G., Sen, S., *et al.* (2020) 'Effects of percutaneous coronary intervention on death and myocardial infarction stratified by stable and unstable coronary artery disease: A meta-analysis of randomized controlled trials', *Circulation: Cardiovascular Quality and Outcomes*, 13(2), p. e006363.

Chang, L., Wang, Z., Ma, F., Tran, B., Zhong, R., Xiong, Y., Dai, T., Wu, J., Xin, X., Guo, W., *et al.* (2019) 'ZYZ-803 mitigates endoplasmic reticulum stress-related necroptosis after acute myocardial infarction through downregulating the RIP3-CaMKII signaling pathway', *Oxidative Medicine and Cellular Longevity*, 2019, p. 6173685.

Chen, Y.-T., Wong, L. L., Liew, O. W. and Richards, A. M. (2019) 'Heart failure with

reduced ejection fraction (HFrEF) and preserved ejection fraction (HFpEF): The diagnostic value of circulating microRNAs', *Cells*, 8(12), p. 1651.

Chen, Y., Yu, Q. and Xu, C. B. (2017) 'A convenient method for quantifying collagen fibers in atherosclerotic lesions by imagej software', *International Journal of Clinical and Experimental Medicine*, 10(10), pp. 14904–14910.

Chen, Z., Chua, C. C., Ho, Y.-S., Hamdy, R. C. and Chua, B. H. L. (2001) 'Overexpression of Bcl-2 attenuates apoptosis and protects against myocardial I/R injury in transgenic mice', *Am J Physiol Heart Circ Physiol*, 280(5), pp. 2313–2320.

Chiong, M., Wang, Z. V., Pedrozo, Z., Cao, D. J., Troncoso, R., Ibacache, M., Criollo, A., Nemchenko, A., Hill, J. A. and Lavandero, S. (2011) 'Cardiomyocyte death: Mechanisms and translational implications', *Cell Death and Disease*, 2(12), p. e244.

Chipurupalli, S., Kannan, E., Tergaonkar, V., D'andrea, R. and Robinson, N. (2019) 'Hypoxia induced ER stress response as an adaptive mechanism in cancer', *International Journal of Molecular Sciences*, 20(3), p. 749.

Chong, W. C., Shastri, M. D. and Eri, R. (2017) 'Endoplasmic reticulum stress and oxidative stress: A vicious nexus implicated in bowel disease pathophysiology', *International Journal of Molecular Sciences*, 18(4), p. 771.

Chung, A. C. K., Dong, Y., Yang, W., Zhong, X., Li, R. and Lan, H. Y. (2013) 'Smad7 suppresses renal fibrosis via altering expression of TGF-β/Smad3-regulated microRNAs', *Molecular Therapy*, 21(2), pp. 388–398.

Cleutjens, J. P. M., Verluyten, M. J. A., Smits, J. F. M. and Daemen, M. J. A. P. (1995) 'Collagen remodeling after myocardial infarction in the rat heart', *American Journal of Pathology*, 147(2), pp. 325–338.

Cnop, M., Foufelle, F. and Velloso, L. A. (2012) 'Endoplasmic reticulum stress, obesity and diabetes', *Trends in Molecular Medicine*, 18(1), pp. 59–68.

Cochain, C., Channon, K. M. and Silvestre, J. S. (2013) 'Angiogenesis in the infarcted myocardium', *Antioxidants and Redox Signaling*, 18(9), pp. 1100–1113.

Coleman, M. L., Sahai, E. A., Yeo, M., Bosch, M., Dewar, A. and Olson, M. F. (2001)

‘Membrane blebbing during apoptosis results from caspase-mediated activation of ROCK I’, *Nature Cell Biology*, 3(4), pp. 339–345.

Colla, E. (2019) ‘Linking the endoplasmic reticulum to Parkinson’s disease and alpha-synucleinopathy’, *Frontiers in Neuroscience*, 13(MAY), p. 560.

Coniglio, S. J., Zavarella, S. and Symons, M. H. (2008) ‘Pak1 and Pak2 mediate tumor cell invasion through distinct signaling mechanisms.’, *Molecular and Cellular Biology*, 28(12), pp. 4162–72.

Conrad, N., Judge, A., Tran, J., Mohseni, H., Hedgecott, D., Crespillo, A. P., Allison, M., Hemingway, H., Cleland, J. G., McMurray, J. J. V., *et al.* (2018) ‘Temporal trends and patterns in heart failure incidence: a population-based study of 4 million individuals’, *The Lancet*, 391(10120), pp. 572–580.

Cox, E. J. and Marsh, S. A. (2014) ‘A systematic review of fetal genes as biomarkers of cardiac hypertrophy in rodent models of diabetes’, *PLoS ONE*, 9(3), p. 92903.

Crawford, E. D. and Wells, J. A. (2011) ‘Caspase substrates and cellular remodeling’, *Annual Review of Biochemistry*, 80, pp. 1055–1087.

Cresti, A., Chiavarelli, M., Glauber, M., Tanganelli, P., Scalese, M., Cesareo, F., Guerrini, F., Capati, E., Focardi, M. and Severi, S. (2016) ‘Incidence rate of primary cardiac tumors: A 14-year population study’, *Journal of Cardiovascular Medicine*, 17(1), pp. 37–43.

Culmsee, C., Zhu, C., Landshamer, S., Becattini, B., Wagner, E., Pellechia, M., Blomgren, K. and Plesnila, N. (2005) ‘Apoptosis-inducing factor triggered by poly(ADP-ribose) polymerase and Bid mediates neuronal cell death after oxygen-glucose deprivation and focal cerebral ischemia’, *Journal of Neuroscience*, 25(44), pp. 10262–10272.

Dai, Y., Song, J., Li, W., Yang, T., Yue, X., Lin, X., Yang, X., Luo, W., Guo, J., Wang, X., *et al.* (2019) ‘RhoE fine-tunes inflammatory response in myocardial infarction’, *Circulation*, 139(9), pp. 1185–1190.

Dally, S., Monceau, V., Corvazier, E., Bredoux, R., Raies, A., Bobe, R., del Monte, F. and Enouf, J. (2009) ‘Compartmentalized expression of three novel sarco/endoplasmic reticulum Ca2+ATPase 3 isoforms including the switch to ER stress, SERCA3f, in non-failing and failing human heart’, *Cell Calcium*, 45(2), pp. 144–154.

Daugas, E., Susin, S. A., Zamzami, N., Ferri, K. F., Irinopoulou, T., Larochette, N., Prévost, M. C., Leber, B., Andrews, D., Penninger, J., *et al.* (2000) 'Mitochondrio-nuclear translocation of AIF in apoptosis and necrosis.', *The FASEB journal : official publication of the Federation of American Societies for Experimental Biology*, 14(5), pp. 729–739.

Davis, R. J. (2000) 'Signal transduction by the JNK group of MAP kinases', *Cell*, 103(2), pp. 239–252.

Davis, R. T., Simon, J. N., Utter, M., Mungai, P., Alvarez, M. G., Chowdhury, S. A. K., Heydemann, A., Ke, Y., Wolska, B. M. and Solaro, R. J. (2015) 'Knockout of p21-activated kinase-1 attenuates exercise-induced cardiac remodelling through altered calcineurin signalling', *Cardiovascular Research*, 108(3), pp. 335–347.

DeSantiago, J., Bare, D. J., Varma, D., Solaro, R. J., Arora, R. and Banach, K. (2018) 'Loss of p21-activated kinase 1 (Pak1) promotes atrial arrhythmic activity', *Heart Rhythm*, 15(8), pp. 1233–1241.

Desmouliere, A., Geinoz, A., Gabbiani, F. and Gabbiani, G. (1993) 'Transforming growth factor-β1 induces α-smooth muscle actin expression in granulation tissue myofibroblasts and in quiescent and growing cultured fibroblasts', *Journal of Cell Biology*, 122(1), pp. 103–111.

Deten, A., Hölzl, A., Leicht, M., Barth, W. and Zimmer, H.-G. (2001) 'Changes in extracellular matrix and in transforming growth factor beta isoforms after coronary artery ligation in rats', *Journal of Molecular and Cellular Cardiology*, 33(6), pp. 1191–1207.

Dewenter, M., von der Lieth, A., Katus, H. A. and Backs, J. (2017) 'Calcium signaling and transcriptional regulation in cardiomyocytes.', *Circulation Research*, 121(8), pp. 1000–1020.

Dhuriya, Y. K. and Sharma, D. (2018) 'Necroptosis: A regulated inflammatory mode of cell death', *Journal of Neuroinflammation*, 15(1), pp. 1–9.

Dirkx, E., da Costa Martins, P. A. and De Windt, L. J. (2013) 'Regulation of fetal gene expression in heart failure', *Biochimica et Biophysica Acta - Molecular Basis of Disease*, 1832(12), pp. 2414–2424.

Dobaczewski, M., Xia, Y., Bujak, M., Gonzalez-Quesada, C. and Frangogiannis, N. G. (2010) 'CCR5 signaling suppresses inflammation and reduces adverse remodeling of the infarcted heart, mediating recruitment of regulatory T cells', *American Journal of Pathology*, 176(5), pp. 2177–2187.

Du, C., Fang, M., Li, Y., Li, L. and Wang, X. (2000) 'Smac, a mitochondrial protein that promotes cytochrome c-dependent caspase activation by eliminating IAP inhibition.', *Cell*, 102(1), pp. 33–42.

Duan, Q., Chen, C., Yang, L., Li, N., Gong, W., Li, S. and Wang, D. W. (2015) 'MicroRNA regulation of unfolded protein response transcription factor XBP1 in the progression of cardiac hypertrophy and heart failure in vivo', *Journal of Translational Medicine*, 13(1), p. 363.

Duarte, K., Heide, S., Poëa-Guyon, S., Rousseau, V., Depienne, C., Rastetter, A., Nava, C., Attié-Bitach, T., Razavi, F., Martinovic, J., *et al.* (2020) 'PAK3 mutations responsible for severe intellectual disability and callosal agenesis inhibit cell migration', *Neurobiology of Disease*, 136, p. 104709.

Dumont, B. L. (2019) 'Significant strain variation in the mutation spectra of inbred laboratory mice', *Molecular Biology and Evolution*, 36(5), pp. 865–874.

Edlinger, L., Berger-Becvar, A., Menzl, I., Hoermann, G., Greiner, G., Grundschober, E., Bago-Horvath, Z., Al-Zoughbi, W., Hoefler, G., Brostjan, C., *et al.* (2017) 'Expansion of *BCR/ABL1* $^{+}$ cells requires PAK2 but not PAK1', *British Journal of Haematology*, 179(2), pp. 229–241.

Eefting, F., Rensing, B., Wigman, J., Pannekoek, W. J., Liu, W. M., Cramer, M. J., Lips, D. J. and Doevendans, P. A. (2004) 'Role of apoptosis in reperfusion injury', *Cardiovascular Research*, 61(3), pp. 414–426.

Eghbali, M., Tomek, R., Sukhatme, V. P., Woods, C. and Bhambi, B. (1991) 'Differential effects of transforming growth factor-beta 1 and phorbol myristate acetate on cardiac fibroblasts. Regulation of fibrillar collagen mRNAs and expression of early transcription factors.', *Circulation Research*, 69(2), pp. 483–490.

Egom, E. E. A., Ke, Y., Musa, H., Mohamed, T. M. A., Wang, T., Cartwright, E., Solaro, R.

J. and Lei, M. (2010) 'FTY720 prevents ischemia/reperfusion injury-associated arrhythmias in an ex vivo rat heart model via activation of Pak1/Akt signaling', *Journal of Molecular and Cellular Cardiology*, 48(2), pp. 406–414.

Egom, E. E. A., Mohamed, T. M. A., Mamas, M. A., Shi, Y., Liu, W., Chirico, D., Stringer, S. E., Ke, Y., Shaheen, M., Wang, T., *et al.* (2011) 'Activation of Pak1/Akt/eNOS signaling following sphingosine-1-phosphate release as part of a mechanism protecting cardiomyocytes against ischemic cell injury', *AJP: Heart and Circulatory Physiology*, 301(4), pp. H1487–H1495.

Elsherif, L., Ozler, M., Zayed, M. A., Shen, J. H., Chernoff, J., Faber, J. E. and Parise, L. V. (2014) 'Potential compensation among group I PAK members in hindlimb ischemia and wound healing', *PLoS ONE*, 9(11), p. e112239.

Elson, E. L., Qian, H., Fee, J. A. and Wakatsuki, T. (2019) 'A model for positive feedback control of the transformation of fibroblasts to myofibroblasts', *Progress in Biophysics and Molecular Biology*, 144, pp. 30–40.

Eltzschig, H. K. and Eckle, T. (2011) 'Ischemia and reperfusion-from mechanism to translation', *Nature Medicine*, pp. 1391–1401.

Eron, S. J., Raghupathi, K. and Hardy, J. A. (2017) 'Dual site phosphorylation of caspase-7 by PAK2 blocks apoptotic activity by two distinct mechanisms', *Structure*, 25(1), pp. 27–39.

Fatigati, V. and Murphy, R. A. (1984) 'Actin and tropomyosin variants in smooth muscles. Dependence on tissue type', *Journal of Biological Chemistry*, 259(23), pp. 14383–14388.

Ferrini, A., Stevens, M. M., Sattler, S. and Rosenthal, N. (2019) 'Toward regeneration of the heart: bioengineering strategies for immunomodulation', *Frontiers in Cardiovascular Medicine*, 6, p. 26.

Finnson, K. W., Almadani, Y. and Philip, A. (2020) 'Non-canonical (non-SMAD2/3) TGF-β signaling in fibrosis: Mechanisms and targets', *Seminars in Cell and Developmental Biology*, 101, pp. 115–122.

Flate, E. and Stalvey, J. R. D. (2014) 'Motility of select ovarian cancer cell lines: Effect of extracellular matrix proteins and the involvement of PAK2', *International Journal of*

Oncology, 45(4), pp. 1401–1411.

Frangogiannis, N. G. (2017) 'The extracellular matrix in myocardial injury, repair, and remodeling', *Journal of Clinical Investigation*, 127(5), pp. 1600–1612.

Frank, S. R., Bell, J. H., Frödin, M. and Hansen, S. H. (2012) 'A βpIX-PAK2 complex confers protection against scrib-dependent and cadherin-mediated apoptosis', *Current Biology*, 22(19), pp. 1747–1754.

Frantz, S., Hu, K., Adamek, A., Wolf, J., Sallam, A., Maier, S. K. G., Lonning, S., Ling, H., Ertl, G. and Bauersachs, J. (2008) 'Transforming growth factor beta inhibition increases mortality and left ventricular dilatation after myocardial infarction', *Basic Research in Cardiology*, 103(5), pp. 485–492.

French, B. A. and Kramer, C. M. (2007) 'Mechanisms of postinfarct left ventricular remodeling', *Drug Discovery Today: Disease Mechanisms*, 4(3), pp. 185–196.

Fritsch, M., Günther, S. D., Schwarzer, R., Albert, M. C., Schorn, F., Werthenbach, J. P., Schiffmann, L. M., Stair, N., Stocks, H., Seeger, J. M., *et al.* (2019) 'Caspase-8 is the molecular switch for apoptosis, necroptosis and pyroptosis', *Nature*, 575, pp. 683–687.

Frobert, A., Valentin, J., Magnin, J. L., Riedo, E., Cook, S. and Giraud, M. N. (2015) 'Prognostic value of troponin I for infarct size to improve preclinical myocardial infarction small animal models', *Frontiers in Physiology*, 6(NOV), p. 353.

Fu, H. Y., Okada, K. -i., Liao, Y., Tsukamoto, O., Isomura, T., Asai, M., Sawada, T., Okuda, K., Asano, Y., Sanada, S., *et al.* (2010) 'Ablation of C/EBP homologous protein attenuates endoplasmic reticulum-mediated apoptosis and cardiac dysfunction induced by pressure overload', *Circulation*, 122(4), pp. 361–369.

Fuchsova, B., Alvarez Juliá, A., Rizavi, H. S., Frasch, A. C. and Pandey, G. N. (2016) 'Expression of p21-activated kinases 1 and 3 is altered in the brain of subjects with depression', *Neuroscience*, 333, pp. 331–344.

Fujio, Y., Nguyen, T., Wencker, D., Kitsis, R. N. and Walsh, K. (2000) 'Akt promotes survival of cardiomyocytes in vitro and protects against Ischemia-reperfusion injury in mouse heart', *Circulation*, 101(6), pp. 660–667.

Galli, A. and Lombardi, F. (2016) 'Postinfarct Left Ventricular Remodelling: A Prevailing Cause of Heart Failure', *Cardiology Research and Practice*, 2016, p. 2579832.

Gao, C., Ma, T., Pang, L. and Xie, R. (2014) 'Activation of P21-activated protein kinase 2 is an independent prognostic predictor for patients with gastric cancer', *Diagnostic Pathology*, 9(1), p. 55.

Gao, X. M., Xu, Q., Kiriazis, H., Dart, A. M. and Du, X. J. (2005) 'Mouse model of post-infarct ventricular rupture: Time course, strain- and gender-dependency, tensile strength, and histopathology', *Cardiovascular Research*, 65(2), pp. 469–477.

Garvin, A. M., Jackson, M. A. and Korzick, D. H. (2018) 'Inhibition of programmed necrosis limits infarct size through altered mitochondrial and immune responses in the aged female rat heart', *American Journal of Physiology - Heart and Circulatory Physiology*, 315(5), pp. H1434–H1442.

Gatti, A., Huang, Z., Tuazon, P. T. and Traugh, J. A. (1999) 'Multisite autophosphorylation of p21-activated protein kinase γ-PAK as a function of activation', *Journal of Biological Chemistry*, 274(12), pp. 8022–8028.

Gerakis, Y. and Hetz, C. (2018) 'Emerging roles of ER stress in the etiology and pathogenesis of Alzheimer's disease', *FEBS Journal*, 285(6), pp. 995–1011.

Ghosh, R., Wang, L., Wang, E. S., Perera, B. G. K., Igbaria, A., Morita, S., Prado, K., Thamsen, M., Caswell, D., Macias, H., *et al.* (2014) 'Allosteric inhibition of the IRE1α RNase preserves cell viability and function during endoplasmic reticulum stress', *Cell*, 158(3), pp. 534–548.

Giacomo, V. di, Rapino, M., Sancilio, S., Patruno, A., Zara, S., Di Pietro, R. and Cataldi, A. (2010) 'PKC-δ signalling pathway is involved in H9c2 cells differentiation', *Differentiation*, 80(4–5), pp. 204–212.

Gintant, G., Burridge, P., Gepstein, L., Harding, S., Herron, T., Hong, C., Jalife, J. and Wu, J. C. (2019) 'Use of human induced pluripotent stem cell-derived cardiomyocytes in preclinical cancer drug cardiotoxicity testing: A scientific statement from the American Heart Association', *Circulation Research*, 125(10), pp. e75–e92.

González-Montero, J., Brito, R., Gajardo, A. I. and Rodrigo, R. (2018) 'Myocardial

reperfusion injury and oxidative stress: Therapeutic opportunities', *World Journal of Cardiology*, 10(9), pp. 74–86.

González, A., Schelbert, E. B., Díez, J. and Butler, J. (2018) 'Myocardial interstitial fibrosis in heart failure: Biological and translational perspectives', *Journal of the American College of Cardiology*, 71(15), pp. 1696–1706.

Gopal, S. K., Greening, D. W., Hanssen, E. G., Zhu, H. J., Simpson, R. J. and Mathias, R. A. (2016) 'Oncogenic epithelial cell-derived exosomes containing Rac1 and PAK2 induce angiogenesis in recipient endothelial cells', *Oncotarget*, 7(15), pp. 19709–19722.

Greulich, S., Mayr, A., Gloekler, S., Seitz, A., Birkmeier, S., Schäufele, T., Bekeredjian, R., Zuern, C. S., Seizer, P., Geisler, T., *et al.* (2019) 'Time-dependent myocardial necrosis in patients with ST-segment–elevation myocardial infarction without angiographic collateral flow visualized by cardiac magnetic resonance imaging: Results from the multicenter STEMI-SCAR project', *Journal of the American Heart Association*, 8(12), p. e012429.

Guan, H. S., Shangguan, H. J., Shang, Z., Yang, L., Meng, X. M. and Qiao, S. Bin (2011) 'Endoplasmic reticulum stress caused by left ventricular hypertrophy in rats: Effects of telmisartan', *American Journal of the Medical Sciences*, 342(4), pp. 318–323.

Györfi, A. H., Matei, A. E. and Distler, J. H. W. (2018) 'Targeting TGF-β signaling for the treatment of fibrosis', *Matrix Biology*, 68–69, pp. 8–27.

Ha, H. C. and Snyder, S. H. (1999) 'Poly(ADP-ribose) polymerase is a mediator of necrotic cell death by ATP depletion.', *Proceedings of the National Academy of Sciences of the United States of America*, 96(24), pp. 13978–82.

Halawa, B.; Salomon, P.; Jołda-Mydłowska, B.; Zysko, D. (1999) 'Levels of tumor necrosis factor (TNF-alpha) and interleukin 6 (IL-6) in serum of patients with acute myocardial infarction', *Polish Archives of Internal Medicine*, 101(3), pp. 197–203.

Han, D., Lerner, A. G., Vande Walle, L., Upton, J. P., Xu, W., Hagen, A., Backes, B. J., Oakes, S. A. and Papa, F. R. (2009) 'IRE1α kinase activation modes control alternate endoribonuclease outputs to determine divergent cell fates', *Cell*, 138(3), pp. 562–575.

Hanna, A. and Frangogiannis, N. G. (2019) 'The Role of the TGF-β Superfamily in

Myocardial Infarction', *Frontiers in Cardiovascular Medicine*, 6, p. 140.

Hao, S., Luo, C., Abukiwan, A., Wang, G., He, J., Huang, L., Weber, C. E. M., Lv, N., Xiao, X., Eichmüller, S. B., *et al.* (2015) 'miR-137 inhibits proliferation of melanoma cells by targeting PAK2', *Experimental Dermatology*, 24(12), pp. 947–952.

Harding, H. P., Zhang, Y. and Ron, D. (1999) 'Protein translation and folding are coupled by an endoplasmic- reticulum-resident kinase', *Nature*, 397(6716), pp. 271–274.

Harjola, V., Parissis, J., Bauersachs, J., Brunner-La Rocca, H., Bueno, H., Čelutkienė, J., Chioncel, O., Coats, A. J. S., Collins, S. P., Boer, R. A., *et al.* (2020) 'Acute coronary syndromes and acute heart failure: a diagnostic dilemma and high-risk combination. A statement from the Acute Heart Failure Committee of the Heart Failure Association of the European Society of Cardiology', *European Journal of Heart Failure*, 22(8), pp. 1298–1314.

Hausenloy, D. J., Botker, H. E., Engstrom, T., Erlinge, D., Heusch, G., Ibanez, B., Kloner, R. A., Ovize, M., Yellon, D. M. and Garcia-Dorado, D. (2017) 'Targeting reperfusion injury in patients with ST-segment elevation myocardial infarction: Trials and tribulations', *European Heart Journal*, 38(13), pp. 935-941d.

Hausenloy, D. and Yellon, D. (2013) 'Myocardial ischemia-reperfusion injury: a neglected therapeutic target', *J Clin Invest*, 123(1), pp. 92–100.

He, B. (2006) 'Viruses, endoplasmic reticulum stress, and interferon responses', *Cell Death and Differentiation*, 13(3), pp. 393–403.

Hillary, R. F. and Fitzgerald, U. (2018) 'A lifetime of stress: ATF6 in development and homeostasis', *Journal of Biomedical Science*, 25(1), p. 48.

Hinderer, C., Katz, N., Buza, E. L., Dyer, C., Goode, T., Bell, P., Richman, L. K. and Wilson, J. M. (2018) 'Severe toxicity in nonhuman primates and piglets following high-dose intravenous administration of an adeno-associated virus vector expressing human SMN', *Human Gene Therapy*, 29(3), pp. 285–298.

Hinderer, S. and Schenke-Layland, K. (2019) 'Cardiac fibrosis – A short review of causes and therapeutic strategies', *Advanced Drug Delivery Reviews*, 146, pp. 77–82.

Hinz, B., Celetta, G., Tomasek, J. J., Gabbiani, G. and Chaponnier, C. (2001) 'Alpha-smooth muscle actin expression upregulates fibroblast contractile activity', *Molecular Biology of the Cell*, 12(9), pp. 2730–2741.

Hinz, Boris, Mastrangelo, D., Iselin, C. E., Chaponnier, C. and Gabbiani, G. (2001) 'Mechanical tension controls granulation tissue contractile activity and myofibroblast differentiation', *American Journal of Pathology*, 159(3), pp. 1009–1020.

Hitomi, J., Katayama, T., Eguchi, Y., Kudo, T., Taniguchi, M., Koyama, Y., Manabe, T., Yamagishi, S., Bando, Y., Imaizumi, K., *et al.* (2004) 'Involvement of caspase-4 in endoplasmic reticulum stress-induced apoptosis and Aβ-induced cell death', *Journal of Cell Biology*, 165(3), pp. 347–356.

Hochhauser, E., Cheporko, Y., Yasovich, N., Pinchas, L., Offen, D., Barhum, Y., Pannet, H., Tobar, A., Vidne, B. A. and Birk, E. (2007) 'Bax deficiency reduces infarct size and improves long-term function after myocardial infarction.', *Cell Biochemistry and Biophysics*, 47(1), pp. 11–20.

Hofmann, C. (2004) 'The genetics of Pak', *Journal of Cell Science*, 117(19), pp. 4343–4354.

Hofmann, U., Burkard, N., Vogt, C., Thoma, A., Frantz, S., Ertl, G., Ritter, O. and Bonz, A. (2009) 'Protective effects of sphingosine-1-phosphate receptor agonist treatment after myocardial ischaemia-reperfusion', *Cardiovascular Research*, 83(2), pp. 285–293.

Hollien, J., Lin, J. H., Li, H., Stevens, N., Walter, P. and Weissman, J. S. (2009) 'Regulated Ire1-dependent decay of messenger RNAs in mammalian cells', *Journal of Cell Biology*, 186(3), pp. 323–331.

Hollien, J. and Weissman, J. S. (2006) 'Decay of endoplasmic reticulum-localized mRNAs during the unfolded protein response', *Science*, 313(5783), pp. 104–107.

Holly, T. A., Drincic, A., Byun, Y., Nakamura, S., Harris, K., Klocke, F. J. and Cryns, V. L. (1999) 'Caspase inhibition reduces myocyte cell death induced by myocardial ischemia and reperfusion in vivo', *Journal of Molecular and Cellular Cardiology*, 31(9), pp. 1709–1715.

Hough, C., Radu, M. and Doré, J. J. E. (2012) 'TGF-beta induced ERK phosphorylation of

Smad linker region regulates Smad signaling', *PLoS ONE*, 7(8), p. 42513.

Hu, H., Tian, M., Ding, C. and Yu, S. (2019) 'The C/EBP homologous protein (CHOP) transcription factor functions in endoplasmic reticulum stress-induced apoptosis and microbial infection', *Frontiers in Immunology*, 10(JAN), p. 3083.

Huang, J., Huang, A., Poplawski, A., DiPino, F., Traugh, J. A. and Ling, J. (2020) 'PAK2 activated by Cdc42 and caspase 3 mediates different cellular responses to oxidative stress-induced apoptosis', *Biochimica et Biophysica Acta - Molecular Cell Research*, 1867(4), p. 118645.

Huang, Z., Ling, J. and Traugh, J. A. (2003) 'Localization of p21-activated protein kinase γ-PAK/Pak2 in the endoplasmic reticulum is required for induction of cytostasis', *Journal of Biological Chemistry*, 278(15), pp. 13101–13109.

Humpton, T. J. and Vousden, K. H. (2016) 'Regulation of cellular metabolism and hypoxia by p53', *Cold Spring Harbor Perspectives in Medicine*, 6(7), p. a026146.

Ikeda, H., Suzuki, Y., Suzuki, M., Koike, M., Tamura, J., Tong, J., Nomura, M. and Itoh, G. (1998) 'Apoptosis is a major mode of cell death caused by ischaemia and ischaemia/reperfusion injury to the rat intestinal epithelium', *Gut*, 42(4), pp. 530–537.

Inamdar, Arati and Inamdar, Ajinkya (2016) 'Heart failure: Diagnosis, management and utilization', *Journal of Clinical Medicine*, 5(7), p. 62.

Institute of Medicine (US) Committee on Social Security Cardiovascular Disability Criteria (2010) 'Heart Failure, cardiomyopathy, and right heart failure', in *Cardiovascular Disability: Updating the Social Security Listings.* National Academies Press (US), p. Chapter 5.

Irwin, M. W., Mak, S., Mann, D. L., Qu, R., Penninger, J. M., Yan, A., Dawood, F., Wen, W.-H., Shou, Z. and Liu, P. (1999) 'Tissue expression and immunolocalization of tumor necrosis factor-α in postinfarction dysfunctional myocardium', *Circulation*, 99(11), pp. 1492–1498.

Jackson, S. J., Andrews, N., Ball, D., Bellantuono, I., Gray, J., Hachoumi, L., Holmes, A., Latcham, J., Petrie, A., Potter, P., *et al.* (2017) 'Does age matter? The impact of rodent age on study outcomes', *Laboratory Animals*, 51(2), pp. 160–169.

Jakobi, R., McCarthy, C. C., Koeppel, M. A. and Stringer, D. K. (2003) 'Caspase-activated PAK-2 is regulated by subcellular targeting and proteasomal degradation', *Journal of Biological Chemistry*, 278(40), pp. 38675–38685.

Jakobi, R., Moertl, E. and Koeppel, M. A. (2001) 'p21-activated protein kinase gamma-PAK suppresses programmed cell death of BALB3T3 fibroblasts', *Journal of Biological Chemistry*, 276(20), pp. 16624–16634.

Jiang, Y., Park, P., Hong, S. M. and Ban, K. (2018) 'Maturation of cardiomyocytes derived from human pluripotent stem cells: Current strategies and limitations', *Molecules and Cells*, pp. 613–621.

Jin, J. L., Lv, R. G., Guo, J., Liu, X. H., Liang, Y. W., Wei, J. R. and Wang, L. (2016) 'Improvement of left ventricular remodelling by inhibition of NF-κB in a rat model of myocardial infarction', *Heart Lung and Circulation*, 25(10), pp. 1007–1012.

St. John Sutton, M. G. and Sharpe, N. (2000) 'Left ventricular remodeling after myocardial infarction: Pathophysiology and therapy', *Circulation*, 101(25), pp. 2981–2988.

Johnston, E. F. and Gillis, T. E. (2017) 'Transforming growth factor beta-1 (TGF-β1) stimulates collagen synthesis in cultured rainbow trout cardiac fibroblasts', *Journal of Experimental Biology*, 220(14), pp. 2645–2653.

Jung, J. H. and Traugh, J. A. (2005) 'Regulation of the interaction of Pak2 with Cdc42 via autophosphorylation of serine 141', *Journal of Biological Chemistry*, 280(48), pp. 40025–40031.

Jung, M., Ma, Y., Iyer, R. P., DeLeon-Pennell, K. Y., Yabluchanskiy, A., Garrett, M. R. and Lindsey, M. L. (2017) 'IL-10 improves cardiac remodeling after myocardial infarction by stimulating M2 macrophage polarization and fibroblast activation', *Basic Research in Cardiology*, 112(3), p. 33.

Kaczmarek, A., Vandenabeele, P. and Krysko, D. V. (2013) 'Necroptosis: The release of damage-associated molecular patterns and its physiological relevance', *Immunity*, 38(2), pp. 209–223.

Kaiser, W. J., Upton, J. W., Long, A. B., Livingston-Rosanoff, D., Daley-Bauer, L. P., Hakem,

R., Caspary, T. and Mocarski, E. S. (2011) 'RIP3 mediates the embryonic lethality of caspase-8-deficient mice', *Nature*, 471(7338), pp. 368–372.

Kalogeris, T., Baines, C. P., Krenz, M. and Korthuis, R. J. (2012) 'Cell biology of ischemia/reperfusion injury', *International Review of Cell and Molecular Biology*, 298, pp. 229–317.

Kania, G., Blyszczuk, P. and Eriksson, U. (2009) 'Mechanisms of cardiac fibrosis in inflammatory heart disease', *Trends in Cardiovascular Medicine*, 19(8), pp. 247–252.

Kaplan, P., Babusikova, E., Lehotsky, J. and Dobrota, D. (2003) 'Free radical-induced protein modification and inhibition of Ca2+-ATPase of cardiac sarcoplasmic reticulum', *Molecular and Cellular Biochemistry*, 248(1–2), pp. 41–47.

Karakikes, I., Ameen, M., Termglinchan, V. and Wu, J. C. (2015) 'Human induced pluripotent stem cell-derived cardiomyocytes: Insights into molecular, cellular, and functional phenotypes', *Circulation Research*, 117(1), pp. 80–88.

Kassan, M., Galán, M., Partyka, M., Saifudeen, Z., Henrion, D., Trebak, M. and Matrougui, K. (2012) 'Endoplasmic reticulum stress is involved in cardiac damage and vascular endothelial dysfunction in hypertensive mice.', *Arteriosclerosis, Thrombosis, and Vascular Biology*, 32(7), pp. 1652–1661.

Kawano, S., Kubota, T., Monden, Y., Tsutsumi, T., Inoue, T., Kawamura, N., Tsutsui, H. and Sunagawa, K. (2006) 'Blockade of NF-κB improves cardiac function and survival after myocardial infarction', *American Journal of Physiology - Heart and Circulatory Physiology*, 291(3), pp. 1337–1344.

Ke, Y., Lei, M., Collins, T. P., Rakovic, S., Mattick, P. A. D., Brodie, M. S., Terrar, D. A., Solaro, R. J. and Yamasaki, M. (2007) 'Regulation of L-type calcium channel and delayed rectifier potassium channel activity by p21-activated kinase-1 in guinea pig sinoatrial node pacemaker cells', *Circulation Research*, 100(9), pp. 1317–1327.

Ke, Y., Lei, M., Wang, X. and Solaro, R. J. (2013) 'Unique catalytic activities and scaffolding of p21 activated kinase-1 in cardiovascular signaling.', *Frontiers in Pharmacology*, 4, p. 116.

Kehat, I. and Molkentin, J. D. (2010) 'Molecular pathways underlying cardiac remodeling

during pathophysiological stimulation', *Circulation*, 122(25), pp. 2727–2735.

Kim, B. J., Ryu, S. W. and Song, B. J. (2006) 'JNK- and p38 kinase-mediated phosphorylation of Bax leads to its activation and mitochondrial translocation and to apoptosis of human hepatoma HepG2 cells', *Journal of Biological Chemistry*, 281(30), pp. 21256–21265.

Kim, S. H., Kwon, D. Y., Kwak, J. H., Lee, S., Lee, Y. H., Yun, J., Son, T. G. and Jung, Y. S. (2018) 'Tunicamycin-induced ER stress is accompanied with oxidative stress via abrogation of sulfur amino acids metabolism in the liver', *International Journal of Molecular Sciences*, 19(12), p. 4114.

Kimes, B. W. and Brandt, B. L. (1976) 'Properties of a clonal muscle cell line from rat heart', *Experimental Cell Research*, 98(2), pp. 367–381.

King, C. C., Gardiner, E. M. M., Zenke, F. T., Bohl, B. P., Newton, A. C., Hemmings, B. A. and Bokoch, G. M. (2000) 'p21-activated kinase (PAK1) is phosphorylated and activated by 3-phosphoinositide-dependent kinase-1 (PDK1)', *Journal of Biological Chemistry*, 275(52), pp. 41201–41209.

Klabunde, R. E. (2017) 'Cardiac electrophysiology: normal and ischemic ionic currents and the ECG', *Advances in Physiology Education*, 41(1), pp. 29–37.

Kloner, R. A. (1993) 'Does reperfusion injury exist in humans?', *Journal of the American College of Cardiology*, 21(2), pp. 537–545.

Koh, D. W., Dawson, T. M. and Dawson, V. L. (2005) 'Mediation of cell death by poly(ADP-ribose) polymerase-1', *Pharmacological Research*, 52(1 SPEC. ISS.), pp. 5–14.

Koh, W., Mahan, R. D. and Davis, G. E. (2008) 'Cdc42- and Rac1-mediated endothelial lumen formation requires Pak2, Pak4 and Par3, and PKC-dependent signaling.', *Journal of Cell Science*, 121(Pt 7), pp. 989–1001.

Koo, K. H. and Kwon, H. (2018) 'MicroRNA miR-4779 suppresses tumor growth by inducing apoptosis and cell cycle arrest through direct targeting of PAK2 and CCND3 article', *Cell Death and Disease*, 9(2), pp. 1–14.

Krown, K. A., Page, M. T., Nguyen, C., Zechner, D., Gutierrez, V., Comstock, K. L.,

Glembotski, C. C., Quintana, P. J. E. and Sabbadini, R. A. (1996) 'Tumor necrosis factor alpha-induced apoptosis in cardiac myocytes: Involvement of the sphingolipid signaling cascade in cardiac cell death', *Journal of Clinical Investigation*, 98(12), pp. 2854–2865.

Kurian, G. A., Rajagopal, R., Vedantham, S. and Rajesh, M. (2016) 'The role of oxidative stress in myocardial ischemia and reperfusion injury and remodeling: Revisited', *Oxidative Medicine and Cellular Longevity*, 2016, p. 1656450.

Kuznetsov, A. V., Javadov, S., Sickinger, S., Frotschnig, S. and Grimm, M. (2015) 'H9c2 and HL-1 cells demonstrate distinct features of energy metabolism, mitochondrial function and sensitivity to hypoxia-reoxygenation', *Biochimica et Biophysica Acta - Molecular Cell Research*, 1853(2), pp. 276–284.

Lage, R., Cebro-Márquez, M., Rodríguez-Mañero, M., González-Juanatey, J. R. and Moscoso, I. (2019) 'Omentin protects H9c2 cells against docetaxel cardiotoxicity', *PLOS ONE*, 14(2), p. e0212782.

Lam, C. S. P., McEntegart, M., Claggett, B., Liu, J., Skali, H., Lewis, E., Køber, L., Rouleau, J., Velazquez, E., Califf, R., *et al.* (2015) 'Sex differences in clinical characteristics and outcomes after myocardial infarction: insights from the Valsartan in Acute Myocardial Infarction Trial (VALIANT)', *European Journal of Heart Failure*, 17(3), pp. 301–312.

Lee, A., Jeong, D., Mitsuyama, S., Oh, J. G., Liang, L., Ikeda, Y., Sadoshima, J., Hajjar, R. J. and Kho, C. (2014) 'The role of SUMO-1 in cardiac oxidative stress and hypertrophy', *Antioxidants & Redox Signaling*, 21(14), pp. 1986–2001.

Lee, A. S. (2005) 'The ER chaperone and signaling regulator GRP78/BiP as a monitor of endoplasmic reticulum stress', *Methods*, 35(4), pp. 373–381.

Lee, N., MacDonald, H., Reinhard, C., Halenbeck, R., Roulston, A., Shi, T. and Williams, L. T. (1997) 'Activation of hPAK65 by caspase cleavage induces some of the morphological and biochemical changes of apoptosis.', *Proceedings of the National Academy of Sciences of the United States of America*, 94(December), pp. 13642–13647.

Lee, P., Sata, M., Lefer, D. J., Factor, S. M., Walsh, K. and Kitsis, R. N. (2003) 'Fas pathway is a critical mediator of cardiac myocyte death and MI during ischemia-reperfusion in vivo.', *American journal of physiology. Heart and circulatory physiology*, 284(2), pp.

H456–H463.

Lenna, S. and Trojanowska, M. (2012) 'The role of endoplasmic reticulum stress and the unfolded protein response in fibrosis', *Current Opinion in Rheumatology*, pp. 663–668.

Lerner, A. G., Upton, J. P., Praveen, P. V. K., Ghosh, R., Nakagawa, Y., Igbaria, A., Shen, S., Nguyen, V., Backes, B. J., Heiman, M., *et al.* (2012) 'IRE1α induces thioredoxin-interacting protein to activate the NLRP3 inflammasome and promote programmed cell death under irremediable ER stress', *Cell Metabolism*, 16(2), pp. 250–264.

Li, G., Mongillo, M., Chin, K. T., Harding, H., Ron, D., Marks, A. R. and Tabas, I. (2009) 'Role of ERO1-α-mediated stimulation of inositol 1,4,5-triphosphate receptor activity in endoplasmic reticulum stress-induced apoptosis', *Journal of Cell Biology*, 186(6), pp. 783–792.

Li, H., Zhu, H., Xu, C. and Yuan, J. (1998) 'Cleavage of BID by caspase 8 mediates the mitochondrial damage in the Fas pathway of apoptosis', *Cell*, 94(4), pp. 491–501.

Li, R. J., He, K. L., Li, X., Wang, L. L., Liu, C. L. and He, Y. Y. (2015) 'Salubrinal protects cardiomyocytes against apoptosis in a rat myocardial infarction model via suppressing the dephosphorylation of eukaryotic translation initiation factor 2α', *Molecular Medicine Reports*, 12(1), pp. 1043–1049.

Li, S., Ma, J., Li, J. B., Lacefield, J. C., Jones, D. L., Peng, T. Q. and Wei, M. (2018) 'Over-expression of calpastatin attenuates myocardial injury following myocardial infarction by inhibiting endoplasmic reticulum stress', *Journal of Thoracic Disease*, 10(9), pp. 5283–5297.

Li, X., Wen, W., Liu, K., Zhu, F., Malakhova, M., Peng, C., Li, T., Kim, H. G., Ma, W., Yeon Cho, Y., *et al.* (2011) 'Phosphorylation of caspase-7 by p21-activated protein kinase (PAK) 2 inhibits chemotherapeutic drug-induced apoptosis of breast cancer cell lines', *Journal of Biological Chemistry*, 286(25), pp. 22291–22299.

Li, X., Murugiah, K., Li, J., Masoudi, F. A., Chan, P. S., Hu, S., Spertus, J. A., Wang, Y., Downing, N. S., Krumholz, H. M., *et al.* (2017) 'Urban-rural comparisons in hospital admission, treatments, and outcomes for ST-segment-elevation myocardial infarction in China from 2001 to 2011: A retrospective analysis from the China PEACE study (Patient-

Centered Evaluative Assessment of Cardiac Event', *Circulation: Cardiovascular Quality and Outcomes*, 10(11), p. e003905.

Liang, Q., Bueno, O. F., Wilkins, B. J., Kuan, C. Y., Xia, Y. and Molkentin, J. D. (2003) 'c-Jun N-terminal kinases (JNK) antagonize cardiac growth through cross-talk with calcineurin-NFAT signaling', *EMBO Journal*, 22(19), pp. 5079–5089.

Lim, S. Y., Davidson, S. M., Mocanu, M. M., Yellon, D. M. and Smith, C. C. T. (2007) 'The cardioprotective effect of necrostatin requires the cyclophilin-D component of the mitochondrial permeability transition pore', *Cardiovascular Drugs and Therapy*, 21(6), pp. 467–469.

Liu, C. L., He, Y. Y., Li, X., Li, R. J., He, K. L. and Wang, L. L. (2014) 'Inhibition of serine/threonine protein phosphatase PP1 protects cardiomyocytes from tunicamycin-induced apoptosis and I/R through the upregulation of p-eIF2a', *International Journal of Molecular Medicine*, 33(3), pp. 499–506.

Liu, H., Shin, S. H., Chen, H., Liu, T., Li, Z., Hu, Y., Liu, F., Zhang, C., Kim, D. J., Liu, K., *et al.* (2020) 'CDK12 and PAK2 as novel therapeutic targets for human gastric cancer', *Theranostics*, 10(14), pp. 6201–6215.

Liu, J., Fraser, S. D., Faloon, P. W., Rollins, E. L., Vom Berg, J., Starovic-Subota, O., Laliberte, A. L., Chen, J. N., Serluca, F. C. and Childs, S. J. (2007) 'A betaPix Pak2a signaling pathway regulates cerebral vascular stability in zebrafish', *Proc Natl Acad Sci U S A*, 104(35), pp. 13990–13995.

Liu, M., Chen, Z. and Chen, L. (2016) 'Endoplasmic reticulum stress: a novel mechanism and therapeutic target for cardiovascular diseases', *Acta Pharmacologica Sinica*, 37(4), pp. 425–443.

Liu, M. and Dudley, S. C. (2016) 'Role for the unfolded protein response in heart disease and cardiac arrhythmias', *International Journal of Molecular Sciences*, 17(1), p. 52.

Liu, W., Zi, M., Naumann, R., Ulm, S., Jin, J., Taglieri, D. M., Prehar, S., Gui, J., Tsui, H., Xiao, R. P., *et al.* (2011) 'Pak1 as a novel therapeutic target for antihypertrophic treatment in the heart', *Circulation*, 124(24), pp. 2702–2715.

Liu, X.-H., Zhang, Z.-Y., Sun, S. and Wu, X.-D. (2008) 'Ischemic postconditioning protects

myocardium from ischemia/reperfusion injury through attenuating endoplasmic reticulum stress.', *Shock*, 30(4), pp. 422–7.

Liu, X., Kwak, D., Lu, Z., Xu, X., Fassett, J., Wang, H., Wei, Y., Cavener, D. R., Hu, X., Hall, J., *et al.* (2014) 'Endoplasmic reticulum stress sensor protein kinase R-like endoplasmic reticulum kinase (PERK) protects against pressure overload-induced heart failure and lung remodeling', *Hypertension*, 64(4), pp. 738–744.

Liu, X. H., Zhang, Z. Y., Andersson, K. B., Husberg, C., Enger, U. H., Ræder, M. G., Christensen, G. and Louch, W. E. (2011) 'Cardiomyocyte-specific disruption of Serca2 in adult mice causes sarco(endo)plasmic reticulum stress and apoptosis', *Cell Calcium*, 49(4), pp. 201–207.

Liu, Z., Cai, H., Zhu, H., Toque, H., Zhao, N., Qiu, C., Guan, G., Dang, Y. and Wang, J. (2014) 'Protein kinase RNA-like endoplasmic reticulum kinase (PERK)/calcineurin signaling is a novel pathway regulating intracellular calcium accumulation which might be involved in ventricular arrhythmias in diabetic cardiomyopathy', *Cellular Signalling*, 26(12), pp. 2591–2600.

Livak, K. J. and Schmittgen, T. D. (2001) 'Analysis of Relative Gene Expression Data Using Real-Time Quantitative PCR and the 2−ΔΔCT Method', *Methods*, 25(4), pp. 402–408.

Loo, T.-H., Ng, Y.-W., Lim, L. and Manser, E. (2004) 'GIT1 activates p21-activated kinase through a mechanism independent of p21 binding.', *Molecular and Cellular Biology*, 24(9), pp. 3849–59.

Luedde, M., Lutz, M., Carter, N., Sosna, J., Jacoby, C., Vucur, M., Gautheron, J., Roderburg, C., Borg, N., Reisinger, F., *et al.* (2014) 'RIP3, a kinase promoting necroptotic cell death, mediates adverse remodelling aftermyocardial infarction', *Cardiovascular Research*, 103(2), pp. 206–216.

Luo, S. and Rubinsztein, D. C. (2009) 'Huntingtin promotes cell survival by preventing Pak2 cleavage.', *Journal of cell science*, 122(Pt 6), pp. 875–85.

Lyons, R. M., Keski-Oja, J. and Moses, H. L. (1988) 'Proteolytic activation of latent transforming growth factor-β from fibroblast-conditioned medium', *Journal of Cell Biology*, 106(5), pp. 1659–1665.

Ma, L.-Q., Yu, Y., Chen, H., Li, M., Ihsan, A., Tong, H.-Y., Huang, X.-J. and Gao, Y. (2018) 'Sweroside alleviated aconitine-induced cardiac toxicity in H9c2 cardiomyoblast cell line', *Frontiers in Pharmacology*, 9(OCT), p. 1138.

Ma, Y., Yabluchanskiy, A. and Lindsey, M. L. (2013) 'Neutrophil roles in left ventricular remodeling following myocardial infarction', *Fibrogenesis and Tissue Repair*, 6(1), p. 11.

Ma, Z. G., Yuan, Y. P., Wu, H. M., Zhang, X. and Tang, Q. Z. (2018) 'Cardiac fibrosis: New insights into the pathogenesis', *International Journal of Biological Sciences*, 14(12), pp. 1645–1657.

Mahfoudh-Boussaid, A., Zaouali, M. A., Hauet, T., Hadj-Ayed, K., Miled, A. H., Ghoul-Mazgar, S., Saidane-Mosbahi, D., Rosello-Catafau, J. and Abdennebi, H. Ben (2012) 'Attenuation of endoplasmic reticulum stress and mitochondrial injury in kidney with ischemic postconditioning application and trimetazidine treatment', *Journal of Biomedical Science*, 19(1), p. 71.

Manser, E., Leung, T., Salihuddin, H., Zhao, Z. and Lim, L. (1994) 'A brain serine/threonine protein kinase activated by Cdc42 and Rac1', *Nature*, 367(6458), pp. 40–46.

Manser, E., Loo, T.-H., Koh, C.-G., Zhao, Z.-S., Chen, X.-Q., Tan, L., Tan, I., Leung, T. and Lim, L. (1998) 'PAK kinases are directly coupled to the PIX family of nucleotide exchange factors', *Molecular Cell*, 1(2), pp. 183–192.

Mao, C., Tai, W. C., Bai, Y., Poizat, C. and Lee, A. S. (2006) 'In vivo regulation of Grp78/BiP transcription in the embryonic heart: Role of the endoplasmic reticulum stress response element and GATA-4', *Journal of Biological Chemistry*, 281(13), pp. 8877–8887.

Mao, J., Lv, Z. and Zhuang, Y. (2014) 'MicroRNA-23a is involved in tumor necrosis factor-α induced apoptosis in mesenchymal stem cells and myocardial infarction', *Experimental and Molecular Pathology*, 97(1), pp. 23–30.

Mao, K., Kobayashi, S., Jaffer, Z. M., Huang, Y., Volden, P., Chernoff, J. and Liang, Q. (2008) 'Regulation of Akt/PKB activity by P21-activated kinase in cardiomyocytes', *Journal of Molecular and Cellular Cardiology*, 44(2), pp. 429–434.

Marciniak, S. J., Yun, C. Y., Oyadomari, S., Novoa, I., Zhang, Y., Jungreis, R., Nagata, K., Harding, H. P. and Ron, D. (2004) 'CHOP induces death by promoting protein synthesis

and oxidation in the stressed endoplasmic reticulum', *Genes and Development*, 18(24), pp. 3066–3077.

Marlin, J. W., Eaton, A., Montano, G. T., Chang, Y.-W. E. and Jakobi, R. (2009) 'Elevated p21-activated kinase 2 activity results in anchorage-independent growth and resistance to anticancer drug-induced cell death.', *Neoplasia*, 11(3), pp. 286–297.

Marlin, J. W., Chang, Y. W. E., Ober, M., Handy, A., Xu, W. and Jakobi, R. (2011) 'Functional PAK-2 knockout and replacement with a caspase cleavage-deficient mutant in mice reveals differential requirements of full-length PAK-2 and caspase-activated PAK-2p34', *Mammalian Genome*, 22(5–6), pp. 306–317.

Maron, B. J., Pelliccia, A., Spataro, A. and Granata, M. (1993) 'Reduction in left ventricular wall thickness after deconditioning in highly trained Olympic athletes', *British Heart Journal*, 69(2), pp. 125–128.

Masaki, T., Yoshida, M. and Noguchi, S. (1999) 'Targeted disruption of CRE-Binding factor TREB5 gene leads to cellular necrosis in cardiac myocytes at the embryonic stage', *Biochemical and Biophysical Research Communications*, 261(2), pp. 350–356.

Matsui, T., Tao, J., Del Monte, F., Lee, K. H., Li, L., Picard, M., Force, T. L., Franke, T. F., Hajjar, R. J. and Rosenzweig, A. (2001) 'Akt activation preserves cardiac function and prevents injury after transient cardiac ischemia in vivo', *Circulation*, 104(3), pp. 330–335.

Maurel, M., Chevet, E., Tavernier, J. and Gerlo, S. (2014) 'Getting RIDD of RNA: IRE1 in cell fate regulation', *Trends in Biochemical Sciences*, 39(5), pp. 245–254.

McCullough, K. D., Martindale, J. L., Klotz, L. O., Aw, T. Y. and Holbrook, N. J. (2001) 'Gadd153 sensitizes cells to endoplasmic reticulum stress by down-regulating Bcl2 and perturbing the cellular redox state.', *Molecular and Cellular Biology*, 21(4), pp. 1249–59.

McLendon, P. M. and Robbins, J. (2015) 'Proteotoxicity and cardiac dysfunction', *Circulation Research*, 116(11), pp. 1863–1882.

McMullen, J. R. and Jennings, G. L. (2007) 'Differences between pathological and physiological cardiac hypertrophy: Novel therapeutic strategies to treat heart failure', *Clinical and Experimental Pharmacology and Physiology*, 34(4), pp. 255–262.

Mei, X., Tan, G. and Qing, W. (2020) 'AMPK activation increases postoperative cognitive impairment in intermittent hypoxia rats via direct activating PAK2', *Behavioural Brain Research*, 379, p. 112344.

Mendell, J. R., Al-Zaidy, S., Shell, R., Arnold, W. D., Rodino-Klapac, L. R., Prior, T. W., Lowes, L., Alfano, L., Berry, K., Church, K., *et al.* (2017) 'Single-dose gene-replacement therapy for spinal muscular atrophy', *New England Journal of Medicine*, 377(18), pp. 1713–1722.

Meng, Q., Bhandary, B., Bhuiyan, M. S., James, J., Osinska, H., Valiente-Alandi, I., Shay-Winkler, K., Gulick, J., Molkentin, J. D., Blaxall, B. C., *et al.* (2018) 'Myofibroblast-specific TGFβ receptor II signaling in the fibrotic response to cardiac myosin binding protein C-induced cardiomyopathy', *Circulation Research*, 123(12), pp. 1285–1297.

Merten, K. E., Jiang, Y. and Kang, Y. J. (2007) 'Zinc inhibits doxorubicin-activated calcineurin signal transduction pathway in H9c2 embryonic rat cardiac cells', *Experimental Biology and Medicine*, 232(5), pp. 682–689.

Meusser, B., Hirsch, C., Jarosch, E. and Sommer, T. (2005) 'ERAD: the long road to destruction', *Nature Cell Biology*, 7(8), pp. 766–772.

Mirkes, P. E. (2008) 'Cell death in normal and abnormal development', *Congenital Anomalies*, 48(1), pp. 7–17.

Monasky, M. M., Taglieri, D. M., Patel, B. G., Chernoff, J., Wolska, B. M., Ke, Y. and Solaro, R. J. (2012) 'p21-activated kinase improves cardiac contractility during ischemia-reperfusion concomitant with changes in troponin-T and myosin light chain 2 phosphorylation', *AJP: Heart and Circulatory Physiology*, 302(1), pp. H224–H230.

Moore, K. and Hollien, J. (2015) 'Ire1-mediated decay in mammalian cells relies on mRNA sequence, structure, and translational status', *Molecular Biology of the Cell*, 26(16), pp. 2873–2884.

Moreno, P. R. (2001) 'Pathophysiology of plaque disruption and thrombosis in acute ischemic syndromes', *Journal of Stroke and Cerebrovascular Diseases*, 10(2 SUPPL. 1), pp. 2–9.

Morishima, N., Nakanishi, K., Takenouchi, H., Shibata, T. and Yasuhiko, Y. (2002) 'An

endoplasmic reticulum stress-specific caspase cascade in apoptosis. Cytochrome c-independent activation of caspase-9 by caspase-12', *Journal of Biological Chemistry*, 277(37), pp. 34287–34294.

Morita, N., Mandel, W. J., Kobayashi, Y. and Karagueuzian, H. S. (2014) 'Cardiac fibrosis as a determinant of ventricular tachyarrhythmias', *Journal of Arrhythmia*, 30(6), pp. 389–394.

Moshki, M., Zareie, M. and Hashemizadeh, H. (2015) 'Sex differences in acute myocardial infarction.', *Nursing and Midwifery Studies*, 4(1), p. e22395.

Moubarak, R. S., Yuste, V. J., Artus, C., Bouharrour, A., Greer, P. A., Menissier-de Murcia, J. and Susin, S. A. (2007) 'Sequential activation of poly(ADP-ribose) polymerase 1, calpains, and Bax is essential in apoptosis-inducing factor-mediated programmed necrosis', *Molecular and Cellular Biology*, 27(13), pp. 4844–62.

Moussa, A. and Li, J. (2012) 'AMPK in myocardial infarction and diabetes: the yin/yang effect', *Acta Pharmaceutica Sinica B*, 2(4), pp. 368–378.

Mouton, A. J., DeLeon-Pennell, K. Y., Rivera Gonzalez, O. J., Flynn, E. R., Freeman, T. C., Saucerman, J. J., Garrett, M. R., Ma, Y., Harmancey, R. and Lindsey, M. L. (2018) 'Mapping macrophage polarization over the myocardial infarction time continuum', *Basic Research in Cardiology*, 113(4), p. 26.

Murry, C. E., Reinecke, H. and Pabon, L. M. (2006) 'Regeneration gaps. Observations on stem cells and cardiac repair', *Journal of the American College of Cardiology*, 47(9), pp. 1777–1785.

Nagaraju, C. K., Robinson, E. L., Abdesselem, M., Trenson, S., Dries, E., Gilbert, G., Janssens, S., Van Cleemput, J., Rega, F., Meyns, B., *et al.* (2019) 'Myofibroblast phenotype and reversibility of fibrosis in patients with end-stage heart failure', *Journal of the American College of Cardiology*, 73(18), pp. 2267–2282.

Nakamura, T., Ueda, Y., Juan, Y., Katsuda, S., Takahashi, H. and Koh, E. (2000) 'Fas-mediated apoptosis in adriamycin-induced cardiomyopathy in rats: In vivo study.', *Circulation*, 102(5), pp. 572–578.

Nakka, V. P., Gusain, A. and Raghubir, R. (2010) 'Endoplasmic reticulum stress plays

critical role in brain damage after cerebral ischemia/reperfusion in rats', *Neurotoxicity Research*, 17(2), pp. 189–202.

Newton, K., Wickliffe, K. E., Dugger, D. L., Maltzman, A., Roose-Girma, M., Dohse, M., Kőműves, L., Webster, J. D. and Dixit, V. M. (2019) 'Cleavage of RIPK1 by caspase-8 is crucial for limiting apoptosis and necroptosis', *Nature*, 574(7778), pp. 428–431.

Ni, L., Scott, L., Campbell, H. M., Pan, X., Alsina, K. M., Reynolds, J., Philippen, L. E., Hulsurkar, M., Lagor, W. R., Li, N., *et al.* (2019) 'Atrial-specific gene delivery using an adeno-associated viral vector', *Circulation Research*, 124(2), pp. 256–262.

Nielsen, S. H., Mouton, A. J., DeLeon-Pennell, K. Y., Genovese, F., Karsdal, M. and Lindsey, M. L. (2019) 'Understanding cardiac extracellular matrix remodeling to develop biomarkers of myocardial infarction outcomes', *Matrix Biology*, 75–76, pp. 43–57.

Nimnual, A. S., Taylor, L. J. and Bar-Sagi, D. (2003) 'Redox-dependent downregulation of Rho by Rac', *Nature Cell Biology*, 5(3), pp. 236–241.

Nishitoh, H., Saitoh, M., Mochida, Y., Takeda, K., Nakano, H., Rothe, M., Miyazono, K. and Ichijo, H. (1998) 'ASK1 is essential for JNK/SAPK activation by TRAF2', *Molecular Cell*, 2(3), pp. 389–395.

O'Donnell, M. A., Perez-Jimenez, E., Oberst, A., Ng, A., Massoumi, R., Xavier, R., Green, D. R. and Ting, A. T. (2011) 'Caspase 8 inhibits programmed necrosis by processing CYLD.', *Nature Cell Biology*, 13(12), pp. 1437–42.

Oerlemans, M. I. F. J., Liu, J., Arslan, F., Den Ouden, K., Van Middelaar, B. J., Doevendans, P. A. and Sluijter, J. P. G. (2012) 'Inhibition of RIP1-dependent necrosis prevents adverse cardiac remodeling after myocardial ischemia-reperfusion in vivo', *Basic Research in Cardiology*, 107(4), p. 270.

Ojha, N., Roy, S., Radtke, J., Simonetti, O., Gnyawali, S., Zweier, J. L., Kuppusamy, P. and Sen, C. K. (2008) 'Characterization of the structural and functional changes in the myocardium following focal ischemia-reperfusion injury', *American Journal of Physiology - Heart and Circulatory Physiology*, 294(6), p. H2435.

Olivetti, G., Abbi, R., Quaini, F., Kajstura, J., Cheng, W., Nitahara, J. A., Quaini, E., Di Loreto, C., Beltrami, C. A., Krajewski, S., *et al.* (1997) 'Apoptosis in the failing human

heart', *New England Journal of Medicine*, 336(16), pp. 1131–1141.

Ong, S. B., Hernández-Reséndiz, S., Crespo-Avilan, G. E., Mukhametshina, R. T., Kwek, X. Y., Cabrera-Fuentes, H. A. and Hausenloy, D. J. (2018) 'Inflammation following acute myocardial infarction: Multiple players, dynamic roles, and novel therapeutic opportunities', *Pharmacology and Therapeutics*, 186, pp. 73–87.

Ono, K., Matsumori, A., Shioi, T., Furukawa, Y. and Sasayama, S. (1998) 'Cytokine gene expression after myocardial infarction in rat hearts: Possible implication in left ventricular remodeling', *Circulation*, 98(2), pp. 149–156.

Opferman, J. T. (2008) 'Apoptosis in the development of the immune system.', *Cell Death and Differentiation*, 15(2), pp. 234–242.

Ortega-Gómez, A., Perretti, M. and Soehnlein, O. (2013) 'Resolution of inflammation: An integrated view', *EMBO Molecular Medicine*, 5(5), pp. 661–674.

Palojoki, E., Saraste, A., Eriksson, A., Pulkki, K., Tikkanen, I., Saraste, A., Eriksson, A. and Kallajoki, M. (2001) 'Cardiomyocyte apoptosis and ventricular remodeling after myocardial infarction in rats', *American Journal of Physiology - Heart and Circulatory Physiology*, 280(6), pp. 2726–2731.

Pandya, K., Pulli, B., Bultman, S. and Smithies, O. (2011) 'Reversible epigenetic modifications of the two cardiac myosin heavy chain genes during changes in expression', *Gene Expression*, 15(2), pp. 51–59.

Park, C. S., Cha, H., Kwon, E. J., Sreenivasaiah, P. K. and Kim, D. H. (2012) 'The chemical chaperone 4-phenylbutyric acid attenuates pressure-overload cardiac hypertrophy by alleviating endoplasmic reticulum stress', *Biochemical and Biophysical Research Communications*, 421(3), pp. 578–584.

Pasparakis, M. and Vandenabeele, P. (2015) 'Necroptosis and its role in inflammation', *Nature*, 517(7534), pp. 311–320.

Peet, C., Ivetic, A., Bromage, D. I. and Shah, A. M. (2020) 'Cardiac monocytes and macrophages after myocardial infarction', *Cardiovascular research*, 116(6), pp. 1101–1112.

Peng, X., He, Q., Li, G., Ma, J. and Zhong, T. P. (2016) 'Rac1-PAK2 pathway is essential for zebrafish heart regeneration', *Biochemical and Biophysical Research Communications*, 472(4), pp. 637–642.

Pincha, N., Saha, D., Bhatt, T., Zirmire, R. and Jamora, C. (2018) 'Activation of fibroblast contractility via cell-cell interactions and soluble signals', *BIO-PROTOCOL*, 8(18), p. e3021.

Pizzino, G., Irrera, N., Cucinotta, M., Pallio, G., Mannino, F., Arcoraci, V., Squadrito, F., Altavilla, D. and Bitto, A. (2017) 'Oxidative stress: Harms and benefits for human health', *Oxidative Medicine and Cellular Longevity*, 2017, p. 8416763.

Ponikowski, P., Anker, S. D., AlHabib, K. F., Cowie, M. R., Force, T. L., Hu, S., Jaarsma, T., Krum, H., Rastogi, V., Rohde, L. E., *et al.* (2014) 'Heart failure: preventing disease and death worldwide', *ESC Heart Failure*, 1(1), pp. 4–25.

Porter, K. E. and Turner, N. A. (2009) 'Cardiac fibroblasts: At the heart of myocardial remodeling', *Pharmacology & Therapeutics*, 123(2), pp. 255–278.

Prabhu, S. D. and Frangogiannis, N. G. (2016) 'The biological basis for cardiac repair after myocardial infarction', *Circulation Research*, 119(1), pp. 91–112.

Puthalakath, H., O'Reilly, L. A., Gunn, P., Lee, L., Kelly, P. N., Huntington, N. D., Hughes, P. D., Michalak, E. M., McKimm-Breschkin, J., Motoyama, N., *et al.* (2007) 'ER stress triggers apoptosis by activating BH3-only protein Bim', *Cell*, 129(7), pp. 1337–1349.

Qi, Z. P., Xia, P., Hou, T. T., Li, D. Y., Zheng, C. J. and Yang, X. Y. (2016) 'Characteristics of mRNA dynamic expression related to spinal cord ischemia/reperfusion injury: A transcriptomics study', *Neural Regeneration Research*, 11(3), pp. 480–486.

Radu, M., Lyle, K., Hoeflich, K. P., Villamar-Cruz, O., Koeppen, H. and Chernoff, J. (2015) 'p21-activated kinase 2 regulates endothelial development and function through the Bmk1/Erk5 pathway', *Molecular and Cellular Biology*, 35(23), pp. 3990–4005.

Ran, M., Weng, B., Cao, R., Li, Z., Peng, F., Luo, H., Gao, H. and Chen, B. (2018) 'miR-26a inhibits proliferation and promotes apoptosis in porcine immature Sertoli cells by targeting the PAK2 gene', *Reproduction in Domestic Animals*, 53(6), pp. 1375–1385.

Rane, C. K. and Minden, A. (2014) 'P21 activated kinases: Structure, regulation, and functions', *Small GTPases*, 5, p. e28003.

Regitz-Zagrosek, V. and Kararigas, G. (2017) 'Mechanistic pathways of sex differences in cardiovascular disease', *Physiological Reviews*, 97(1), pp. 1–37.

Reimer, K. A., Lowe, J. E., Rasmussen, M. M. and Jennings, R. B. (1977) 'The wavefront phenomenon of ischemic cell death. 1. Myocardial infarct size vs duration of coronary occlusion in dogs.', *Circulation*, 56(5), pp. 786–794.

Renkema, G. H., Pulkkinen, K. and Saksela, K. (2002) 'Cdc42/Rac1-mediated activation primes PAK2 for superactivation by tyrosine phosphorylation.', *Molecular and Cellular Biology*, 22(19), pp. 6719–25.

Rienks, M., Papageorgiou, A. P., Frangogiannis, N. G. and Heymans, S. (2014) 'Myocardial extracellular matrix: An ever-changing and diverse entity', *Circulation Research*, 114(5), pp. 872–888.

Ronzitti, G., Gross, D. A. and Mingozzi, F. (2020) 'Human immune responses to adeno-associated virus (AAV) vectors', *Frontiers in Immunology*, 11, p. 670.

Rousseau, V., Goupille, O., Morin, N. and Barnier, J. V. (2003) 'A new constitutively active brain PAK3 isoform displays modified specificities toward Rac and Cdc42 GTPases', *Journal of Biological Chemistry*, 278(6), pp. 3912–3920.

Rozpedek, W., Pytel, D., Mucha, B., Leszczynska, H., Diehl, J. A. and Majsterek, I. (2016) 'The role of the PERK/eIF2α/ATF4/CHOP signaling pathway in tumor progression during endoplasmic reticulum stress', *Current Molecular Medicine*, 16(6), pp. 533–544.

Rudel, T., Zenke, F. T., Chuang, T. H. and Bokoch, G. M. (1998) 'p21-activated kinase (PAK) is required for Fas-induced JNK activation in Jurkat cells', *Journal of Immunology*, 160(1), pp. 7–11.

Rudel, T. and Bokoch, G. M. (1997) 'Membrane and morphological changes in apoptotic cells regulated by caspase-mediated activation of PAK2.', *Science*, 276(5318), pp. 1571–4.

Rusinkevich, V., Huang, Y., Chen, Z. yan, Qiang, W., Wang, Y. gang, Shi, Y. fang and Yang,

H. tian (2019) ‘Temporal dynamics of immune response following prolonged myocardial ischemia/reperfusion with and without cyclosporine A’, *Acta Pharmacologica Sinica*, 40(9), pp. 1168–1183.

Russell, R. C., Yuan, H. X. and Guan, K. L. (2014) ‘Autophagy regulation by nutrient signaling’, *Cell Research*, 24(1), pp. 42–57.

Russell, R. R., Li, J., Coven, D. L., Pypaert, M., Zechner, C., Palmeri, M., Giordano, F. J., Mu, J., Birnbaum, M. J. and Young, L. H. (2004) ‘AMP-activated protein kinase mediates ischemic glucose uptake and prevents postischemic cardiac dysfunction, apoptosis, and injury’, *Journal of Clinical Investigation*, 114(4), pp. 495–503.

Sander, E. E., Ten Klooster, J. P., Van Delft, S., Van Der Kammen, R. A. and Collard, J. G. (1999) ‘Rac downregulates Rho activity: Reciprocal balance between both GTPases determines cellular morphology and migratory behavior’, *Journal of Cell Biology*, 147(5), pp. 1009–1021.

Sanjabi, S., Oh, S. A. and Li, M. O. (2017) ‘Regulation of the immune response by TGF-β: From conception to autoimmunity and infection’, *Cold Spring Harbor Perspectives in Biology*, 9(6), p. a022236.

Sawada, T., Minamino, T., Fu, H. Y., Asai, M., Okuda, K., Isomura, T., Yamazaki, S., Asano, Y., Okada, K. ichiro, Tsukamoto, O., *et al.* (2010) ‘X-box binding protein 1 regulates brain natriuretic peptide through a novel AP1/CRE-like element in cardiomyocytes’, *Journal of Molecular and Cellular Cardiology*, 48(6), pp. 1280–1289.

Schultz-Cherry, S. and Murphy-Ullrich, J. E. (1993) ‘Thrombospondin causes activation of latent transforming growth factor-β secreted by endothelial cells by a novel mechanism’, *Journal of Cell Biology*, 122(4), pp. 923–932.

Scull, C. M. and Tabas, I. (2011) ‘Mechanisms of ER stress-induced apoptosis in atherosclerosis’, *Arteriosclerosis, Thrombosis, and Vascular Biology*, 31(12), pp. 2792–2797.

Sebbagh, M., Renvoizé, C., Hamelin, J., Riché, N., Bertoglio, J. and Bréard, J. (2001) ‘Caspase-3-mediated cleavage of ROCK I induces MLC phosphorylation and apoptotic membrane blebbing.’, *Nature cell biology*, 3(April), pp. 346–352.

Severino, A., Campioni, M., Straino, S., Salloum, F. N., Schmidt, N., Herbrand, U., Frede, S., Toietta, G., Di Rocco, G., Bussani, R., *et al.* (2007) 'Identification of protein disulfide isomerase as a cardiomyocyte survival factor in ischemic cardiomyopathy', *Journal of the American College of Cardiology*, 50(11), pp. 1029–1037.

Sheehan, K. A., Ke, Y., Wolska, B. M. and Solaro, R. J. (2009) 'Expression of active p21-activated kinase-1 induces Ca2+ flux modification with altered regulatory protein phosphorylation in cardiac myocytes.', *American journal of physiology. Cell physiology*, 296(1), pp. C47-58.

Shimazaki, M., Nakamura, K., Kii, I., Kashima, T., Amizuka, N., Li, M., Saito, M., Fukuda, K., Nishiyama, T., Kitajima, S., *et al.* (2008) 'Periostin is essential for cardiac healing after acute myocardial infarction', *Journal of Experimental Medicine*, 205(2), pp. 295–303.

Skalli, O., Pelte, M. F., Peclet, M. C., Gabbiani, G., Gugliotta, P., Bussolati, G., Ravazzola, M. and Orci, L. (1989) 'α-Smooth muscle actin, a differentiation marker of smooth muscle cells, is present in microfilamentous bundles of pericytes', *Journal of Histochemistry and Cytochemistry*, 37(3), pp. 315–321.

Smith, C. C. T., Davidson, S. M., Lim, S. Y., Simpkin, J. C., Hothersall, J. S. and Yellon, D. M. (2007) 'Necrostatin: A potentially novel cardioprotective agent?', *Cardiovascular Drugs and Therapy*, 21(4), pp. 227–233.

Somanathan, S., Breous, E., Bell, P. and Wilson, J. M. (2010) 'AAV vectors avoid inflammatory signals necessary to render transduced hepatocyte targets for destructive t cells', *Molecular Therapy*, 18(5), pp. 977–982.

Son, S. M., Byun, J., Roh, S.-E., Kim, S. J. and Mook-Jung, I. (2014) 'Reduced IRE1α mediates apoptotic cell death by disrupting calcium homeostasis via the InsP3 receptor', *Cell Death and Disease*, 5(4), p. e1188.

Song, X. J., Yang, C. Y., Liu, B., Wei, Q., Korkor, M. T., Liu, J. Y. and Yang, P. (2011) 'Atorvastatin inhibits myocardial cell apoptosis in a rat model with post-myocardial infarction heart failure by downregulating ER stress response', *International Journal of Medical Sciences*, 8(7), pp. 564–572.

Su, H. C. and Lenardo, M. J. (2008) 'Genetic defects of apoptosis and primary

immunodeficiency', *Immunology and Allergy Clinics of North America*, 28(2), pp. 329–351.

Suen, D. F., Norris, K. L. and Youle, R. J. (2008) 'Mitochondrial dynamics and apoptosis', *Genes and Development*, 22(12), pp. 1577–1590.

Svensson, E. C., Marshall, D. J., Woodard, K., Lin, H., Jiang, F., Chu, L. and Leiden, J. M. (1999) 'Efficient and stable transduction of cardiomyocytes after intramyocardial injection or intracoronary perfusion with recombinant adeno- associated virus vectors', *Circulation*, 99(2), pp. 201–205.

Szegezdi, E., Duffy, A., O'Mahoney, M. E., Logue, S. E., Mylotte, L. A., O'Brien, T. and Samali, A. (2006) 'ER stress contributes to ischemia-induced cardiomyocyte apoptosis', *Biochemical and Biophysical Research Communications*, 349(4), pp. 1406–1411.

Szegezdi, E., Logue, S. E., Gorman, A. M. and Samali, A. (2006) 'Mediators of endoplasmic reticulum stress-induced apoptosis', *EMBO Reports*, 7(9), pp. 880–885.

Szobi, A., Gonçalvesová, E., Varga, Z., Leszek, P., Kuśmierczyk, M., Hulman, M., Kyselovič, J., Ferdinandy, P. and Adameová, A. (2017) 'Analysis of necroptotic proteins in failing human hearts', *Journal of Translational Medicine*, 15(1), p. 86.

Taglieri, D. M., Monasky, M. M., Knezevic, I., Sheehan, K. A., Lei, M., Wang, X., Chernoff, J., Wolska, B. M., Ke, Y. and Solaro, R. J. (2011) 'Ablation of p21-activated kinase-1 in mice promotes isoproterenol-induced cardiac hypertrophy in association with activation of Erk1/2 and inhibition of protein phosphatase 2A', *Journal of Molecular and Cellular Cardiology*, 51(6), pp. 988–996.

Taglieri, D. M., Ushio-Fukai, M. and Monasky, M. M. (2014) 'P21-activated kinase in inflammatory and cardiovascular disease', *Cellular Signalling*, 26(9), pp. 2060–2069.

Talman, V. and Ruskoaho, H. (2016) 'Cardiac fibrosis in myocardial infarction-from repair and remodeling to regeneration.', *Cell and tissue research*, 365(3), pp. 563–81.

Tam, A. B., Mercado, E. L., Hoffmann, A. and Niwa, M. (2012) 'ER stress activates NF-κB by integrating functions of basal IKK activity, IRE1 and PERK', *PLoS ONE*, 7(10), p. e45078.

Tamaki, N., Hatano, E., Taura, K., Tada, M., Kodama, Y., Nitta, T., Iwaisako, K., Seo, S.,

Nakajima, A., Ikai, I., *et al.* (2008) 'CHOP deficiency attenuates cholestasis-induced liver fibrosis by reduction of hepatocyte injury', *American Journal of Physiology - Gastrointestinal and Liver Physiology*, 294(2), pp. 498–505.

Tang, Y., Zhou, H., Chen, A., Pittman, R. N. and Field, J. (2000) 'The Akt proto-oncogene links Ras to Pak and cell survival signals', *Journal of Biological Chemistry*, 275(13), pp. 9106–9109.

Taylor, C. J., Ryan, R., Nichols, L., Gale, N., Hobbs, F. R. and Marshall, T. (2017) 'Survival following a diagnosis of heart failure in primary care', *Family Practice*, 34(19), p. cmw145.

Taylor, R. C., Cullen, S. P. and Martin, S. J. (2008) 'Apoptosis: controlled demolition at the cellular level.', *Nature Reviews. Molecular cell biology*, 9(3), pp. 231–241.

Teiger, E., Dam, T. V., Richard, L., Wisnewsky, C., Tea, B. S., Gaboury, L., Tremblay, J., Schwartz, K. and Hamet, P. (1996) 'Apoptosis in pressure overload-induced heart hypertrophy in the rat', *Journal of Clinical Investigation*, 97(12), pp. 2891–2897.

Teng, C., Li, P., Wu, L. and Howes, C. (2020) 'An updated examination of comorbidities among patients presenting with acute myocardial infarction', *Journal of the American College of Cardiology*, 75(11), p. 166.

Teske, B. F., Wek, S. A., Bunpo, P., Cundiff, J. K., McClintick, J. N., Anthony, T. G. and Wek, R. C. (2011) 'The eIF2 kinase PERK and the integrated stress response facilitate activation of ATF6 during endoplasmic reticulum stress', *Molecular Biology of the Cell*, 22(22), pp. 4390–4405.

Thuerauf, D. J., Marcinko, M., Gude, N., Rubio, M., Sussman, M. A. and Glembotski, C. C. (2006) 'Activation of the unfolded protein response in infarcted mouse heart and hypoxic cultured cardiac myocytes', *Circulation Research*, 99(3), pp. 275–282.

Tomasek, J. J., Gabbiani, G., Hinz, B., Chaponnier, C. and Brown, R. A. (2002) 'Myofibroblasts and mechano: Regulation of connective tissue remodelling', *Nature Reviews Molecular Cell Biology*, 3(5), pp. 349–363.

Tournier, C., Hess, P., Yang, D. D., Xu, J., Turner, T. K., Nimnual, A., Bar-Sagi, D., Jones, S. N., Flavell, R. A. and Davis, R. J. (2000) 'Requirement of JNK for stress-induced activation

of the cytochrome c- mediated death pathway', *Science*, 288(5467), pp. 870–874.

Tsujita, K., Shimomura, H., Kaikita, K., Kawano, H., Hokamaki, J., Nagayoshi, Y., Yamashita, T., Fukuda, M., Nakamura, Y., Sakamoto, T., *et al.* (2006) 'Long-term efficacy of edaravone in patients with acute myocardial infarction', *Circulation Journal*, 70(7), pp. 832–837.

Upton, J. P., Wang, L., Han, D., Wang, E. S., Huskey, N. E., Lim, L., Truitt, M., McManus, M. T., Ruggero, D., Goga, A., *et al.* (2012) 'IRE1α cleaves select microRNAs during ER stress to derepress translation of proapoptotic caspase-2', *Science*, 338(6108), pp. 818–822.

Urra, H., Dufey, E., Avril, T., Chevet, E. and Hetz, C. (2016) 'Endoplasmic reticulum stress and the hallmarks of cancer', *Trends in Cancer*, 2(5), pp. 252–262.

Vaccarino, V., Parsons, L., Every, N. R., Barron, H. V. and Krumholz, H. M. (1999) 'Sex-based differences in early mortality after myocardial infarction', *New England Journal of Medicine*, 341(4), pp. 217–225.

Velagaleti, R. S., Pencina, M. J., Murabito, J. M., Wang, T. J., Parikh, N. I., D'Agostino, R. B., Levy, D., Kannel, W. B. and Vasan, R. S. (2008) 'Long-term trends in the incidence of heart failure after myocardial infarction', *Circulation*, 118(20), pp. 2057–2062.

Verdera, H. C., Kuranda, K. and Mingozzi, F. (2020) 'AAV vector immunogenicity in humans: A long journey to successful gene transfer', *Molecular Therapy*, 28(3), pp. 723–746.

Vettel, C., Wittig, K., Vogt, A., Wuertz, C. M., El-Armouche, A., Lutz, S. and Wieland, T. (2012) 'A novel player in cellular hypertrophy: G iβγ/PI3K-dependent activation of the RacGEF TIAM-1 is required for α 1-adrenoceptor induced hypertrophy in neonatal rat cardiomyocytes', *Journal of Molecular and Cellular Cardiology*, 53(2), pp. 165–175.

Vilas, G. L., Corvi, M. M., Plummer, G. J., Seime, A. M., Lambkin, G. R. and Berthiaume, L. G. (2006) 'Posttranslational myristoylation of caspase-activated p21-activated protein kinase 2 (PAK2) potentiates late apoptotic events.', *Proceedings of the National Academy of Sciences of the United States of America*, 103(17), pp. 6542–6547.

Virag, J. A. I. and Lust, R. M. (2011) 'Coronary artery ligation and intramyocardial

injection in a murine model of infarction', *Journal of Visualized Experiments*, (52), p. 2581.

Walsh, J. G., Cullen, S. P., Sheridan, C., Lüthi, A. U., Gerner, C. and Martin, S. J. (2008) 'Executioner caspase-3 and caspase-7 are functionally distinct proteases', *Proceedings of the National Academy of Sciences of the United States of America*, 105(35), pp. 12815–12819.

Wang, B., Hao, J., Jones, S. C., Yee, M. S., Roth, J. C. and Dixon, I. M. C. (2002) 'Decreased Smad 7 expression contributes to cardiac fibrosis in the infarcted rat heart', *American Journal of Physiology - Heart and Circulatory Physiology*, 282(5), pp. H1685-96.

Wang, H., Sun, L., Su, L., Rizo, J., Liu, L., Wang, L. F., Wang, F. S. and Wang, X. (2014) 'Mixed lineage kinase domain-like protein MLKL causes necrotic membrane disruption upon phosphorylation by RIP3', *Molecular Cell*, 54(1), pp. 133–146.

Wang, R., Wang, Y., Lin, W. K., Zhang, Y., Liu, W., Huang, K., Terrar, D. A., Solaro, R. J., Wang, X., Ke, Y., *et al.* (2014) 'Inhibition of angiotensin II-induced cardiac hypertrophy and associated ventricular arrhythmias by a p21 activated kinase 1 bioactive peptide', *PLoS ONE*, 9(7), p. e101974.

Wang, S., Binder, P., Fang, Q., Wang, Z., Xiao, W., Liu, W. and Wang, X. (2018) 'Endoplasmic reticulum stress in the heart: insights into mechanisms and drug targets', *British Journal of Pharmacology*, 175(8), pp. 1293–1304.

Wang, S., Bian, W., Zhen, J., Zhao, L. and Chen, W. (2019) 'Melatonin-mediated Pak2 activation reduces cardiomyocyte death through suppressing hypoxia reoxygenation injury–induced endoplasmic reticulum stress', *Journal of Cardiovascular Pharmacology*, 74(1), pp. 20–29.

Wang, X., Ma, S. and Qi, G. (2012) 'Effect of hypoxia-inducible factor 1-alpha on hypoxia/reoxygenation-induced apoptosis in primary neonatal rat cardiomyocytes', *Biochemical and Biophysical Research Communications*, 417(4), pp. 1227–1234.

Wang, X. Z. and Ron, D. (1996) 'Stress-induced phosphorylation and activation of the transcription factor CHOP (GADD153) by p38 MAP kinase', *Science*, 272(5266), pp. 1347–1349.

Wang, Y., Tsui, H., Ke, Y., Shi, Y., Li, Y., Davies, L., Cartwright, E. J., Venetucci, L., Zhang, H., Terrar, D. A., *et al.* (2014) 'Pak1 is required to maintain ventricular Ca2+ homeostasis and electrophysiological stability through SERCA2a regulation in mice', *Circulation: Arrhythmia and Electrophysiology*, 7(5), pp. 938–948.

Wang, Y., Wang, S., Lei, M., Boyett, M., Tsui, H., Liu, W. and Wang, X. (2018) 'The p21-activated kinase 1 (Pak1) signalling pathway in cardiac disease: from mechanistic study to therapeutic exploration', *British Journal of Pharmacology*, 175(8), pp. 1362–1374.

Wang, Z., Jiang, H., Chen, S., Du, F. and Wang, X. (2012) 'The mitochondrial phosphatase PGAM5 functions at the convergence point of multiple necrotic death pathways', *Cell*, 148(1–2), pp. 228–243.

Wang, Z. V., Deng, Y., Gao, N., Pedrozo, Z., Li, D. L., Morales, C. R., Criollo, A., Luo, X., Tan, W., Jiang, N., *et al.* (2014) 'Spliced X-box binding protein 1 couples the unfolded protein response to hexosamine biosynthetic pathway', *Cell*, 156(6), pp. 1179–1192.

Wei, L., Lu, J., Feng, L., Long, D., Shan, J., Li, S. and Li, Y. (2010) 'HIF-1α accumulation upregulates MICA and MICB expression on human cardiomyocytes and enhances NK cell cytotoxicity during hypoxia-reoxygenation', *Life Sciences*, 87(3–4), pp. 111–119.

Weil, B. R. and Neelamegham, S. (2019) 'Selectins and immune cells in aucte mycardial infarction and post-infarction ventricular remodelings: Pathophysiology and novel treatments', *Frontiers in Immunology*, 10(FEB), p. 300.

Westphal, R. S., Coffee, R. L., Marotta, A., Pelech, S. L. and Wadzinski, B. E. (1999) 'Identification of kinase-phosphatase signaling modules composed of p70 S6 kinase-protein phosphatase 2A (PP2A) and p21-activated kinase-PP2A', *Journal of Biological Chemistry*, 274(2), pp. 687–692.

Whelan, R. S., Konstantinidis, K., Wei, A. C., Chen, Y., Reyna, D. E., Jha, S., Yang, Y., Calvert, J. W., Lindsten, T., Thompson, C. B., *et al.* (2012) 'Bax regulates primary necrosis through mitochondrial dynamics', *Proceedings of the National Academy of Sciences of the United States of America*, 109(17), pp. 6566–6571.

Wiley, S. R., Schooley, K., Smolak, P. J., Din, W. S., Huang, C. P., Nicholl, J. K., Sutherland, G. R., Smith, T. D., Rauch, C., Smith, C. A., *et al.* (1995) 'Identification and characterization

of a new member of the TNF family that induces apoptosis', *Immunity*, 3(6), pp. 673–682.

Wilkes, M. C., Murphy, S. J., Garamszegi, N. and Leof, E. B. (2003) 'Cell-type-specific activation of PAK2 by transforming growth factor beta independent of Smad2 and Smad3.', *Molecular and Cellular Biology*, 23(23), pp. 8878–89.

Wilkes, M. C., Mitchell, H., Penheiter, S. G., Doré, J. J., Suzuki, K., Edens, M., Sharma, D. K., Pagano, R. E. and Leof, E. B. (2005) 'Transforming growth factor-beta activation of phosphatidylinositol 3-kinase is independent of Smad2 and Smad3 and regulates fibroblast responses via p21-activated kinase-2.', *Cancer Research*, 65(22), pp. 10431–40.

Wilkes, M. C. and Leof, E. B. (2006) 'Transforming growth factor beta activation of c-Abl is independent of receptor internalization and regulated by phosphatidylinositol 3-kinase and PAK2 in mesenchymal cultures.', *The Journal of Biological Chemistry*, 281(38), pp. 27846–54.

Witek, P., Korga, A., Burdan, F., Ostrowska, M., Nosowska, B., Iwan, M. and Dudka, J. (2016) 'The effect of a number of H9C2 rat cardiomyocytes passage on repeatability of cytotoxicity study results', *Cytotechnology*, 68(6), pp. 2407–2415.

Wong, A.-P., Niedzwiecki, A. and Rath, M. (2016) 'Myocardial energetics and the role of micronutrients in heart failure: a critical review.', *American Journal of Cardiovascular Disease*, 6(3), pp. 81–92.

World Health Organisation (2020) *Cardiovascular diseases (CVDs) factsheet*.

Wu, H. and Wang, Z. X. (2003) 'The mechanism of p21-activated kinase 2 autoactivation', *Journal of Biological Chemistry*, 278(43), pp. 41768–41778.

Wu, J., Jackson-Weaver, O. and Xu, J. (2018) 'The TGFβ superfamily in cardiac dysfunction', *Acta Biochimica et Biophysica Sinica*, 50(4), pp. 323–335.

Wünsch, M., Sharma, H. S., Markert, T., Bernotat-Danielowski, S., Schott, R. J., Kremer, P., Bleese, N. and Schaper, W. (1991) 'In situ localization of transforming growth factor β1 in porcine heart: Enhanced expression after chronic coronary artery constriction', *Journal of Molecular and Cellular Cardiology*, 23(9), pp. 1051–1062.

Xiao, Y. Q., Freire-de-Lima, C. G., Schiemann, W. P., Bratton, D. L., Vandivier, R. W. and Henson, P. M. (2008) 'Transcriptional and translational regulation of TGF-β production in response to apoptotic cells', *The Journal of Immunology*, 181(5), pp. 3575–3585.

Xie, J. and Xu, B. (2017) 'P2309PAK3 aggravates pathological cardiac hypertrophy in mice', *European Heart Journal*, 38(suppl_1).

Xu, L., Cai, Y., Wang, Y. and Xu, C. (2020) 'Meteorin-like (METRNL) attenuates myocardial ischemia/reperfusion injury-induced cardiomyocytes apoptosis by alleviating endoplasmic reticulum stress via activation of AMPK-PAK2 signaling in H9C2 Cells', *Medical Science Monitor: International Medical Journal of Experimental and Clinical Research*, 26, p. e924564.

Yadav, S., Yuan, C. C., Kazmierczak, K., Liang, J., Huang, W., Takeuchi, L. M., Kanashiro-Takeuchi, R. M. and Szczesna-Cordary, D. (2019) 'Therapeutic potential of AAV9-S15D-RLC gene delivery in humanized MYL2 mouse model of HCM', *Journal of Molecular Medicine*, 97(7), pp. 1033–1047.

Yamauchi-Takihara, K., Ihara, Y., Ogata, A., Yoshizaki, K., Azuma, J. and Kishimoto, T. (1995) 'Hypoxic stress induces cardiac myocyte-derived interleukin-6', *Circulation*, 91(5), pp. 1520–1524.

Yan, X., Zhang, J., Sun, Q., Tuazon, P. T., Wu, X., Traugh, J. A. and Chen, Y.-G. (2012) 'p21-Activated kinase 2 (PAK2) inhibits TGF-β signaling in Madin-Darby canine kidney (MDCK) epithelial cells by interfering with the receptor-Smad interaction.', *The Journal of Biological Chemistry*, 287(17), pp. 13705–12.

Yang, X., Pabon, L. and Murry, C. E. (2014) 'Engineering adolescence: Maturation of human pluripotent stem cell-derived cardiomyocytes', *Circulation Research*, 114(3), pp. 511–523.

Yao, G. W., Bai, J. R. and Zhang, D. P. (2019) 'P21 activated kinase 2 promotes pancreatic cancer growth and metastasis', *Oncology Letters*, 17(4), pp. 3709–3718.

Yellon, D. M. and Hausenloy, D. J. (2007) 'Myocardial reperfusion injury', *New England Journal of Medicine*, 357(11), pp. 1121–1135.

Yu, Q. and Stamenkovic, I. (2000) 'Cell surface-localized matrix metalloproteinase-9

proteolytically activates TGF-β and promotes tumor invasion and angiogenesis', *Genes and Development*, 14(2), pp. 163–176.

Zaman, S. and Kovoor, P. (2014) 'Sudden cardiac death early after myocardial infarction: pathogenesis, risk stratification, and primary prevention', *Circulation*, 129(23), pp. 2426–2435.

Zebrowski, D. C., Vergarajauregui, S., Wu, C. C., Piatkowski, T., Becker, R., Leone, M., Hirth, S., Ricciardi, F., Falk, N., Giessl, A., *et al.* (2015) 'Developmental alterations in centrosome integrity contribute to the post-mitotic state of mammalian cardiomyocytes', *eLife*, 4, p. e05563.

Zeisberg, E. M., Tarnavski, O., Zeisberg, M., Dorfman, A. L., McMullen, J. R., Gustafsson, E., Chandraker, A., Yuan, X., Pu, W. T., Roberts, A. B., *et al.* (2007) 'Endothelial-to-mesenchymal transition contributes to cardiac fibrosis', *Nature Medicine*, 13(8), pp. 952–961.

Zeldovich, L. (2017) 'Genetic drift: The ghost in the genome', *Lab Animal*, 46(6), pp. 255–257.

Zeng, Q., Lagunoff, D., Masaracchia, R., Goeckeler, Z., Côté, G. and Wysolmerski, R. (2000) 'Endothelial cell retraction is induced by PAK2 monophosphorylation of myosin II', *Journal of Cell Science*, 113(3), pp. 471–482.

Zeng, Y., Broxmeyer, H. E., Staser, K., Chitteti, B. R., Park, S. J., Hahn, S., Cooper, S., Sun, Z., Jiang, L., Yang, X., *et al.* (2015) 'Pak2 regulates hematopoietic progenitor cell proliferation, survival, and differentiation', *Stem Cells*, 33(5), pp. 1630–1641.

Zenke, F. T., King, C. C., Bohl, B. P. and Bokoch, G. M. (1999) 'Identification of a central phosphorylation site in p21-activated kinase regulating autoinhibition and kinase activity', *Journal of Biological Chemistry*, 274(46), pp. 32565–32573.

Zeymer, U., Suryapranata, H., Monassier, J. P., Opolski, G., Davies, J., Rasmanis, G., Linssen, G., Tebbe, U., Schröder, R., Tiemann, R., *et al.* (2001) 'The Na+/H+ exchange inhibitor eniporide as an adjunct to early reperfusion therapy for acute myocardial infarction: Results of the Evaluation of the Safety and Cardioprotective Effects of Eniporide in Ecute Myocardial Infarction (ESCAMI) trial', *Journal of the American College*

of Cardiology, 38(6), pp. E1644–E1650.

Zhang, A., Zhang, J., Sun, P., Yao, C., Su, C., Sui, T., Huang, H., Cao, X. and Ge, Y. (2010) 'EIF2α and caspase-12 activation are involved in oxygen-glucose-serum deprivation/restoration-induced apoptosis of spinal cord astrocytes', *Neuroscience Letters*, 478(1), pp. 32–36.

Zhang, C., Tang, Y., Li, Y., Xie, L., Zhuang, W., Liu, J. and Gong, J. (2017) 'Unfolded protein response plays a critical role in heart damage after myocardial ischemia/reperfusion in rats', *PLOS ONE*, 12(6), p. e0179042.

Zhang, D. W., Shao, J., Lin, J., Zhang, N., Lu, B. J., Lin, S. C., Dong, M. Q. and Han, J. (2009) 'RIP3, an energy metabolism regulator that switches TNF-induced cell death from apoptosis to necrosis', *Science*, 325(5938), pp. 332–336.

Zhang, F., Huang, B., Zhao, Y., Tang, S., Xu, H., Wang, L., Liang, R. and Yang, H. (2013) 'BNC protects H9c2 cardiomyoblasts from H2O2-induced oxidative injury through ERK1/2 signaling pathway', *Evidence-based Complementary and Alternative Medicine*, 2013, p. 802784.

Zhang, L., Zhang, C. and Wang, A. (2016) 'Divergence and conservation of the major UPR branch IRE1-bZIP signaling pathway across eukaryotes', *Scientific Reports*, 6(1), pp. 1–14.

Zhang, Z., Tan, Y., Zhu, L., Zhang, B., Feng, P., Gao, E., Xu, C., Wang, X., Yi, W. and Sun, Y. (2019) 'Asprosin improves the survival of mesenchymal stromal cells in myocardial infarction by inhibiting apoptosis via the activated ERK1/2-SOD2 pathway', *Life Sciences*, 231, p. 116554.

Zhao, W. S., Xu, L., Wang, L. F., Zheng, L., Zhang, Z. Y., Liu, Y., Liu, X. L., Yang, X. C., Cui, L. and Zhang, L. (2009) 'A 60-s postconditioning protocol by percutaneous coronary intervention inhibits myocardial apoptosis in patients with acute myocardial infarction', *Apoptosis*, 14(10), pp. 1204–1211.

Zhao, Z., Manser, E. and Lim, L. (2000) 'Interaction between PAK and Nck: A template for Nck targets and role of PAK autophosphorylation', *Molecular and Cellular Biology*, 20(11), pp. 3906–3917.

Zhao, Z. Q., Nakamura, M., Wang, N. P., Wilcox, J. N., Shearer, S., Ronson, R. S., Guyton, R. A. and Vinten-Johansen, J. (2000) 'Reperfusion induces myocardial apoptotic cell death', *Cardiovascular Research*, 45(3), pp. 651–660.

Zhao, Z. Q., Corvera, J. S., Halkos, M. E., Kerendi, F., Wang, N. P., Guyton, R. A. and Vinten-Johansen, J. (2003) 'Inhibition of myocardial injury by ischemic postconditioning during reperfusion: Comparison with ischemic preconditioning', *American Journal of Physiology - Heart and Circulatory Physiology*, 285(2), pp. H579-88.

Zhou, G.-L., Zhuo, Y., King, C. C., Fryer, B. H., Bokoch, G. M. and Field, J. (2003) 'Akt phosphorylation of serine 21 on Pak1 modulates Nck binding and cell migration', *Molecular and Cellular Biology*, 23(22), pp. 8058–8069.

Zhou, T., Prather, E. R., Garrison, D. E. and Zuo, L. (2018) 'Interplay between ROS and antioxidants during ischemia-reperfusion injuries in cardiac and skeletal muscle', *International Journal of Molecular Sciences*, 19(2), p. 417.

Zhu, G. and Lee, A. S. (2015) 'Role of the unfolded protein response, GRP78 and GRP94 in organ homeostasis', *Journal of Cellular Physiology*, 230(7), pp. 1413–1420.

Zhu, P., Hu, S., Jin, Q., Li, D., Tian, F., Toan, S., Li, Y., Zhou, H. and Chen, Y. (2018) 'Ripk3 promotes ER stress-induced necroptosis in cardiac IR injury: A mechanism involving calcium overload/XO/ROS/mPTP pathway', *Redox Biology*, 16, pp. 157–168.

Zinszner, H., Kuroda, M., Wang, X. Z., Batchvarova, N., Lightfoot, R. T., Remotti, H., Stevens, J. L. and Ron, D. (1998) 'CHOP is implicated in programmed cell death in response to impaired function of the endoplasmic reticulum', *Genes and Development*, 12(7), pp. 982–995.